The circulation of the Norwegian Sea- An investigation from space and ocean

Roshin Pappukutty Raj

Dissertation for the degree philosophiae doctor (PhD)

at the University of Bergen

October 2013

Preface

An introductory part and a collection of papers constitute my thesis presented in partial fulfilment of the requirements for the degree philosophiae doctor (PhD) in physical oceanography at the Geophysical Institute, University of Bergen, Norway.

In this thesis, the circulation of the Norwegian Sea known for its influence on the local climate in the northwestern Europe, is studied using a suite of different satellite, hydrographic, numerical ocean model, surface drifter and re-analysis datasets. The findings of this thesis are presented in the form of four scientific papers. Paper 1 focuses on the circulation of the Norwegian Sea, its seasonal and inter-annual variability, connecting flows between the two branches of the Norwegian Atlantic Current, the relationship between the surface flows and the Atlantic Water beneath, and the volume transports at six key locations. Paper 2 zooms into the Lofoten Basin, and addresses the processes influencing the spatial and temporal evolution of dense water formation in the basin and its link to the overflow waters exiting at the Faroe Shetland Channel. Paper 3, zooms further into the western Lofoten Basin and presents a comprehensive study focusing on a most anomalous anticyclonic vortex of the Nordic Seas. In a step towards more precise satellite measurements, Paper 4 shows estimates of a new mean dynamic topography (MDT) for the North Atlantic and the Arctic from Gravity field and steady-state Ocean Circulation Explorer (GOCE) satellite gravity anomaly data. Employing the newly estimated data, the circulation of the region is revisited.

This introductory part is organised as follows: The first chapter describes the background for the research done here. The second chapter gives the motivation for the research work and the main objectives. The next chapter presents the different datasets and methods used in this research. The final two chapters present the summary of the four papers of this thesis and future perspectives.

Acknowledgements

First of all I thank my supervisor and good friend Jan Even Øie Nilsen for working with me, teaching me and motivating me all through the time during the last five years. I am also grateful to my co-supervisors Tor Eldevik and Tore Furevik for their guidance and friendliness. Without the help of my supervisors this thesis would have been a distant dream.

I express my sincere gratitude to Prof. Johnny. A. Johannessen with whom I am currently working with, for his continuous support and encouragement. I also thank Anne Britt Sandø and Yongqi Gao for helping me with the MICOM model.

I am grateful to the University of Bergen and Bjerknes Center for Climate Research for funding my PhD (through POCAHONTAS project) and in particular Nansen Environmental and Remote Sensing Center for providing financial assistance (MONARCH-A project) after the official tenure of my PhD. Next I thank Swapna George, Leon Chafik, Muralidhar Adakudlu, Ingo Bethke, my friends and all the administrative staffs at NERSC, BCCR and GFI for their support.

Last but not the least I thank my dear wife, Dhanya and our parents and sisters for their support and prayers.

Roshin Pappukutty Raj
Bergen, October 2013

Contents

Abbreviations

ADT	Absolute Dynamic Topography
AMOC	Atlantic Meridional Overturning Circulation
ATL12	North Atlantic and Mediterranean Sea Mercator-Océan model
AVHRR	Advanced Very-High Resolution Radiometer
AVISO	Archiving, Validation and Interpretation of Satellite Oceanographic data
AW	Atlantic Water
BF	Bjørnøya-Fugløya
Chl	Chlorophyll
CLS	Collecte, Localisation, Satellites
CNES	The Centre national d'études spatiales
CO	Crossover flows
CTD	Conductivity, Temperature, Depth
DIR	Direct approach
DTU	Technical University of Denmark
EGC	East Greenland Current
EI	Eddy Intensity
EKE	Eddy Kinetic Energy
ELB	Eastern Lofoten Basin
ESA	European Space Agency
FC	Faroe Current
FN	Faroe North
FSC	Faroe Shetland Channel
FSCOW	Faroe Shetland Channel Overflow Waters
GOCE	Gravity field and steady-state Ocean Circulation Explorer
GRACE	Gravity Recovery and Climate Experiment
GUT	GOCE User Toolbox
HPF	High level Processing Facility
HYCOM	The Hybrid Coordinate Ocean Model
ICES	International Council for the Exploration of the Seas

ICESat	Ice Cloud and Land Elevation Satellite
IFR	Iceland Faroe Ridge
LAGEOS	Laser Geodynamics Satellites
LS	Lofoten Slope
MDT	Mean Dynamic Topography
MICOM	Miami Isopycnic Coordinate Ocean Model
MLD	Mixed Layer Depth
MODAS	Modular Oceanographic Data Assimilation System
MR	Mohn Ridge
MSS	Mean Sea Surface
NAW	North Atlantic Water
NCC	Norwegian Coastal Current
NCEP	National Centers for Environmental Prediction
NISE	Norwegian Iceland Seas Experiment
NNAW	Norwegian North Atlantic Water
NwAC	Norwegian Atlantic Current
NwAFC	Norwegian Atlantic Front Current
NwASC	Norwegian Atlantic Slope Current
RMS	Root Mean Square
SeaWiFS	Sea-viewing Wide Field-of-view Sensor
SC	Shetland Current
SLA	Sea Level Anomaly
SPW	Space Wise
SSH	Sea Surface Height
SST	Sea Surface Temperature
SV	Svinøy
TW	Time Wise
VJ	Vøring Jet
WLB	Western Lofoten Basin
WOCE	World Ocean Circulation Experiment
WSC	West Spitsbergen Current

Abstract

The Norwegian Sea circulation plays a key role in maintaining the mild climate of the northwestern Europe via the transport of warm Atlantic Water pole-ward. The first paper addresses the advective currents connecting the two branches of the Norwegian Atlantic Current and shows the general spin up of the Norwegian Sea circulation during winter with the exception of the flow over the Mohn Ridge. The variability in the surface velocities in the Norwegian Sea is found to be deep reaching, which supports the use of altimetry to monitor the variability of the poleward transport of Atlantic Water. A strengthening and weakening of the Atlantic inflow east of the Faroe Islands has a consistent response along the entire slope current. However, a stronger western inflow, observed north of the Faroe Islands, is associated with more flow of Atlantic Water into the slope current. This finding suggest that a substantial fraction of Atlantic Water that eventually enters the Barents Sea or the Arctic through the Fram Strait, may originate from the western inflowing branch of Atlantic Water to the Nordic Seas, and that the two branches of northward flowing Atlantic Water cannot be considered as separate flows. Paper 2 examines the influence of the surface circulation, eddy activity and local heat loss on the spatial distribution and temporal evolution of dense water formation in the Lofoten Basin. Evidence of intrusion of Atlantic Water into the central Lofoten Basin due to buoyant waters in the eastern part of the basin is found. With the support of hydrographic and satellite datasets, the concept of separate western and eastern regions of the Lofoten Basin is introduced and a link between the western Lofoten Basin and Faroe Shetland overflow waters is identified. Paper 3 addresses an anomalous anticyclonic vortex in the Nordic Seas, which is situated in the western Lofoten Basin. The vortex' surface and vertical characteristics on seasonal, inter-annual, and climatological time-scales are quantified, relevant forcing mechanisms are addressed, and its uniqueness in the Nordic Seas is documented. In the final paper, a new mean dynamic topography (MDT) is estimated for the North Atlantic and the Arctic from the Gravity field and steady-state Ocean Circulation Explorer (GOCE) satellite gravity anomaly data. The new GOCE-based MDT is assessed and compared to independent steric height observations, other state-of-the-art

MDTs and three coupled sea-ice-ocean models, showing its usefulness in studies of high latitude ocean circulation.

List of publications

1. **Raj, R. P**., J. E. Ø. Nilsen and T. Furevik (2013): The two-branch structure of the Norwegian Atlantic Current-transport variability and connecting flows. *Journal of Geophysical Research-Oceans, submitted.*

2. **Raj, R. P**., and J. E. Ø. Nilsen (2013): Processes influencing the dense water formation in the Lofoten Basin. *Journal of Geophysical Research-Oceans, submitted.*

3. **Raj, R**. **P**., L. Chafik, J. E. Ø. Nilsen and T. Eldevik (2013): The Lofoten vortex of the Nordic Seas. *Deep Sea Research, Part 1, in revision*.

4. Johannessen, J.A., **R. P. Raj**, J. E. Ø. Nilsen, T. Pripp, P. Knudsen, F. Counillon, L. Bertino, D. Stammer, N. Serra and N. Koldunov (2013): Towards improved estimation of the dynamic topography and ocean circulation in the high latitude and Arctic Ocean: The importance of GOCE, in The Earth's Hydrological Cycle. Edited by Bengtsson et al., *Springer*. Accepted.

Chapter 1

Introduction

The Norwegian Sea circulation (see Figure 1) with its transport of warm Atlantic Water pole-ward is a key component in maintaining a relatively mild climate in the northwestern Europe (e.g., *Rhines et al.,* 2008). This heat further regulates the local climate by its influence on the sea ice cover in the Barents Sea (*Årthun et al.,* 2012) and near Svalbard (*Walczowski and Piechura,* 2011). The circulation of the Norwegian Sea also plays a key role on the biological productivity of the region which in turn is linked to the fisheries (*Mork and Skagseth,* 2010). In a global perspective, the Atlantic Water entering the Norwegian Sea and its densification are important to the formation of overflow waters in the Nordic Seas which further contributes to the North Atlantic Deep Water and maintains the Atlantic Meridional Overturning Circulation (AMOC; *Dickson and Brown,* 1994; *Medhaug et al.,* 2011). Thus the circulation of the Norwegian Sea is important to the global climate.

1.1. The Region

The Nordic Seas (Figure 1) is a buffer zone between the North Atlantic Ocean to the south and the Arctic Ocean to the North. The surface layers of the Nordic Seas are dominated by relatively salty and warm Atlantic Water to the east while it is dominated by rather fresh and cold Polar Water to the west. This thesis primarily focuses on the circulation of the Norwegian Sea situated in the eastern part of the Nordic Seas. The Norwegian Sea is comprised of the Norwegian Basin and the Lofoten Basin, of which the latter is the largest heat reservoir in the Nordic Seas since it is occupied by the Atlantic Water, down to 800 m depth (*Blindheim and Rey,* 2004; *Skagseth and Mork,* 2012). Geographically, the Lofoten Basin is separated from the Greenland Basin by the Mohn Ridge and from the Norwegian Basin by the Vøring Plateau and the Helgeland Ridge stretching towards Jan Mayen. In the Lofoten Basin, the Atlantic Water has a bowl shaped structure having a width of 800 km (e.g., *Orvik,* 2004). In the Norwegian Basin the penetration of Atlantic Water is limited to shallower depths.

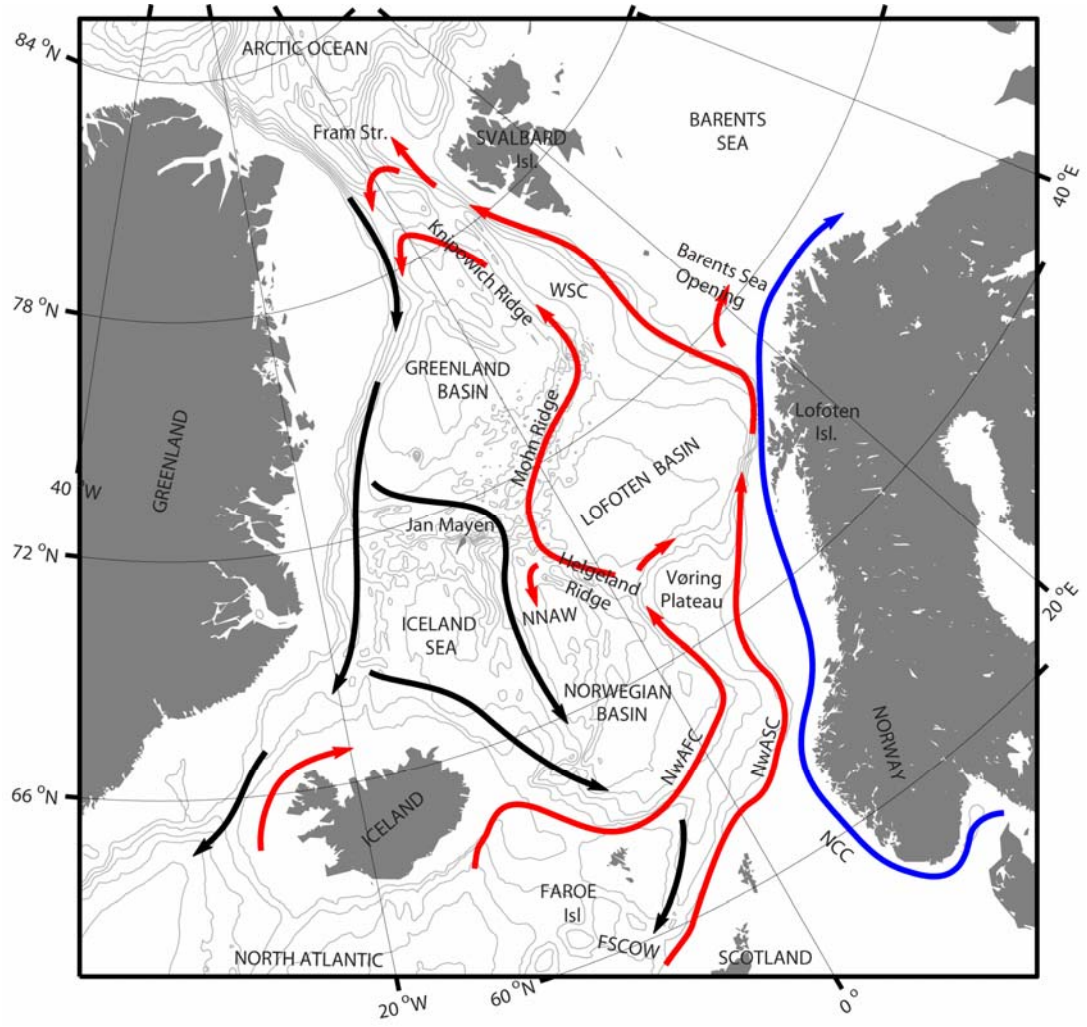

Figure 1. The Nordic Seas with schematic water pathways showing its overturning circulation from inflowing Atlantic Water in the surface (red) to deeper transformed waters returning to become overflows to the deep North Atlantic (black). The Norwegian Atlantic slope current (NwASC), Norwegian Atlantic front current (NwAFC), and West Spitsbergen Current (WSC) are represented by red arrows. The fresh Norwegian Coastal Current (NCC) is indicated in blue. The Norwegian North Atlantic Water (NNAW), and the overflow waters exiting at Faroe Shetland Channel (FSCOW) are also indicated. Grey isobaths are drawn for every 600 m. Surface circulation in this figure is based on the review of the Nordic Seas circulation presented in *Furevik and Nilsen* (2005), while deep flows (in black) are simplified from *Hansen and Østerhus* (2000).

1.2. Norwegian Sea circulation

The circulation of the Norwegian Sea was first comprehensively described by *Helland-Hansen and Nansen* in 1909. The Norwegian Atlantic current (NwAC) is the extension of the Gulf Stream in the Nordic Seas and is fed into the Norwegian Sea mainly via two inflows (see Figure 1): The Faroe-Shetland inflow and the Iceland-Faroe inflow. The NwAC which is considered as the northern limb of AMOC is the

source for salt and heat into the Norwegian Sea (e.g., *Rhines et al.,* 2008). The NwAC is a two branch current system of which the eastern branch follows the Norwegian shelf edge as a barotropic slope current, while the western branch is topographically guided from the Iceland-Faroe front (*Poulain et al.,* 1996; *Orvik and Niiler,* 2002). Atlantic Water fills the volume between the two branches of NwAC. The western and eastern branches of NwAC are known as the Norwegian Atlantic Front Current (*Mork and Skagseth,* 2010) and the Norwegian Atlantic Slope Current (*Skagseth and Orvik,* 2002), respectively (see Figure 1). In this thesis, the terms "front current" and "slope current" are used to represent the two branches respectively. At the inflow, the volume of Atlantic Water transported poleward by the slope current and front current respectively are in the range of 2.7-4.4 Sv (*Orvik and Skagseth,* 2003; *Hughes et al.,* 2006; *Sherwin et al.,* 2008; *Berx et al.,* 2013) and 1.7-3.5 Sv (*Orvik et al.,* 2001; *Hansen et al.,* 2010; *Mork and Skagseth,* 2010). The heat transport associated with the inflow of Atlantic Water to the Norwegian Sea (relative to 0°C) is estimated to be in the order of 250 TW (*Hansen et al.,* 2003; *Furevik et al.,* 2007; *Segtnan et al.*, 2011). About half of this is heat is lost due to air-sea interaction or lateral eddy mixing before the Atlantic Water leaves the Norwegian Sea to the Barents Sea Opening or through the Fram Strait (*Segtnan et al.*, 2011). While the variability of the slope current has been found to be associated with both the local wind field (*Gordon and Huthnance,* 1987; *Skagseth and Orvik,* 2002) and the large-scale wind field (e.g., *Skagseth et al.,* 2004; *Chafik,* 2012), the variability of the front current, at its beginning, is associated with local wind stress and sea surface height near the Iceland-Faroe Ridge (*Hansen et al.,* 2010; *Richter et al.,* 2012).

Further downstream in the Norwegian Sea, the front current and the slope current form the western and eastern boundaries of the Lofoten basin (Figure 1). The front current flows along the Mohn Ridge while the slope current continues along the continental slope, partly branching into the Barents Sea, and flows northwards as the West Spitsbergen Current (WSC; *Saloranta and Haugan,* 2001; *Walczowski and Piechura,* 2011). The strongest topographic steering of the front current is along the western slope of the Vøring Plateau (*Nilsen and Nilsen*, 2007). A returning branch of the front

current to the east of Jan Mayen flows southward into the Norwegian Basin (*Read and Pollard,* 1992). This is part of the cyclonic circulation of Atlantic Water in the Norwegian Basin. This recirculation of Atlantic Water together with the northward flowing NwAC and Norwegian Coastal Current (NCC) which flows along the coast of Norway into the Barents Sea constitute the surface circulation of the Norwegian Sea.

1.3. Eddies in the Norwegian Sea

Mesoscale eddies in the ocean are vortices or flows with scales ranging from the baroclinic Rossby radius of deformation to as large as hundred kilometre. Mesoscale eddies contribute to the stirring of water masses and thus results in mixing. Eddies are known to feed momentum and energy back into the mean flow and help drive the deep ocean circulation (*Morrow et al.,* 1994; *Lozier,* 1997). Eddies also carry heat, salt, carbon, and nutrients and play an important role in the global budgets of these tracers. Most of the eddy energy is generated by instabilities of the mean flow (*Stammer and Wunsch,* 1999), and by fluctuating winds (*Frankignoul and Muller,* 1979).

Helland-Hansen and Nansen (1909) first observed mesoscale eddies in the Norwegian Sea and termed these ocean features as ‘‘puzzling waves’’. In the Norwegian Sea, eddies are found to play an important role in heat exchanges and dense water formation (*Rossby et al.,* 2009b; *Spall,* 2010). The eddies form due to baroclinic instability (*Ikeda et al.,* 1989; *Spall,* 2010) and also through a combination of topographic steering, vortex stretching and barotropic instability (*Johannessen et al.,* 1989). The Lofoten Basin is the highest eddy active region in the Nordic Seas (*Poulain et al.,* 1996; *Jakobsen et al.,* 2003). *Volkov et al.* (2013) recently termed Lofoten Basin as a “hot spot” of intense synoptic scale variability. The key feature of the Lofoten Basin circulation is the spinning of anticyclonic eddies from the slope current and its southwestward propagation towards the deep Lofoten Basin (*Köhl,* 2007; *Andersson et al.,* 2011). Other main eddy active regions in the Norwegian Sea are the two inflows (*Sherwin et al.,* 2006; *Richter et al.,* 2009; *Koszalka et al.,* 2011).

1.4. Dense water formation in the Norwegian Sea

Overflow waters from the Nordic Seas and Arctic Ocean is the main source of North Atlantic Deep Water (*Dickson and Brown,* 1994). Several studies have shown the gradual transformation of Atlantic Water along its advective path in the Nordic Seas to play a major role in the formation of overflow waters (*Mauritzen,* 1996a,b; *Isachsen et al.,* 2007; *Eldevik et al.,* 2009). The importance of water mass transformation in the Norwegian Sea is highlighted by *Isachsen et al.* (2007), where they showed that the bulk of the light to dense water mass transformation occurring in the Nordic Seas takes place in the deep Lofoten and Norwegian Basin. Later *Eldevik et al.* (2009) showed that dense waters formed in the Norwegian Basin may have a direct influence on the overflow waters exiting at the Faroe Shetland Channel (FSC). The residence time of Atlantic Water circulating in the Lofoten Basin is longer than in any other region of the Nordic Seas possibly due to the deep cyclonic recirculation prevailing there (*Gascard and Mork,* 2008). The longer residence time combined with strong atmospheric cooling results in densification of Atlantic Water in the Lofoten Basin, which in turn has been argued to influence overflow waters. However, the link between the Atlantic Water in the Lofoten Basin and the overflow waters has not been shown yet.

Chapter 2

Motivation and Objectives

The motivation of this research stems from the potential importance of the Norwegian Sea circulation (see Figure 1) to the Atlantic Water transformation. The overall aim of the thesis is to revisit the circulation of the Norwegian Sea and to add new insight to our current understanding of the flow pattern, eddy activity, hydrography, deep convection and dense water formation in the region. The motivations and objectives for the four manuscripts included in this thesis are listed below.

Paper 1. **The two-branch structure of the Norwegian Atlantic Current-transport variability and connecting flows.**

The circulation of the Norwegian Sea has been subject to investigations since *Mohn* (1887) and *Helland-Hansen and Nansen* (1909). In recent years, the variability in Atlantic Water transport in the Norwegian Sea has received much attention due to its significance influence on the sea ice cover in the Barents Sea (*Sandø et al.,* 2010; *Årthun et al.,* 2012) and near Svalbard (*Walczowski and Piechura,* 2009). *Mork and Skagseth* (2010) estimated Atlantic Water volume transport from satellite derived surface velocities and hydrography, which showed the usefulness of satellite data for studies of variability in Atlantic Water transport. Although their analysis was limited to Svinøy section, the results suggested that the method could be consistently applied for other locations in the Norwegian Sea, as done here. Unlike the temporal variability, the spatial features of the circulation in the Norwegian Sea, has been thoroughly studied using drifters and floats (e.g., *Jakobsen et al.*, 2003; *Rossby et al.,* 2009a*; Andersson et al.,* 2011; *Koszalka et al.,* 2011, 2013). However, still it remains to be decided whether the two branches of NwAC can be considered as separate flows after entering on each sides of the Faroe Islands (*Helland-Hansen and Nansen*, 1909; *Orvik and Niiler,* 2002*; Nilsen and Nilsen,* 2007). *Rossby et al.* (2009a) using floats showed connecting flows and mixing between the two branches of NwAC and argued that the two branches cannot be considered as separate. However, evidence of persistent flow between the front current and the slope current based on long term and continuous data

like altimetry, has not yet been presented. The main objectives of Paper 1 are:

- To examine the spatial and temporal variability of the surface circulation of the Norwegian Sea using satellite altimetry;
- To examine the vertical structure of the circulation observed from satellites, using hydrography;
- To identify regions where flow (surface waters in this study) between the two branches of the Norwegian Atlantic Current may take place;
- To assess effects of these inter-connections on the downstream flow variability.

Paper 2. **Processes influencing the dense water formation in the Lofoten Basin.**

In recent times, the Lofoten Basin, which is the largest heat reservoir in the Nordic Seas, has received some attention due to the dense water formation there and its possible link to the overflow waters exiting from the Nordic Seas. The identification of the Lofoten Basin as a major location in the Nordic Seas where strong dense water formation takes place (*Isachsen et al*., 2007), further highlights the importance of dense waters formed there. However, a thorough description of the water mass distribution or a link between the Lofoten Basin and overflow waters from the Nordic Seas has not been shown in earlier studies. The main objectives of Paper 2 are:

- To identify the influence of surface circulation, eddy activity, and heat loss of the Lofoten Basin on the spatial distribution and temporal evolution of dense water formation in the Lofoten Basin;
- To study the temporal variability in the hydrographic properties of Atlantic Water in the Lofoten Basin during a six decade time period;
- To quantify the influence of North Atlantic inflow and atmospheric heat loss on the Atlantic Water density in the Lofoten Basin;
- To assess the Atlantic Water transformation in the Lofoten Basin as an integral part of the cyclonic overturning loop in the Nordic Seas, which is part of AMOC.

Paper 3. **The Lofoten vortex of the Nordic Seas.**

A most anomalous circulation feature in the Nordic Seas is the anticyclonic vortex seated in the deep part of the Lofoten Basin. Since the vortex is also situated in the

deep convective region in the basin it is likely to play an active role in the ventilation of Atlantic Water. Several studies have observed the existence of this quasi-permanent Lofoten vortex (*Ivanov and Korablev*, 1995a, b; *Kohl*, 2007; *Rossby et al.,* 2009a; *Andersson et al.,* 2011; *Koszalka et al.,* 2011; *Søiland and Rossby,* 2013; *Volkov et al.,* 2013). This study performs a more comprehensive observational based quantitative analysis of the vortex using satellite and long-term hydrographic datasets. The main objectives of Paper 3 are:

- To document the uniqueness of the Lofoten Vortex in the Nordic Seas;
- To quantify the vortex' surface and vertical characteristics;
- To quantify its variability on seasonal, inter-annual, and climatological time-scales;
- To assess relevant forcing mechanisms.

Paper 4. Towards improved estimation of the dynamic topography and ocean circulation in the high latitude and Arctic Ocean: The importance of GOCE.

Changes in the North Atlantic and the Arctic have far reaching influences on regional and global environment and climate variability, thus emphasizing the need for advanced quantitative understanding of the ocean circulation and transport variability in the high latitude and Arctic Ocean. The main objectives of Paper 4 are:

- To estimate a new mean dynamic topography for the North Atlantic and the Arctic from the highly precise gravity field from GOCE data, to facilitate improvements in future analyses of the circulation in the Nordic Seas and Arctic Ocean;
- To assess the quality, usefulness and validity of the new GOCE derived MDT for studies of the ocean circulation and transport estimates in the Nordic Seas and Arctic Ocean;
- To estimate the barotopic contribution to the mean dynamic topography in the Nordic Seas.

Chapter 3

Data and Methods

3.1. Ocean Currents from remote sensing

3.1.1. Satellite altimetry

Accurate measurements of the sea surface relative to a reference ellipsoid have been provided by several (TOPEX/POSEIDON, ERS-1 and 2, Envisat, JASON-1 and 2) satellite altimeter missions (e.g., *Fu et al.,* 2001) for the past two decades. An altimeter emits signal to the earth surface and receives the reflected echo and thus measures the sea surface height (SSH). Instantaneous SSH is measured relative to a reference ellipsoid (Figure 2). Sea level anomalies (SLA) are estimated from the instantaneous SSH after subtracting the mean sea surface (MSS). Currently, MSS derived from altimetry is known with a centimeter accuracy (*Schaffer et al.,* 2012).

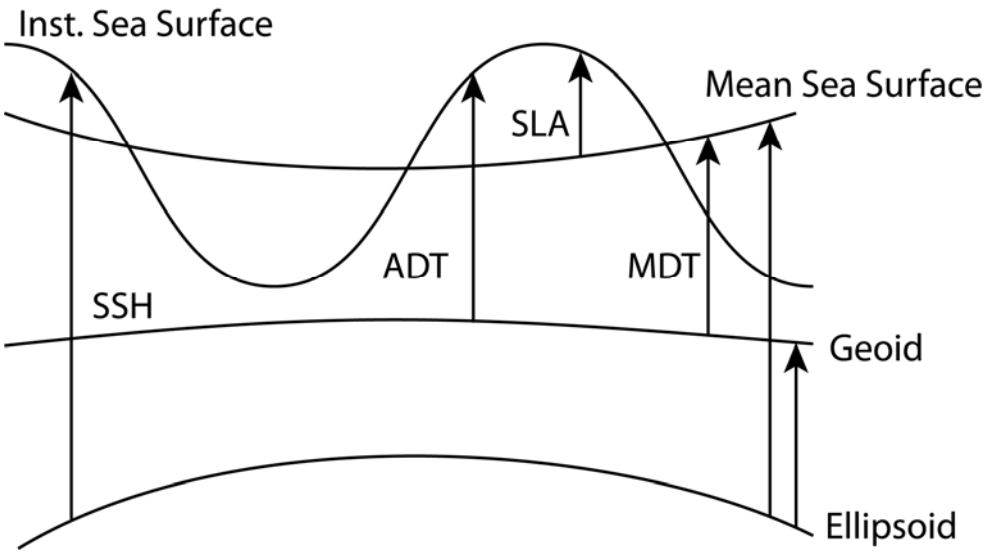

Figure 2. Schematic illustration of the relationship between the mean dynamic topography (MDT), the mean sea surface and the geoid referenced to the same ellipsoid.

The SLA fields, corrected for the inverted barometer effect, tides, and tropospheric effects (*Le Traon and Ogor,* 1998) are based on merged TOPEX/POSEIDON (T/P), ERS-1 and 2 and Envisat data (*Ducet et al.,* 2000; *Volkov and Pujol,* 2012). Note that

the TOPEX/POSEIDON data is not available north of 66°N. The SLA fields and the errors associated with it are obtained from AVISO. AVISO stands for Archiving, Validation and Interpretation of Satellite Oceanographic data, and was set up in 1992 to process, archive and distribute ocean radar altimeter data. In the Norwegian Sea, the SLA fields provided are of roughly 12 to 18 km resolution. Figure 3 shows an example of a (randomly chosen) weekly SLA field in the Norwegian Sea and the magnitude of its errors. The root mean square (RMS) difference between the altimeter data and tide gauge measurements in the Norwegian Sea is generally 3 cm (*Volkov and Pujol*, 2012).

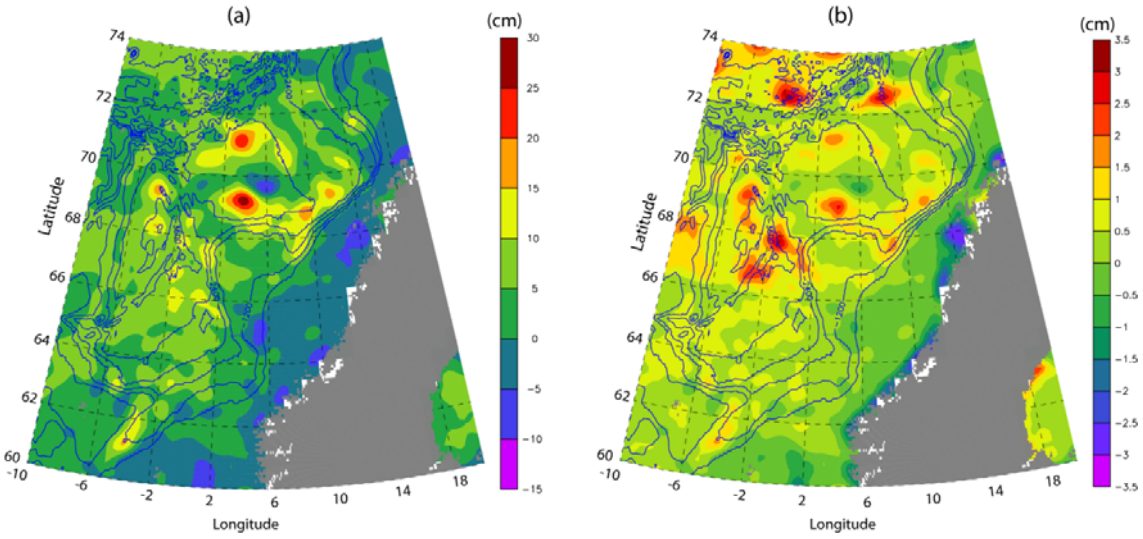

Figure 3. (a) An example of weekly sea level anomaly data and (b) the error associated with it during 19-25 June 2008. Blue lines are isobaths drawn for every 600 m.

3.1.2. Mean Dynamic Topography

Mean dynamic topography used to study the circulation of the global ocean, is the difference between MSS and the geoid (Figure 2; *Knudsen et al*., 2011). The geoid is the equipotential surface of earth's gravity field, or more precisely it is the sea surface in the absence of winds, currents and tides and only influenced by gravity. Thus, MDT yields the long term averaged strength of the ocean currents, i.e. the mean circulation. The lack of an accurate geoid has until recently prevented precise computation of the ocean's geostrophic circulation from satellite altimetry (*Knudsen et al.,* 2007*; Bingham et al.,* 2008). Various methods have been used to calculate the MDT from *in*

situ ocean data. The simplest method is to compute dynamic height relative to an assumed level of no motion from climatology of temperature and salinity, based on measurement profiles made over many decades (*Levitus and Boyer*, 1994; *Levitus* et al., 1994). A modification of this method uses an inverse model with certain dynamical constraints to get the barotropic signal (*LeGrand et al.,* 2003). However, these two methods cannot represent a uniform time average due to the inhomogeneity of hydrography data. In another approach, *Niiler* et al. (2003), from a 10-year set of near-surface drifter velocities derived MDT which is corrected for temporal bias using altimeter data. Later, *Rio & Hernandez* (2004) created another MDT (Rio03 MDT) by blending ocean observation without the use of a model. During the last decade, the introduction of satellite gravity measurements from Gravity Recovery and Climate Experiment (GRACE) drastically improved the knowledge of the marine geoid (*Rio et al.,* 2005; *Maximenko et al.,* 2009). An update of Rio03 MDT (Rio05 MDT) was released after the incorporation of the GRACE geoid model (*Rio et al.,* 2005). Currently, the CNES-CLS09 MDT (*Rio et al.,* 2011; Figure 4a), an updated version of Rio05 MDT, is the state-of-the-art MDT.

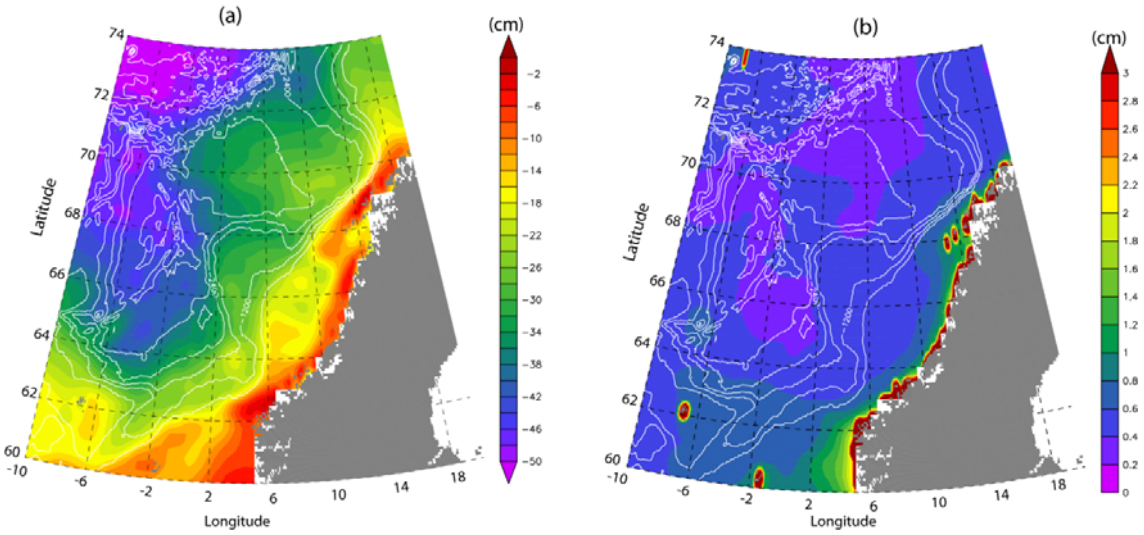

Figure 4. Spatial distribution of MDT from (a) CNES-CLS09 MDT, and (b) the error associated with it in the Norwegian Sea. White lines are isobaths drawn for every 600 m.

The CNES-CLS09 MDT is based on altimetry, surface buoys, Argo floats, in situ measurements, and a GRACE geoid model. This MDT has been estimated on a 1/4^{o} regular grid using a combination of direct and synthetic methods (*Rio and Hernandez*,

2004; *Rio et al*., 2005). The main improvements from the previous Rio05 MDT are: (1) the use of 4.5 years of GRACE gravity anomaly data instead of 2 years; (2) updated drifting buoy velocities (1993-2008) and dynamic heights estimated from Conductivity, Temperature and Depth (CTD) casts and Argo floats (1993-2008); (3) an improved Ekman model for the extraction of the geostrophic component of the buoy velocities; (4) an improved processing method for the estimation of dynamic heights; (5) the estimation of the MDT is done on a 1/4° resolution grid instead of 1/2°. Figure 4 shows the MDT in the Norwegian Sea, which ranges from -45 cm to 5 cm. The errors associated with the estimation of MDT are provided together with the dataset (*Rio et al.,* 2011). These errors are computed using multivariate objective analysis of both observational errors and the a-priori MDT covariance field (see *Rio et al.,* 2011, for more details). In the Norwegian Sea, from the continental plateau and outwards, the errors are less than 1.0 cm (Figure 4b).

3.1.3. Absolute Dynamic Topography

SLA added to MDT gives Absolute Dynamic Topography (ADT) which can be further used to determine the surface velocities (u_s and v_s):

$$ADT = SLA + MDT, \tag{1}$$

$$u_s = \frac{-g}{f}\frac{\partial ADT}{\partial y}, \tag{2}$$

$$v_s = \frac{g}{f}\frac{\partial ADT}{\partial x}, \tag{3}$$

where g is the acceleration due to gravity, f is the Coriolis parameter, h is SLA, and x and y are the longitudinal and latitudinal directions. ADT and surface geostrophic velocities determined from the CNES-CLS09 MDT and the AVISO SLA are used in Paper 1, 2 and 3, in order to study the circulation of the Norwegian Sea.

Eddy kinetic energy, *EKE,* is computed using the relation (*Chaigneau et al.,* 2008):

$$EKE = \frac{u'^2 + v'^2}{2}, \tag{4}$$

where u' and v' are geostrophic velocity anomalies determined using only the altimeter derived SLA instead of the full ADT in equations (2) and (3). The SLA derived EKE is used to quantify the Lofoten Vortex of the Nordic Seas in Paper 3.

3.1.4. Evaluation of the absolute velocities

Volkov and Pujol (2012) validated this satellite data in the Norwegian Sea and argued that the velocities can be successfully used to study the variability in the surface circulation of the region.

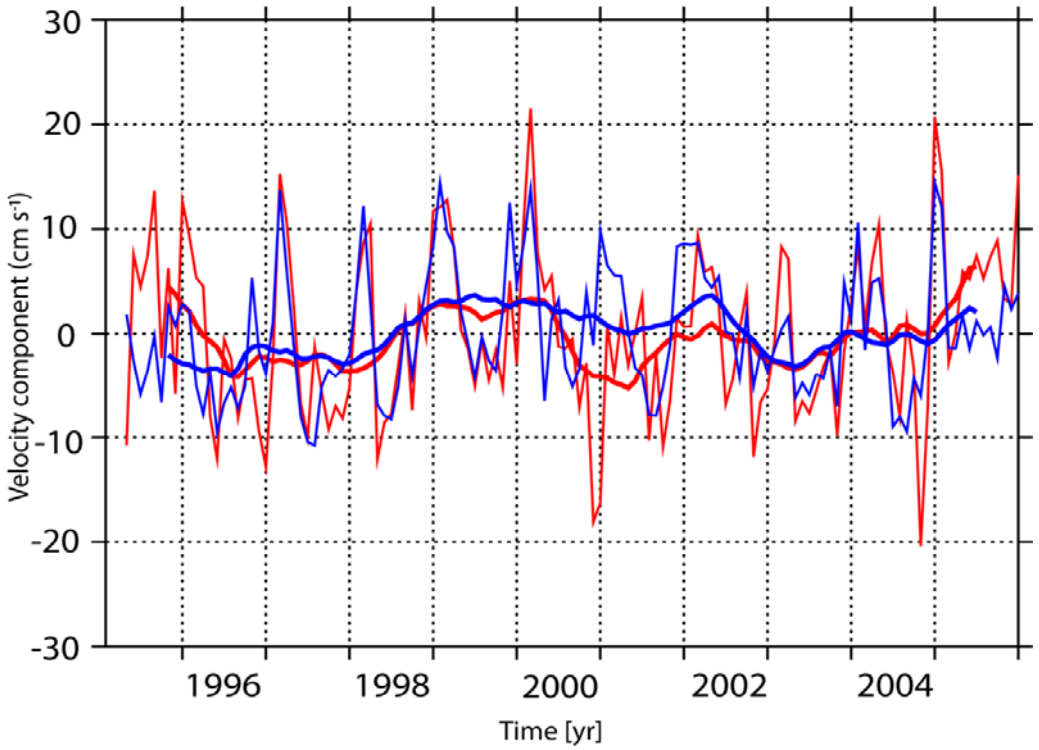

Figure 5. Monthly surface geostrophic velocity anomaly from altimetry (blue) and independent current meter velocity anomaly at 100 m depth (red) in the slope current at Svinøy section. Thick lines are 12 month running mean of their respective datasets. The monthly velocity anomalies are determined after removing the time-mean. This figure is from Paper 1 of this thesis.

Mork and Skagseth (2010) compared the temporal mean of satellite derived absolute velocities across the Svinøy Section to the temporal mean of independent current measurements and found good similarity between the satellite and current meter velocities. We compared the monthly variability of altimeter derived surface velocities with the current meter velocities in the slope current at Svinøy Section (Figure 5). The figure shows good comparison and there is a significant correlation (r=0.61) between the two independent velocity measurements (correlation obtained after de-trending and de-seasoning). Note that this comparison between satellite and current meter data is

done in a location very near to the coast (Figure 2a in Paper 1). It is known that the errors in the altimeter data near to the coast are higher than in the open ocean. However, the good agreement between the altimeter data and current meter at Svinøy demonstrate the usefulness and validity of the dataset in studies of the variability in the circulation of the Norwegian Sea.

3.2. A New Mean Dynamic Topography of the North Atlantic and Arctic Ocean from the new GOCE data

The first three scientific papers of this thesis used the CNES-CLS09 MDT dataset (*Rio et al.,* 2011; Section 3.1.2). As a step towards higher precision, a new mean dynamic topography estimated from GOCE (Paper 4) is described below.

The gravity field over the earth's surface varies from place to place due to the rotation of the earth, positions of mountains and ocean trenches and variations in density of the ocean interior. The GOCE mission of the European Space Agency (ESA) was successfully launched in October 2009. GOCE is dedicated to measuring the Earth's gravity field and the geoid with unprecedented accuracy (gravity: ~1-2 mgal; geoid: ~1-2 cm) at a spatial resolution of ~100 km. Recent studies show the improvements of the GOCE derived geoid and MDT over the GRACE satellite data at higher spatial resolution of around 100 km (*Bingham et al.* 2011; *Knudsen et al.* 2011; *Bruinsma et al.,* 2013).

3.2.1. The GOCE geoid

The GOCE High level Processing Facility (HPF) delivers the level 2 global gravity model from which geoid heights can be determined (*Johannessen et al.,* 2003*; Koop et al.,* 2007; *Bingham et al.,* 2011). Three versions of the GOCE gravity model are provided by three distinct methods: the direct approach (DIR), the space-wise (SPW), and time-wise (TW) methods (see *Bruinsma et al.*, 2010 and *Pail et al.*, 2011 for details). Here we use the third release of the DIR and TW models. While the TW model is a GOCE-only model (12 months of GOCE data), i.e., no external gravity field information has been used, neither as reference model, nor for constraining the solution, the DIR gravity field model is constructed with 12 months of GOCE data and 7 years of GRACE and Laser Geodynamics Satellites (LAGEOS) data. Thus, the TW gravity model is the GOCE-only product which gives the best demonstration of the capabilities of GOCE. The TW and DIR geoids (0.25º latitude and 0.25º longitude grids) are herein determined from their respective gravity models in the mean-tide system and relative to the Topex-ellipsoid, in order to be consistent with the two

different MSS datasets used in this study. All technical details associated with the estimation of the geoid from gravity anomalies are given in *Johannessen et al.* (2003). The two different MSS data sets used in this study are: (1) CNES-CLS11 MSS (*Schaffer et al.,* 2012) and DTU10 MSS (*Knudsen et al.,* 2011).

3.2.2. Estimation of Mean Dynamic Topography and velocity fields

As explained in section 3.1.2, the computation of MDT from MSS and geoid is conceptually very simple as expressed by the equation *MDT = MSS – geoid*. However as indicated by *Benveniste et al.,* (2007) there are several issues that must be considered in order to obtain a good MDT product. All these issues are considered in the estimation of MDT shown below (Table 1). The computation of the MDT is done according to the recommendations from the GOCE User Toolbox (GUT) tutorials and is carried out using GUT tools (*Benveniste et al.,* 2007; *Knudsen et al.,* 2011).

Table 1. Mean Dynamic Topography products (first column) and the geoids (second column) and the mean sea surfaces (third Column) they are based on.

MDT	Geoids	MSS
TW_CNES	TW	CNES-CLS11
TW_DTU	TW	DTU10
DIR_CNES	DIR	CNES-CLS11
DIR_DTU	DIR	DTU10

After the estimation, a filter should be applied to the MDT in order to remove the noise. In a recent study, *Knudsen et al.,* (2011) applied a Gaussian filter (140 km) to the MDT. However in the high latitudes, it is found that large spatial filtering removes signatures of ocean currents. The influence of the spatial filtering on the estimation of MDT is demonstrated in Figure 6 comparing profiles of MDT across the Greenland Basin (a), the Lofoten Basin (b), the Norwegian Basin (c) and the Greenland-Scotland ridge (d). Although, the maximum difference between the MDTs is less than 5 cm, the signatures of the mesoscale circulation features in the Nordic Seas are gradually lost as the filter-width increases from 80 km. This is particularly evident for the two branches of the Norwegian Atlantic Current (panel b and c) as well as for the inflow of Atlantic Water in the Denmark Strait (panel d). Hence, for high latitudinal studies, a Gaussian filter of 80 km is chosen.

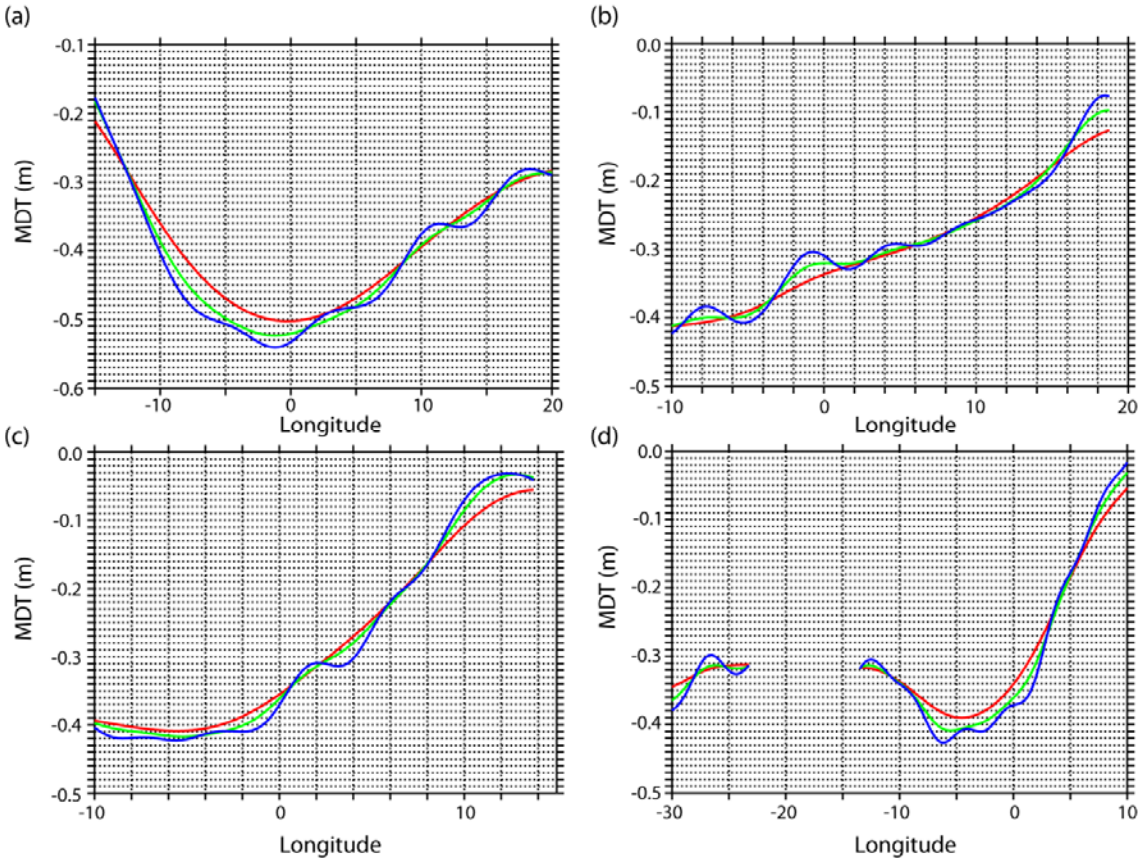

Figure 6. DIR_DTU mean dynamic topography with a spatial resolution of 140 km (red), 100 km (green), 80 km (blue) across (a) 75°N, (b) 70°N, (c) 67°N and (d) 65°N. The discontinuous lines in panel d is due to presence of land.

The four MDTs (Table 1) of the North Atlantic and the Arctic prepared from two GOCE geoid models and MSS are shown in Figure 7. All four MDTs reproduced the distinct minima in MDT in the Labrador Sea and the Greenland Sea as well as the maxima in the Beaufort Gyre and in the northern Pacific Ocean. The comparison of the four solutions show that the MDT estimated from the DIR geoid and DTU10 MSS provides the best representation of known circulation features in the Arctic Ocean and Nordic Seas (Figure 7a). Interestingly, the TW_DTU MDT (based solely on the GOCE geoid) is comparable to DIR_DTU MDT, south of about 85ºN. All in all, this clearly demonstrates the potential of the GOCE mission for studying high latitude ocean circulation. Note that in Paper 4, MDT is estimated (as described above) from the Eigen 6C gravity model which uses the combination of DIR gravity model and terrestrial data (*Förste et al.,* 2011).

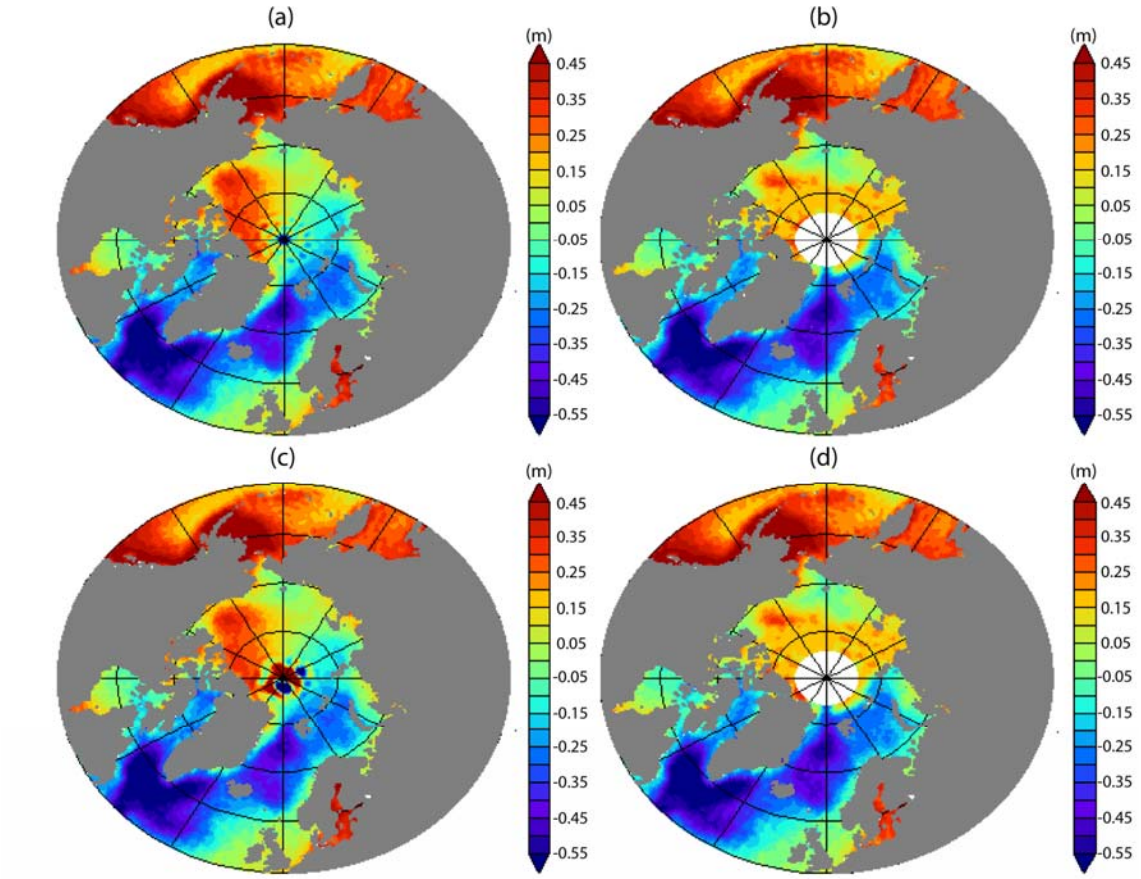

Figure 7. Mean dynamic topography of the North Atlantic and the Arctic Ocean: (a) DIR_DTU MDT, (b) DIR_CNES MDT, (c) TW_DTU MDT, (d) TW_CNES MDT.

3.3. Other remote sensing data

Sea surface temperature (SST; 1993-2010) is obtained from 1/8º global fields of SST produced by the Modular Ocean Data Assimilation System (MODAS). MODAS SST is produced by an optimal interpolation of Advanced Very-High Resolution Radiometer (AVHRR) nonlinear SST observations (*Barron and Kara*, 2006). Note that the spatial coverage of AVHRR SST is influenced by cloud cover. Hence, MODAS SST is used in this study. MODAS SST is used as a proxy to show the effect of buoyancy forcing on the eddy intensity of the anticyclonic vortex of the Lofoten Basin (Paper 3).

Chlorophyll-a (chl-a; 1997-2010; 9 km grid) pigment concentration is obtained from Sea-viewing Wide Field-of-view Sensor (SeaWiFS). SeaWiFS chl-a data has been used to study phytoplankton blooms in the Nordic Seas (*Engelsen et al.,* 2002). In this thesis (Paper 2), it is used as a proxy to study the surface circulation pattern of the Lofoten Basin.

3.4. Hydrography

Hydrographic data is obtained from the long term (1949-2008) hydrographic NISE database (Norwegian Iceland Seas Experiment; *Nilsen et al.,* 2008). Similar to the satellite altimetry, the NISE data is a major dataset used in all four papers of this thesis. The NISE dataset consists of CTD data decimated to 5 m, and bottle data. The hydrographic variables included in the latest version (V3) of the NISE dataset are temperature and salinity. The major source of the NISE dataset is the public database maintained by the International Council for the Exploration of the Seas (ICES). The NISE database also includes data obtained from the Marine Research Institute, Iceland; Institute of Marine Research, Norway; the Faroese Fisheries Laboratory, Faroe Islands; Geophysical Institute, University of Bergen, Norway and the World Ocean Circulation Experiment (WOCE). The NISE dataset has been used to study the variability of different water masses in the Nordic Seas (e.g., *Eldevik et al.,* 2009). The spatial distribution of the number of observations (salinity samples) in the NISE dataset is shown in Figure 8.

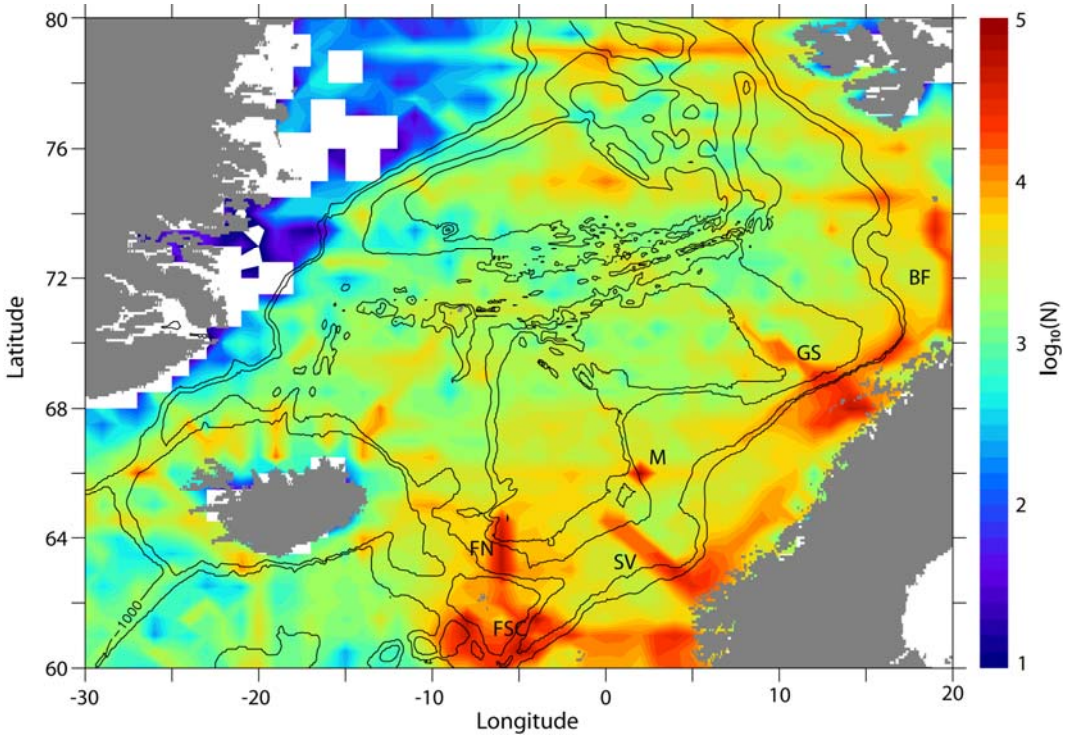

Figure 8. Number of observations (salinity samples; N) included in the NISE dataset. Colour (logarithmic scale) indicates number of observations on 1° x 0.5° longitude and latitude grids. White areas have no data. The symbols FN, FSC, SV, GS, BF respectively denotes the Faroe North, Faroe Shetland Channel, Svinøy, Gimsøy and Bjørnøya-Fugløya hydrographic sections. The hydrographic station Mike is denoted by the symbol 'M'. Black lines represent isobaths for 500, 1000, 2500 and 3000 m depths.

In this thesis, bin averaging methods are used for creating homogeneous fields from in-homogeneously sampled data. A "bin" is a limited area in space or time, and the division into bins are done by making a grid of points (evenly or unevenly distributed) to which mean values are assigned. The mean values determined using the regular population (POP) mean are from those data with positions nearer than halfway to the next grid point in all directions. In doing so, the geographical cells are represented by a mean value positioned in the middle of the cell. The variance of the population mean is calculated by the single observations' squared standard deviation divided by the number of observations. More details of the bin averaging methods are given in *Nilsen* (2003). Different length units can form the basis for a division of an area into bins. The vertical binning of the data is done to the 'standard' depths 0, 10, 25, 50, 75, 100, 150, 200, 300, 400, 500, 600, 800, 1000, 1200, 1300, 1400, 1500 m. However, the horizontal binning of the dataset is done differently according to the objective of the

study. In Paper 1, the length of the sections are selected to cover the study region, and horizontal bin sizes are selected according to the availability of observations to give the best spatial resolution while still ensuring that climatic monthly mean sections can be made in order to eliminate seasonal bias. For some sections the horizontal bins are centered on stations on standard repeated sections, and are thus small, while for others the data are much more scattered, and larger bins are used. In Paper 2, hydrographic properties of Atlantic Water in the eastern and western Lofoten Basin are estimated as area averages of the two regions. In Paper 2 and 4, 1° x 0.5° longitude and latitude horizontal bins are used to estimate the spatial variability of steric height. In Paper 3, a hydrographic section along 70°N is selected in order to study the hydrographic properties of an anticyclonic vortex situated in the Lofoten Basin. Mixed layer depth (MLD) in Paper 2 and 3 are estimated on 1° x 0.5° horizontal bins. The time dimension is also incorporated when binning. Binning on separate weeks is done in Paper 1 for composite studies. Binning on inter-annual time scales is used in Paper 2 to study the inter-annual variability of hydrographic properties of Atlantic Water in the Lofoten Basin.

Mixed layer depths are calculated by a finite density difference method, following *Nilsen and Falck* (2006). In the same way as the maximum gradient method, a finite difference method finds the pycnocline, and not the depth of the homogeneous layer per se. A difference criterion between the surface density and MLD-base density is calculated by subtracting a temperature of 0.8°C from the surface value, and applied to individual density profiles. The climatological mean MLD is calculated by horizontally binning the individual MLD estimates. Steric heights from hydrographic climatologies are calculated according to *Siegismund et al.* (2007), where the steric height is referenced to depths (e.g., 500 m in Paper 2), and a constant density ρ_0 from salinity of 35 and temperature of 0°C. More information on the concept and application of steric height is given by *Tomczak and Godfrey* (2003). Subsurface velocities are calculated using the surface geostrophic velocities (v_s) and the thermal wind relation according to *Mork and Skagseth* (2010):

$$v(z) = v_s + \frac{g}{\rho_0 f} \int_z \frac{\partial \rho}{\partial x} dz \,, \tag{5}$$

where, f is the Coriolis parameter, g is the acceleration due to gravity, ρ is the density and ρ_0 is a reference density and x is directed along the section. Volume transports of Atlantic Water are found by integrating the velocities vertically over the depth interval with salinities 35 and above, and then laterally between defined limits.

3.5. Surface drifter and Re-analysis datasets

Surface drifter tracks used in Paper 1 are obtained from the WOCE surface drifter expedition database (*Schlitzer,* 2000). WOCE drifter tracks have been used in several studies of the near surface circulation in the Nordic Seas (e.g., *Jakobsen et al*., 2003). Surface geostrophic velocities (1ºx1º grid) and the errors associated with it obtained from the dataset "Drifter derived climatology of global near-surface currents" are used in Paper 2 and 4. The dataset obtained is derived from satellite-tracked surface drifting buoy observations (*Lumpkin and Garraffo*, 2005).

Heat flux datasets (short wave radiation, long wave radiation, latent heat flux, and sensible heat flux; 1949-2008) obtained from National Centers for Environmental Predictions (NCEP; *Kalnay et al*., 1996) are the re-analysis datasets used in this thesis (Paper 2). The NCEP heat flux data, one of the widely referenced re-analysis dataset in studies related to air-sea interaction in the Nordic Seas, are also used in many numerical ocean models as the atmospheric forcing (e.g., *Sandø et al*., 2010).

3.6. Numerical Ocean Model

The output from a regional version of Miami Isopycnic Coordinate Ocean Model (MICOM; *Sandø et al.,* 2012) covering the North Atlantic, the Nordic Seas, and the Arctic Ocean during the time period 1993-2007 is used in Paper 4. The model data is used for the estimation of volume transports in the Norwegian Sea and for the estimation of MDT (time-mean of model SSH) in the North Atlantic and the Arctic. A brief description of the MICOM model is given below.

Output data from a global version of MICOM (*Orre et al.,* 2009) is used as boundary conditions. The global model has a grid spacing of about 40 km whereas the resolution of the regional model is about 13 km in the Nordic Seas. The model has 35 vertical

layers of fixed potential densities, and an uppermost mixed layer with temporal and spatial varying density. The nesting boundaries are located in the South Atlantic and in the Bering Strait. A dynamic and thermodynamic sea-ice model is coupled to MICOM (*Bentsen*, 2002). The models share the horizontal grid, the exchange of fluxes are handled internally and hence the sea-ice model can be considered as an integrated part of MICOM. The atmospheric forcing is taken from daily NCEP/NCAR reanalysis fields (*Kalnay et al.,* 1996) and the forcing scheme and procedure are described in *Bentsen and Drange* (2000). For more detailed description of the model physics and performance, see *Hátún et al.* (2005); *Sandø and Furevik* (2008); *Sandø et al.* (2010) and *Sandø et al.* (2012). The regional version of the MICOM model has been evaluated with good results at FSC and Barents Sea Opening (*Sandø et al*., 2010, 2012).

Chapter 4

Summary of results

The present study revisits the circulation of the Norwegian Sea using measurements taken from space and in the ocean. A summary of the thesis is given below.

In the Norwegian Sea (Figure 1), there is a general spin up of the surface circulation during winter, with the exception of the flow along the Mohn Ridge, which is strongest in summer. This seasonal intensification is due to more buoyant waters in the Lofoten Basin during summer, which results in the elevation of sea surface height there. Similarly, buoyant waters in the eastern Lofoten Basin results in a weak mean surface flow in the central Lofoten Basin, but stronger during winter. In the Norwegian Sea, topographic steering results in local intensification of the slope current at the Svinøy and Lofoten slope regions. In the front current, topographic steering is prominent at the western slope of the Vøring Plateau and along the northern part of the Mohn Ridge.

Four major surface flows connecting the front current and the slope current are identified, out of which two show distinct seasonality (Paper 1). The major factors influencing these flows are: topographic steering, surface winds and buoyancy loss. A strengthening of the front current upstream of the Lofoten Basin is associated with a larger eastward flow of Atlantic Water towards the slope current, which also increases the probability of Atlantic Water from the front current to enter the Barents Sea. This implies that the Iceland-Faroe inflow of Atlantic Water may have more importance for the Barents Sea and Arctic Ocean than previously assumed, and the two branches of northward flowing Atlantic water in the Nordic Seas cannot be considered as two independent flows.

The variability in the surface velocities in the Norwegian Sea is found to be representative also of the subsurface Atlantic Water flow, and the relationship is more pronounced in the slope current. Compared to the front current, there is large variability in the amount of Atlantic Water transported pole-ward by the slope current

(front current, the range being up to 1 Sv; slope current, the range being up to 5 Sv).

This thesis confirms the Lofoten Basin as the most eddy active region outside the boundary currents of the Nordic Seas. The northeastern part of the basin is found to be an important location of eddy shedding from the slope current (Paper 2). The eddy kinetic energy maxima in this region during early winter coincides with the maxima in the slope current transport during January, supporting the link between the strength of the slope current and eddy shedding. Two strong eddy active regions with distinctly different annual cycles on either side of the Lofoten Basin are found to exist. There is a two month lag between the eddy kinetic energy of the western and eastern region of the Lofoten Basin which indicates propagation of eddies from the east and into the western basin. The maxima in mergers between the quasi-permanent anticyclonic Lofoten Vortex situated in the western Lofoten Basin and other anticyclonic eddies during March is consistent with two months travel time of eddies into the western basin from the east. Observational evidence confirm transfer of energy from other anticyclones to the Lofoten Vortex via vortex merging process (Paper 3). The vortex merger further explains the seasonality in the *eddy intensity* of the Lofoten Vortex which is maximum during late winter-spring and minimum during late autumn-early winter. On the other hand, the long term variability in the *Eddy Intensity* of the Lofoten Vortex is significantly influenced by the buoyancy forcing. The Lofoten Vortex persistently residing in the deepest part of the basin, follows a cyclonic drift path, and also plays an active role in ventilating the Atlantic Water in the Nordic Seas.

The spatial distribution and temporal evolution of dense water formation in the Lofoten Basin is influenced by the surface circulation, eddy activity, and heat loss in the basin (Paper 2). The variability in temperature dominates the Atlantic Water density variability of the Lofoten Basin, which in turn is influenced by the variability in the inflowing North Atlantic Water and the heat loss in the basin. The inter-annual variability in both local heat loss and upstream North Atlantic Water density influences the Atlantic Water density of the eastern Lofoten Basin more than in the western. A lag of two years is found between the Atlantic Water densities in the Lofoten Basin and the North Atlantic Water density at Faroe Shetland Channel.

The density of Atlantic Water in the Lofoten Basin after 2000, which is the lightest during 60 year time-period, is linked to the warming of the inflowing North Atlantic Water since the mid 1990s. A strong connection is found between the Atlantic Water (in both salinity and temperature) in the western Lofoten Basin and the Norwegian North Atlantic Water (NNAW), and the further connection to the Faroe Shetland overflow found by *Eldevik et al.* (2009), points to the possibility of a returning circulation connecting the Lofoten Basin to the overflows.

A new mean dynamic topography is estimated for the North Atlantic and the Arctic from the GOCE gravity anomaly data (in Paper 4). The MDT resolves major circulation features in the North Atlantic and the Arctic concurring with previous knowledge. Combined with the steric height estimated from hydrographic data, the pure barotropic contribution to the MDT shows distinct features in consistence with the known existence of deep barotropic circulations in the central regions of the Norwegian and Greenland Seas. There is notable improvement in the representation of the circulation of the Western Nordic Seas compared to the current state-of-the-art MDTs. The slope current contains approximately 60% of the total volume flux across the Svinøy section with a distinct transport maximum in winter (Dec-Jan) and a minimum in summer (Jun-Aug). This transport is moreover dominated by the barotropic component. The outcome of GOCE MDT is also promising with respect to improving the capabilities to evaluate ocean models.

All in all, the results of this thesis add new insights into the ocean circulation of the Norwegian Sea. This thesis also shows the importance of the initiatives taken by different space agencies around the world for providing higher resolution and more accurate remote sensing observations.

Chapter 5

Future Perspectives

The importance of the circulation of the Nordic Seas to global climate has been mentioned in several studies (e.g., Rhines *et al.,* 2008). However, only few attempts has been made to study the circulation of the Nordic Seas using the state-of-the-art CNES-CLS09 MDT (*Mork and Skagseth,* 2010; *Chafik,* 2012; Paper 1, 2, 3 in this thesis). Notably, none of these studies analysed the circulation of the western Nordic Seas. Moreover, Paper 4 showed the limitation of the CNES-CLS09 MDT in reproducing the mean circulation of the northwestern Nordic Seas. As a solution, a new MDT is estimated for the North Atlantic and the Arctic from GOCE data in Paper 4. But, it should be noted that since a Gaussian filter (80 km) is applied to the MDT in order to remove the noise, this MDT cannot be used to study mesoscale circulation features of the Nordic Seas. In this section, a new more accurate high resolution MDT of the Nordic Seas is estimated (described below), facilitating future studies of both large-scale and mesoscale features.

In a recent study, *Bruinsma et al.* (2013) showed that the latest release (Release 4) of the GOCE data is found to be closer to observations compared to the previous releases. The Release 4 direct approach gravity anomaly (DIR4) data is constructed with 28 months of GOCE data, 9 years of GRACE data and 25 years of LAGEOS data. This is roughly two-times the amount of data used in the Release 3 DIR gravity anomaly data (Section 3.2.1).

In here, a new geoid is estimated from DIR4 data in the mean-tide system and relative to the Topex-ellipsoid (as described in Section 3.2.2). The DIR4 MDT is determined by subtracting this new geoid from DTU10 MSS (*Knudsen et al.,* 2011). The next step after low-pass filtering the DIR4 MDT with a Gaussian filter (80 km), is to re-incorporate smaller spatial scales of MDT (<80 km) back onto it. This is achieved using the CNES-CLS09 MDT used in Paper 1, 2, and 3. As mentioned in Section 3.1.2, this MDT is based on altimetry, in situ measurements, surface buoys, Argo floats, and a GRACE geoid model (*Rio et al.,* 2011). Its shorter spatial scales are

obtained by high-pass filtering it with the 80 km Gaussian filter. Finally, the combined MDT is estimated by adding these shorter spatial scales (< 80 km) from the CNES-CLS09 MDT to the longer spatial scales (> 80 km) from the DIR4 MDT.

Compared to the CNES-CLS09 MDT, the new combined MDT significantly improves the estimation of the mean circulation of the Nordic Seas, mainly in the western Nordic Seas (Figure 9). The shape of the combined MDT and orientation of the dominant slopes reveals the distinct minima in the Greenland Basin and shows the circulation pathways including the northward flow of NwAC and southward flow of East Greenland Current (e.g., Jakobsen *et al*., 2003).

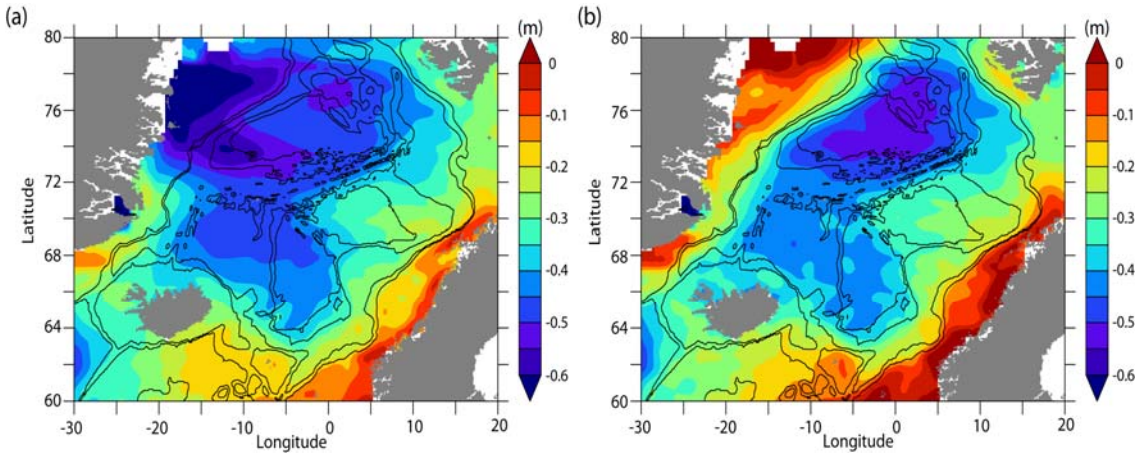

Figure 9. Mean dynamic topography of the Nordic Seas: (a) CNES-CLS09 MDT, (b) Combined MDT. Black lines represent the isobaths for 500, 1000, 2500 and 3000 m depths.

In future studies, this combined MDT together with sea level anomalies can be used to estimate more accurate ADTs. Surface velocities estimated from these ADTs can be further used to study the seasonal and inter-annual variability of the circulation of the Nordic Seas. In an upcoming project (GLOBCURRENT) funded by ESA, the circulation of the Nordic Seas will be investigated in detail using surface currents derived from GOCE, altimetry, Synthetic Aperture Radar data and microwave SST. In view of the promising GOCE-based results, they are also providing a new opportunity for the evaluation of Coupled Model Intercomparison Project Phase 5 (CMIP5) models. From such an evaluation, the best CMIP5 models in the Nordic Seas can be categorized, which further can be used to study changes in Nordic Seas circulation in scenarios, for e.g., enhanced greenhouse gas emission, additional fresh water input etc.

References

Andersson, M., K. A. Orvik, J. H. LaCasce, I. Koszalka, and C. Mauritzen, 2011: Variability of the Norwegian Atlantic Current and associated eddy field from surface drifters. *J. Geophys. Res.*, *116*, C08032, doi:10.1029/2011JC007078.

Barron, C. N., and A. B. Kara, 2006: Satellite-based daily SSTs over the global ocean. *Geophys. Res. Lett., 33*, L15603, doi:10.1029/2006GL026356.

Benveniste, J., P. Knudsen, and the GUTS Team, 2007: The GOCE user toolbox. In: Fletcher K (ed). *Proceedings of the 3rd international GOCE user workshop, 6–8 November 2006*, Frascati, Italy. European Space Agency, Noordwijk.

Bentsen, M., and H. Drange, 2000: Parameterizing surface fluxes in ocean models using the NCEP/NCAR reanalysis data. *RegClim Gen.Tech. Rep. 4*, Norw. Inst. for Air Res., Kjeller, Norway.

Bentsen, M., 2002: Modelling ocean climate variability of the North Atlantic and the Nordic Seas. *Ph.D. thesis,* Nansen Environmental and Remote Sensing Center, Bergen, Norway.

Berx, B., B. Hansen, S. Østerhus, K.M. Larsen, T. Sherwin, and K. Jochumsen, 2013: Combining in situ measurements and altimetry to estimate volume, heat and salt transport variability through the Faroe–Shetland Channel. *Ocean Sci., 9*, 639-654, doi:10.5194/os-9-639-2013.

Bingham, R. J., K. Haines and C.W. Hughes, 2008: Calculating the Oceans Mean dynamic topography from a Mean sea surface and a Geoid. *J. Atmos. Ocean. Tech. 25*, 1808-1822, doi:10.1175/2008JTECHO568.

Bingham, R. J., P. Knudsen, O. Andersen, and R. Pail, 2011: An initial estimate of the North Atlantic steady-state geostrophic circulation from GOCE. *Geophys. Res. Lett., 38*, L01606, doi:10.1029/2010GL045633.

Blindheim, J., and F. Rey, 2004: Water-mass formation and distribution in the Nordic seas during the 1990s. *ICES J. Mar.Sci., 61***,** 846–863.

Bruinsma, S. L., J. C. Marty, G. Balmino, R. Biancale, C. Foerste, O. Abrikosov and H. Neumayer, 2010: GOCE Gravity Field Recovery by Means of the Direct Numerical Method. ESA Living Planet Symposium (presented), 27th June - 2nd July 2010, Bergen, Norway; See also: earth.esa.int/GOCE.

Bruinsma, S. L., C. Förste, O. Abrikosov, J.-C. Marty, M.-H. Rio, S. Mulet, and S. Bonvalot, 2013: The new ESA satellite-only gravity field model via the direct approach. *Geophys. Res. Lett.,* 40,3607–3612, doi:10.1002/grl.50716.

Chafik, L., 2012: The response of the circulation in the Faroe-Shetland Channel to the North Atlantic Oscillation. *Tellus A, 64*.

Chaigneau, A., A. Gizolme, and C. Grados, 2008: Mesoscale eddies off Peru in altimeter records: Identification algorithms and eddy spatiotemporal patterns. *Prog. Oceanogr., 79,* 106–119, doi:10.1016/j.pocean.2008.10.013.

Ducet, N., P. Y. LeTraon, and G. Reverdin, 2000: Global high-resolution mapping of ocean circulation from TOPEX/Poseidon and ERS-1 and 2. *J. Geophys. Res.*, *105*, 19477–19498.

Dickson, R. R., and J. Brown, 1994: The production of North Atlantic Deep Water, sources rates and pathways. *J. Geophys. Res.,*99, 12319-12341.

Eldevik, T., J. E. Ø. Nilsen, D. Iovino, K. A. Olsson, A. B. Sandø, and H. Drange, 2009: Observed sources and variability of Nordic seas overflow. *Nat. Geosci.*, *2*, 406-410, doi: 10.1038/ngeo518.

Engelsen, O., N. E. Hegseth, H. Hop, E. Hansen, and S. Falk-Petersen, 2002: Spatial variability of chlorophyll-a in the Marginal Ice Zone of the Barents Sea, with relations to sea ice and oceanographic conditions. *J. Marine Syst.,* 35, 79-97.

Frankignoul, C., and P. Müller, 1979: Quasigeostrophic response of an infinite beta-plane ocean to stochastic forcing by the atmosphere. *J. Phys. Oceanogr.*,**9**, 104-127.

Friehe, C. A., W. J. Shaw, D. P. Rogers, K. L. Davidson, W. G. Large, S. A. Stage, G. H. Crescenti, S. J. S. Khalsa, G. K. Greenhut, and F. Li, 1991: Air-sea fluxes and surface layer turbulence around a sea surface temperature front. *J. Geophys. Res., 96*, 8593–8609.

Fu, L-L., B. Cheng, and B. Qiu, 2001: 25-day period large-scale oscillations in the Argentine Basin revealed by the TOPEX/POSEIDON altimeter. *J. Phys. Oceanogr* .31, 506–517.

Furevik, T., and J. E. Ø. Nilsen, 2005: Large-Scale Atmospheric Circulation Variability and its Impacts on the Nordic Seas Ocean Climate - a Review. The Nordic Seas: An Integrated Perspective. *AGU Geophy Monog. Series.*, *158*,105-136.

Furevik, T., C. Mauritzen, and R. Ingvaldsen, 2007: The Flow of Atlantic Water to the Nordic Seas and Arctic Ocean, in Arctic-Alpine Ecosystems and People in a Changing Environment. edited by J.B. Ørbæk, R Kallenborn, I Tombre, E Nøst Hegseth, S Falk-Petersen, A.H. Hoel, *Springer Verlag*, pp 123-146.

Förste, C., S. Bruinsma, R. Shako, J-C. Marty, F. Flechtner, O. Abrikosov, C. Dahle, J.M. Lemoine, K. H. Neumayer, R. Biancale, F. Barthelmes, R. König, and G. Balmino, 2011: EIGEN-6 - A new combined global gravity field model including GOCE data from the collaboration of GFZPotsdam and GRGS-Toulouse. *Geophysical Research Abstracts*, *13*, EGU2011-3242-2, EGU General Assembly.

Gascard, J. C., and K. A. Mork, 2008: Climatic importance of large scale and mesoscale circulation in the Lofoten Basin deduced from lagrangian observations during ASOF, in Arctic - Subarctic Ocean Fluxes: Defining the role of the Northern Seas in Climate. edited by R. R. Dickson et al., pp. 131-143, Springer Verlag, Netherland, doi: 10.1007/978-1-4020-6774-7_7.

Gordon, R. L., and J. M. Huthnance, 1987: Storm-driven continental shelf waves over the Scottish continental shelf. *Cont. Shelf Res*., 7 (9), 1015-1048.

Hansen, B., and S. Østerhus, 2000: North Atlantic – Nordic Seas Exchanges. *Prog. Oceanogr.,* 45, 109–208.

Hansen, B., S. Østerhus, H. H´at ´un, R. Kristiansen, and K. M. H. Larsen, 2003: The Iceland-Faroe inflow of Atlantic water to the Nordic Seas. *Prog. Oceanogr.,* 59, 443-474.

Hansen, B., H. Hátún, R. Kristiansen, S. M. Olsen, and S. Østerhus, 2010: Stability and forcing of the Iceland-Faroe inflow of water, heat, and salt to the Arctic. *Ocean Sci., 6*, 1013–1026, 2010.

Helland-Hansen, B., and F. Nansen, 1909: The Norwegian Sea: its physical oceanography based upon the Norwegian Researches 1900–1904. *Report on Norwegian Fishery and Marine Investigation, vol. II*. The Royal Department of Trade, Navigation and Industries, Mallingske, Kristiania, 390 pp.

Hughes, S. L., Turrell, W. R., Hansen, B., and Østerhus, S, 2006: Fluxes of Atlantic Water (Volume, Heat and Salt) in the Faroe-Shetland Channel calculated from a decade of Acoustic Doppler Current Profiler data (1994–2005). Fisheries Research Services Collaborative Report No 01/06. Marine Laboratory, Victoria Road, Aberdeen AB11 9DB, Scotland.

Hátún, H., A. B. Sandø, H. Drange, and M. Bentsen, 2005: Seasonal to decadal temperature variations in the Faroe-Shetland inflow waters, in The Nordic Seas: An Integrated Perspective Oceanography, Climatology, Biogeochemistry, and Modeling. edited by H. Drange et al., pp. 239–250, *Geophys. Monogr. Ser., 158*, AGU, Washington, D. C.

Ikeda, M., J. A. Johannessen, K. Lygre, and S. Sandven, 1989: A process study of mesoscale meanders and eddies in the Norwegian Coastal Current. *J. Phys. Oceanogr.* 19, 20–35.

Isachsen, P. E., C. Mauritzen, and H. Svendsen, 2007: Dense water formation in the Nordic Seas diagnosed from sea surface buoyancy fluxes. *Deep Sea Res.*, *Part 1*, *54*, 22-41, doi:10.1016/j.dsr.2006.09.008.

Ivanov, V., and A. Korablev, 1995a: Formation and regeneration of the pycnocline lens in the Norwegian Sea. *Russ. Meteor. Hydrol.,* 9, 62–69.

Ivanov, V., and A. Korablev, 1995b: Interpycnocline lens dynamics in the Norwegian Sea. *Russ, Meteor. Hydrol., 10***,** 32–37.

Jakobsen, P. K., M. H. Ribergaard, D. Quadfasel, T. Schmith, and C. W. Hughes, 2003: Near-surface circulation in the northern North Atlantic as inferred from Lagrangian drifters: Variability from the mesoscale to interannual. *J. Geophys. Res.*, 108(C8), 3251, doi:10.1029/2002JC001554.

Johannessen, J. A., E. Svendsen, S. Sandven, O. Johannessen, and K. Lygre, 1989: Three- dimensional structure of mesoscale eddies in the Norwegian Coastal Current. *J. Phys. Oceanogr.* 19, 3–19.

Johannessen, J. A., G. Balmino, C. Le Provost, R. Rummel, R. Sabadini,, H. Sünkel, C.C. Tscherning, P. Visser, P. Woodworth, C. W. Hughes, P. LeGrand, N. Sneeuw, F. Perosanz, M. Aguirre-Martinez, H. Rebhan, and M. Drinkwater, 2003: The European Gravity Field and Steady-State Ocean Circulation Explorer Satellite Mission: Impact in Geophysics. *Survey in Geophysics*, 24, 339-386.

Kalnay, E., M. Kanamitsu, R. Kistler, W. Collins, D. Deaven, L. Gandin, M. Iredell, S. Saha, G. White, J. Woollen, Y. Zhu, M. Chelliah, W. Ebisuzaki, W.Higgins, J. Janowiak, K. C. Mo, C. Ropelewski, J. Wang, A. Leetmaa, R. Reynolds, R. Jenne, and D. Joseph, 1996: The NCEP/NCAR 40-Year Reanalysis Project. B. Am. Meteorol. Soc., 77 (3), 437–471.

Knudsen, P., O. B. Andersen, R. Forsberg, H.P. Föh, A.V. Olesen, A.L. Vest, D. Solheim, O. D. Omang, R. Hipkin, A. Hunegnaw, K. Haines, R. Bingham, J.-P. Drecourt, J.A. Johannessen, H. Drange, F. Siegismund, F. Hernandez, G. Larnicol, M.-H. Rio, and P. Schaeffer, 2007: Combining altimetric/gravimetric and ocean model mean dynamic topography models in the GOCINA region. *IAG symposia*, Vol. 130, Springer Verlag, ISBN-10 3-540-49349-5, 3-10.

Knudsen, P., R. Bingham, O. Andersen, and M-H. Rio, 2011: A global mean dynamic topography and ocean circulation estimation using a preliminary GOCE gravity field. *J. Geodesy*, *85*(*11*), *861-879*. DOI 10.1007/s00190-011-0485-8.

Koop, R., T. Gruber, and R. Rummel, 2007: The status of the GOCE high level processing facility (HPF). *Proceedings of the 3rd GOCE User Workshop*, Eur. Space Res. Inst., Eur. Space Agency, Frascati, Italy.199-204.

Koszalka. I., J. H. LaCasce , M. Andersson , K. A. Orvik , and C. Mauritzen, 2011: Surface circulation in the Nordic Seas from clustered drifters. *Deep Sea Res., Part 1., 58*, 468-485, doi:10.1016/j.dsr.2011.01.007.

Koszalka. I., J. H. LaCasce, and C.Mauritzen, 2013: In pursuit of anomalies-Analyzing the poleward transport of Atlantic Water with surface drifters. *Deep Sea Res., Part II., 85,* 96-108, http://dx.doi.org/10.1016/j.dsr2.2012.07.035.

Köhl, A., 2007: Generation and stability of a quasi-permanent vortex in the Lofoten basin. *J. Phys. Oceanogr,. 37*, 2637-2651.

LeGrand, P., E. J. O. Schrama, and J. Tournadre, 2003: An inverse estimate of the dynamic topography of the ocean. *Geophys. Res. Lett. 30 (2)*, 1062, doi:10.1029/2002GL014917.

LeTraon, P. Y., and F. Ogor, 1998: ERS-1/2 orbit improvement using TOPEX/Poseidon: The 2 cm challenge. *J. Geophys. Res*., *103*, 8045–8057.

Levitus, S., and T. P. Boyer, 1994: World ocean atlas 1994 volume 4: temperature NOAA Atlas NESDIS 117(4). National Ocean and Atmosphere Administration USA.

Levitus, S., R. Burgett, and T. P. Boyer, 1994: World Ocean Atlas 1994, Salinity, NOAA Atlas NESDIS. vol. 3, 111 pp., NOAA, Silver Spring, Md.

Lozier, M. S., 1997: Evidence of large-scale eddy-driven gyres in the North Atlantic. *Science*, 277, 361-364.

Lumpkin, R., and Z. Garraffo, 2005: Evaluating the Decomposition of Tropical Atlantic Drifter Observations. *J. Atmos. Ocean Tech.,* I 22, 1403-1415.

Mauritzen, C., 1996a: Production of dense overflow water feeding the North Atlantic across the Greenland-Scotland Ridge. Part 1: Evidence of revised circulation scheme. *Deep Sea Res.*, *Part 1,43*, 769– 806.

Mauritzen, C., 1996b: Production of dense overflow waters feeding the North Atlantic across the Greenland–Scotland Ridge. Part 2. An inverse model. *Deep-Sea Res. I., 43,* 807–835.

Maximenko, N., P. Niiler, M-H. Rio, O. Melnichenko, L. Centurioni, D. Chambers, V. Zlotnicki, and B. Galperin, 2009: Mean dynamic topography of the ocean derived from satellite and drifting buoy data using three different techniques. *J Atmos Ocean Tech., 26(9)*,1910–1919.

Medhaugh, I., H. R. Langehaug, T. Eldevik, T. Furevik, and M. Bentsen, 2011: Mechanisms for decadal variability in a simulated Atlantic Meridional Overturning Circulation. *Clim. Dyn.,* doi: 10.1007/s00382-011-1124-z.

Mohn, H., 1887: The Northern Ocean, its Depths, Temperature and Circulation. The Norwegian North-Atlantic Expedition 1876-1878. Christiania, 1887 (in Norwegian).

Mork, K. A., and Ø. Skagseth, 2010: A quantitative description of the Norwegian Atlantic Current by combining altimetry and hydrography. *Ocean Sci.., 6*, 901–911.

Morrow, R. A., R. Coleman, J. A. Church, and D. B. Chelton, 1994: Surface eddy momentum flux and velocity variances in the Southern Ocean from Geosat altimetry. *J. Phys. Oceanogr*., 24, 2050-2071.

Niiler, P. P., N. A. Maximenko, and J. C. McWilliams, 2003: Dynamically balanced absolute sea level of the global ocean derived from near-surface velocity observations. *Geophys Res. Lett.* 30(22):2164. doi:10.1029/2003GL018628.

Nilsen, J. E. Ø ., 2003: Aspects of the Atlantic Flow through the Norwegian Sea . University of Bergen, Geophysical institute / G.C. Rieber Climate Institute, Nansen Environmental and Remote Sensing Center . Doctoral Thesis No. 40, UiB Reports in meteorology and oceanography no. 3-2003 (http://www.nersc.no/pub/aspects-atlantic-flow-through-norwegian-sea).

Nilsen, J. E. Ø., and E. Falck 2006: Variation of mixed layer properties in the Norwegian Sea for the period 1948–1999. *Prog. Oceanogr., 70,* 58–90, doi:10.1016/j.pocean.2006.03.014.

Nilsen, J. E. Ø., and F. Nilsen, 2007: The Atlantic Water Flow along the Vøring Plateau: Detecting Front Structures in Oceanic Station Time Series. *Deep Sea Res.*, *Part 1, 54(3)*, 297-319, doi:10.1016/j.dSV.2006.12.012.

Nilsen, J. E. Ø., H. H´at´un, K. A. Mork, and H. Valdimarsson, 2008: The NISE Data Set. *Technical Report 08-01*, Faroese Fisheries Laboratory, Box 3051, T´orshavn, Faroe Islands.

Orre, S., J. N. Smith, V. Alfimov, and M. Bentsen, 2009: Simulating transport of 129I and idealized tracers in the northern North Atlantic Ocean. *Environ. Fluid Mech.*, 10, 213–233.

Orvik, K. A., Ø. Skagseth, and M. Mork, 2001: Atlantic inflow to the Nordic Seas. Current structure and volume fluxes from moored current meters, VM-ADCM and SeasSoar-CTD observations. *Deep Sea Res. I, 48*, 937-957.

Orvik, K. A., and P. Niiler, 2002: Major pathways of Atlantic water in the northern North Atlantic and Nordic Seas toward Arctic. *Geophys. Res.Lett.,* 29(19), 1896, doi:10.1029/2002GL015002.

Orvik, K. A., and Ø. Skagseth, 2003: Monitoring the Norwegian Atlantic slope current using a single moored current meter. *Cont. Shelf Res.,23*, 159–176.

Orvik, K. A., 2004: The deepening of the Atlantic water in the Lofoten Basin of the Norwegian Sea, demonstrated by using an active reduced gravity model. *Geophys. Res. Lett., 31*, L01306, doi:10.1029/2003GL018687.

Pail, R., S. Bruinsma, F. Migliaccio, C. Foerste, H. Goiginger, W.-D. Schuh, E. Hoeck, M. Reguzzoni, J. M. Brockmann, O. Abrikosov, M. Veicherts, T. Fecher, R. Mayrhofer, I. Krasbutter, F. Sanso, and C. C. Tscherning, 2011: First

GOCE gravity field models derived by three different approaches. *J. Geodesy., 85,* 11, 819-843.

Poulain, P. M., A. Warn-Varnas, and P. P. Niiler, 1996: Near-surface circulation of the Nordic seas as measured by Lagrangian drifters. *J. Geophys. Res.*, *101(C8)*, 237–258.

Read, J., and R. Pollard, 1992: Water Masses in the Region of the Iceland–Faroes Front. *J. Phys. Oceanogr,*. 22 (11), 1365–1378.

Rhines, P. B., S. Hakkinen, and S. Josey, 2008: Is oceanic heat transport significant in the climate system?, *in Arctic-Subarctic Ocean Flux: defining the role of the northern seas in climate.* edited by Dickson et al., 87-109, Springer, Newyork.

Rio, M. H., and F. Hernandez, 2004: A mean dynamic topography computed over the world ocean from altimetry, in situ measurements, and a geoid model. *J. Geophys. Res*., *109*, C12032, doi:10.1029/2003JC002226.

Rio, M. H., P. Schaeffer, J. M. Lemoine, and F. Hernandez, 2005: Estimation of the ocean Mean Dynamic Topography through the combination of altimetric data, in-situ measurements and GRACE geoid: From global to regional studies. Paper presented at GOCINA international workshop, Luxembourg.

Rio, M. H., S. Guinehut, and G. Larnicol, 2011: New CNES-CLS09 global mean dynamic topography computed from the combination of GRACE data, altimetry, and in situ measurements. *J. Geophys. Res.,*116, C07018, doi: 10.1029/2010JC006505.

Richter, K., T. Furevik, and K. A. Orvik, 2009: Effect of wintertime low-pressure systems on the Atlantic inflow to the Nordic seas. *J. Geophys. Res.,* 114, doi:10.1029/2009JC005392, 2009.

Richter, K., Segtnan O. H. A, and T. Furevik, 2012: Variability of the Atlantic inflow to the Nordic Seas and its causes inferred from observations of sea surface height. *J. Geophys. Res. Oceans*, doi:10.1029/2011JC007719.

Rossby, T., M. Prater, and H. Søiland, 2009a: Pathways of inflow and dispersion of warm waters in the Nordic Seas. *J. Geophys. Res.*, *114*, C04011, doi:10.1029/2008JC005073.

Rossby, T., V. Ozhigin, V. Ivshin, and S. Bacon, 2009b: An isopycnal view of the Nordic Seas hydrography with focus on properties of the Lofoten Basin. *Deep Sea Res.*, *Part 1, 56*, doi:10.1016/j.dsr.2009.07.005.

Saloranta, T. M., and P. M. Haugan, 2001: Interannual variability in the hydrography of Atlantic water northwest of Svalbard. *J Geophys. Res.*, 106, 13931-13943.

Sandø, A. B., and T. Furevik, 2008: The relation between the wind stress curl in the

North Atlantic and the Atlantic inflow to the Nordic seas. *J. Geophys. Res*., 113, C06028, doi:10.1029/2007JC004236.

Sandø, A. B., J. E. Ø. Nilsen, Y. Gao, and K. Lohmann, 2010: The importance of heat transports and local air-sea heat fluxes for the Barents Sea climate variability. *J. Geophys. Res.*, 115, C07013, doi:10.1029/2009JC005884.

Sandø, A. B., J. E. Ø. Nilsen, T. Eldevik , and M. Bentsen, 2012: Mechanisms for variable North Atlantic-Nordic Seas exchanges. *J. Geophys. Res., 117*, C07013, doi:10.1029/2009JC005884.

Schaeffer, P., Y. Faugere, J. F. Legeais, N. Picot, and E. Bronner, 2012: The CNES-CLS11 global mean sea surface computed from 16 years of satellite altimeter data. *Mar. Geod*., doi:10.1080/01490419.2012.718231.

Schlitzer, R., 2000: Electronic Atlas of WOCE hydrographic and tracer data now available. *Eos Trans. AGU*, *81(5),* 45.

Segtnan, O. H., T. Furevik, and A. D. Jenkins, 2011: Heat and freshwater budgets of the Nordic seas computed from atmospheric reanalysis and ocean observation. *J. Geophys. Res., 116,* C11003, doi:10.1029/2011JC006939.

Sherwin, T. J., M. O. Williams, W.R. Turrell, S. Hughes, and P. I. Miller, 2006: A description and analysis of mesoscale variability in the Froe-Shetland Channel. *J. Geophys. Res. 111,*C03003. DOI: 10.1029/2005JC002867.

Sherwin, T., S. Hughes, W. Turrell,B. Hansen, S. Østerhus, 2008: Wind-driven monthly variations in transport and the flow field in the Faroe–Shetland Channel. *Polar Research.*, 27.

Siegismund, F., J. A. Johannessen, H. Drange, K. A. Mork, A. Korablev (2007), Steric height variability in the Nordic Seas. *J. Geophys. Res., 112*, C12010, doi:10.1029/2007/JC004221.

Skagseth, Ø. and K. A. Orvik, 2002: Identifying fluctuations in the Norwegian Atlantic Slope Current by means of empirical orthogonal functions. *Cont. Shelf Res., 22,* 547–563.

Skagseth, Ø., K. A. Orvik, and T. Furevik, 2004: Coherent variability of the Norwegian Atlantic slope current determined by using TOPEX/ERS altimeter data. *Geophys. Res. Lett., 31*, L14304, doi:10.1029/2004GL020057.

Skagseth, Ø., and K. A. Mork, 2012: Heat content in the Norwegian Sea during 1995-2005. *ICES J. Mar. Sci*., 69 (5), 826-832, doi: 10.1093/icesjms/fss026.

Spall, M. A., 2010: Non-local topographic influences on deep convection: An idealized model for the Nordic Seas. *Ocean Model., 32*, 72-85.

Stammer, D., and C. Wunsch, 1999: Temporal changes in eddy energy of the oceans. *Deep Sea Res.*, 46, 77-108.

Søiland, H., and T. Rossby (2013): On the structure of the Lofoten Basin Eddy. *J. Geophys. Res. Oceans., 118,* doi:10.1002/jgrc.20301.

Tomczak, M., and J. S. Godfrey (2003), Regional Oceanograhy: An Introduction (2nd edition). Daya Publishing House, New Delhi, India.

Volkov, D. L., and I. Pujol, 2012: Quality assessment of a satellite altimetry data product in the Nordic Seas, Barents, and Kara seas. *J. Geophys. Res.,* 117, 1978-2012. doi: 10.1029/2011JC007557.

Volkov, D. L., T. V. Belonenko, and V. R. Foux, 2013: Puzzling over the dynamics of the Lofoten Basin - a sub-Arctic hot spot of ocean variability. *Geophys. Res. Lett., 40,* 738–743, doi:10.1002/grl.50126.

Walczowski, W., and J. Piechura, 2009: Warming of the west Spitsbergen Current and sea ice north of Svalbard. *Oceanologia,*, 51 (2), 147–164.

Walczowski, W., and J. Piechura, 2011: Influence of the West Spitsbergen Current on the local climate. *Int. J. Climatol.,* 31,1088–1093, DOI: 10.1002/joc.2338.

Årthun, M., T. Eldevik, L. H. Smedsrud, Ø. Skagseth, and R. B. Ingvaldsen, 2012: Quantifying the Influence of Atlantic Heat on Barents Sea Ice Variability and Retreat. *J. Climate*, *25*: 4736–4743, doi:10.1175/JCLI-D-11-00266.1.

Papers

PAPER 1

The two-branch structure of the Norwegian Atlantic Current-transport variability and connecting flows

Roshin P. Raj, J. Even Ø. Nilsen, Tore Furevik (2013)

Submitted to Journal of Geophysical Research-Oceans

The two-branch structure of the Norwegian Atlantic Current - transport variability and connecting flows

Roshin P. Raj [1, 2, 3], J. Even Ø. Nilsen [1, 3], Tore Furevik [2, 3]

[1] Nansen Environmental and Remote Sensing Center, Thormøhlensgate 47, Bergen, Norway
[2] Geophysical Institute, University of Bergen, Allegaten 70, Bergen, Norway
[3] Bjerknes Centre for Climate Research, Allegaten 70, Bergen, Norway

Abstract

The Norwegian Atlantic Current (NwAC) in the Norwegian Sea is studied using remote sensing, surface drifters, and hydrography. Focus has been on the northward transport of Atlantic Water (AW) in the two branches of NwAC. Analysis of satellite derived absolute geostrophic velocity fields (1993-2010) shows a general spin up of the circulation in winter. An exception is over the Mohn Ridge where it is strongest in summer. We identify four regions in the Norwegian Sea where water is flowing from the western to the eastern branch of the NwAC, and highlight the dynamical importance of topographic steering. Combining altimetry with hydrographic data, we demonstrate that the variability in surface velocities of the Norwegian Sea is deep reaching, and that altimetry therefore can be used to monitor the variability of the poleward transport of AW. As expected, strengthening and weakening of the Atlantic inflow east of the Faroe Islands has a consistent response along the entire slope current. However, a stronger western inflow, observed north of the Faroe Islands, is to a lesser degree associated with velocities downstream in the front current, and instead associated with more flow of AW into the slope current increasing the transports here. Consequences of this finding are that a substantial fraction of AW that eventually enters the Barents Sea or the Arctic through the Fram Strait, may originate from the western inflowing branch of AW to the Nordic Seas, and that the two branches of northward flowing AW cannot be considered separate flows.

Key words: Norwegian Atlantic Current, Eddy kinetic energy, Norwegian Basin, Lofoten Basin, Volume transports, Poleward heat transport.

1. Introduction

The Norwegian Sea comprises the Norwegian Basin and the Lofoten Basin (Figure 1), and is the area in the Nordic Seas where the majority of the light to dense Atlantic Water transformation occurs [*Furevik et al.,* 2002*; Isachsen et al.,* 2007]. The heat and salt is supplied to the Norwegian Sea by the Norwegian Atlantic Current (NwAC), a two-branch current system having an eastern branch following the shelf edge as a barotropic slope current, and a western branch following the western rim of the Norwegian Sea as a topographically guided front current from the Iceland-Faroe front to the Fram Strait [*Poulain et al.,* 1996; *Orvik and Niiler,* 2002; *Skagseth and Orvik,* 2002; *Orvik and Skagseth,* 2003, *Høydalsvik et al.,* 2013]. The two branches are known as the Norwegian Atlantic Front Current [NwAFC; *Mork and Skagseth,* 2010] and the Norwegian Atlantic Slope Current [NwASC; *Skagseth and Orvik,* 2002] respectively, here for simplicity termed the "front current" and the "slope current. The volume of Atlantic Water (AW) transported poleward by the slope current and the front current are estimated to be in the range of 3.4-4.4 Sv [*Orvik and Skagseth,* 2003; *Skagseth et al.,* 2008; *Mork and Skagseth,* 2010] and 1.7-6.8 Sv [*Orvik et al.,* 2001; *Hansen et al.,* 2010; *Mork and Skagseth,* 2010, *Høydalsvik et al.,* 2013], with the highest estimate for the front current being the only based on direct measurements [nine glider transects, *Høydalsvik et al.,* 2013]. The heat transport associated with the inflow of AW to the Norwegian Sea (relative to 0°C) is estimated to be in the order of 250 TW [*Hansen et al.,* 2003, *Furevik et al.,* 2007, *Segtnan et al*, 2011]. About half of this heat is lost due to air-sea interaction or lateral eddy mixing before the Atlantic water leaves the Norwegian Sea through the Barents Sea opening or through the Fram Strait [*Segtnan et al*, 2011]. A returning branch of AW to the south of Jan Mayen flows into the Norwegian Basin [*Read and Pollard,* 1992]. This forms the southward component of the cyclonic circulation of AW in the Norwegian Basin, which together with the northward flowing NwAC and the Norwegian Coastal Current completes the surface circulation of the Norwegian Sea.

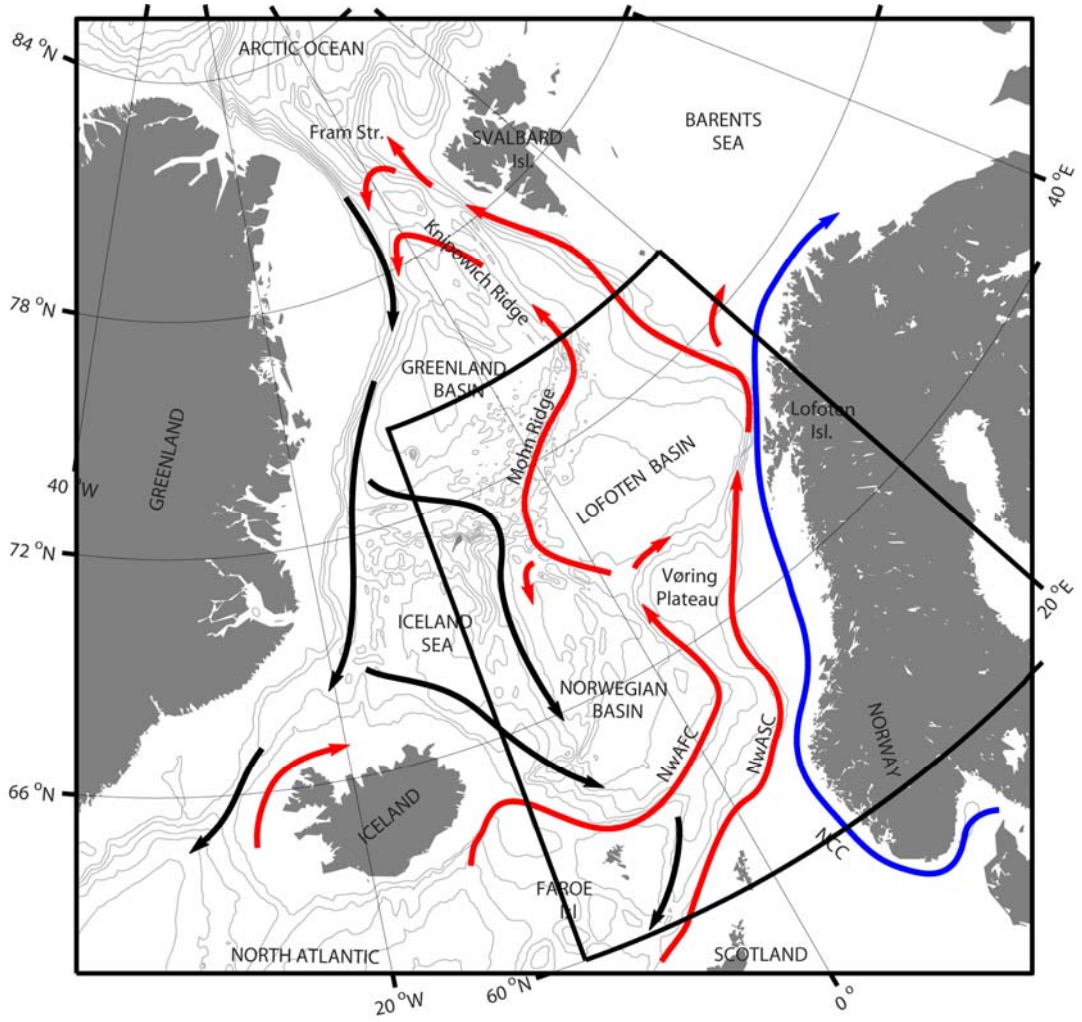

Figure 1. The Nordic Seas with schematic water pathways showing its overturning circulation from northward flowing Atlantic Water in the surface (red) to southward flowing transformed waters at depth (black). The Norwegian Atlantic slope current (NwASC) and Norwegian Atlantic front current (NwAFC) are represented by red arrows. The fresh Norwegian Coastal Current (NCC) is indicated in blue. See *Orvik and Niiler* [2002], *Furevik and Nilsen* [2005], and *Eldevik et al.* [2009] for details. Grey isobaths are drawn for every 600 m. The black frame indicates the area shown in Figures 2, 3b, 7, 8.

The circulation of the Norwegian Sea has been subject to investigations since the Norwegian North-Atlantic Expedition during 1876-1878 [*Mohn*, 1887; *Helland-Hansen and Nansen* 1909]. The AW flow through the Norwegian Sea and its associated heat loss and densification are important factors for the overflow waters formed in the region [*Mauritzen,* 1996; *Eldevik et al.,* 2009]. These overflow waters further contribute to the North Atlantic Deep Water and thus play an important role in

the Atlantic Meridional Overturning Circulation and its associated northward transport of heat [*Mauritzen,* 1996; *Hansen and Østerhus,* 2000; *Isachsen et al.,* 2007; *Eldevik et al.,* 2009; *Medhaug et al.,* 2011]. In recent years, the variability in AW transport in the Norwegian Sea has received much attention due to its significant influence on the sea ice cover in the Barents Sea [*Sandø et al.,* 2010; *Årthun et al.,* 2012] and near Svalbard [*Walczowski and Piechura,* 2009]. *Mork and Skagseth* [2010] estimated AW volume transport from satellite derived surface velocities and hydrography, which showed the usefulness of satellite data for studies of variability in AW transport. Although their analysis was limited to Svinøy section, the results suggested that the method could be consistently applied for other locations in the Norwegian Sea.

The spatial features of the circulation in the Norwegian Sea has been thoroughly studied using drifters and floats [e.g., *Jakobsen et al.*, 2003; *Rossby et al.,* 2009*; Andersson et al.,* 2011; *Koszalka et al.,* 2011, 2013]. Still it remains to be decided whether the two branches of NwAC can be considered as separate flows after entering on each sides of the Faroe Islands [*Helland-Hansen and Nansen*, 1909; *Orvik and Niiler,* 2002*; Nilsen and Nilsen,* 2007]. *Rossby et al.* [2009] using floats showed crossover flow and mixing between the two branches of NwAC, and argued that the two branches therefore could not be considered as separate. However, the time variability of the crossover flow and the impact on the downstream transports of heat, salt and volume has still not been assessed.

The main objectives of this study are to: (1) Quantify the spatial and temporal variability of the surface circulation of the Norwegian Sea using satellite altimetry; (2) Examine the vertical structure of the circulation observed from satellites, using hydrography; (3) Identify regions where flow (surface waters in this study) between the two branches of the Norwegian Atlantic Current may take place; (4) Assess effects of these inter-connections on the downstream flow variability. The outline of the paper is as following: In Section 2 we describe the different datasets and methods being used in this study. The main results are presented in Section 3 and the implications for our

understanding of the flow through the Norwegian Sea are discussed in Section 4. The paper is then summarized and concluded in Section 5.

2. Data and Methods

2.1. Altimeter data

Weekly sea level anomalies (SLA) from 1993 to 2010 are used to study the surface circulation of the Norwegian Sea. The SLA fields from AVISO, corrected for the inverted barometer effect, tides, and tropospheric effects [*Le Traon and Ogor,* 1998], are based on merged TOPEX/POSEIDON (T/P), ERS-1 and 2 and Envisat data [*Ducet et al.,* 2000; *Volkov and Pujol,* 2012]. In the Norwegian Sea, the SLA fields provided have roughly 12 to 18 km resolution. In this study, we have used the state of the art Mean Dynamic Topography (MDT), from CNES-CLS09 [*Rio et al.,* 2011]. The CNES-CLS09 MDT is based on altimetry, in situ measurements, Argo floats, surface buoys and the Gravity Recovery and Climate Experiment (GRACE) geoid model on a $1/4^{o}$ regular grid using a combination of direct and synthetic methods [*Rio and Hernandez,* 2004*; Rio et al.,* 2011]. The errors associated with the estimation of CNES-CLS09 MDT are provided together with the MDT dataset [*Rio et al.,* 2011]. In the Norwegian Sea, from the continental plateau and outwards, the errors are less than 1.0 cm (not shown). The provided errors are computed using multivariate objective analysis of both observational errors and the a-priori MDT covariance field (see *Rio et al.* [2011] for more details).

Weekly absolute dynamic topography (ADT) is the sum of MDT and SLA. *Volkov and Pujol* [2012] evaluated this satellite ADT data in the Norwegian Sea and found that the altimeter data can be successfully used to study the variability in the sea level and surface circulation of the region. Absolute surface geostrophic velocities are here computed from weekly absolute dynamic topography (ADT) gridded data, using the geostrophic relation:

$$u_s = \frac{-g}{f}\frac{\partial h}{\partial y}, \quad (1)$$

$$v_s = \frac{g}{f}\frac{\partial h}{\partial x}, \quad (2)$$

where u_s and v_s are the components of the surface velocity, g is the acceleration due to gravity, f is the Coriolis parameter, h is the sea surface height (dynamic topography), while x and y are distances along positive longitudinal and latitudinal directions respectively.

Mean fields of monthly and winter climatology of velocity are based on the weekly velocities derived using equations (1) and (2). The corresponding error estimates in the mean velocities become $s_m=s/(N-1)^{1/2}$, where s is the standard deviation for the N weekly velocities the mean is based on. Note that this error estimate does not include any uncertainties in the data, only in calculating statistical means from a limited data set. Eddy Kinetic Energy (EKE) is calculated on a weekly basis using the relation:

$$EKE=\frac{u'^2+v'^2}{2}, \tag{3}$$

where u' and v' are geostrophic velocity anomalies determined using SLA instead of ADT in equations (1) and (2) [*Chaigneau et al.,* 2008].

In order to study the seasonal and inter-annual variability of the surface circulation of the Norwegian Sea in detail, six key regions with enhanced flow speeds are selected (see Section 3.1 and Figure 2). Monthly velocity components along the direction of the mean flow are determined for each location. For composite studies, the high/low periods at each location are weeks with velocity components above/below mean plus/minus one standard deviation calculated over the entire period. Typically 150 weeks of altimeter and hydrographic data are included in the determination of each composite map. All correlations in this study are based on de-trended and de-seasoned data. The effective degrees of freedom are found according to *Chelton* [1983], i.e., taking into consideration the autocovariance of all time series. Significance levels are calculated by the standard Student's t test.

2.2. Hydrography

Hydrographic data used in this study are from the long term hydrographic NISE database [Norwegian Iceland Seas Experiment; *Nilsen et al.,* 2008]. The NISE dataset consists of CTD data decimated to 5 m, and bottle data. The hydrographic variables

included in this study are temperature and salinity from 1993-2008. Hydrographic sections are based on bin means along chosen lines (see Figure 8) and on 'standard' depths 0, 10, 25, 50, 75, 100, 150, 200, 300, 400, 500, 600, 800, 1000, and 1200 m. The length of the sections are selected to cover the flow of interest, and the horizontal bin sizes are selected according to the availability of stations to give the best spatial resolution while still ensuring that climatic monthly mean sections can be made in order to eliminate seasonal bias. For some sections the horizontal bins are centered on stations on standard repeated sections, and distances are thus small, while for others the data are much more scattered, and larger bins are used. The number of observations in each single bin of the composite sections varies approximately from 10 to 100.

Subsurface velocities are calculated using the surface geostrophic velocities (v_s) and the thermal wind relations:

$$v(z) = v_s + \frac{g}{\rho_0 f} \int_z \frac{\partial \rho}{\partial x} dz \,. \qquad (4)$$

where, ρ is the density, ρ_0 is a reference density, and x is directed along the section. Volume transports of AW are then found by integrating the velocities vertically over the depth interval with salinities 35 or above, and then laterally between limits defined to include the mean core of the current as well as the main differences between the composite periods.

2.3. Surface drifter data

Surface drifter tracks are obtained from WOCE (World Ocean Circulation Experiment) surface drifter dataset [*Schlitzer,* 2000]. Note that only those drifters that cross from the front current into the slope current are used in this study (34 in number). This is roughly 60% of the total number of drifter releases in the Iceland-Faroe region throughout the 1990s [*Koszalka et al.,* 2013]. After identifying major regions of flow from the front current into the slope current (see Section 3.3), separate colors (e.g., green, blue, red) are assigned to drifters following the different flow pathways (Figure 7a).

3. Results

In this section we first utilize the altimeter data to examine the spatial and temporal variability of the surface velocities of NwAC in the Norwegian Sea. Next we identify regions of flow between the two branches of NwAC, before hydrography data is combined with altimetry to estimate strengths and co-variability in volume transports in key regions in the Norwegian Sea.

3.1. The features of the flow through the Norwegian Sea

Winter and summer climatologies of surface geostrophic velocities in the Norwegian Sea (Figure 2) show a two-branch structure similar to what has been found earlier using drifters [e.g., *Jakobsen et al.,* 2003*; Andersson et al.,* 2011; *Koszalka et al.,* 2011]. The two branches of NwAC (front current and slope current) are clearly resolved in the seasonal climatologies of the absolute surface geostrophic velocities, and the reported strengthening of the mean circulation of the Norwegian Sea during winter [*Mork and Skagseth,* 2005; *Jakobsen et al.*, 2003] is also seen. The surface velocities of NwAC are highly intensified at two key locations in the Norwegian Sea (Figure 2), here termed the Svinøy (SV) and Lofoten Slope (LS) regions. This regional intensification of NwAC is most pronounced in winter climatology, when area-mean surface velocities exceed 25 cm s^{-1}. In addition to the above two locations, four other regions are selected for a detailed study of surface velocity, hydrography and volume transports (Figure 2). These are the Vøring Jet (VJ) region, with a well-defined, topographically steered narrow swift current near the western Vøring Plateau [*Poulain et al.,* 1996; *Orvik and Niiler*, 2002; *Nilsen and Nilsen*, 2007]; the Mohn Ridge (MR) region with a local maximum in the front current; and the two regions to the south covering the Shetland Current (SC) and Faroe Current (FC) inflow branches to the Norwegian Sea. Thus there are three regions selected along the slope current (SC, SV, LS), and three along the front current (FC, VJ, MR).

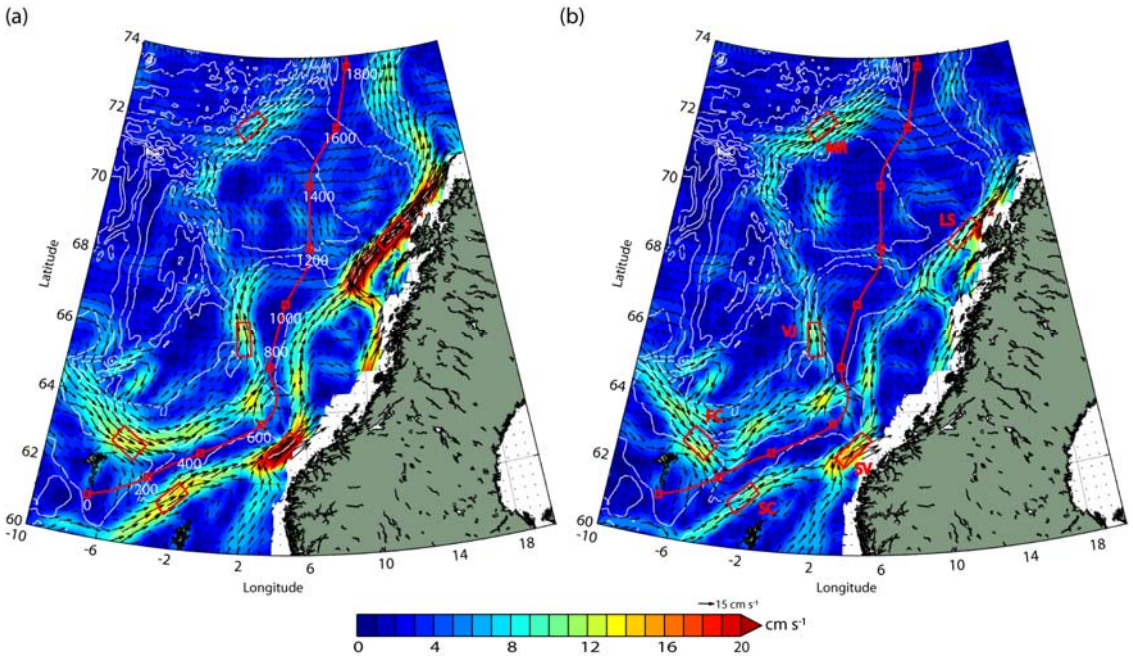

Figure 2. Climatologies (1993-2010) of surface geostrophic velocity (speed in colors) for winter (December-February; a) and summer (June-August; b) from satellite altimetry. White isobaths are drawn for every 600 m. The symbols SC, SV, LS, FC, VJ, and MR in panel b denote Shetland Current, Svinøy region, Lofoten Slope, Faroe Current, Vøring Jet, and Mohn Ridge respectively, whereas red boxes represent the areas used for averaging. Seasonal climatologies of perpendicular velocity component shown in Figure 6 are calculated at grid points along the red line at approximately 15 km interval. Numbers by the red squares along the line indicate distance in kilometer.

3.2. Seasonal and inter-annual variability

During winter, the velocities at LS and SV are twice as high as the velocities at the two inflows FC and SC, while in summer this is only the case for the SV flow (Figure 3a). The seasonal cycle in the velocities at LS and SV are three times (10-15 cm s^{-1}) larger than in any other part of the Norwegian Sea. A distinct seasonality is also seen in the SC inflow, where the current is twice as large in winter compared to summer. While the speed of the slope current peaks in January, maximum in FC is seen in February and for VJ in March. For MR, a weak maximum in velocity occurs during late summer. This opposite phase of the velocities over the Mohn Ridge compared to other parts of the Norwegian Sea is also seen in the winter minus summer climatology (Figure 3b). A minimum in the surface velocities is also noted along the southern Norwegian Basin.

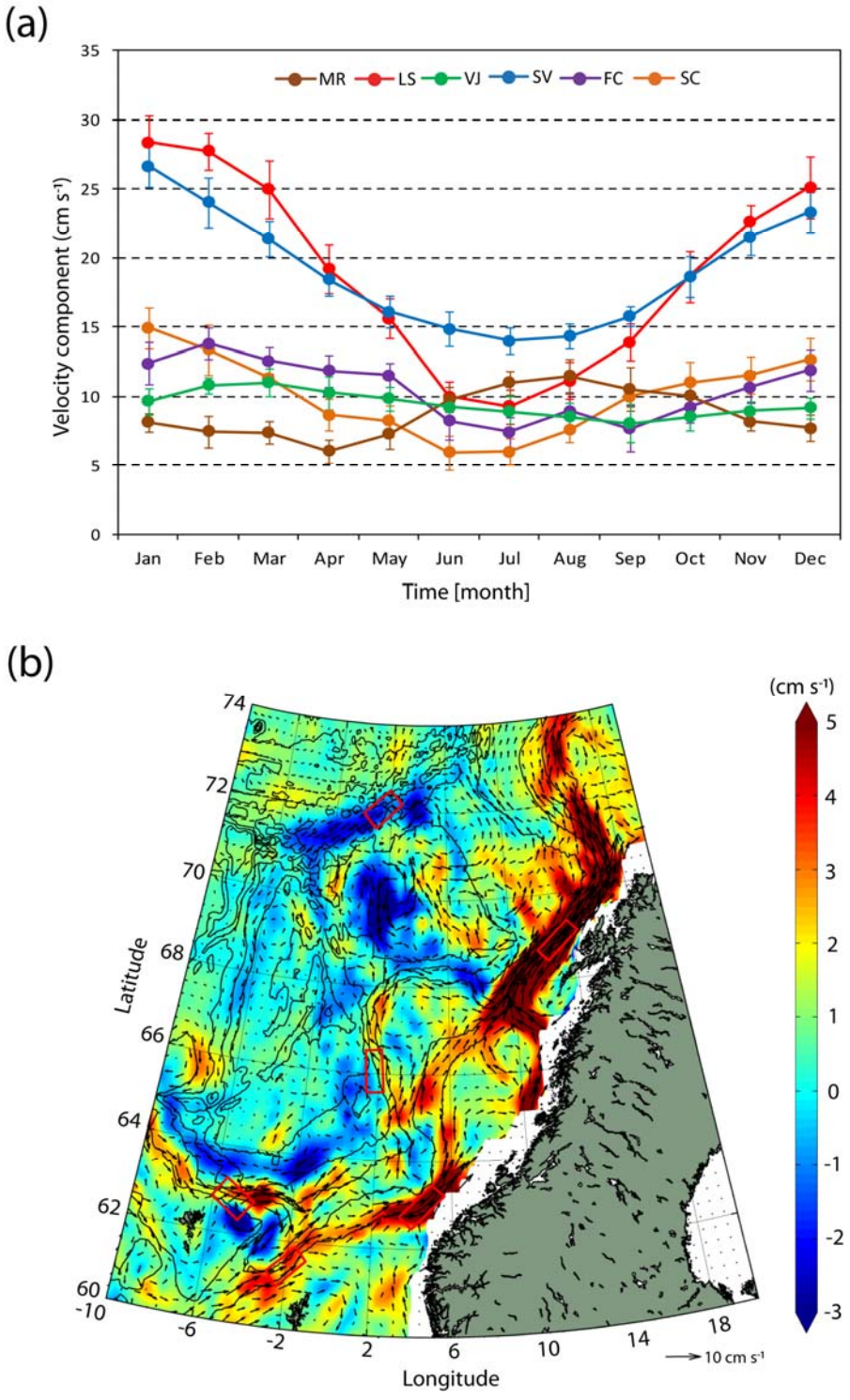

Figure 3. (a) Annual climatology (1993-2010) of absolute surface geostrophic velocity component along the mean flow (cm s^{-1}) together with error estimates based on the averaging at locations SC, SV, LS, FC, VJ and, MR. (b) Winter (DJF) minus summer (JJA) climatology of absolute surface geostrophic speed (cm s^{-1}). Corresponding seasonal difference in surface geostrophic velocities are indicated by arrows. Blue isobaths are drawn for every 600 m.

Eleven years (1995-2005) of monthly mean absolute geostrophic surface velocities at SV is compared with current meter velocities measured at 100 m depth (Figure 4a) in order to test the validity of the altimeter dataset for studying the temporal variability of NwAC. The analysis shows high and significant correlation both for the monthly variability (r=0.61) and for the inter-annual variability (r=0.65). The monthly velocity anomalies, determined after subtracting the annual cycle, are constrained within -20 to 20 cm s^{-1} during the 11-year period. In the Faroe current, the observed monthly and inter-annual variability of the volume transports of AW [*Hansen et al.,* 2010] is also seen to be significantly correlated with the surface velocities, during 1997-2010 (Figure 4b; r=0.45 and r=0.80 respectively). The average Iceland Faroe inflow is 3.5 Sv, while the mean surface velocity is observed to be 10 cm s^{-1}.

The temporal evolution of NwAC velocities during the past two decades (Figure 5) shows a substantial inter-annual variability, but with no significant long-term trends. Visual inspection of the figure shows a high degree of covariance between the velocities of the two strongest currents, SV and LS. Monthly and winter correlations of the velocities at the six locations are given in Table 1. There is significant correlation between the two inflow branches SC and FC (r=0.31), but this is not significant for the winter months. Surface velocities in both inflowing regions correlate with surface velocities in the SV and LS regions. An unexpected result is that the correlations with the inflows are higher for the Lofoten slope region than for the Svinøy region, and that the highest correlation between inflowing regions and slope current regions is found between the Lofoten slope and the Faroe Current regions (r=0.42), in particular in winter time (r=0.55). The overall highest correlation among the selected locations was found between SV and LS (r=0.60). There is also a significant correlation between the velocities of the FC and VJ (r=0.29), while no significant correlations are found between MR and any other locations.

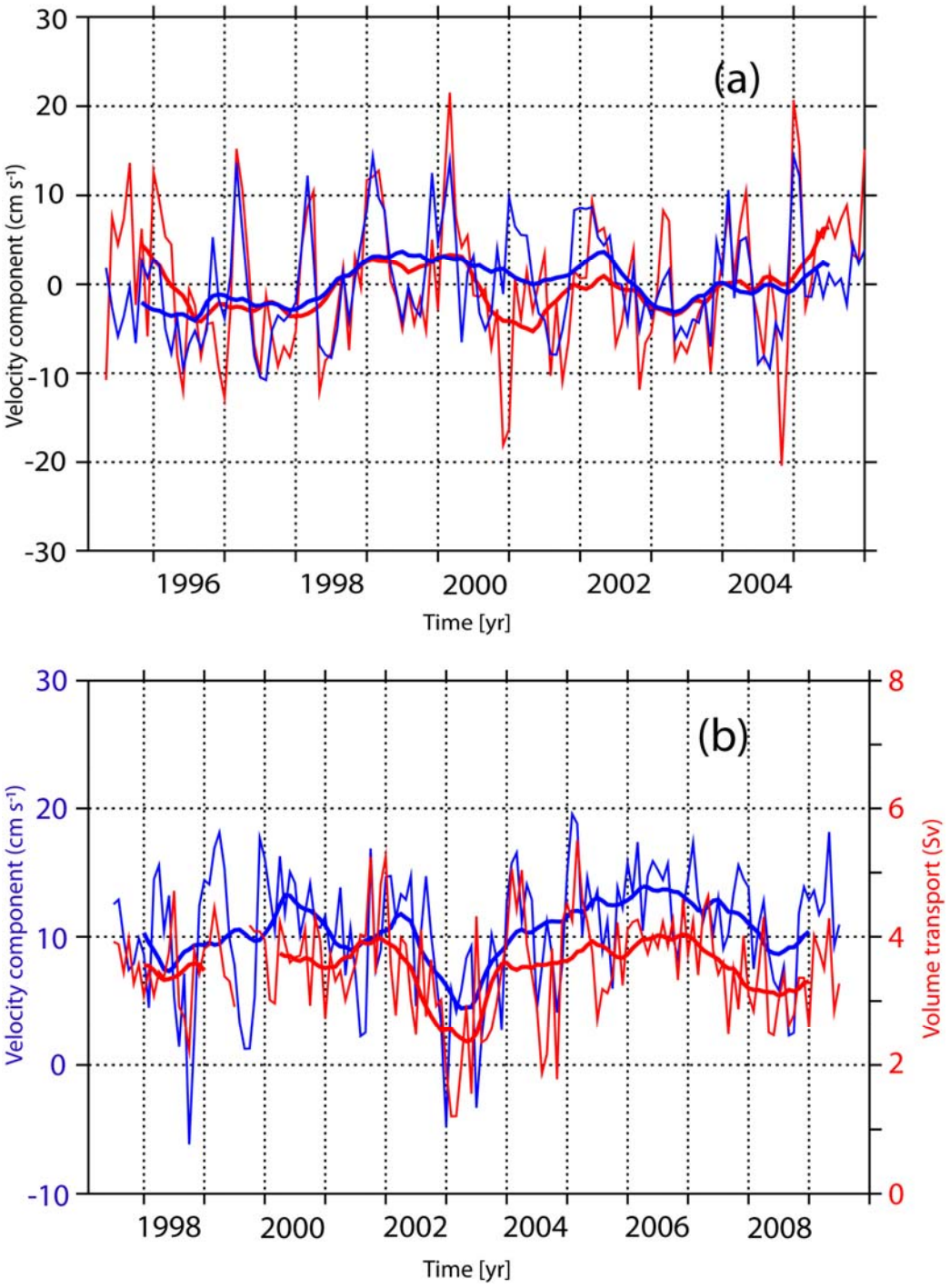

Figure 4. (a) Monthly surface geostrophic velocity anomaly from altimetry (blue) and independent current meter velocity anomaly at 100 m depth (red), at SV. (b) Monthly surface geostrophic velocity at location FC from altimetry (blue) and monthly volume transports at FC [red; *Hansen et al.,* 2010]. Thick lines are 12 month running mean of the respective datasets.

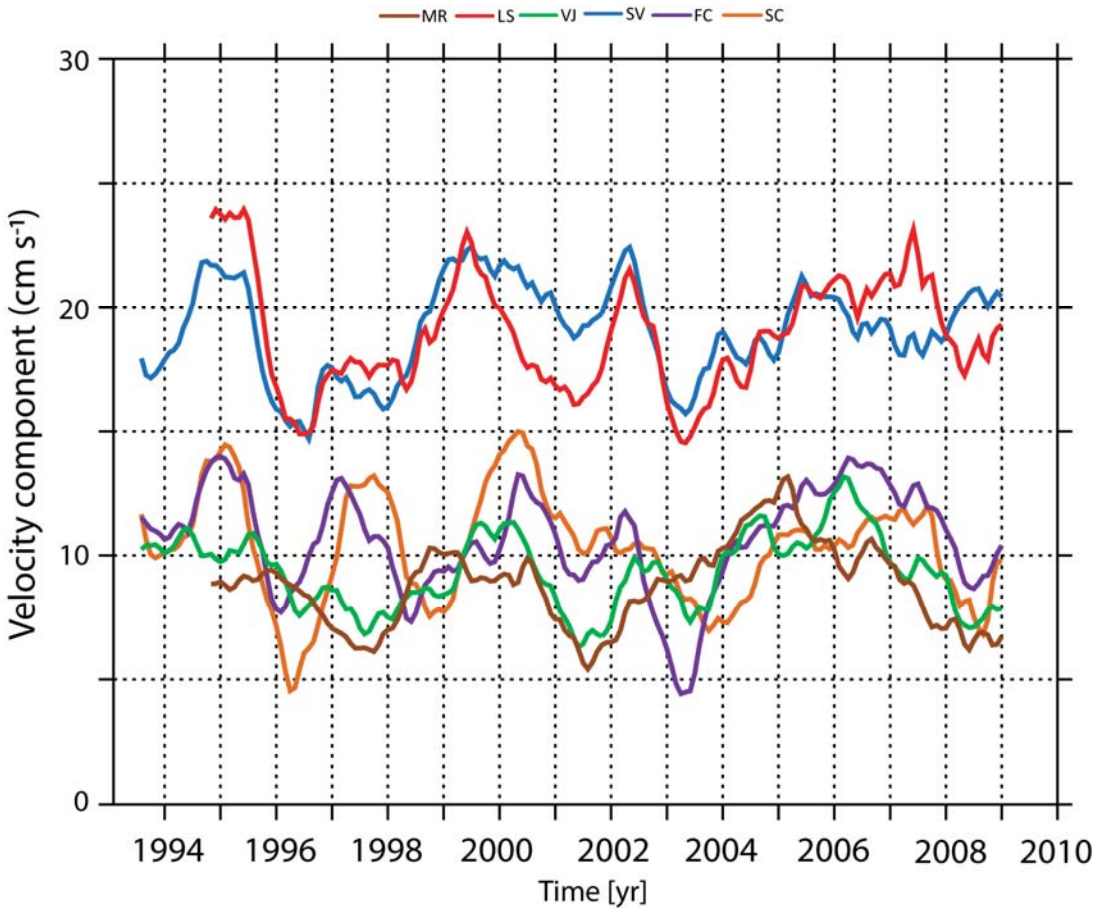

Figure 5. Temporal evolution (12 month running mean) of surface geostrophic velocity at locations MR, LS, VJ, SV, FC, and SC.

Table 1. Correlations between velocities at the 6 locations shown in Figure 2 during 1993-2010. Winter (Dec-Feb) correlations are given in parenthesis. All tabulated correlations (*r*) were calculated using de-trended and de-seasoned monthly time series. Values highlighted in bold are above the 5% significance level.

	MR	LS	VJ	SV	FC	SC
MR		-0.03 (0.02)	0.19 (0.01)	-0.03 (-0.06)	0.01 (0.14)	-0.02 (-0.03)
LS	-0.03 (0.02)		**0.32** **(0.34)**	**0.60** **(0.61)**	**0.42** **(0.55)**	**0.28** **(0.36)**
VJ	0.19 (0.01)	**0.32** **(0.34)**		0.19 (0.06)	**0.29** **(0.38)**	0.1 (0.05)
SV	-0.03 (-0.06)	**0.60** **(0.61)**	0.19 (0.06)		**0.32** **(0.42)**	**0.23** **(0.39)**
FC	0.01 (0.14)	**0.42** **(0.55)**	**0.29** **(0.38)**	**0.32** **(0.42)**		**0.31** (0.22)
SC	-0.02 (-0.03)	**0.28** **(0.36)**	0.1 (0.05)	**0.23** **(0.39)**	**0.31** (0.22)	

3.3. Interconnections between the two branches of the Norwegian Atlantic Current

In order to identify regions where there is flow from the front current into the slope current, winter and summer climatologies of the surface velocity components normal to a line separating the two branches of the NwAC (Figure 2) are estimated (Figure 6). The significance of these seasonal mean normal velocities at each location along the section is tested using the one sample Student's t test (in Figure 6, a red line joins the locations with positive mean values significantly different from zero at the 99% confidence level) and significant, shoreward regions which are wider than 50 km are categorized as regions of surface flow towards the slope current, and hereafter termed "crossover flows" or "CO".

The crossover flows identified exist mainly at four locations, at around 200-300 km, 500 km, 700 km, and 1100 km along the line (Figure 6). Distinct seasonality is observed at CO-1, and CO-2, where normal velocity at CO-1 has a maximum (and is only seen) during summer, while CO-2 is only defined during winter. On the other hand, no clear seasonality is observed at the crossover flows CO-3 and CO-4. These two regions are defined in Figure 7 by their (marginally broader) winter extent. There is also a weak flow perpendicular to the mid-line at 1400-1700 km in the northern Lofoten Basin, but being downstream of our study regions it is not assigned a number nor discussed further. The existence and path of these flows can to some extent be seen in the surface velocity fields of Figure 2.

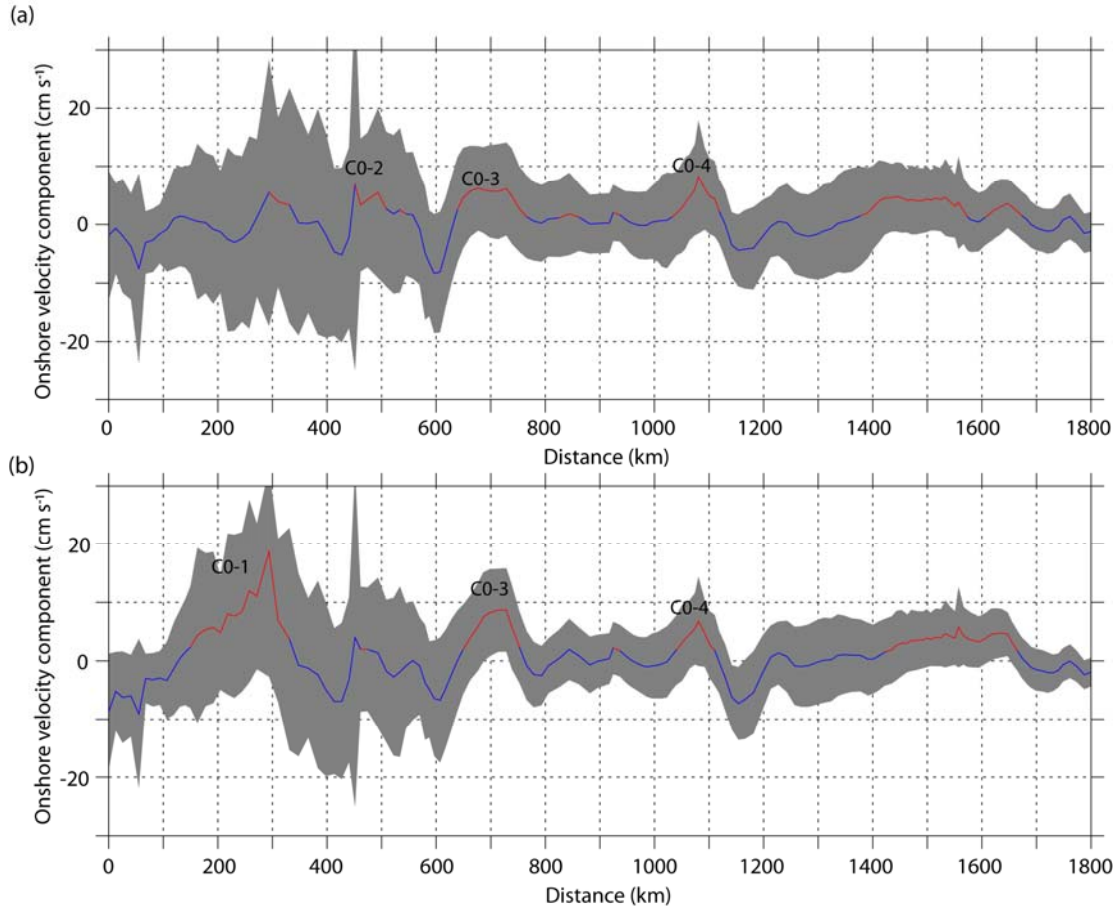

Figure 6. Velocity component (blue) normal to the red line shown in Figure 2, positive towards the southeastern side. (a) Winter (DJF) and (b) summer (JJA) climatology derived from altimeter. Positive mean values significantly different from zero at the 99% confidence level are marked with red. The shaded region represents the mean plus/minus one standard deviation. CO-1, 2, 3, and 4 represents the four major crossover locations identified.

In order to study the flows between the branches in more detail, surface drifter tracks that cross from the front current into the slope current in the WOCE data archive, are analyzed (Figure 7a). In this study, only those drifters crossing from the front current into the slope current are selected, in order to emphasize the CO-regions as *the* main regions where crossovers exist, and not so much elsewhere. All of these surface drifters enter the NwAC north of the Faroes (i.e., in the FC). It is found that out of the total 34 surface drifters that cross from front current into the slope current, 27 cross at either of the four crossover regions identified from altimetry. Quantitatively, 12 surface drifters cross the front current into the slope current at CO-1, 1 at CO-2, 8 at CO-3, 6 at CO-4, while 7 are found to cross outside these regions. Note that a few surface drifters which crossed at CO-1 are also seen drifting back to the front current. Analysis of altimeter derived EKE (Figure 7b) shows high eddy activity near two major crossover regions (CO-1 and CO-3).

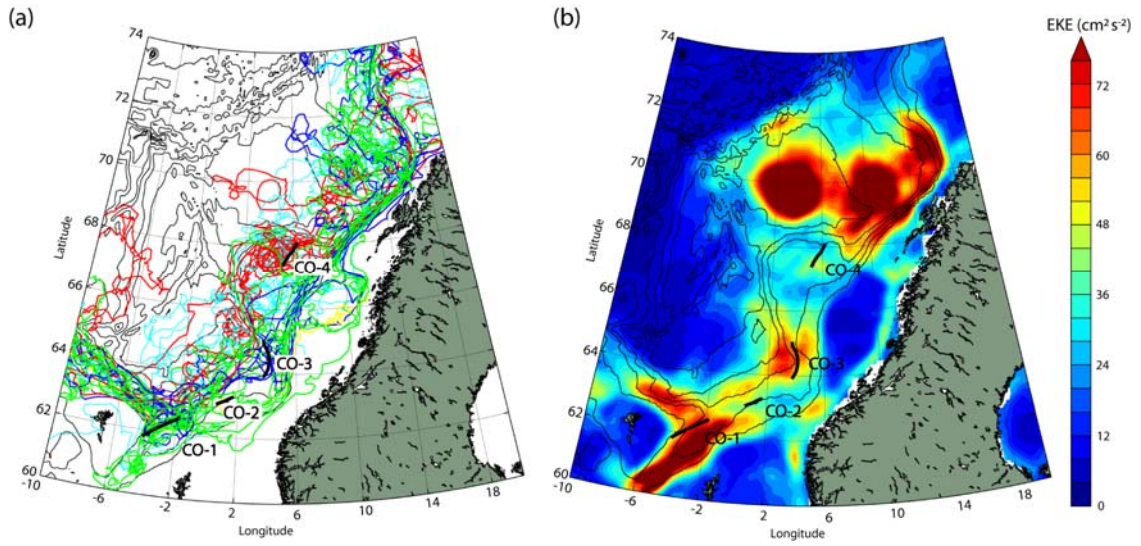

Figure 7. (a) WOCE surface drifter tracks showing crossovers from the front current into the slope current. The drifter tracks colored in green, yellow, blue and red indicates the drifters crossing at the major crossover locations, CO-1, 2, 3, and 4 respectively. The locations (bold black line) and width of crossover regions are determined from Figure 6. Drifter tracks colored in cyan are those drifters crossing outside the major crossover regions. (b) Climatology (1993-2010) of altimeter derived EKE in the Norwegian Sea. Black isobaths are drawn for every 600 m.

3.4. The relationship between surface flow and ocean interior

In Figure 8, composite maps show the difference between weeks with anomalously high velocities (exceeding one standard deviation above the mean of the whole period) minus weeks with anomalously low velocities (lower than one standard deviation below the mean) during 1993-2010 at the respective locations. All three slope current locations (SC, SV, and LS) show signatures of a strengthened, topographically trapped, eastern branch of NwAC (Figure 8b, d, f). The relationship between the locations in the front current is different. Any positive response in the front current to enhanced FC inflow is limited to the Vøring Escarpment where the flow becomes topographically steered around the whole Vøring plateau and into the slope current (Figure 8e). This scenario is characterized by strong topographic control and enhanced cyclonic circulation all around the Norwegian Sea, including the slope current positions SC, SV, and LS, as well as an increase in the recirculation of AW in the Faroe Shetland Channel (FSC). Further downstream in the front current, no coherence is found between the velocities at VJ and MR (Figure 8c, a). In particular, the composite velocities for strong MR current show weakening of the currents at all other locations, emphasizing the out of phase behavior of this flow (Figure 8a). Strong VJ currents, on the other hand, are associated with topographic steering towards the slope current, also when not connected to a general spin up in the Norwegian Sea (Figure 8c).

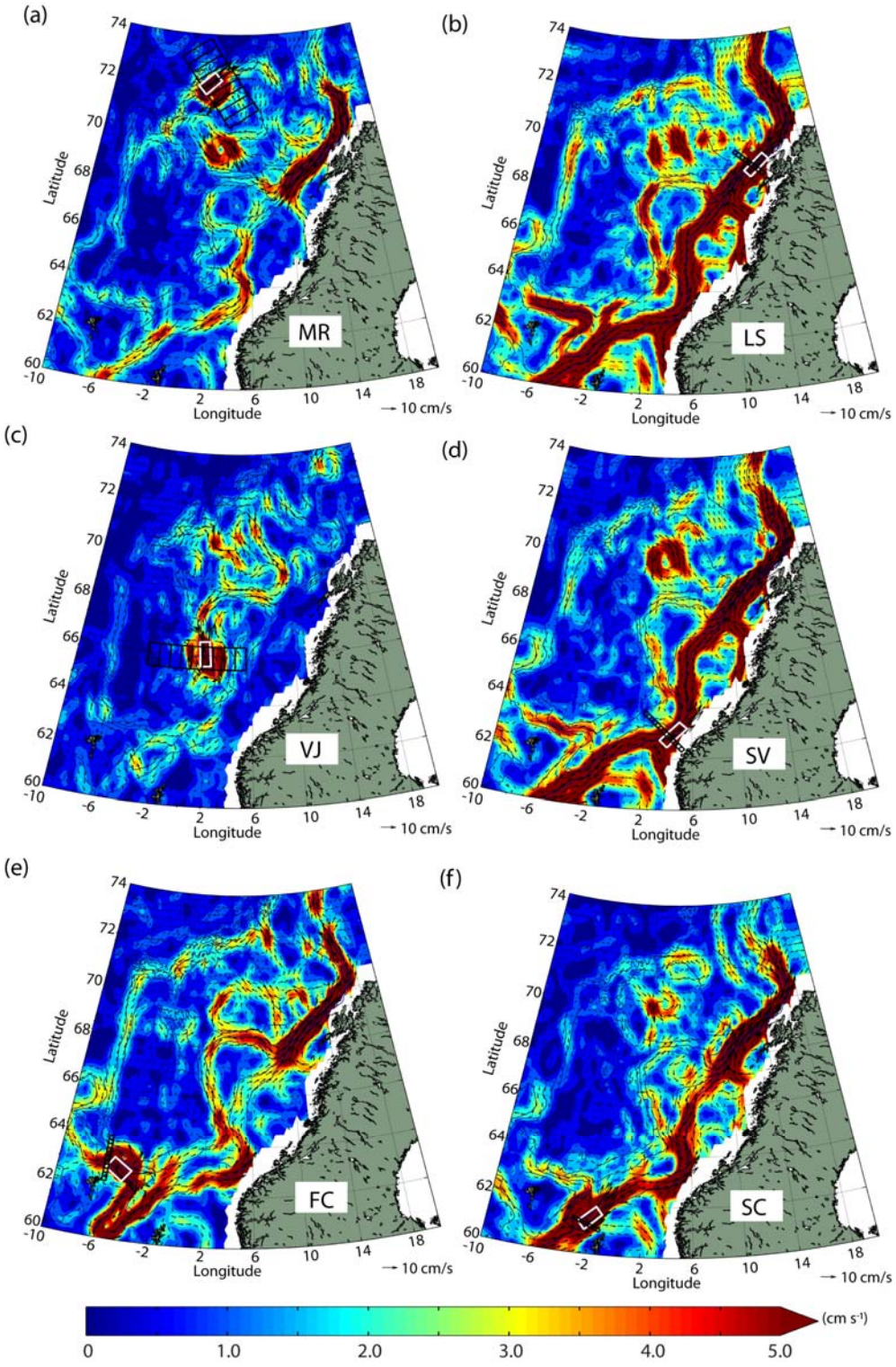

Figure 8. Composite maps of the difference in the mean high and low component velocities (speed in colors) at locations (a) MR, (b) LS, (c) VJ, (d) SV, (e) FC, and (f) SC. Approximately 150 weeks of surface geostrophic velocity datasets during the period 1993-2010 are included in the determination of each composite maps. The location of the hydrographic sections used in Figures 9 and 10 are shown as black bins. Blue isobaths are drawn for every 600 m.

The local variations in hydrography associated with variability in the surface circulation shown above, is analyzed by performing the same composite analysis on the cross-section surface velocities and subsurface densities, velocities, and volume transports for sections crossing through each of the six target regions (Figure 9-10). The difference in sea surface height gradients between high and low surface velocity periods is maximum in the slope current (Figure 9 b,d). Similarly, the change in horizontal subsurface density gradients is also found to be larger in the slope current. The average surface flows (not shown) as well as the composite anomalies are in general deep reaching, i.e., representative of the AW layer with only weak attenuation with depth (Figure 10). The increase in subsurface velocities at MR in the core of the front current is limited to the upper 200 m, and the composite difference in the velocity of this layer reaches 9 cm s^{-1}. Associated with increased flow at MR, isopycnals are deeper at the inshore side of the section, indicating that the reason for the increased northward flow is an influx of more light water from the east (Figure 9a). Moving upstream along the front current, at VJ, the composite difference in subsurface velocities is found to be roughly 12 cm s^{-1}. Unlike at MR, the subsurface velocities at VJ during high surface velocity periods increase throughout the entire water column. Focusing on the slope current, the local intensification of surface currents at SV and LS is also reflected in the hydrography. The composite difference in Atlantic-layer velocities is the largest at these two locations, exceeding 20 cm s^{-1}. The Atlantic layer velocities at the two inflows also increase in accordance with the increase in surface flow (at FC by roughly 10 cm s^{-1} and at SC by roughly 15 cm s^{-1}). Curiously, the strongest increase in subsurface velocities at SC occurs in the deep, associated with a lateral shift of the deep southward flow (see mean current field in Figure 10f).

The composite difference of AW volume transports, integrated over the selected regions in the respective sections are shown in Figure 10, and in Table 2. The results show that the changes in the volume transports associated with strong or weak surface flows are maximum along the slope current (with 4.1, 4.0, and 5.2 Sv, respectively). In contrast, the differences in volume transports at the front current locations are only in the range of -0.1 to 1.1 Sv. The narrow swift Vøring Jet shows the maximum

difference in transport, the MR shows negligible difference, while the difference in volume transport at FC is 0.6 Sv. The overall mean transports are also shown in Table 2, and will be compared to other estimates in the next section.

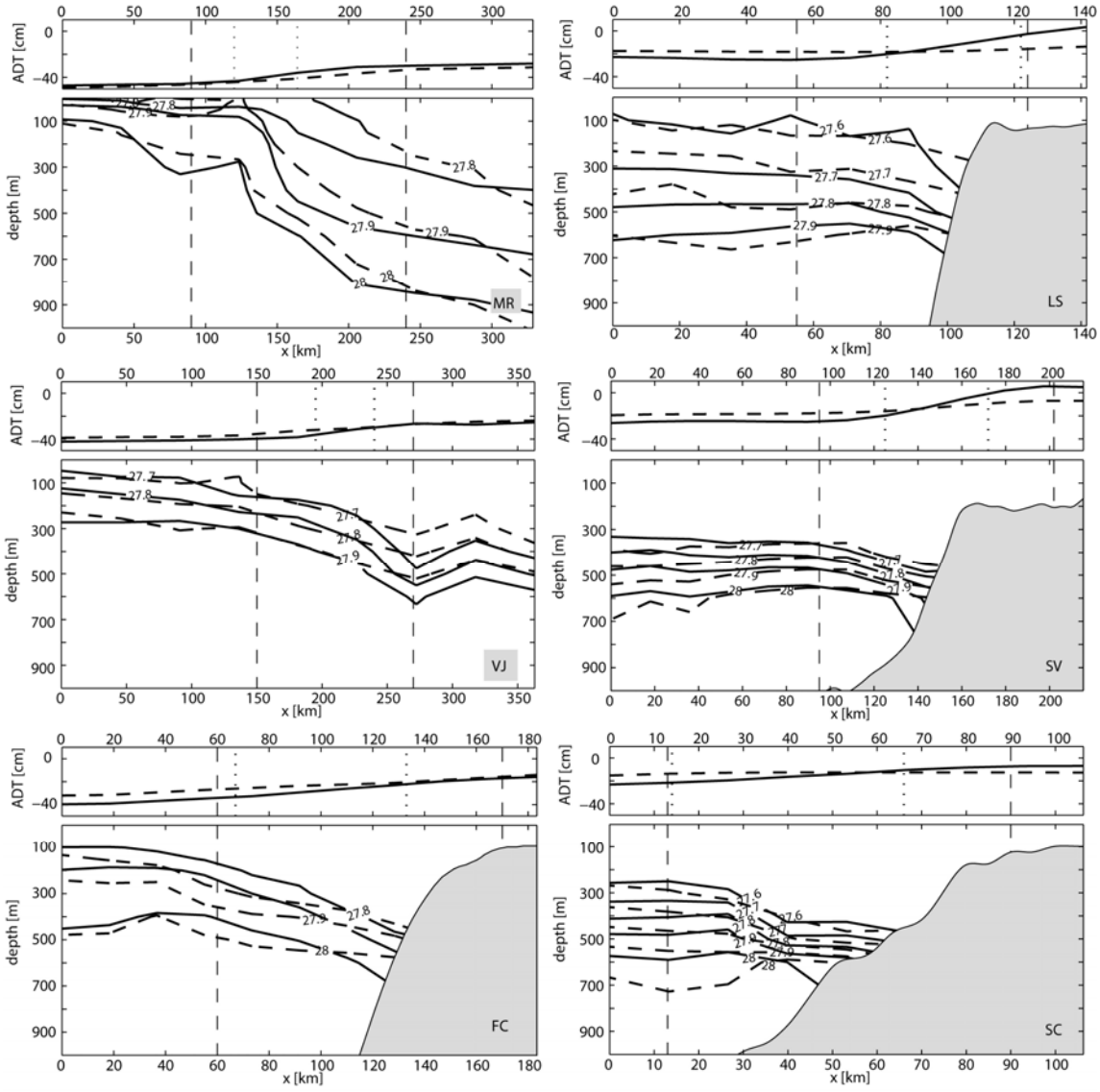

Figure 9. Sea surface height (ADT; upper panels) and composite mean hydrographic sections of chosen isopycnals (σ_0; lower panels) for the periods of strong (full lines) and weak (dashed lines) surface velocities for (a) MR, (b) LS, (c) VJ, (d) SV, (e) FC and, (f) SC. See Figure 8 for positions of the sections. *Dotted* vertical lines indicate the location of the defining boxes for the composites, found in the fields of surface velocities (white boxes in Figure 8), while *dashed* vertical lines (all panels) indicate the region used to calculate the volume transport of main current cores.

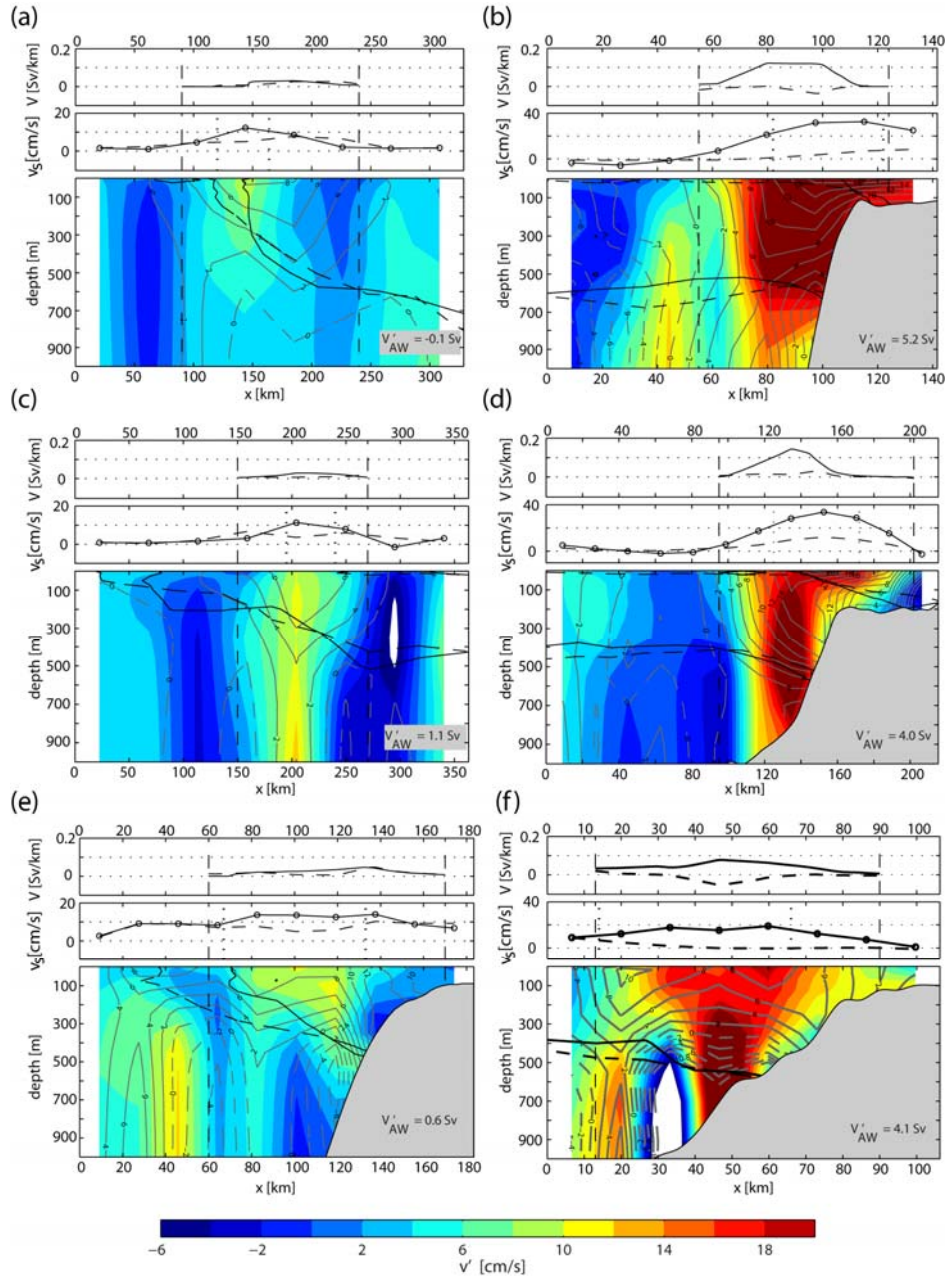

Figure 10. Along section volume transport density of AW (V, upper panels), surface velocities (v_s, middle panels) and subsurface velocities (mean as grey contours and composite, v', in colour, lower panels) for (a) MR, (b) LS, (c) VJ, (d) SV, (e) FC and, (f) SC. In the top panels (upper and middle) full lines are for the positive composite case, and dashed lines for the negative case. The lower panels show the composite difference in the subsurface velocities. *Dotted* vertical lines in the middle panels indicate the location of the defining boxes for the composites, found in the fields of surface velocities (white boxes in Figure 8). Dashed vertical lines (all panels) indicate the region used to calculate the volume transport of main current cores, chosen so that both mean flow and composite difference is included. Full and dashed curves in the lower panels indicate the depth of the 35 isohaline (typical definition of salinity minimum for Atlantic Water) during positive case and negative case respectively, to which vertical integration of velocities are done in the calculation of horizontal volume transport densities, V. Total AW transport, V_{AW}, is calculated by horizontal integration of V between the dashed vertical lines.

Table 2. Atlantic Water (S≥35) volume transports (Sv) across the 6 boxes shown in Figure 2 during respective mean, high, low and composite surface velocities. Total AW transport, $V_{AW,}$ is calculated by horizontal integration of volume transports, $V,$ between the vertical dashed lines in Figure 10. The composite not being shown as 0.0 at MR is a result of rounding when calculating the composite volume-transport difference.

	Mean V_{AW} (Sv)	High V_{AW} (Sv)	Low V_{AW} (Sv)	Composite: V_{AW} (Sv)
MR	2.0	2.1	2.1	-0.1
LS	1.9	4.5	-0.7	5.2
VJ	1.8	2.2	1.1	1.1
SV	2.8	5.0	1.0	4.0
FC	2.3	2.6	2.0	0.6
SC	1.2	3.4	-0.8	4.1

4. Discussion

In this study, absolute velocities are determined from the CNES-CLS09 MDT in order to study the surface circulation of the Norwegian Sea. *Mork and Skagseth* [2010] showed similarity between the climatology of satellite derived surface velocities and the independent current measurements along the Svinøy Section and estimated the inter-annual variability in volume transports using satellite and hydrographic data. In an earlier study, *Skagseth et al.* [2004] showed good correlation between the geostrophic velocity anomalies derived from SLA and current meter measurements at Svinøy Section. Our study also shows that the current meter velocities and altimeter derived surface velocities along the Svinøy Section are correlated on monthly time

scales (r=0.61; Figure 4a). Monthly current-meter velocities used for the comparison are obtained from one current meter located at the core of the slope current at 100 m depth [*Orvik and Skagseth,* 2005], while altimeter velocities used are surface velocities averaged over a box (SV region as shown in Figure 2b). They are therefore not directly comparable, but they do show much of the same variability. It should be further noted that this comparison between the satellite and current meter data is done relatively close to the coast, and since satellite altimetry is more accurate away from the coast [*Volkov and Pujol,* 2012], this supports the use of altimeter data to study the open ocean circulation of the Norwegian Sea.

In the Norwegian Sea, the altimeter derived velocities successfully reproduce the mean circulation as reported in earlier studies [e.g., *Jakobsen et al.,* 2003]. Regional intensification of NwAC at SV and LS found in altimeter derived velocities and hydrography is concurrent with the observations of *Skagseth et al.* [2004] and *Poulain et al.* [1996]. *Skagseth et al.* [2004] argued that near Svinøy and Lofoten sections the continental slope becomes steeper and due to topographic steering of geostrophic currents along isobaths (f/H contours), the converging isobaths will accelerate the flow. Traditionally, the slope current is considered as a narrow swift current flowing north [eg: *Orvik and Niiler,* 2002]. *Gascard and Mork* [2008] using floats argued that the slope current near the eastern Lofoten Basin is a broad and turbulent current due to the presence of mesoscale eddies, as has been further demonstrated by *Koszalka et al*. [2011, 2013] . From climatologies we find that the slope current at the eastern border of the Lofoten Basin is a narrow swift current during winter (Figure 2, 3). This explains the large correlation (r=0.60) between the surface velocities at locations SV and LS. Moreover, we show that a stronger slope current transports additional volume of AW pole-ward (Figure 8, 10).

According to the current understanding, NwAC is stronger during winter than during summer [*Jakobsen et al.,* 2003; *Mork and Skagseth,* 2005]. Our study captures this seasonality in all parts of the NwAC except over the Mohn Ridge. Contrary to the other regions studied, surface velocities of the front current over MR are weak during

winter and strong during late summer (Figure 2, 3). The increase in surface velocities here during summer can be linked to the presence of more buoyant waters in the Lofoten Basin, mainly due to prevalence of northerly winds and increased Ekman transport of buoyant waters offshore [*Nilsen and Falck,* 2006]. These buoyant waters in turn increase the sea surface slope at the MR, thereby increasing the surface currents there. Additional evidence supporting this is provided from the composite analysis of the high and low surface velocities and associated density fields in the hydrographic sections at MR (Figure 9a).

In a recent RAFOS-float study, *Rossby et al.* [2009] showed flow of AW between the two branches of NwAC in several regions. They suggested that these crossover flows are due to the influence of topographic steering and due to the substantial loss of heat as the AW moves northward. Earlier *Walin et al.* [2004] has argued that the subsequent loss of buoyancy may result in a transition of the AW from a baroclinic front current into a barotropic slope current. From altimeter derived surface velocities we identify four major crossover flows of surface waters (Figure 6). The fact that most drifters that cross, do so through our altimeter defined CO regions, is also a strong indication that our CO regions are not simply meanders on the mean flow, but a real crossover of water from one branch to another. Of the four crossover regions identified, two of them (CO-1 and CO-2) show seasonality while the other two are present throughout the year (CO-3 and CO-4). Crossover flow CO-1 associated with the transport of AW from FC into SC is observed mainly during summer. In particular, all floats shown by *Rossby et al.* [2009] to be crossing from FC towards SC (their Figure 8) pass through the exact same crossover region identified herein from altimetry (CO-1). This result supports our use of altimeter derived surface velocities for the detection of flow between the branches of the Norwegian Atlantic Current. *Rossby et al.* [2009] stated that topographic steering of the Faroe Plateau results in the entry of FC waters into FSC. Furthermore, a strong FC is herein shown to be associated with an increased topographically controlled cyclonic circulation in the whole Norwegian Sea (Figure 8e), a flow pattern which has been coupled to the regional variability in the wind field [*Isachsen et al.,* 2003]. Unlike CO-1, crossover

flow at CO-3 is found to be associated with diverging topography as seen in Figures 2 and 7, where topographic steering is less prominent. Also, high eddy activity is seen near these two crossover flows (CO-1 and CO-3; Figure 7b). In the case of CO-1 it is likely that the high eddy activity in the FSC plays a role in entrainment into the slope current after topographic steering has aided water in passing through CO-1. The prominence of eddy activity in these regions is also seen in drifter studies [*Koszalka et al.,* 2011]. The forcing mechanism which affects the crossover flow at CO-2 is not clear. The mean crossover flow CO-4 is located over the Vøring Plateau (Figure 2, 6), while during strong wind induced topographic steering (e.g., Figure 8e), the maximum flow from the front current into the slope current in this region is found slightly to the north, over the Vøring Escarpment, indicating different forcing regimes. In sum, depending on location, the effect of buoyancy loss, topographic steering, and surface winds all can play important roles for the flows between the front current and the slope current.

Focusing on the correlation analysis (Table 1), this study reveals higher correlation between FC and SV velocities ($r=0.31$), than between SC and SV velocities ($r=0.23$). This is surprising since SC and SV are both located in the slope current, while FC represents the western Atlantic inflow. A similar low correlation between volume transports of SC and SV has earlier been shown by *Richter et al.* [2009]. They stated that eddy activity in the SC region and subsequent sampling problems as the likely cause. We support their observation and argue that both the recirculation of FC inflow into SC inflow, represented by crossover flow CO-1, and the large eddy activity in the SC region seen in Figure 7b, results in the lower correlation between the velocities at SC and SV regions. Notably the correlation between FC and SC is not significant during winter, and is consistent with the seasonal difference in crossover flow at CO-1. On the other hand, the higher correlation found between FC inflow and SV velocities during winter may be attributed to the increased crossover flow via CO-2. While the non-seasonal crossover flow CO-3 is likely to justify the high correlation between the velocities of FC and LS, the non-seasonal crossover flow CO-4 may contribute to the positive correlation between velocities at VJ and LS. All in all, the correlation analysis

thus supports the earlier studies [*Helland-Hansen and Nansen*, 1909; *Nilsen and Nilsen,* 2007; *Rossby et al.,* 2009], suggesting that the two branches of the NwAC cannot be considered as two distinct separate currents flowing northward because of substantial exchanges of water masses between the two.

Variability in the altimeter derived surface velocities in the Norwegian Atlantic Current is shown to correlate with variability in the depth-integrated transport of Atlantic Water pole-ward. In the composite analyses, changes in velocities detected at the surface are seen to be deep reaching in both the front current and the slope current (Figure 10). This is supported by the correlation between the surface velocities and current meter derived volume transports at FC (Figure 4b). Volume transport is the integration of velocity over depth and width, and similarity between the surface velocities and the volume transport indicates either a baroclinic structure in phase with the surface flow or a predominant barotropic structure. The deep reaching influence of the changes in surface velocities here (roughly 250 m; Figure 10e) supports the latter. *Hansen et al.,* [2010] showed that there is no trend in the volume transports at FC. However, their study is limited to shorter time period due to non-availability of continuous current meter measurements at FC prior to 1997. Since altimeter derived surface velocities and the volume transports at FC are strongly correlated on inter-annual timescales (Figure 4b; r=0.80), it can be used as a proxy for the variability in volume transports also prior to 1997. The temporal evolution of altimeter derived surface velocities at FC, supports that there is no significant trend in the volume transport during the past two decades. *Richter et al*. [2012] combined tide gauge data with altimetry and arrived at a similar result. Unlike the front current, the whole water column of the slope current is in phase with the surface velocities due to its barotropic structure. These results underline the importance of remote sensing in high latitudes where acquiring current meter observations are difficult.

Mean and composite volume transports at six locations in the Norwegian Sea are determined from satellite surface velocities and hydrography. The calculated mean volume transports are significantly smaller than those determined from current meters

(Table 2). These differences in estimated volume transports can have several reasons, the most important probably the accuracy of the satellite-derived geoid. Note that the longer spatial scales of CNES-CLS09 MDT are determined mainly from the 4.5 years GRACE data. Even though the mean sea surface is known with a centimeter accuracy [*Schaeffer et al.,* 2012], the errors in the estimation of the geoid may be important.

According to *Rio et al.* [2011], north of 60°N in the Atlantic, e.g. in the Norwegian Sea, drifter velocities are not used for the calculation of the CNES-CLS09 MDT. We have taken advantage of this to independently assess relative accuracies through computation of mean geostrophic velocities, using MDT in equations 1 and 2, and comparing with drifter derived mean geostrophic velocities obtained from *Lumpkin and Garraffo,* [2005]. At the front current regions studied herein, it is found that the MDT derived velocities are 4-10 cm s^{-1} weaker than the drifter velocities (not shown). Although the drifter data has a relatively smaller sampling rate, this indicates that the MDT may be somewhat smoother than reality in these locations. A future version of the CNES-CLS09 MDT to be constructed with 28 months (01-11-2009 to 01-08-2012) of Gravity field and steady-state Ocean Circulation Explorer (GOCE) data, 9 years (2003 to 2012) of GRACE data, and 25 years (1985-2010) of Laser Geodynamics Satellites (LAGEOS) data, instead of the 4.5 years GRACE data currently used, is expected to decrease the uncertainties associated with the estimation of the geoid.

Another reason for weaker mean volume transports is that they are determined from mean hydrography and mean surface velocities for the whole time period, rather than from monthly current meter time series. Hence, our estimation does not take into account any non-linearity associated. The available, scattered hydrographic observations do not permit this analysis to be done on weekly time scales at all six locations. Even the standard sections such as Faroe North (in FC) and Svinøy (in SV) are taken at most 5 times a year. For the composite differences in volume transports, the time-invariant MDT cancels out in the calculation, and thus has no effect on the results. But the NISE dataset consists of scattered available observations, so the composite hydrographic sections will inherently be of a smoothed character, which

likely leads to somewhat weaker volume-transport contrasts between the composite-extremes. However, this is general and not likely to affect the overall comparison between the six locations. Seasonal bias is not expected to affect the composite hydrographic sections, since weeks of strong and weak surface flows are in this case considered separately.

An important finding in this study is the large variability in the volume transport in the slope current compared to the front current (Table 2; front current, 0-1 Sv; slope current, 4-5 Sv). This highlights the importance of the North Atlantic storm tracks, since cyclones entering the Nordic Seas are known to speed up the slope current [*Orvik and Skagseth*, 2003; *Sandø and Furevik,* 2008; *Richter et al.,* 2009; *Sandø et al.,* 2012]. Since it is known that heat loss is larger in a broader and slower current than that in a narrow swift current [e.g., *Furevik*, 2001], a topographically trapped slope current is expected to carry a larger amount of heat to the Arctic. Most of the AW in the front current downstream of the Lofoten Basin is continuing as the western branch of the West Spitsbergen Current and re-circulates in the Nordic Seas, while the slope current provides AW to both the Barents Sea and the eastern branch of the West Spitsbergen Current, which enters the Arctic interior through the Farm Strait [*Walczowski and Piechura,* 2011]. The crossover flows upstream of the Lofoten Basin, demonstrated herein, shows that the source of Atlantic Water to the Barents Sea and Arctic is not only the Faroe-Shetland inflow but to some extent also the Iceland-Faroe inflow. Furthermore, we have shown that a strengthening of the front current (Figure 8) increases the flow of AW from the front current to the slope current. Thus, considering the significant influence of AW on the sea ice cover in the Barents Sea [*Sandø et al.,* 2010; *Årthun et al.,* 2012] and near Svalbard [*Walczowski and Piechura,* 2009], an intensification of the front current may play a larger role for the Arctic Ocean climate than previously assumed.

5. Summary

This study demonstrates the usefulness of altimeter derived surface velocities for monitoring long term variability in the subsurface circulation of Atlantic Water in the

Nordic Seas. The variability in the surface velocities in the Norwegian Sea is found to be representative of the subsurface Atlantic Water flow, and the relationship is more pronounced in the slope current. Compared to the front current, there is large variability in the amount of Atlantic Water transported pole-ward by the slope current. In the Norwegian Sea, there is a general spin up of the surface circulation during winter with the exception of the flow over the Mohn Ridge, which has a maximum in summer due to more buoyant waters in the western Lofoten Basin at that time. Four major flows connecting the front current and the slope current are identified. The major factors influencing these are topographic steering, surface winds and buoyancy loss. A strengthening of the front current upstream of the Lofoten Basin is associated with a larger eastward flow of Atlantic Water towards the slope current, which also increases the probability of warm Atlantic Water from the front current to enter the Barents Sea and Arctic Ocean. Thus, the features revealed herein, directly implies that the Iceland Faroe inflow of Atlantic Water has more importance for the Barents Sea and Arctic Ocean than previously assumed, and that we cannot consider the two branches of northward flowing Atlantic water in the Nordic Seas as two independent flows.

Acknowledgements

This research was supported by the European Union and Norwegian Research Council through the projects MONARCH-A (grant 242446), BIAC, NORCLIM, and DECCEN. The altimeter products were produced by Ssalto/Duacs and distributed by *Aviso*, with support from *CNES* (http://www.aviso.oceanobs.com/duacs/). The hydrographic data were provided by the Marine Research Institute, Iceland; Institute of Marine Research, Norway; the Faroese Fisheries Laboratory and Geophysical Institute, University of Bergen, Norway through the NISE project. We thank Kjell Arild Orvik and Bogi Hansen for providing the Svinoy current-meter data and Faroe Current volume transport data respectively. The work is partly funded by the Centre for Climate Dynamics and is publication no. AXXX from the Bjerknes Centre for Climate Research.

References

Andersson, M., K. A. Orvik, J. H. LaCasce, I. Koszalka, and C. Mauritzen (2011), Variability of the Norwegian Atlantic Current and associated eddy field from surface drifters, *J. Geophys. Res.,116,* C08032, doi:10.1029/2011JC007078.

Chaigneau, A., A. Gizolme, and C.Grados (2008), Mesoscale eddies off Peru in altimeter records: Identification algorithms and eddy spatiotemporal patterns, *Prog. Oceanogr., 79,* 106–119, doi:10.1016/j.pocean.2008.10.013.

Chelton, D. B. (1983), Effects of sampling errors in statistical estimation*, Deep Sea Res., Part A, 30*, 1083–1103.

Ducet, N., P. Y. LeTraon, and G. Reverdin (2000), Global high-resolution mapping of ocean circulation from TOPEX/Poseidon and ERS-1 and 2, *J. Geophys. Res.*, *105*, 19477–19498.

Eldevik, T., J. E. Ø. Nilsen, D. Iovino, K. A. Olsson, A. B. Sandø, and H. Drange (2009), Observed sources and variability of Nordic seas overflow**,** *Nat. Geosci.*, *2*, 406-410, doi: 10.1038/ngeo518.

Furevik, T. (2001), Annual and interannual variability of Atlantic Water temperatures in the Norwegian and Barents Seas: 1980-1996, *Deep Sea Res.*, *Part I*, *48* (2), 383-404.

Furevik, T., M. Bentsen, H. Drange, J. A. Johannessen and A. Korablev (2002), Temporal and spatial variability in the sea surface salinity in the Nordic Seas, *J. Geophys. Res.*, 107(C12),8009, doi: 10.1029/2001JC001118.

Furevik, T., and J. E. Ø. Nilsen (2005), Large-Scale Atmospheric Circulation Variability and its Impacts on the Nordic Seas Ocean Climate - a Review, *in The Nordic Seas: An Integrated Perspective, Oceanography, Climatology, Biogeochemistry and Modeling,* edited by H. Drange, T. Dokken, T. Furevik, R. Gerdes, and W. Berger, pp. 105-136, AGU Geophysical Monograph Series.

Furevik, T., C. Mauritzen, and R. Ingvaldsen (2007), The Flow of Atlantic Water to the Nordic Seas and Arctic Ocean, in Arctic-Alpine Ecosystems and People in a Changing Environment, edited by J.B. Ørbæk, R Kallenborn, I Tombre, E Nøst Hegseth, S Falk-Petersen, A.H. Hoel, *Springer Verlag*, pp 123-146.

Gascard, J. C., and K. A. Mork (2008), Climatic importance of large scale and mesoscale circulation in the Lofoten Basin deduced from lagrangian observations during ASOF, *in Arctic–Subarctic Ocean Fluxes: Defining the*

Role of the Northern Seas in Climate, edited by R. R. Dickson, J. Meincke, and P. Rhines, pp. 131-143, Springer, New York.

Hansen, B., and S. Østerhus, S (2000), North Atlantic – Nordic Seas Exchanges, *Prog. Oceanogr.,* 45, 109–208.

Hansen. B., S. Østerhus, H. Hátún, R. Kristiansen, and K. M. H. Larsen (2003), The Iceland-Faroe inflow of Atlantic water to the Nordic Seas, *Prog. Oceanogr.,* 59, 443-474.

Hansen. B., H. H´at ´un, R. Kristiansen, S. M. Olsen, and S. Østerhus (2010), Stability and forcing of the Iceland-Faroe inflow of water, heat, and salt to the Arctic, *Ocean Sci., 6*, 1013–1026.

Helland-Hansen, B., and F. Nansen (1909), The Norwegian Sea: its physical oceanography based upon the Norwegian Researches 1900–1904, *Report on Norwegian Fishery and Marine Investigation, vol. II.* The Royal Department of Trade, Navigation and Industries, Mallingske, Kristiania, 390 pp.

Høydalsvik. F., C. Mauritzen, K. A. Orvik, J. H. LaCasce, C. M. Lee, and J. Gobat (2013), Transport estimates of the Western Branch of the Norwegian Atlantic Current from glider surveys, *Deep Sea Res.*, *Part 1*, *75*, 86-95, doi.org/10.1016/j.dsr.2013.05.005.

Isachsen, P. E., J. H. LaCasce, C. Mauritzen, and S. Häkkinen (2003), Wind-driven variability of the large-scale recirculating flow in the Nordic Seas and Arctic Ocean, *J. Phys. Oceanogr.* 33, 2534–2550.

Isachsen, P. E., C. Mauritzen, and H. Svendsen (2007), Dense water formation in the Nordic Seas diagnosed from sea surface buoyancy fluxes, *Deep Sea Res.*, *Part 1*, *54*, 22-41, doi:10.1016/j.dsr.2006.09.008.

Jakobsen, P. K., M. H. Ribergaard, D. Quadfasel, T. Schmith, and C. W. Hughes (2003), Near-surface circulation in the northern North Atlantic as inferred from Lagrangian drifters: Variability from the mesoscale to interannual, *J. Geophys. Res.,108*(C8), 3251, doi:10.1029/2002JC001554.

Koszalka. I., J.H. LaCasce , M. Andersson , K.A. Orvik , C. Mauritzen (2011) Surface circulation in the Nordic Seas from clustered drifters, *Deep Sea Res., Part 1., 58*, 468-485, doi:10.1016/j.dsr.2011.01.007.

Koszalka. I., J. H. LaCasce, and C.Mauritzen (2013), In pursuit of anomalies—Analyzing the poleward transport of Atlantic Water with surface drifters, *Deep Sea Res., Part II., 85*, 96-108, doi.org/10.1016/j.dsr2.2012.07.035.

LeTraon, P. Y., and F. Ogor (1998), ERS-1/2 orbit improvement using TOPEX/Poseidon: The 2 cm challenge, *J. Geophys. Res.,103*, 8045–8057.

Lumpkin, R., and Z. Garraffo (2005), Evaluating the Decomposition of Tropical Atlantic Drifter Observations, *J. Atmos. Ocean. Tech., 22*, 1403-1415.

Mauritzen, C. (1996), Production of dense overflow water feeding the North Atlantic across the Greenland-Scotland Ridge. Part 1: Evidence of revised circulation scheme, *Deep Sea Res.*, *Part 1,43*, 769– 806.

Medhaugh. I., H. R. Langehaug, T. Eldevik, T. Furevik, and M. Bentsen (2011), Mechanisms for decadal variability in a simulated Atlantic Meridional Overturning Circulation, *Clim. Dyn.,* doi: 10.1007/s00382-011-1124-z.

Mohn, H. (1887), The Northern Ocean, its Depths, Temperature and Circulation. The Norwegian North-Atlantic Expedition 1876-1878. Christiania, 1887 (in Norwegian).

Mork, K. A., and Ø. Skagseth (2005), Annual Sea Surface Height Variability in the Nordic Seas, *The Nordic Seas: An Integrated Perspective, AGU Geophysical Monograph Series*, *158*, 51-64.

Mork, K. A., and Ø. Skagseth (2010), A quantitative description of the Norwegian Atlantic Current by combining altimetry and hydrography, *Ocean Sci., 6*, 901–911.

Nilsen, J. E. Ø., and E. Falck (2006), Variation of mixed layer properties in the Norwegian Sea for the period 1948–1999, *Prog. Oceanogr., 70*, 58–90, doi:10.1016/j.pocean.2006.03.014.

Nilsen, J. E. Ø., and F. Nilsen (2007), The Atlantic Water Flow along the Vøring Plateau: Detecting Front Structures in Oceanic Station Time Series, *Deep Sea Res.*, *Part 1, 54(3)*, 297-319, doi:10.1016/j.dSV.2006.12.012.

Nilsen, J. E. Ø., H. H´at´un, K. A. Mork, and H. Valdimarsson (2008), The NISE Data Set. *Technical Report 08-01*, Faroese Fisheries Laboratory, Box 3051, T´orshavn, Faroe Islands.

Orvik, K. A., Ø. Skagseth, and M. Mork (2001), Atlantic inflow to the Nordic Seas. Current structure and volume fluxes from moored current meters, VM-ADCM and SeasSoar-CTD observations, *Deep Sea Res, Part I, 48*, 937-957.

Orvik, K. A., and P. Niiler (2002), Major pathways of Atlantic water in the northern North Atlantic and Nordic Seas toward Arctic, *Geophys. Res.Lett.,* 29(19), 1896, doi:10.1029/2002GL015002.

Orvik, K. A., and Ø. Skagseth (2003), Monitoring the Norwegian Atlantic slope current using a single moored current meter, *Cont. Shelf. Res., 23*, 159–176.

Orvik, K. A., and O. Skagseth (2005), Heat flux variations in the eastern Norwegian Atlantic Current toward the Arctic from moored instruments, 1995-2005, *Geophy. Res. Lett.*, *32*, L14610, doi:10.1029/2005GL023487.

Poulain, P. M., A. Warn-Varnas, and P. P. Niiler (1996), Near-surface circulation of the Nordic seas as measured by Lagrangian drifters, *J. Geophys. Res.*, *101(C8)*, 237–258.

Read, J., and R. Pollard (1992), Water Masses in the Region of the Iceland–Faroes Front, *J. Phys. Oceanog,.* 22 (11), 1365–1378.

Richter, K., T. Furevik, and K. A. Orvik (2009), Effect of wintertime low-pressure systems on the Atlantic inflow to the Nordic seas, *J. Geophys. Res.,* 114, doi:10.1029/2009JC005392, 2009.

Richter, K., O. H. Segtnan, and T. Furevik (2012), Variability of the Atlantic inflow to the Nordic Seas and its causes inferred from observations of sea surface height, *J. Geophys. Res.,* 117, C04004, doi:10.1029/2011JC007719.

Rio, M. H., and F. Hernandez (2004), A mean dynamic topography computed over the world ocean from altimetry, in situ measurements, and a geoid model, *J. Geophys. Res*., *109*, C12032, doi:10.1029/2003JC002226.

Rio, M. H., S. Guinehut, and G. Larnicol (2011), New CNES-CLS09 global mean dynamic topography computed from the combination of GRACE data, altimetry, and in situ measurements, *J. Geophys. Res.,*116, C07018, doi: 10.1029/2010JC006505.

Rossby, T., M. Prater, and H. Søiland (2009), Pathways of inflow and dispersion of warm waters in the Nordic Seas, *J. Geophys. Res.*, *114*, C04011, doi:10.1029/2008JC005073.

Sandø, A. B., and T. Furevik (2008), Relation between the wind stress curl in the North Atlantic and the Atlantic inflow to the Nordic Seas, *J. Geophys. Res., 113*, C06028, doi:10.1029/2007JC004236.

Sandø, A. B., J. E. Ø. Nilsen, Y. Gao, and K. Lohmann (2010), The importance of heat transports and local air-sea heat fluxes for the Barents Sea climate variability, *J. Geophys. Res.*, 115, C07013, doi:10.1029/2009JC005884.

Sandø, A.B., J. E. Ø. Nilsen, T. Eldevik , M. Bentsen (2012), Mechanisms for variable North Atlantic-Nordic Seas exchanges, J. Geophys. Res., *117*, C07013, doi:10.1029/2009JC005884.

Schlitzer, R. (2000) Electronic Atlas of WOCE hydrographic and tracer data now available, *Eos Trans. AGU*, *81(5),* 45.

Segtnan, O. H., T. Furevik, and A. D. Jenkins (2011), Heat and freshwater budgets of the Nordic seas computed from atmospheric reanalysis and ocean observations, J. Geophys. Res., 116, C11003, doi:10.1029/2011JC006939.

Schaeffer, P., Y. Faugere, J. F. Legeais, N. Picot, and E. Bronner (2012), The CNES-CLS11 global mean sea surface computed from 16 years of satellite altimeter data, *Mar. Geod*., doi:10.1080/01490419.2012.718231.

Skagseth, Ø. and K. A. Orvik (2002), Identifying fluctuations in the Norwegian Atlantic Slope Current by means of empirical orthogonal functions, *Cont. Shelf Res., 22,* 547–563, 2002.

Skagseth. Ø., K. A. Orvik, and T. Furevik (2004), Coherent variability of the Norwegian Atlantic slope current determined by using TOPEX/ERS altimeter data, *Geophys. Res. Lett., 31*, L14304, doi:10.1029/2004GL020057.

Skagseth, Ø., T. Furevik, R. Ingvaldsen, H. Loeng, K. A. Mork, K. A. Orvik, and V. Ozhigin (2008), Volume and heat transports to the Arctic Ocean via the Norwegian and Barents Seas, in Arctic - Subarctic Ocean Fluxes (R. Dickson, J. Meincke, and P. Rhines, Eds.) Springer Verlag, 25-64.

Volkov, D. L. and I. Pujol (2012), Quality assessment of a satellite altimetry data product in the Nordic Seas, Barents, and Kara seas, *J. Geophys. Res.,* 117, 1978-2012, doi: 10.1029/2011JC007557.

Walczowski, W., and J. Piechura, 2009: Warming of the west Spitsbergen Current and sea ice north of Svalbard, *Oceanologia*, 51 (2), 147–164.

Walczowski. W and J. Piechura (2011), Influence of the West Spitsbergen Current on the local climate, *Int. J. Climatol.* 31: 1088–1093, doi: 10.1002/joc.2338.

Walin, G., G. Brostrom, J. Nilsson, and O. Dahl (2004), Baroclinic boundary currents with downstream decreasing buoyancy: A study of an idealized Nordic Seas system, *J. Mar. Res.,* 62,517–54.

Årthun, M., T. Eldevik, L. H. Smedsrud, Ø. Skagseth, and R. B. Ingvaldsen (2012), Quantifying the Influence of Atlantic Heat on Barents Sea Ice Variability and Retreat, *J. Climate*, *25*, 4736–4743, doi:10.1175/JCLI-D-11-00266.1.

PAPER 2

Processes influencing the dense water formation in the Lofoten Basin

Roshin P. Raj, J. Even Ø. Nilsen (2013)

Submitted to Journal of Geophysical Research-Oceans

Processes influencing the dense water formation in the Lofoten Basin

Roshin. P. Raj [1, 2, 3] and J. Even Ø. Nilsen [1,3]

[1] Nansen Environmental and Remote Sensing Center, Thormøhlensgate 47, Bergen, Norway
[2] Geophysical Institute, University of Bergen, Allegaten 70, Bergen, Norway
[3] Bjerknes Centre for Climate Research, Allegaten 70, Bergen, Norway

Abstract

The Lofoten Basin holds the largest volume of Atlantic Water in the Nordic Seas. The variability of advective flow, eddy activity, and heat loss, all influencing dense water formation in the Lofoten Basin, are studied using a range of satellite, drifter, re-analysis, and hydrographic datasets. The Lofoten Basin is shown to consist of two almost equally sized but different regions in terms of hydrography, convection depth, and eddy activity. There are two distinct eddy active regions with different annual cycles, on either side of the basin, and evidence for eddy propagation from the eastern to the western part of the basin. Altimeter and drifter datasets show two local maxima in the two branches of the Norwegian Atlantic Current, on both sides of the basin. Also, intrusion of Atlantic Water from the south into the central Lofoten Basin is found. The temporal variability in the density of Atlantic Water in the Lofoten Basin during the past six decades is dominated by the variability in temperature, and governed by North Atlantic Water advected into the basin and the heat loss from the basin. Finally, we confirm the Atlantic Water transformation in the Lofoten Basin as an integral part of the cyclonic overturning loop in the Nordic Seas, with a possible more direct link to the Faroe Shetland Channel overflow.

Keywords: Norwegian Atlantic Current, dense water formation, mesoscale eddies, heat loss, mixed layer depth, eddy kinetic energy.

1. Introduction

The Lofoten Basin, situated in the Norwegian Sea (Figure 1) is the largest heat reservoir in the Nordic Seas since it is occupied by Atlantic Water (AW) down to a depth of 800 m [*Blindheim and Rey*, 2004]. The Lofoten Basin, which is also the region of highest eddy activity in the Nordic seas [*Poulain et al.,* 1996; *Köhl,* 2007], has a net mean heat loss of ~70 Wm^{-2} with a maximum above 100 Wm^{-2} [*Mauritzen,* 1996b; *Segtnan et al.,* 2011] resulting in strong surface cooling and buoyancy loss. The surface circulation of the Lofoten Basin has been studied earlier using drifters and floats [*Poulain et al.,* 1996; *Jakobsen et al.,* 2003a,b; *Rossby et al.,* 2009a; *Koszalka et al.,* 2011; *Andersson et al.,* 2011]. According to the current understanding, the heat and salt is transported into the Lofoten Basin from the Norwegian Atlantic Current via mesoscale eddies since there is no mean flow into the basin [*Andersson et al.,* 2011]. The Norwegian Atlantic Current is basically a two branch current system of which the eastern branch follows the shelf edge as a barotropic slope current, while the western branch is considered to be a topographically guided jet current [*Poulain et al.,* 1996; *Orvik and Niiler,* 2002; *Skagseth and Orvik,* 2002; *Orvik and Skagseth,* 2003]. Here we use the terms "slope current" and "front current" for the eastern and western branches of the Norwegian Atlantic Current, respectively. The Lofoten Basin is bordered by the front current on the western side and the slope current on the eastern side [*Orvik and Niiler*, 2002; *Mork and Skagseth*, 2010].

The Norwegian Atlantic Current, originating from inflowing North Atlantic Water (NAW), and the returning overflow waters to the deep Atlantic Ocean forms the northern limb of the Atlantic Meridional Overturning Circulation [AMOC; *Eldevik et al.,* 2009]. Overflow waters from the Nordic Seas and Arctic Ocean is the main source of the North Atlantic Deep Water [*Dickson and Brown,* 1994] and earlier studies have shown the gradual transformation of AW along its advective path in the Nordic Seas to play a major role in the formation of overflow waters [*Mauritzen,* 1996a,b; *Isachsen et al.,* 2007; *Eldevik et al.,* 2009] contradicting the traditional claim that the main overflow waters originate in the Greenland Basin. This again underlines the

importance of water mass transformation in the Lofoten Basin, since it is situated in the advective path of AW in the Nordic Seas and the Arctic.

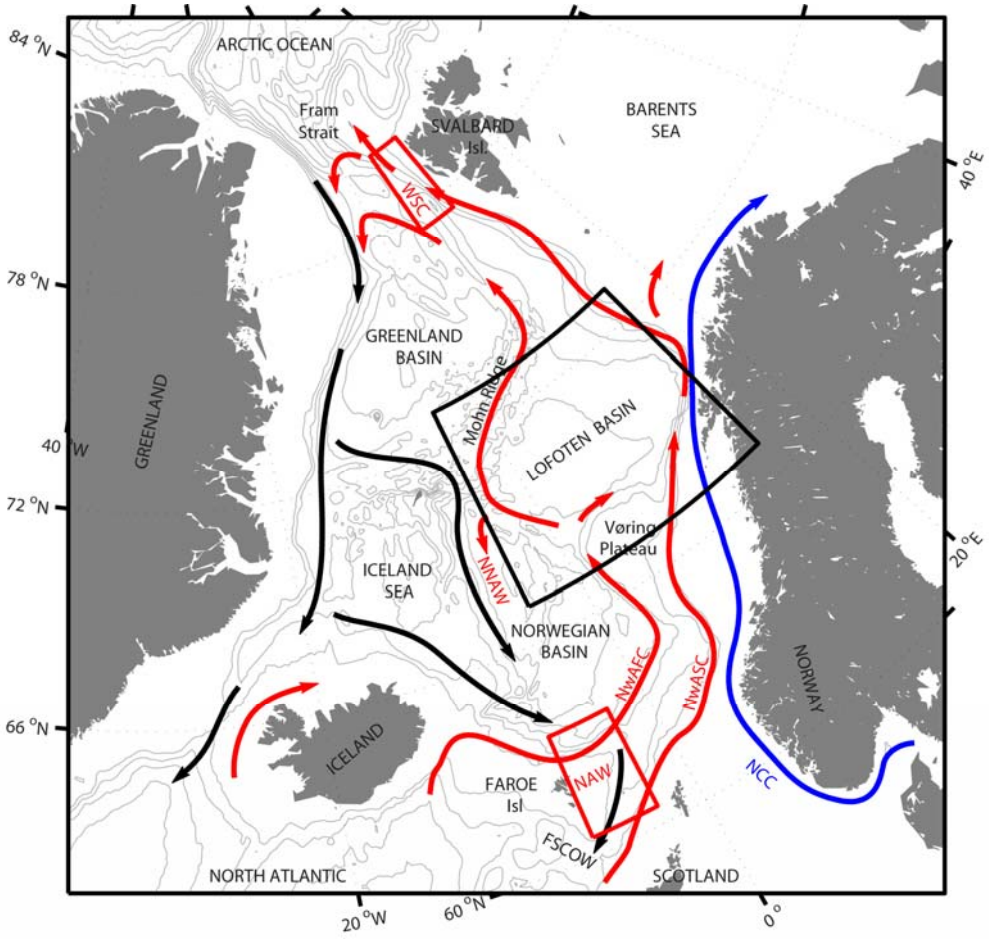

Figure 1. The Nordic Seas with schematic pathways indicating the overturning circulation from warm inflowing Atlantic Water in the surface (red) to cold and dense overflows to the deep North Atlantic (black). The Norwegian Atlantic slope current (NwASC) and Norwegian Atlantic front current (NwAFC) are represented by the longer red arrows. The fresh Norwegian Coastal Current (NCC) is indicated in blue. See *Furevik and Nilsen* [2005] and *Eldevik et al.* [2009] for details. Grey isobaths are drawn for every 600 m and black frame indicates the area shown in Figures 2-6 and 9. The red frames show regions from which time series for the North Atlantic Water inflow (NAW) and the West Spitsbergen Current (WSC) are extracted in this study. The overflow waters at the Faroe Shetland Channel (FSCOW) and the Norwegian North Atlantic Water (NNAW) are also indicated.

It is also important to note that the bulk of light to dense water mass transformation occurring in the Nordic Seas takes place in the deep Lofoten Basin [*Isachsen et al.,* 2007]. The residence time of AW circulating in the Lofoten Basin is larger than any other region in the Nordic Seas due to the deep cyclonic recirculation prevailing there which in turn has the important effect of storing large quantities of AW [*Orvik*, 2004;

Gascard and Mork, 2008]. The longer residence time of AW in the Lofoten Basin combined with strong atmospheric cooling results in loss of heat from AW before it reaches the Arctic proper. The AW entering the Lofoten Basin and associated heat loss thus has potential importance for the dense water formation in the AMOC [*Orvik*, 2004; *Eldevik et al.,* 2009]. Any process influencing the dense water formation in the basin can alter the AW downstream, thereby influencing AMOC.

The dense water formation in the Lofoten Basin can be influenced by surface circulation, eddy activity, and heat loss as will be described below. Surface circulation of the Lofoten Basin plays an important role in eddy shedding [*Gascard and Mork*, 2008; *Köhl,* 2007]. These eddies carry heat into the basin from the east, thereby balancing the heat loss in the basin interior [*Rossby et al.,* 2009b; *Spall*, 2010, 2011]. The eddies also carry fresh coastal waters [*Gascard et al.,* 2004] influencing the salinity of the basin from the east. The heat loss to the atmosphere represents cooling and densification of AW in the basin. A combined influence of all these three factors results in variability of AW temperature and salinity and governs the variability in dense water formation in the Lofoten Basin. The main objective of this study is to examine the surface circulation, eddy activity, and heat loss of the Lofoten Basin as well as to investigate their role on the spatial distribution and temporal evolution of dense water formation in the basin. A suite of different high resolution satellite datasets, drifter, reanalysis, and long term hydrographic datasets are used to address this objective. The outline of the paper is as follows: In Section 2 we describe the different data sets and methods used in this study, and in Section 3 results of our analysis are presented. In Section 4, we discuss the results presented and the paper is summarized and concluded in Section 5.

2. Data and Methods

2.1. Altimeter data

High-resolution weekly sea level anomalies (SLA) during the past 16 years (1995-2010) are used to study the surface circulation and eddy activity of the Lofoten Basin. The SLA fields, corrected for the inverted barometer effect, tides, and tropospheric

effects [*Le Traon and Ogor,* 1998] are based on merged Envisat and ERS-1 and 2 data [*Ducet et al.,* 2000; *Volkov and Pujol,* 2012]. In the Lofoten Basin, the SLA fields provided are of roughly 12 km resolution. In this study, we have used the state of the art Mean Dynamic Topography (MDT), the CNES-CLS09 dataset [*Rio et al.,* 2011]. This MDT is based on altimetry, in situ measurements, surface buoys, Argo floats and Gravity Recovery and Climate Experiment (GRACE) geoid model using a combination of direct and synthetic methods [*Rio and Hernandez, 2004*]. The errors associated with the estimation of CNES-CLS09 MDT are provided together with the MDT dataset, and in the Lofoten Basin the errors are less than 1.0 cm (not shown). Weekly absolute dynamic topography (ADT) is the sum of MDT and SLA. *Volkov and Pujol* [2012] evaluated this ADT dataset in the Norwegian Sea and found that the altimeter data can be successfully used to study the variability of the surface circulation in the region.

Absolute surface geostrophic velocities are computed from weekly absolute dynamic topography (ADT) gridded data, using the geostrophic relation:

$$u_s = \frac{-g}{f}\frac{\partial ADT}{\partial y}, \tag{1}$$

$$v_s = \frac{g}{f}\frac{\partial ADT}{\partial x}, \tag{2}$$

where x and y are the longitudinal and latitudinal directions, u_s and v_s are the respective components of velocity, g is the acceleration due to gravity, and f is the coriolis parameter. *Mork and Skagseth* [2010] showed that the absolute velocities used in this study are in good agreement with independent current measurements at the Svinøy section in the Norwegian Sea. Recently, *Raj et al.* [2013a, submitted], showed that the monthly variability (de-trended and de-seasoned; 1995-2005) in the current meter velocities in the core of the slope current at Svinøy section is also highly correlated with the altimeter derived velocities.

Eddy Kinetic Energy (EKE) is calculated on a weekly basis using the relation [*Chaigneau et al.,* 2008]:

$$EKE=\frac{u'^2+v'^2}{2}, \quad (3)$$

where u' and v' are geostrophic velocity anomalies determined using SLA instead of ADT in equations (1) and (2).

Mean fields of velocity (monthly means and climatologies) are based on the weekly velocity components found by equations (1) and (2), and the corresponding error estimates for each component are $s_m=s/(N-1)^{1/2}$, where s is the standard deviation for the N weekly data points the mean is based on. Seasonal mean EKE fields and error estimates are calculated the same way as for velocity. Annual climatologies of regional EKE are made from weekly spatial averages.

2.2. Hydrographic data

Hydrographic data used in this study are from the long term (1949-2008) hydrographic NISE database [Norwegian Iceland Seas Experiment; *Nilsen et al.,* 2008]. The NISE dataset consists of both CTD and bottle data of which the former is decimated up to 5 m.

Winter mixed layer depth (MLD) climatology (1949-2008; 0.5° x 1° grid) for the Norwegian Sea is calculated by a finite density difference method, following *Nilsen and Falck* [2006]. A difference criterion between the surface density and MLD-base density is calculated by subtracting a temperature of 0.8°C from the surface value, and applied to individual density profiles, before calculating the climatological mean MLD. In the same way as the maximum gradient method, a finite difference method finds the pycnocline, and not the depth of the homogeneous layer per se.

Steric heights from hydrographic climatologies (0.5° x 1° grid) are calculated according to *Siegismund et al.* [2007], where the steric height is referenced to 500 m depth, and a constant density ρ_0 from salinity of 35 and temperature of 0°C. More information on the concept and application of steric height is given by *Tomczak and Godfrey* [2003].

Annual time series of AW properties in the Atlantic inflow (i.e. NAW) and the Lofoten Basin (regions shown in Figure 1 and 6a, respectively) are calculated from the

NISE data using the criteria T≥3ºC and S≥35. In this study, the Atlantic Water in the West Spitsbergen Current (WSC; Figure 1) in the Fram Strait is defined using the criteria T>2 and S>34.9 [*Beszczynska-Moller et al.,* 2012]. Time series of annual temperatures and salinities for Norwegian North Atlantic Water [NNAW; *Read and Pollard*, 1992] are obtained from *Eldevik et al.* [2009]. All correlations are done on de-trended annual time series. The effective degrees of freedom are found according to *Chelton* [1983], i.e. taking into consideration the autocovariance of all time series. Significance levels are calculated by the standard Student's t test.

2.3. Other datasets

Climatology of Chlorophyll-a (chl-a) pigment concentration (9 km grid) are prepared from SeaWiFS chlorophyll-a concentration. Climatology of surface geostrophic velocities from drifters (1º x 1º grid) is obtained from *Lumpkin and Garraffo,* [2005].

Net heat loss from the Lofoten Basin is determined from National Centers for Environmental Predictions (NCEP) dataset [*Kalnay et al.,* 1996] using the equation

$$Qnet=(SW+LW+LH+SH), \quad (4)$$

where *SW, LW, LH* and *SH* are respectively the short wave radiation, long wave radiation, latent heat flux, and sensible heat flux (Wm^{-2}). Positive values of heat flux are directed upwards, i.e. indicating heat loss to the atmosphere.

3. Results

This section starts with the examination of the surface circulation of the Lofoten Basin. Next we address the convection in the deep Atlantic Water layer of the Lofoten Basin. This is followed by the examination of the eddy activity in the Lofoten Basin. Inter-annual variability of AW properties in the Lofoten Basin during past 60 years is presented next, followed by the examination of the variability in the heat loss of the basin. Finally, we trace AW salinity and temperature anomalies to and from the Lofoten Basin using correlation analysis in order to confirm AW of the Lofoten Basin as integral part of the overturning cyclonic loop of AW in the Nordic Seas.

3.1. Mean surface circulation of the Lofoten Basin

Winter and summer climatology of absolute geostrophic surface velocity (Figure 2a,b) reproduce the mean surface circulation of the Lofoten Basin as shown earlier [e.g., *Jakobsen et al.,* 2003a,b]. Altimeter derived surface velocities resolves imprints of the front current and the slope current bordering the western and eastern rim of the Lofoten Basin [*Orvik and Niiler,* 2002]. A clear winter intensification of the slope current and the eastward flow of the front current north of the Vøring Plateau towards the slope current is seen. The figure also shows the local intensification of the front current along the Mohn Ridge, especially in the summer.

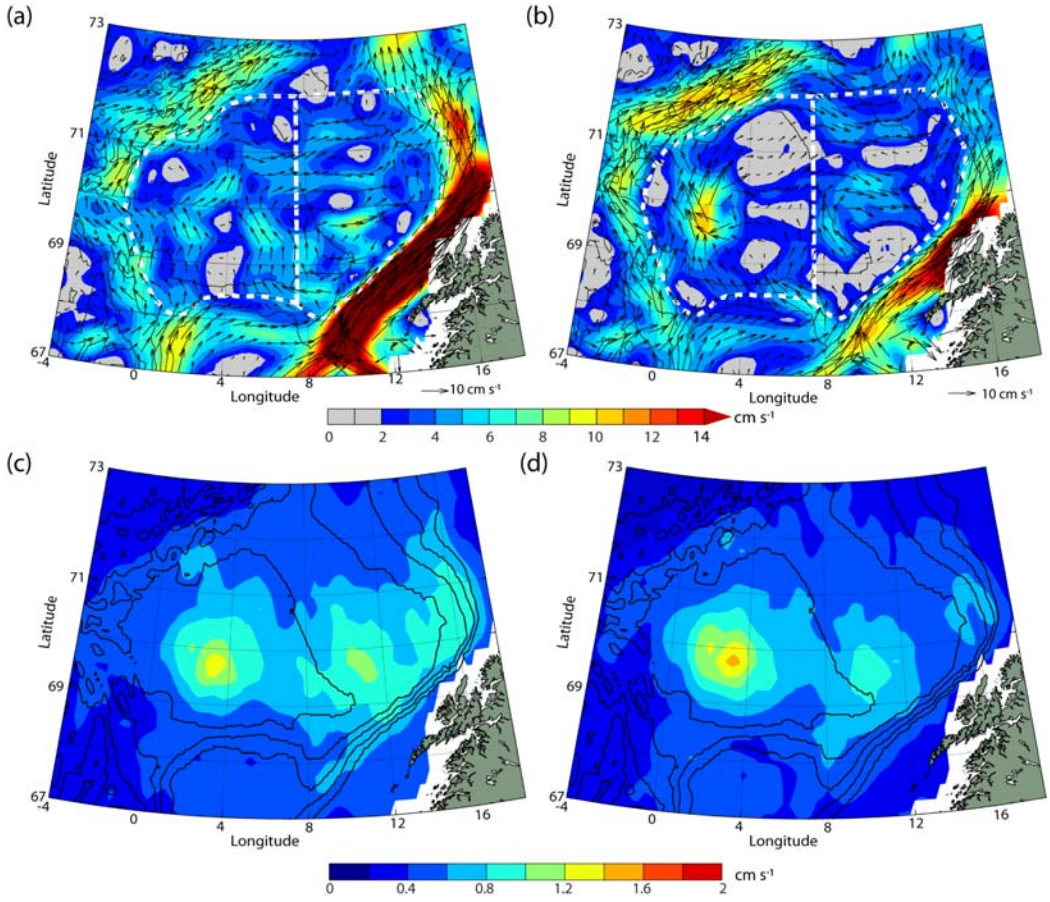

Figure 2. Climatologies (1995-2010) of absolute surface geostrophic velocities (a,b; speed in color) and errors for the speed (c,d) for winter (December-February; a,c) and summer (June-August; b, d). Black isobaths are drawn for every 600 m. The error range shown in bottom panels is chosen as the grey range in top panels. Dashed white lines in panels a and b indicate the fixed regions of western Lofoten Basin (WLB) and the eastern Lofoten Basin (ELB), also shown in Figure 6. The two regions are determined from the *overall* mean geostrophic velocity field (see Section 3.3 for details).

In addition, the two climatologies show a weak AW flow into the central Lofoten Basin (5-8ºE) from the Vøring Escarpment. This surface flow is seen to extend from the flow along the Vøring Escarpment and northward over the middle of the Lofoten Basin. The mean geostrophic velocity of this flow is in the range of 3 to 6 cm s^{-1} and is a weaker flow compared to the front current and the slope current. Notably the errors associated with mean absolute speed in the Lofoten Basin is the largest (<2 cm s^{-1}) in the deepest part of the basin (Figure 2c-d).

The annual climatology of surface geostrophic velocities obtained from surface drifters [*Lumpkin and Garaffo*, 2005] in the Lofoten Basin and the associated errors are shown in Figure 3. The drifter derived climatology shows the signature of the slope current and the front current. The local intensification of the front current over the Mohn Ridge is also seen in the drifter derived climatology of surface currents. The errors associated with the surface velocities from drifters in this region are large (3.5 to 5 cm s^{-1}), but less than 50% of the mean velocity (10 to 14 cm s^{-1}). A signature of weak mean flow from south in the eastern Lofoten Basin is also seen in the drifter data (5-8°E).

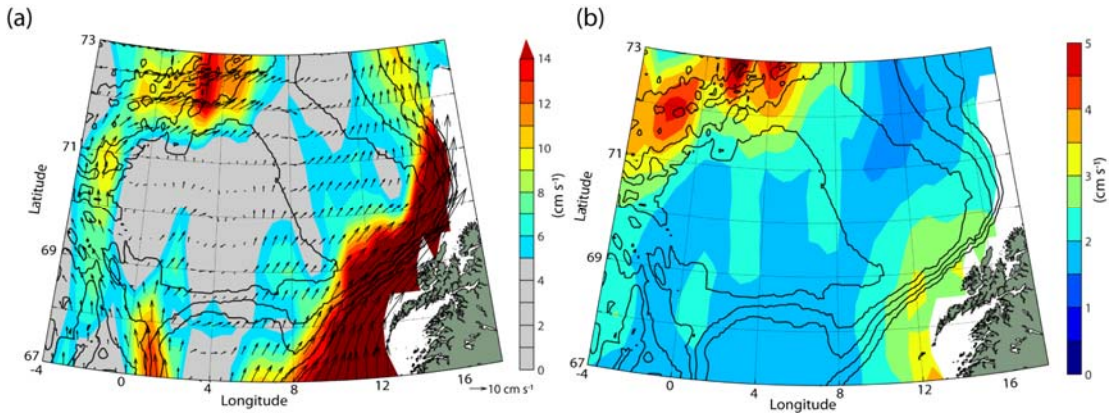

Figure 3. Climatology of (a) surface geostrophic velocities and (b) error, obtained from one degree bin surface drifter data. Black isobaths are drawn for every 600 m. The error range in panel b is chosen as the grey range in panel a.

Ocean circulation is known to influence the spatial distribution of chlorophyll [*Raj et al.,* 2010], hence climatology of chlorophyll-a concentration is used as a proxy to study the mean circulation pattern of the Lofoten Basin further (Figure 4). The spatial distribution of chl-a concentration indicates advection of high chlorophyll waters from

the Norwegian Coastal Current into the Lofoten Basin. As expected, the coastal waters have the highest chl-a concentration (>1.0 mg m^{-3}) near and in the Lofoten Basin. Infiltration of the coastal waters into the Lofoten Basin is strongest in the northeast. The figure shows a distinct difference in chl-a concentration between the eastern and western parts of the Lofoten Basin. The mean chl-a concentration of the eastern Lofoten Basin is 0.2 mg m^{-3} higher than in the western.

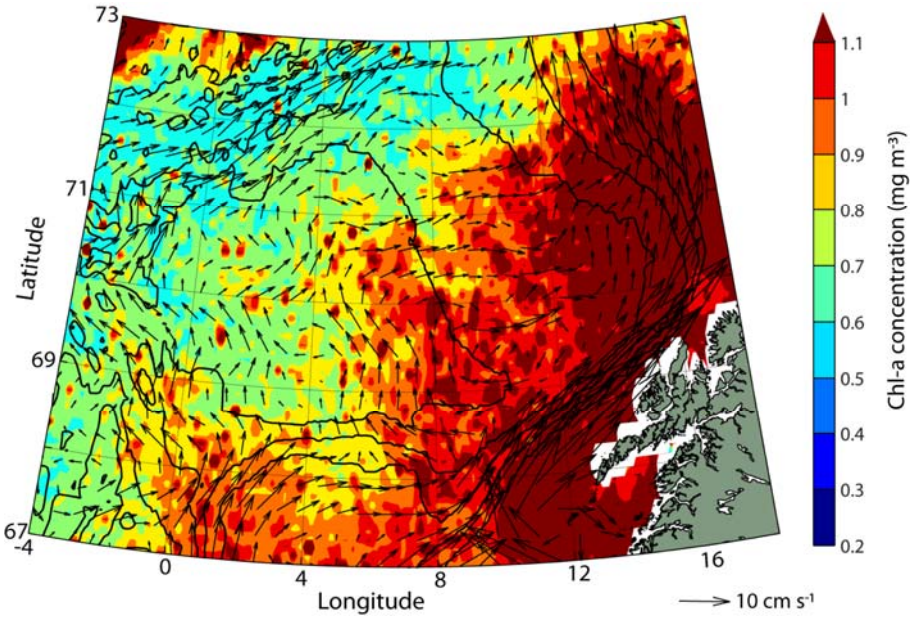

Figure 4. Climatology of SeaWiFS chlorophyll-a concentration (1997-2010; mg m^{-3}). Winter climatology (December-February; 1995-2010) of absolute geostrophic velocity is superimposed in order to indicate the mean winter flow of the Lofoten Basin. Black lines are isobaths drawn for every 600 m.

3.2. Convection in the Lofoten Basin

In order to study the convection in the Lofoten Basin, winter climatology (1949-2008) of MLD is prepared (Figure 5). The spatial distribution of winter MLD shows it to be significantly larger in the western than in the eastern Lofoten Basin. The MLD maximum in the Lofoten Basin coincides with the location of the anticyclonic vortex situated in the deepest part of the Lofoten Basin [*Köhl*, 2007; *Koszalka, et al.,* 2011; *Raj et al.,* 2013b, submitted]. The main result is a deep MLD constrained to the western Lofoten Basin, possibly by both bathymetry and water masses from the east. The winter mean MLD in the western part of the basin reaches about 550 m, while in the eastern part it reaches only about 350 m. This difference of 200 m between the

eastern and western part of the Lofoten Basin is important in terms of transformation of AW in the Lofoten Basin.

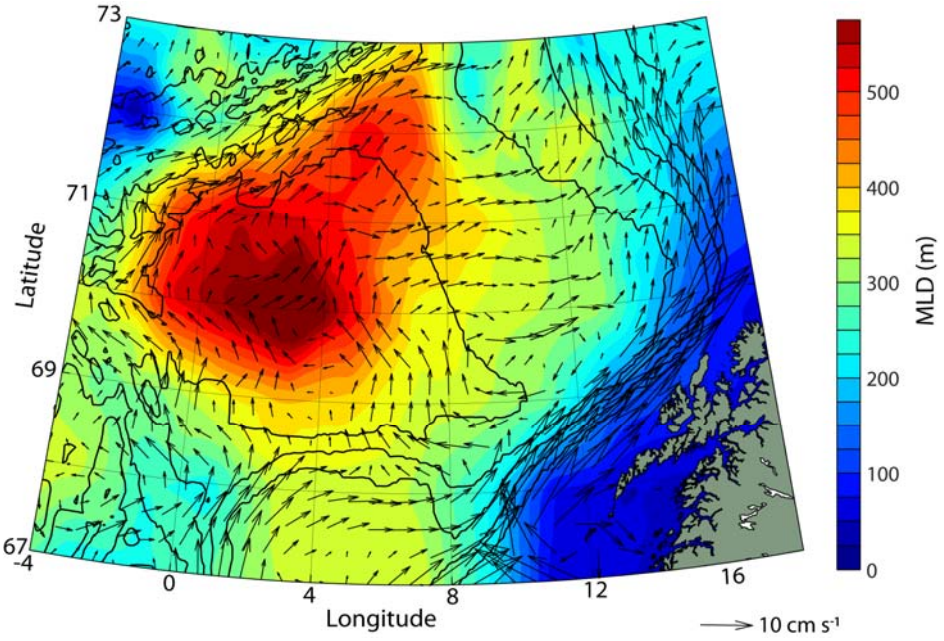

Figure 5.Winter climatology (December-February; 1949-2008) of mixed layer depth (m). Winter climatology (December-February; 1995-2010) of absolute surface geostrophic velocity from altimeter is superimposed in order to indicate the mean flow. Black lines are isobaths drawn for every 600 m.

3.3. Eddy activity in the Lofoten Basin

The Lofoten Basin is the highest eddy active region in the Nordic Seas [*Poulain et al.,* 1996] and the eddy activity of the basin is generally considered to be dominated by eddies spun from the slope current. Here, we use high resolution altimeter data in order to determine and study the spatial, seasonal and inter-annual variability of the eddy kinetic energy in the Lofoten Basin. Seasonal climatologies of EKE show two distinct regions of high eddy activity in the Lofoten Basin (> 100 cm^2 s^{-2}; Figure 6). The figure also shows connection between EKE of the two regions, and this connection is more distinct during winter and spring. Also, EKE of the northeastern part of the Lofoten Basin exhibits seasonality with maximum in winter. The MLD climatology (Figure 5), mean chl-a concentration (Figure 4) and seasonal EKE (Figure 6), all show two distinct western and eastern regions in the Lofoten Basin.

In order to conduct a detailed study, from here onwards the Lofoten Basin will be considered as two separate regions: the western Lofoten Basin (WLB) and the eastern Lofoten Basin (ELB), shown in Figure 6a). The western and eastern boundaries of the Lofoten Basin are determined from the mean geostrophic surface velocity (i.e. mean of Figure 2a and b), and the borders are selected such that the topographically steered front current and the slope current are excluded. While the Vøring Escarpment represents the southern boundary, we simply choose 72°N as the northern boundary since there is no natural meeting point of the front current and slope current, or any bathymetric northern boundary. The separation line in the middle (7.5°E), placed half way between the two high EKE regions in the Lofoten Basin (Figure 6), divides the full basin into a western and an eastern region.

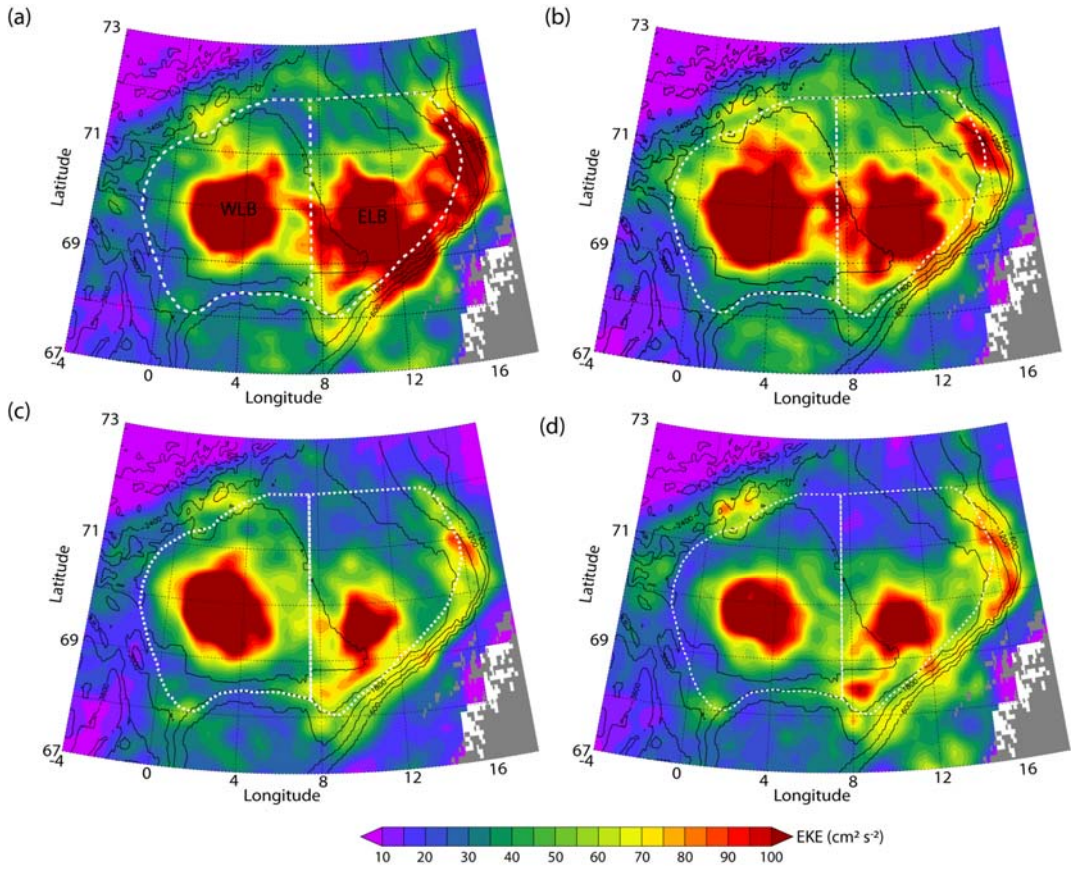

Figure 6. Seasonal climatologies of EKE ($cm^2\ s^{-2}$) for (a) December-February, (b) March-May, (c) June-August, (d) September-November. Dashed white lines indicate the western Lofoten Basin (WLB) and the eastern Lofoten Basin (ELB). Black solid lines are isobaths drawn for every 600 m.

Annual climatologies of EKE for the two regions (Figure 7a) show that while peak EKE of the eastern Lofoten Basin is during early winter, maximum EKE in the western Lofoten Basin is delayed by two months and peaks during spring. Hence, the eddy regimes on either side of the Lofoten Basin are different. Also the inter-annual variability of EKE in the two regions of the Lofoten Basin have different characteristics (Figure 7b). The western region shows stronger and more irregular variations in the level of EKE, while a more regular oscillation of 4 years period is found from spectral analysis (not shown) in the eastern region. In both regions EKE is weaker during the period 1995-1999 (~60 cm^2 s^{-2}) than during 2000-2010 (~80 cm^2 s^{-2}). The maximum in EKE of the western region during 2003 is concurring with a maximum in the strength of the anticyclonic vortex residing there [*Raj et al.,* 2013b, submitted].

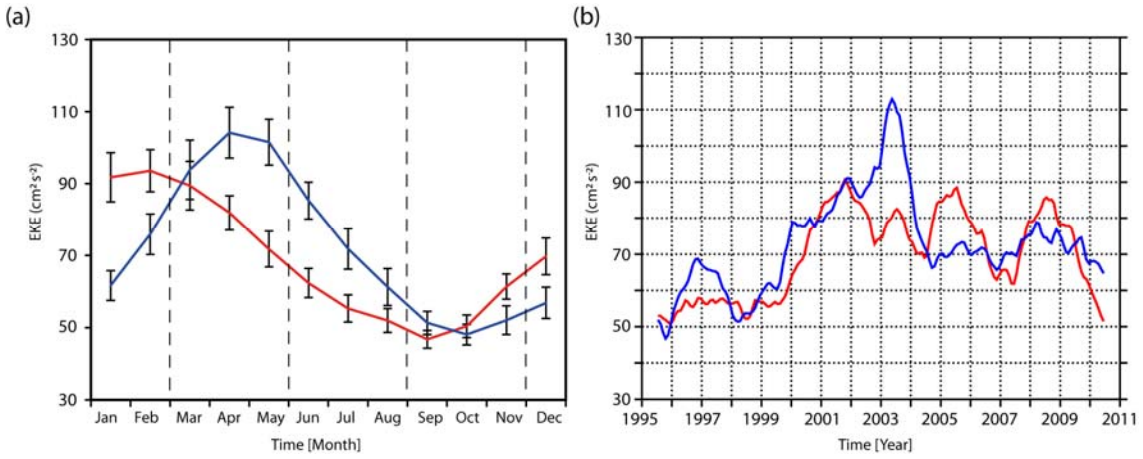

Figure 7. (a) Annual climatologies (1995-2010) and (b) inter-annual variability of EKE for the regions western Lofoten Basin (WLB; blue) and eastern Lofoten Basin (ELB; red), as defined in Figure 6. Error bars in panel a show plus minus s_m, the error of the mean. A twelve month running mean filter is applied to the monthly time series in panel b in order to remove seasonal variability. Dashed grid lines in panel a indicate the different seasons as used in Figure 6.

3.4. Atlantic Water properties in the two regions of the Lofoten Basin

Climatological (1949-2008) monthly mean salinity, temperature and density profiles from the western and eastern Lofoten Basin are shown in Figure 8. These regional average profiles show low salinity surface waters in the ELB, indicating the presence of coastal waters, in clear contrast to the western side (Figure 8a, d). The offshore advection of coastal waters into the Lofoten Basin is largest during late summer and

autumn. There is also a difference of ~1°C between the two regions in the upper 150 m (Figure 8b, e). In accordance, the density of the surface waters is lower in the eastern Lofoten Basin compared to the western. Notably, the densities of the lower AW in the Lofoten Basin (at around 400 m to 600 m) is in the range of overflow water densities [σ_θ>27.8 kg m^{-3}; *Dickson and Brown,* 1994].

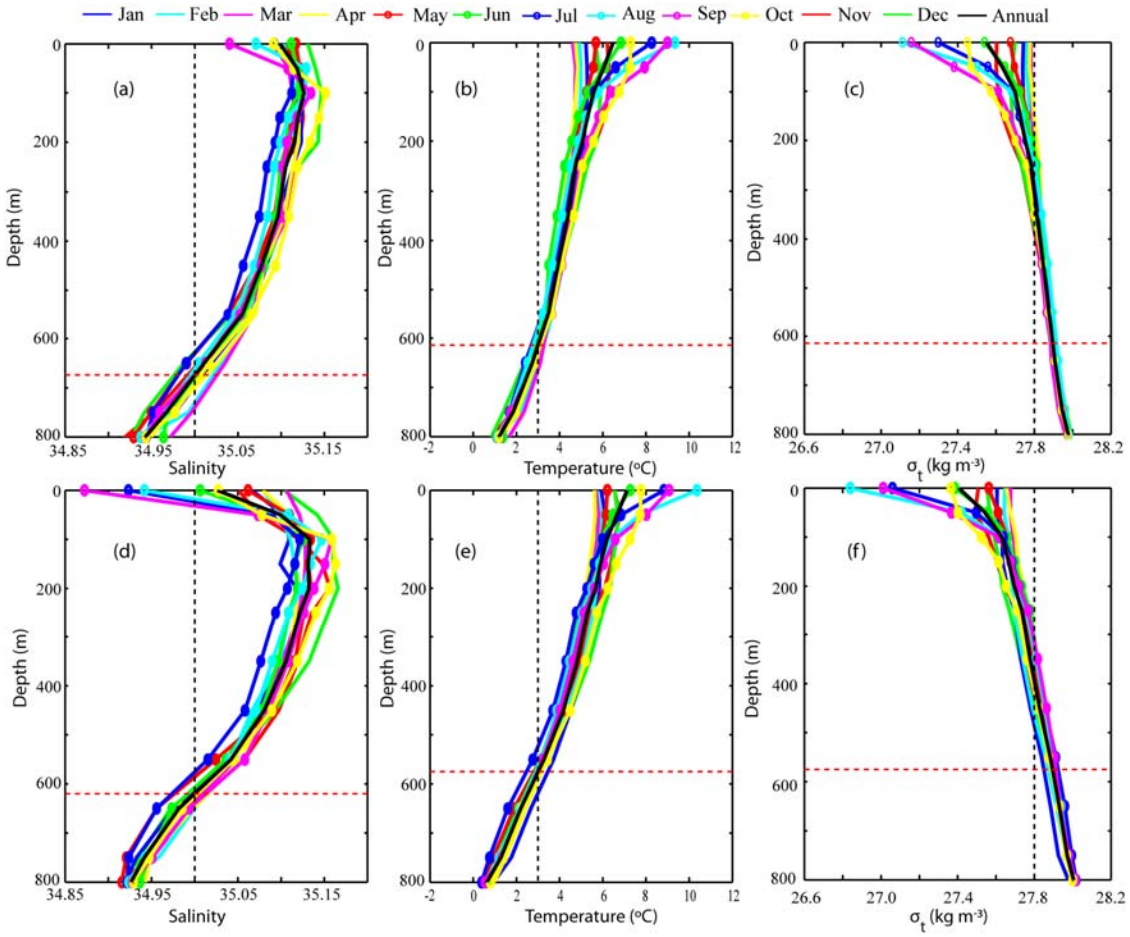

Figure 8. Mean monthly and overall mean profiles of salinity, temperature and density for the (a, b, c) western and (d, e, f) eastern Lofoten Basin. Regions are shown in Figure 6. Dashed horizontal red lines in panels (a,d) and (b,e) represents the mean depth S=35 and T=3 (shown as dashed vertical black lines), respectively. In panels c and f, the dashed horizontal lines indicate the mean Atlantic Water depth respectively in the western and eastern Lofoten Basin satisfying both criteria S≥35 and T≥3, while vertical line represent σ_t=27.8, a normal definition of overflow water densities.

The spatial distribution of steric height in the Lofoten Basin (Figure 9) shows the existence of more buoyant surface waters in the eastern compared to the western region. On average, the steric height contribution from 0-500 m varies within a range of 10-20 cm in the western and 20-30 cm in the eastern region, with a north-south

gradient alignment in the middle of the basin, most evident in winter. In winter, the flow pattern (i.e., the ADT) in the central Lofoten Basin is found to largely align itself with the steric field. Note that Figure 9 only shows the steric contribution to ADT (no barotropic component included), and thus confirms that the buoyant waters that extend to the middle basin give an effective contribution to the sea level gradient/surface geostrophic flow there. In summer, the fields are less coinciding, most likely since warm and fresh waters are more evenly spread in the shallow summer surface layer [Figure 8; *Nilsen and Falck,* 2006].

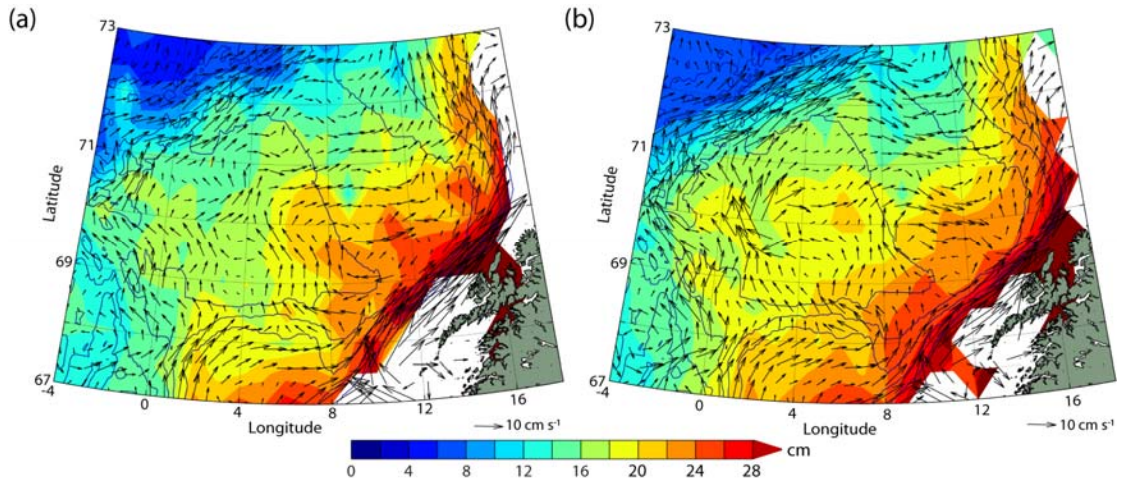

Figure 9. Observed mean (1949-2008) steric height for the 500 m reference depth during winter (December-February; a) and summer (June-August; b). Winter and summer climatologies (1995-2010) of altimeter derived absolute geostrophic velocity are superimposed on the respective panels. Blue isobaths are drawn for every 600 m.

The salinity and temperature profiles in Figure 8 show that the standard AW-definitions lies in the middle and upper part of the deep halo- and thermoclines, and thus supports the validity of these definitions also in this region. That the mean climatological MLD (Figure 5) is somewhat shallower, does not imply that mixing is not occurring throughout the AW depth, it merely indicates that mixing depths are temporally highly variable, which is reflected in the density gradient that exists throughout most of the AW column (Figure 8 c,f).

3.5. Inter-annual variability of Atlantic Water properties and heat loss in the Lofoten Basin

Inter-annual variability in depth, temperature, salinity, and density of AW inside the two regions of the Lofoten Basin (as defined in Figure 6a) during the past 6 decades is shown in Figure 10. A distinct decadal variability is present in the depth of AW inside both regions (Figure 10a). Spectral analysis of the annual time-series (not shown) revealed a more regular AW-depth oscillation of 12 years period in the western region compared to the eastern. In general, AW penetrates deeper in the western than the eastern region. The depth of AW shows a distinct shallowing to 500 m in both regions, in the years around 1980.

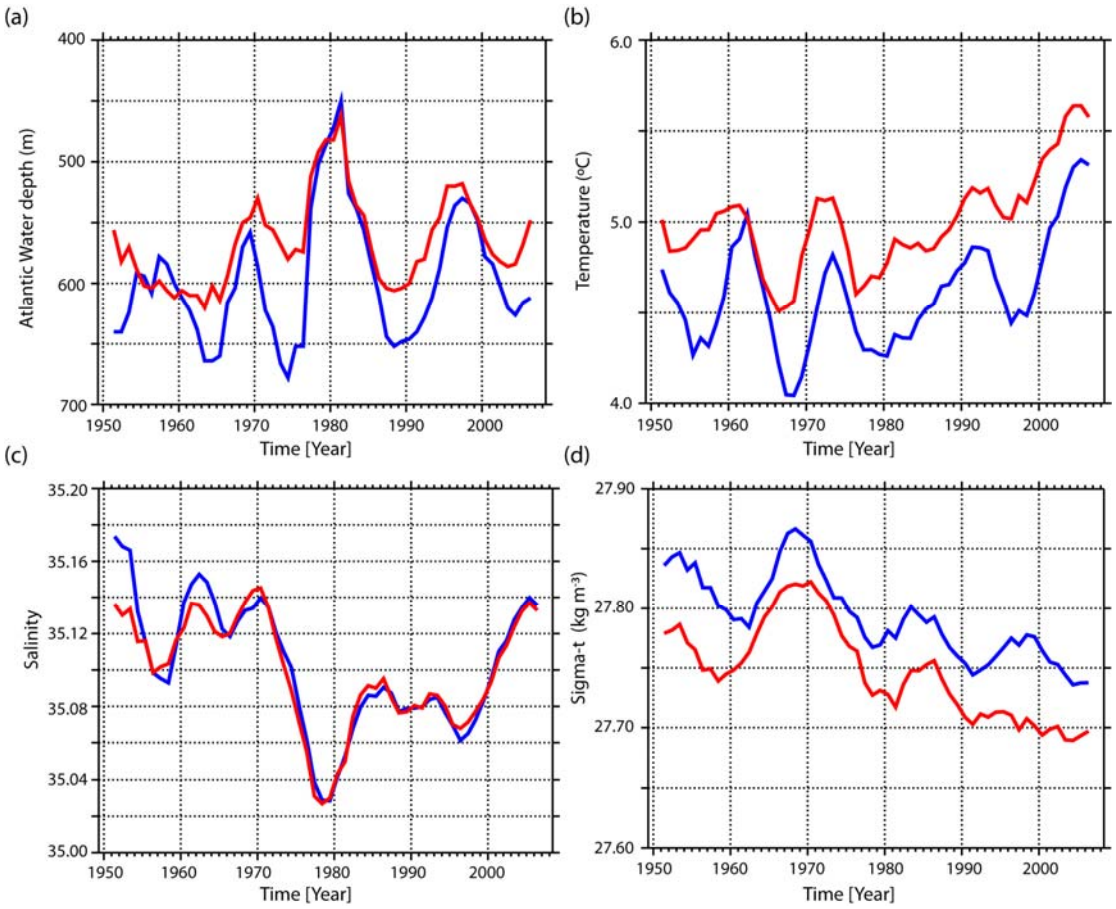

Figure 10. Long term variability in (a) depth, and (b) temperature, (c) salinity, and (d) density of the area and depth averaged Atlantic Water ($T \geq 3^{o}C$ and $S \geq 35$) in the western (blue) and eastern (red) Lofoten Basin. Regions are defined in Figure 6. A five year running mean is applied to the annual time series in all panels.

Figure 10b shows that the AW in the eastern region is warmer than the AW in the western region every year (mean difference=0.4ºC). Apart from this offset, the long

term variability in the temperature of both regions shows strong correlation (r=0.70) and a rising trend since around 1980. Unlike in temperature, there is no offset between the salinity of AW in the two regions (Figure 10c) and the correlation is stronger (r=0.91). There is a strong salinity minimum corresponding to the AW depth minimum around 1980, and after that there is a positive trend as also seen in the temperatures. Note that these results concern the full AW column, and not only the buoyant surface waters presented in Section 3.2.

The density of AW (Figure 10d) is higher in the western than in the eastern region by approximately 0.1 kg m^{-3}. Note that before the mid '70s, the density of AW in the western Lofoten Basin is either higher than or very close to overflow water densities [σ_θ>27.8 kg m^{-3}]. The AW in both regions is seen to get lighter from the 1970s. The long term variability in the densities in both regions resembles the respective temperature variability (Figure 10b,d). Strong correlations are found between the AW temperature and density of the two regions on inter-annual time scales (r_{WLB}=-0.62; r_{ELB}=-0.50).

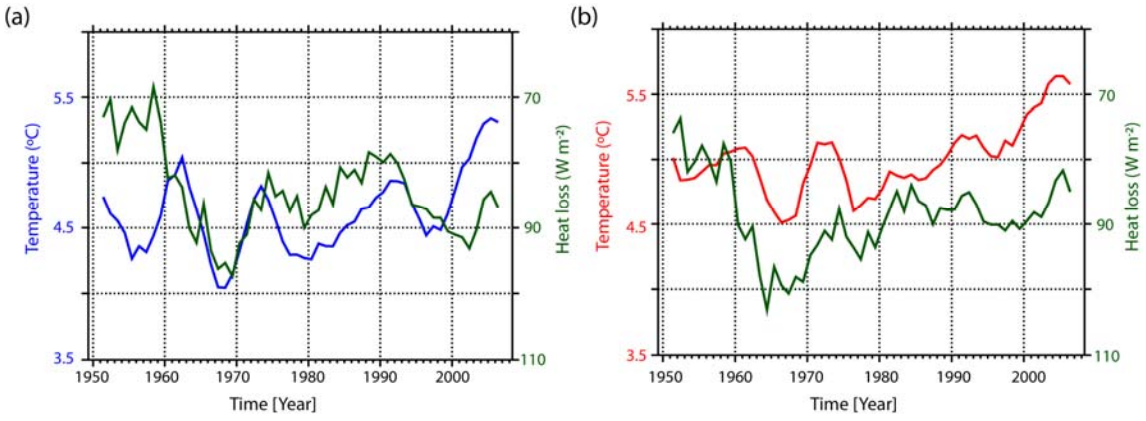

Figure 11. Long term variability in area averaged heat loss and temperature in the (a) western and (b) eastern Lofoten Basin as defined in Figure 6. A five year running mean is applied to the annual time series in both panels. Note the reversal in the axis of heat loss.

The role of atmospheric forcing on the AW temperature variability in the Lofoten Basin is analyzed by investigating the variability in the heat loss in the Lofoten Basin (Figure 11). The net mean (1949-2008) heat loss in the eastern region (88 W m^{-2}) is marginally larger than that in the western region (84 W m^{-2}). The heat loss in the two

regions of the Lofoten Basin shows a distinct maximum in the years around late 1960s. On inter-annual time scales the heat loss in the eastern Lofoten Basin is significantly correlated with the AW temperature there (r=-0.30). Interestingly, no corresponding significant correlation is found in the western region.

3.6. Lofoten Basin Atlantic Water variability and the overturning loop in the Nordic Seas

The AW in the Lofoten Basin has been considered an integral part of the overturning cyclonic loop of AW in the Nordic Seas [*Mauritzen,* 1996a,b; *Eldevik et al.,* 2009]. In order to assess this, annual time series of temperature and salinity of inflowing North Atlantic Water, the Norwegian North Atlantic Water in the Norwegian Basin (shown to be linked to the Faroe Shetland Channel overflow by *Eldevik et al.,* 2009), and the West Spitsbergen Current in the Fram Strait are correlated with the AW temperature and salinity in the two regions of the Lofoten Basin for the time period 1950-2005 (Table 1; locations of NAW, NNAW, and WSC are shown in Figure 1).

Table 1. Lagged peak correlations of time series of hydrographic properties of Atlantic Water in the western (WLB) and eastern (ELB) Lofoten Basin with that of North Atlantic Water (NAW), Norwegian North Atlantic Water (NNAW) and West Spitsbergen Current (WSC). Data source given in Section 2.2 and locations in Figure 1. Time lags are given relative to the water masses in the left column. All tabulated correlation coefficients were calculated using detrended annual time series, and are above the 10% significance level. Symbol '÷' indicates no significant correlation.

	WLB		ELB	
	Temperature	Salinity	Temperature	Salinity
NAW	÷	0.68@2 yr	÷	0.66@2 yr
NNAW	0.56@0 yr	0.70@0 yr	÷	0.61@0 yr
WSC	÷	0.61@0 yr	÷	0.62@0 yr

Starting with the inflowing NAW, we find significant correlations with the AW salinity of both western and eastern regions of the Lofoten Basin with two year lag.

However, the temperature of NAW is not significantly correlated with the Lofoten Basin. Moving downstream of the Lofoten Basin, both salinity and temperature of NNAW is found to correlate with AW in the western region of the Lofoten Basin, while for the eastern region it is only salinity that correlates significantly. Peak correlations are at zero lag, but there is a tendency in both salinity and temperature towards higher correlations when NNAW is lagging slightly (not shown). Further north, in the Fram Strait, we find salinity variations of WSC to be correlated with salinity in both regions of the Lofoten Basin. Even though the peak correlation between these water masses is at zero lag, it should be noted that there are also significant lagged correlations, up to two years both ways.

In order to quantify the combined influence of ocean advection and atmospheric forcing on the density of AW in the Lofoten Basin, a multiple regression analysis of the upstream NAW inflow density and Lofoten Basin heat loss (Figure 11), on the AW density of the Lofoten Basin (Figure 10d) is performed (Table 2). The analysis is done for the two regions of the basin separately. Quantitatively, on inter-annual time scales, the two factors explain 15% of the western and 31% of the eastern Lofoten Basin AW density variability. The individual correlations show that the influence of upstream NAW density variability and local heat loss is higher in the eastern Lofoten Basin compared to the western. A lag of two years is found between the upstream NAW density and AW density of both regions. There is no yearly lag between the heat loss and the AW density of the eastern Lofoten Basin, but the peak correlation in the western basin is found at one year lag. However, the correlation at zero lag is not very different, although it does not test as significant.

Table 2. Lagged peak correlations of time series of Atlantic Water density in the western (WLB) and eastern (ELB) Lofoten Basin with that of North Atlantic Water (NAW) density and local heat loss in the two regions of the Lofoten Basin.Time lags are relative to the variables in the left column. All tabulated correlation coefficients were calculated using detrended annual time series and are above the 10% significance level. The variance in the Atlantic Water density of the two regions of the Lofoten Basin explained by the combined variability in the two year lagged upstream North Atlantic Water (NAW) density and local heat loss (one year lag in the western and zero year lag in the eastern Lofoten Basin) is shown in columns 3 and 5.

	WLB AW density		ELB AW density	
	Correlation Coefficient	Variance explained	Correlation coefficient	Variance explained
NAW density	0.35@2yr	15%	0.48@2yr	31%
Heat loss	0.27@1yr		0.38@0yr	

4. Discussion

4.1. The two distinct regions of the Lofoten Basin

Starting with the surface circulation of the Lofoten Basin, we show the two main branches of the Norwegian Atlantic Current bordering the Lofoten Basin and their local intensification respectively on either side of the basin. Local intensification of the slope current along the eastern rim of the Lofoten Basin is reported by *Skagseth et al.* [2004]. They argue that near the eastern rim of the Lofoten Basin, the slope becomes steep and due to strong topographic steering of geostrophic currents along isobaths (f/H contours), the converging isobaths will accelerate the flow. The topography in the southern part of the Mohn Ridge is not continuous and has gaps [Figure 6; *Voet et al.,* 2010]. The presence of continuous topography over the northern part of Mohn Ridge favors stronger topographic steering and intensifies the front current locally. The intensification of the front current, locked to topography has been addressed in several studies [e.g., *Nilsen and Nilsen,* 2007].

The Lofoten Basin is traditionally considered as a region of large winter heat loss with no considerable mean flow into it (see Figure 1), where heat is believed to be carried into the basin only via lateral eddy fluxes [*Spall,* 2010] and released during water mass transformation. Here, we point to the existence of a mean inflow into the central and eastern Lofoten Basin from the south, which is weaker than the slope current and the front current. *Rossby et al.,* [2009a] using floats (300m), also showed separation of Atlantic Water into the central Lofoten Basin from this area. We further hypothesize that the difference in the buoyancy of surface waters between the western and eastern Lofoten Basin, as will be discussed in Section 4.2, is likely to result in the continuation of this flow in the central Lofoten Basin. The more buoyant waters to the east (Figure 9) increase the sea surface slope and result in a geostrophic surface flow as seen in the altimeter and drifter data.

A key feature of the eddy activity in the Lofoten Basin is the spinning of anticyclonic eddies from the slope current and their southwestward propagation towards the deep Lofoten Basin [*Köhl,* 2007; *Andersson et al.,* 2011]. *Gascard and Mork* [2008] identified the northeastern Lofoten Basin as one of the major eddy detachment regions in the Lofoten Basin. Recently *Raj et al.,* [2013b, submitted] suggested that where the isobaths diverge in the northeastern Lofoten Basin there is a tendency of the flow to become unstable, which triggers growth of eddies from this region. These findings are further supported by the spatial distribution of mean chlorophyll-a concentration where advection from the slope current into the Lofoten Basin is found maximum at the northeastern part of the basin (Figure 4). Moreover, EKE of the northeastern Lofoten Basin is maximum during winter (Figure 6), resembling the strength of the slope current which is also strongest during winter [*Mork and Skagseth,* 2010; *Raj et al.,* 2013b, submitted]. This supports the connection between the surface circulation and the eddy shedding into the Lofoten Basin suggested earlier [*Köhl,* 2007].

The spatial distribution of EKE in the Lofoten Basin reveals two pronounced eddy active regions with distinct annual cycles. The strength of the slope current [*Mork and Skagseth,* 2010] matches the seasonality in EKE of the eastern Lofoten Basin, while

the seasonal cycle in EKE of the western region is dominated by the anticyclonic vortex residing there [*Köhl,* 2007; *Raj et al.,* 2013b, submitted]. The ~2 month lag between the annual EKE climatologies of the two regions and the connection between them seen in the spatial climatologies indicate transfer of energy from eastern to western region via mesoscale eddies during winter and spring. This again supports the argument of earlier studies that the eddies spun from the slope current propagates south-westward into the western Lofoten Basin [*Poulain et al.,* 1996; *Köhl*, 2007; *Rossby et al.,* 2009b; *Andersson et al.,* 2011; *Raj et al.,* 2013b, submitted].

4.2. Spatial variability of the dense water formation in the Lofoten Basin

Convection in the marginal seas of the North Atlantic Ocean has long been considered a key process in forming the dense waters that fill much of the global deep ocean [*Oliver et al.,* 2008]. Eddies spun from the slope current carry fresher coastal waters offshore due to interaction between the Norwegian Coastal Current and the slope current [*Gascard and Mork,* 2008]. Since decrease in salinity dampens convection [*Blindheim and Rey*, 2004] this is important for the dense water formation in the region. The influx of coastal waters into the Lofoten Basin is maximum during summer and autumn (Figure 8a,d). This is due to the dominance of the north easterly winds and associated Ekman transports [*Nilsen and Falck,* 2006]. This larger influx of low saline waters can dampen the pre-conditioning of winter convection. Eddies are also known to flux heat from the slope current into the Lofoten Basin interior balancing the net heat loss to the atmosphere [*Spall,* 2010, 2011]. The proximity of the eastern Lofoten Basin to the slope current also causes it to have warmer waters. There is containment of more buoyant surface waters (less saline and warmer) in the eastern than the western Lofoten Basin. Heat loss, the major factor to influence the water mass transformation of the Norwegian Sea [*Isachsen et al.,* 2007], enhance convection by triggering the overturning of AW inside anticyclonic eddies in the Lofoten Basin [*Rossby et al.,* 2009b]. Hence it is likely that even though there are two high eddy active regions on either side of the Lofoten Basin, the less buoyant waters in the western Lofoten Basin facilitates deeper convection there. Thus surface circulation,

eddy activity and heat loss all influence the spatial distribution of dense water formation in the Lofoten Basin.

4.3. Temporal variability of the dense water formation in the Lofoten Basin

In this section we discuss the long term variability of dense water formation in the basin, the factors influencing it and its implications. First we discuss the factors influencing the long term variability of AW properties in the Lofoten Basin during 1949-2008 (Figure 10). Focusing on the anomalous events, it is found that the minimum in AW temperature and maximum in density of the Lofoten Basin during the late 1960s is associated with maximum heat loss during some anomalously cold winters [Figure 11; *Blindheim and Østerhus*, 2005]. A similar result was also observed by *Rossby et al.,* [2009b] for this period, where they found reduction of AW temperatures in the Lofoten Basin due to excessive heat loss. The lightest AW in the Lofoten Basin is found after 2000 (Figure 10), after an increase in temperature linked to the warming of the inflowing NAW since the mid 1990s [*Orvik and Skagseth*, 2005; *Skagseth and Mork*, 2012]. The increase in salinity together with temperature during this period also points to the influence of NAW. However, the influence of temperature on density can be overpowered by anomalous salinity events. This is especially the case for the "Great Salinity Anomaly" event known to be advected via NAW [*Dickson et al.,* 1988; *Curry and Mauritzen*, 2005], and clearly seen in the Lofoten Basin during the late 1970s.

The influence of the inflowing NAW and heat loss on the density of the Lofoten Basin is statistically significant on inter-annual timescales (Table 2). A lag of two years is found between the AW densities in the Lofoten Basin and the NAW density. Nevertheless, the lag associated with NAW is in agreement with earlier studies showing a transit time of 1-3 years from the Atlantic inflow region to the Fram Strait [e.g., *Furevik,* 2001; *Holliday et al.,* 2008]. Note that the time series in Table 1 and Table 2 are only approximations, as the time series are auto correlated to a varying degree (WLB and ELB densities have integral time scales up to 2.5 years). The influence of NAW densities on the Lofoten Basin's AW densities is stronger in the

eastern region than in the western (Table 2). This is expected due to the proximity of the eastern Lofoten Basin to the slope current from which eddies are shed. It is also revealed that the influence of local heat loss on AW density is higher in the eastern Lofoten Basin. One of the reasons could be the difference in depth of AW in the two regions. The thinner AW layer in the eastern Lofoten Basin is likely more susceptible to the effects of heat loss on density. The reason for the one year lag between the heatloss and AW density of the western Lofoten Basin is not clear but can be linked to the ocean processes in the region. One such process is the ventilation of AW by the quasi permanent anticyclonic vortex situated in the western Lofoten Basin [e.g., *Köhl,* 2007]. In a recent study, *Raj et al.* [2013b, submitted] showed that the SST of the deep Lofoten Basin is significantly correlated with the surface eddy intensity of the anticyclonic vortex at a lag of 11 months, where SST leads. Heat loss via its influence on SST [e.g., *Furevik,* 2000] is linked to a stretching of the vortex by conservation of potential vorticity [*Raj et al.,* 2013b, submitted]. Since deeper convection associated with a deeper vortex will have a stronger influence on the density, a similar lag between heat loss and AW density can be expected. In any case, this study establishes that while the variability in both local heat loss and upstream density influences the AW density of the two regions of the Lofoten Basin, there is a stronger influence in the eastern region. Note that the influence of NAW on the Lofoten Basin AW is aided by the surface circulation and eddy activity which transports the temperature and salinity anomalies into the basin. Hence, it can be argued that the surface circulation, eddy activity, and heat loss in the Lofoten Basin play a key role in the inter-annual variability of dense water formation there.

Next we discuss the main implications of the temporal variability of AW in the Lofoten Basin. In a global perspective, several studies [e.g., *Orvik,* 2004] argued that since Lofoten Basin is situated in the advective path of AW circulating in the Nordic Seas and owning to the large residence time of AW inside the basin which facilitates heat loss, the AW transformation in the basin can influence AMOC. However, no statistical analysis regarding this influence has been provided yet. Here we use correlation analysis as a tool for tracing AW variability to and from the Lofoten Basin.

It is found that the variability of the AW in the Lofoten Basin co-varies with the downstream Norwegian North Atlantic Water and AW in the Fram Strait. Note that an earlier study by *Eldevik et al.* [2009] categorized NNAW (identified at 75-350 m depth) as a water mass in the Nordic Seas that significantly influence the overflow waters exiting at Faroe Shetland Channel (FSCOW). The high co-variance found herein, between the salinities and temperatures of AW in the adjacent western region of Lofoten Basin and NNAW indicates the possibility of inter-basin exchange of AW between the Lofoten and Norwegian basins and is in line with the observations of *Voet et al.,* [2010]. They documented exchanges between the Lofoten and Norwegian Basin due to gaps in the topographic barrier between these two basins and also noted that floats only transfer from the Lofoten Basin into the Norwegian Basin. Since the isopycnal surfaces slope upward out of the Lofoten Basin [*Rossby et al.,* 2009b], also the deepest AW can exit at depths were NNAW is found. Also note that the AW densities of the western region of the Lofoten Basin were either very close to or in the range of overflow water densities [σ_θ>27.8 kg m^{-3}; *Dickson and Brown,* 1994] during the first two and half decades of the time series (Figure 10d). In addition this study found that the mid depth (300 m to 600 m) AW densities in the western Lofoten Basin, which lies above the sill depth are in the range of the overflow water densities. These are evidence that AW variability in the herein identified western region of the Lofoten Basin, can influence NNAW. The correlation between the AW variability in the Lofoten Basin and the WSC is expected since the Lofoten Basin lies in the advective path of AW transport into the Fram Strait. The strong connection between the Lofoten Basin and the NNAW, found herein, and the further connection to the Faroe Shetland overflow found by *Eldevik et al.* [2009], points to the possibility of a returning circulation connecting the Lofoten Basin and the overflows. Due to the scarcity of hydrographic data, analysis based on monthly time series is not possible and a dedicated approach using numerical models is needed to further investigate this issue. In summary, the above discussion provide more support to the argument that the AW transformation in the Lofoten Basin can influence overflow waters and hence is important to AMOC.

5. Concluding remarks

Analysis of the surface circulation of the Lofoten Basin identified local maxima in the front current along the northern part of the Mohn Ridge due to topographic steering, and a weak flow from the Vøring Escarpment into the central Lofoten Basin due to elevation in sea surface height associated with buoyant waters in the eastern Lofoten Basin. The Lofoten Basin is shown to consist of two almost equally sized but different regions in terms of hydrography, convection depth, and eddy activity. The strength of the slope current can influence the spatial distribution of dense water formation in the Lofoten Basin, through the associated eddy shedding carrying fresh and warm waters into the basin. The long term variability in Atlantic Water density in the Lofoten Basin is dominated by the variability in its temperature. On inter-annual timescales, the variability in both local heat loss and upstream North Atlantic Water density influence the Atlantic Water density of the eastern Lofoten Basin more than in the western. The Atlantic Water transformation in the Lofoten Basin is confirmed as an integral part of the overturning cyclonic loop in the Nordic Seas which maintains AMOC, with a possible link from the western Lofoten Basin to the Faroe Shetland Channel Overflow.

Acknowledgements

This research was supported by the European Union and Norwegian Research Council through the project MONARCH-A (grant 242446), and BIAC. We are grateful to Tore Furevik and Tor Eldevik, *Center for Climate Dynamics, Norway,* for their encouragement. The altimeter data are distributed by AVISO (http://www.aviso.oceanobs.com). The hydrographic data were provided by the Marine Research Institute, Iceland; Institute of Marine Research, Norway; the Faroese Fisheries Laboratory and Geophysical Institute, University of Bergen, Norway, through the NISE project. This is publication no. AXXX from the Bjerknes Centre for Climate Research.

References

Andersson, M., K. A. Orvik, J. H. LaCasce, I. Koszalka, and C. Mauritzen (2011), Variability of the Norwegian Atlantic Current and associated eddy field from surface drifters, *J. Geophys. Res.,116,* C08032, doi:10.1029/2011JC007078.

Beszczynska-Möller, A., E. Fahrbach, U. Schauer, and E. Hansen (2012), Variability in Atlantic water temperature and transport at the entrance to the Arctic Ocean, 1997–2010, *ICES. J. Mar. Sci.*, doi:10.1093/icesjms/fss056.

Blindheim, J., and F. Rey (2004), Water-mass formation and distribution in the Nordic seas during the 1990s, *ICES. J. Mar. Sci., 61***,** 846–863.

Blindheim, J., and S. Østerhus (2005), The Nordic Seas, Main Oceanographic Features, *in The Nordic Seas: An Integrated Perspective, Oceanography, Climatology, Biogeochemistry and Modeling,* edited by H. Drange, T. Dokken, T. Furevik, R. Gerdes, and W. Berger, pp. 11-38, AGU Geophysical Monograph Series.

Chaigneau, A., A. Gizolme, and C. Grados (2008), Mesoscale eddies off Peru in altimeter records: Identification algorithms and eddy spatiotemporal patterns, *Prog. Oceanogr., 79,* 106–119, doi:10.1016/j.pocean.2008.10.013.

Chelton, D. B. (1983), Effects of sampling errors in statistical estimation*, Deep Sea Res., Part A, 30*, 1083–1103.

Curry, R., and C. Mauritzen (2005), Dilution of the northern North Atlantic Ocean in recent decades, *Science., 308* (5729), 1772-1774.

Dickson, R. R., J. Meincke, S. Malmberg, and A. J. Lee (1988), The great salinity anomaly in the Northern North Atlantic 1968-1982, *Prog. Oceanogr., 20*, 103-151.

Dickson, R. R., and J. Brown (1994), The production of North Atlantic Deep Water, sources rates and pathways, *J. Geophys. Res.,99*, 12,319–12,341.

Ducet, N., P. Y. LeTraon, and G. Reverdin (2000), Global high-resolution mapping of ocean circulation from TOPEX/Poseidon and ERS-1 and 2, *J. Geophys. Res., 105*, 19477–19498.

Eldevik, T., J. E. Ø. Nilsen, D. Iovino, K. A. Olsson, A. B. Sandø, and H. Drange (2009), Observed sources and variability of Nordic seas overflow**,** *Nat. Geosci.*, *2*, 406-410, doi: 10.1038/ngeo518.

Furevik, T. (2000), On anomalous sea surface temperatures in the Nordic Seas, *J. Climate*., *13* (5), 1044-1053.

Furevik, T. (2001), Annual and interannual variability of Atlantic Water temperatures in the Norwegian and Barents Seas: 1980-1996, *Deep Sea Res.*, *Part I*, *48* (2), 383-404.

Furevik, T., and J. E. Ø. Nilsen (2005), Large-Scale Atmospheric Circulation Variability and its Impacts on the Nordic Seas Ocean Climate - a Review, *in The Nordic Seas: An Integrated Perspective, Oceanography, Climatology, Biogeochemistry and Modeling,* edited by H. Drange, T. Dokken, T. Furevik, R. Gerdes, and W. Berger, pp. 105-136, AGU Geophysical Monograph Series.

Gascard, J. C., G. Raisbeck, S. Sequeira, F.¸Yiou, and K. A. Mork (2004), The Norwegian Atlantic Current in the Lofoten basin inferred from hydrological and tracer data (129I) and its interaction with the Norwegian Coastal Current, *Geophys. Res. Lett., 31,* L01308, doi:10.1029/2003GL018303.

Gascard, J. C., and K. A. Mork (2008), Climatic importance of large scale and mesoscale circulation in the Lofoten Basin deduced from lagrangian observations during ASOF, *in Arctic–Subarctic Ocean Fluxes: Defining the Role of the Northern Seas in Climate,* edited by R. R. Dickson, J. Meincke, and P. Rhines, pp. 131-143, Springer, New York.

Holliday, N. P., S. L. Hughes, S. Bacon, A. Beszczynska-Möller, B. Hansen, A. Lavín, H. Loeng, K. A. Mork, S. Østerhus, T. Sherwin, and W. Walczowski (2008), Reversal of the 1960s to 1990s freshening trend in the northeast North Atlantic and Nordic Seas, *Geophys. Res. Lett., 35*, L03614, doi: 10.1029/2007GL032675.

Isachsen, P. E., C. Mauritzen, and H. Svendsen (2007), Dense water formation in the Nordic Seas diagnosed from sea surface buoyancy fluxes, *Deep Sea Res.*, *Part I*, *54*, 22-41, doi:10.1016/j.dsr.2006.09.008.

Jakobsen, P. K., M. H. Ribergaard, D. Quadfasel, T. Schmith, and C. W. Hughes (2003a), Near-surface circulation in the northern North Atlantic as inferred from Lagrangian drifters: Variability from the mesoscale to interannual, *J. Geophys. Res.,108*(C8), 3251, doi:10.1029/2002JC001554.

Jakobsen, P. K., M. H. Nielsen, D. Quadfasel, and T. Schmith (2003b), Variability of the surface circulation of the Nordic Seas during the 1990s, *ICES. Mar. Sc., 219, 367-370.*

Kalnay, E., M. Kanamitsu, R. Kistler, W. Collins, D. Deaven, L. Gandin, M. Iredell, S. Saha, G. White, J. Woollen, Y. Zhu, M. Chelliah, W. Ebisuzaki, W.Higgins, J.

Janowiak, K. C. Mo, C. Ropelewski, J. Wang, A. Leetmaa, R. Reynolds, R. Jenne, and D. Joseph (1996), The NCEP/NCAR 40-Year Reanalysis Project, *Bull. Am. Meteorol. Soc., 77* (3), 437–471.

Köhl, A. (2007), Generation and stability of a quasi-permanent vortex in the Lofoten basin, *J. Phys. Oceanog,. 37*, 2637-2651.

Koszalka, I., J. H. LaCasce , M. Andersson , K. A. Orvik , and C. Mauritzen (2011) Surface circulation in the Nordic Seas from clustered drifters, *Deep Sea Res., Part I., 58*, 468-485, doi:10.1016/j.dsr.2011.01.007.

LeTraon, P. Y., and F. Ogor (1998), ERS-1/2 orbit improvement using TOPEX/Poseidon: The 2 cm challenge, *J. Geophys. Res.,103*, 8045–8057.

Lumpkin, R., and Z. Garraffo (2005), Evaluating the Decomposition of Tropical Atlantic Drifter Observations, *J. Atmos. Ocean. Tech., 22*, 1403-1415.

Mauritzen, C. (1996a), Production of dense overflow water feeding the North Atlantic across the Greenland-Scotland Ridge. Part 1: Evidence of revised circulation scheme, *Deep Sea Res.*, *Part I, 43*, 769– 806.

Mauritzen, C. (1996b), Production of dense overflow waters feeding the North Atlantic across the Greenland–Scotland Ridge. Part 2. An inverse model, *Deep Sea Res., Part I, 43,* 807–835.

Mork, K. A., and Ø. Skagseth (2010), A quantitative description of the Norwegian Atlantic Current by combining altimetry and hydrography, *Ocean Sci., 6*, 901–911.

Nilsen, J. E. Ø., and E. Falck (2006), Variation of mixed layer properties in the Norwegian Sea for the period 1948–1999, *Prog. Oceanogr., 70*, 58–90, doi:10.1016/j.pocean.2006.03.014.

Nilsen, J. E. Ø., and F. Nilsen (2007), The Atlantic Water Flow along the Vøring Plateau: Detecting Frontal Structures in Oceanic Station Time Series, *Deep Sea Res.*, *Part I, 54*(3), 297-319, doi:10.1016/j.dSV.2006.12.012.

Nilsen, J. E. Ø., H. Hátún, K. A. Mork, and H. Valdimarsson (2008), The NISE Data Set, *Tech. Rep. 08-01*, Faroese Fish. Lab., T´orshavn, Faroe Islands.

Oliver, K. I. C., T. Eldevik, D. P. Stevens, and A. J. Watson (2008), A Greenland Sea perspective on the dynamics of postconvective eddies, *J. Phys. Oceanog,. 38*(12), 2755-2771.

Orvik, K. A., and P. Niiler (2002), Major pathways of Atlantic water in the northern North Atlantic and Nordic Seas toward Arctic, *Geophys. Res. Lett., 29*(19), 1896, doi:10.1029/2002GL015002.

Orvik, K. A., and Ø. Skagseth (2003), Monitoring the Norwegian Atlantic slope current using a single moored current meter, *Cont. Shelf. Res., 23*, 159–176.

Orvik, K. A. (2004), The deepening of the Atlantic water in the Lofoten Basin of the Norwegian Sea, demonstrated by using an active reduced gravity model, *Geophys. Res. Lett., 31*, L01306, doi:10.1029/2003GL018687.

Orvik, K. A., and Ø. Skagseth (2005), Heat flux variations in the eastern Norwegian Atlantic Current toward the Arctic from moored instruments, 1995–2005, *Geophys. Res. Lett., 32*(14), L14610, doi:10.1029/2005GL023487.

Poulain, P. M., A. Warn-Varnas, and P. P. Niiler (1996), Near-surface circulation of the Nordic seas as measured by Lagrangian drifters, *J. Geophys. Res.*, *101*(C8), 237–258.

Raj, R. P., B. N. Peter, and D. Pushpadas (2010), Oceanic and atmospheric influences on the variability of phytoplankton bloom in the Southwestern Indian Ocean, *J. Marine. Syst., 82*, 217-229, doi:10.1016/j.jmarsys.2010.05.009.

Read, J., and R. Pollard (1992), Water Masses in the Region of the Iceland–Faroes Front, *J. Phys. Oceanog,. 22*(11), 1365–1378, doi: http://dx.doi.org/10.1175/1520-0485(1992)022<1365:WMITRO>2.0.CO;2.

Rio, M. H., and F. Hernandez (2004), A mean dynamic topography computed over the world ocean from altimetry, in situ measurements, and a geoid model, *J. Geophys. Res*., *109*, C12032, doi:10.1029/2003JC002226.

Rio, M. H., S. Guinehut, and G. Larnicol (2011), New CNES-CLS09 global mean dynamic topography computed from the combination of GRACE data, altimetry, and in situ measurements, *J. Geophys. Res.,116*, C07018, doi: 10.1029/2010JC006505.

Rossby, T., M. Prater, and H.Søiland (2009a), Pathways of inflow and dispersion of warm waters in the Nordic Seas, *J. Geophys. Res.,114,* C04011, doi:10.1029/2008JC005073.

Rossby, T., V. Ozhigin, V. Ivshin, and S. Bacon (2009b), An isopycnal view of the Nordic Seas hydrography with focus on properties of the Lofoten Basin, *Deep Sea Res.*, *Part I, 56*, doi:10.1016/j.dsr.2009.07.005.

Siegismund, F., J. A. Johannessen, H. Drange, K. A. Mork, A. Korablev (2007), Steric height variability in the Nordic Seas, *J. Geophys. Res., 112*, C12010, doi:10.1029/2007/JC004221.

Segtnan, O. H., Furevik, T., and Jenkins A.D (2011), Heat and freshwater budgets of the Nordic Seas computed from atmospheric reanalysis and direct ocean observations, *J. Geophys. Res., 116*, C11003, doi: 10.1029/2011JC006939.

Skagseth, Ø., and K. A. Orvik (2002), Identifying fluctuations in the Norwegian Atlantic Slope Current by means of empirical orthogonal functions, *Cont. Shelf Res., 22,* 547–563, 2002.

Skagseth. Ø., K. A. Orvik, and T. Furevik (2004), Coherent variability of the Norwegian Atlantic slope current determined by using TOPEX/ERS altimeter data, *Geophys. Res. Lett., 31,* L14304, doi:10.1029/2004GL020057.

Skagseth, Ø., and K. A. Mork (2012), Heat content in the Norwegian Sea during 1995-2005, *ICES. J. Mar. Sci.*, *69* (5), 826-832, doi: 10.1093/icesjms/fss026.

Spall, M. A. (2010), Non-local topographic influences on deep convection: An idealized model for the Nordic Seas, *Ocean Model., 32*, 72-85, doi:10.1016/j.ocemod.2009.10.009.

Spall, M. A. (2011), On the role of eddies and surface forcing in the heat transport and overturning circulation in marginal seas, *J. Climate., 24*, 4844-4858.

Tomczak, M., and J. S. Godfrey (2003), Regional Oceanograhy: An Introduction (2nd edition), Daya Publishing House, New Delhi, India.

Voet, G., D. Quadfasel, K. A. Mork, and H. Søiland (2010), The mid-depth circulation of the Nordic Seas derived from profiling float observations, *Tellus A., 62*(4), 516–529. doi:10.1111/j.1600-0870.2010.00444.x.

Volkov, D. L. and I. Pujol (2012), Quality assessment of a satellite altimetry data product in the Nordic Seas, Barents, and Kara seas, *J. Geophys. Res., 117*, 1978-2012, doi: 10.1029/2011JC007557.

PAPER 3

The Lofoten Vortex of the Nordic Seas

Roshin P. Raj, Léon Chafik, J. Even Ø. Nilsen , Tor Eldevik

In revision Deep Sea Research Part 1

The Lofoten Vortex of the Nordic Seas

Roshin P. Raj [a, b, c,*], Léon Chafik [d], J. Even Ø. Nilsen [a, c], Tor Eldevik [b, c]

[a] Nansen Environmental and Remote Sensing Center, Thormøhlens gate 47, Bergen, Norway
[b] Geophysical Institute, University of Bergen, Allegaten 70, Bergen, Norway
[c] Bjerknes Center for Climate Research, Allegaten 55, Bergen, 5007, Norway
[d] Department of Meteorology, Stockholm University, S-106 91, Stockholm, Sweden

Abstract

The Lofoten Basin is the largest reservoir of ocean heat in the Nordic Seas. A particular feature of the basin is 'the Lofoten Vortex', arguably a most anomalous mesoscale structure in the Nordic Seas. The vortex resides in one of the major winter convection sites in the Norwegian Sea, and is likely to influence the dense water formation of the region. Here, we document this quasi-permanent anticyclonic vortex using hydrographic and satellite data. The vortex' uniqueness in the Nordic Seas, its surface and vertical characteristics on seasonal, inter-annual, and climatological time-scales, are examined together with relevant forcing mechanisms acting on it. We show that the Atlantic Water in the Nordic Seas penetrate the deepest inside the Lofoten Vortex. We confirm the persistent existence of the vortex in the deepest part of the Lofoten Basin, its dominant cyclonic drift and reveal a seasonality in its eddy intensity with maximum during late winter and minimum during late autumn. Finally, we show that while the seasonality in the eddy intensity of the vortex is mainly influenced by mergers with incoming anticyclonic vortices, its long term variability can be explained by buoyancy forcing.

Keywords: Norwegian Atlantic Current, Lofoten Vortex, eddy kinetic energy, convection, Lofoten Basin, heat loss.

1. Introduction

The warm and saline Atlantic Water (AW) entering the Norwegian Sea transports heat towards the Arctic, and is thus a key component in maintaining the region's relatively mild climate and ice-free oceans (Rhines et al., 2008). Northern heat loss is one of the major processes resulting in dense water formation in the Nordic Seas, an important component of the Atlantic Meridional Overturning Circulation (Mauritzen, 1996; Isachsen et al., 2007; Eldevik et al., 2009). The Lofoten Basin of the Norwegian Sea (Fig. 1) is both the largest heat reservoir of the Nordic Seas (Blindheim and Rey, 2004) and a region with strong atmospheric heat loss (Bunker, 1976; Mauritzen, 1996). The Lofoten Basin is also the region of highest eddy activity in the Nordic Seas (Poulain et al., 1996). The residence time of AW circulating in the Lofoten Basin is longer than any other region in the Nordic Seas due to the deep cyclonic recirculation prevailing there which in turn has the important effect of storing large quantities of AW (Orvik, 2004; Gascard and Mork, 2008). The long residence time of AW in the Lofoten Basin results in additional cooling of AW before it reaches the Arctic proper.

The Lofoten Basin, bordered by the baroclinic Norwegian Atlantic Front Current (front current) on the western side and barotropic Norwegian Atlantic Slope Current (slope current) on the eastern side (Orvik and Niiler, 2002; Mork and Skagseth, 2010), seats a large anticyclonic vortex in its western part. This vortex have been reported in several studies (Ivanov and Korablev, 1995a, b; Köhl, 2007, Voet et al., 2010; Andersson et al., 2011; Koszalka et al., 2011). Ivanov and Korablev (1995a, b) first identified this feature and reported it as a quasi-permanent anticyclonic vortex in the Lofoten basin. They concluded winter convection as the main mechanism responsible for the stability of the vortex. Later, Köhl (2007), using a numerical ocean model, studied the generation mechanisms and conditions for stability of the vortex. He proposed that it results primarily from anticyclonic eddies shed from the slope current, propagating south-westward into the central Lofoten Basin. The shedding of eddies from the slope current

has been discussed in many studies (e.g., Rossby et al., 2009; Spall, 2010; Andersson et al., 2011). Recently, Koszalka et al. (2011) using surface drifters reported the vortex to be of 150 km in diameter.

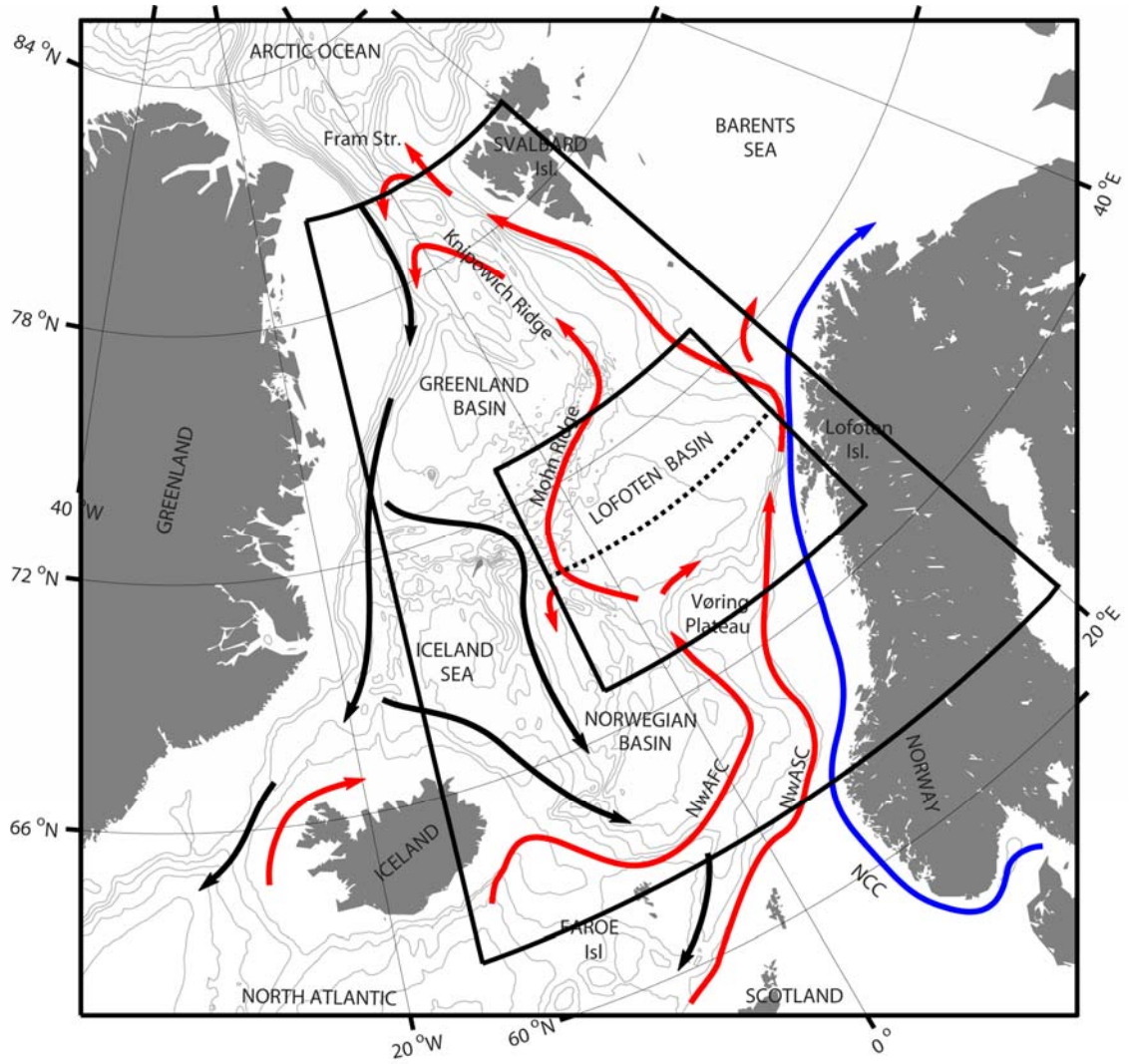

Fig. 1. The Nordic Seas with schematic pathways indicating the overturning circulation from warm inflowing Atlantic Water in the surface (red) to cold and dense overflows to the deep North Atlantic (black). The Norwegian Atlantic slope current (NwASC), here termed as slope current and Norwegian Atlantic front current (NwAFC) are represented by red arrows. The fresh Norwegian Coastal Current (NCC) is indicated in blue. See Furevik and Nilsen (2005) and Eldevik et al. (2009) for details. Grey isobaths are drawn for every 600 m. The large and small black frames indicate the area shown in Fig. 2, 3 and in Fig. 4, 5a respectively. The dashed line indicates the vertical section shown in Fig. 8.

Even though earlier studies showed the existence of the anticyclonic vortex, a comprehensive, observation-based analysis of it is lacking. Here we document the

anticyclonic vortex hereafter termed 'the Lofoten Vortex', using a suite of long term hydrographic and satellite observations. The study addresses and quantifies key issues such as the vortex' surface and vertical structure on seasonal, inter-annual, and climatological time-scales, including relevant forcing mechanisms, and thereby documents the uniqueness of the Lofoten Vortex in the Nordic Seas.

2. Data and Methods

2.1. Altimeter data

High-resolution weekly sea level anomalies (SLA) during the past 18 years (1993-2010) are used to study the vortex. SLA fields, corrected for the inverted barometer effect, tides, and tropospheric effects (Le Traon and Ogor, 1998), are based on merged Envisat and ERS-I and II data (Ducet et al., 2000). In the Lofoten Basin, the SLA fields provided are of roughly 12 km resolution. In a recent study, Volkov and Pujol, (2012) showed that the root mean square (RMS) difference between the altimeter data and tide gauge measurements in the Norwegian Sea is generally 3 cm. Sea surface geostrophic velocity anomaly components, u' and v', are computed from the SLA gradients using the conventional geostrophic relation:

$$u' = \frac{-g}{f}\frac{\partial h}{\partial y} \tag{1}$$

$$v' = \frac{g}{f}\frac{\partial h}{\partial x}, \tag{2}$$

where g is the acceleration due to gravity, f is the Coriolis parameter, h is SLA, and x and y are the longitudinal and latitudinal directions. Eddy kinetic energy, *EKE,* is computed using the standard relation (Chaigneau et al., 2008)

$$EKE = \frac{u'^2 + v'^2}{2}. \tag{3}$$

Vorticity (ω), shearing deformation rate (s_{11}), and stretching deformation rate (s_{12}) are the other eddy kinematic variables determined from geostrophic velocity anomalies (Isern-Fontanet et al., 2006; Chaigneau et al., 2008; Hwang et al., 2004),

$$\omega = \frac{\partial v'}{\partial x} - \frac{\partial u'}{\partial y}, \tag{4}$$

$$s_{11} = \frac{\partial v'}{\partial x} + \frac{\partial u'}{\partial y}, \tag{5}$$

$$s_{12} = \frac{\partial u'}{\partial x} - \frac{\partial v'}{\partial y}. \tag{6}$$

These are used to calculate the Okubo-Weiss parameter, W (Okubo, 1970; Weiss, 1991), which quantifies the relative importance of stretch, strain, and vorticity in the flow:

$$W = (s_{11}^2 + s_{12}^2) - \omega^2. \tag{7}$$

Dominance of rotation over shear and stretch, results in negative values of W (Chaigneau et al., 2008). In order to objectively define the area, *A,* of the vortex, we use the criterion

$$W < -0.2\sigma_w, \tag{8}$$

where σ_w is the spatial standard deviation of *W*. This criterion has been successfully used in earlier studies for detecting ocean vortices from altimetry (Isern-Fontanet et al., 2003, 2006; Morrow et al., 2004).

In order to quantify the relation between the seasonality of the slope current, and the strength of Lofoten Vortex, we employ an along-isobath approach utilizing the weekly altimetric absolute dynamic topography (ADT) from 1992-10-14 until 2010-12-29. The ADT dataset is the sum of the time invariant CNES-CLS09 mean dynamic topography (Rio et al., 2011) and the time variant weekly SLA data described above. The volume transport (Sv=10^6 m^3 s^{-1}) is estimated from ADT using the following equation:

$$\Psi(l,t) = \frac{gH}{f} \Delta_H ADT, \tag{9}$$

where l being the along-slope coordinate, and H is the mean depth between the 500 m and 800 m isobaths. Here, $\Delta_H ADT = ADT(H_{500m}, l, t) - ADT(H_{800m}, l, t)$ and represents the difference in the cross-slope ADT between these two isobaths. In order to extract the flow parallel to the isobaths, the nearest points on the 800 m contour from the 500 m isobath (see Fig. 13) were initially determined. It deserves mentioning that this barotropic estimate of the transport is reasonable, since the slope current is a nearly barotropic shelf-edge current (Orvik and Niiler, 2002).

2.2. Vortex identification and tracking

All weekly SLA and geostrophic velocity anomaly maps were visually inspected in order to identify the vortices of the Lofoten Basin. An anticyclonic vortex is defined by a maximum in SLA. The Lofoten Vortex is both described as strong and quasi-permanent (Köhl, 2007; Andersson et al., 2011; Koszalka et al., 2011). These two distinct features of the Lofoten Vortex were employed in this study in order to identify it from other anticyclonic vortices. The vortex area, A, is identified using Eq. (8). Weekly drift velocities of the center of the vortex are estimated from the displacement of its center during consecutive weeks. The radius of the Lofoten Vortex is estimated using the relation,

$$R=\left(\frac{A}{\pi}\right)^{1/2}. \tag{10}$$

Finally, the eddy intensity, EI, is defined as the area-weighted mean EKE over the vortex area (e.g., Chaigneau et al., 2008):

$$EI = \frac{1}{A} \int_A EKE \, dA \, . \tag{11}$$

Monthly time series of EI are calculated from the weekly values and the corresponding error estimates are determined by the standard error of the mean, $s_m=s/(N-1)^{1/2}$, where s is the standard deviation for the N weekly data the mean is based on. Annual climatologies are based on the monthly mean values. Note that in order to secure a continuous time

series consisting of full years, the analysis of inter-annual variability and annual climatology of the Lofoten Vortex is limited to 16 years (1995-2010; satellite data are absent in January through March 1994). Here, the deep Lofoten Basin is defined by the 3000 m isobath.

2.3. Hydrography

Long term climatology (1949-2008) of temperature and salinity along 70ºN are prepared from the hydrographic NISE dataset (Norwegian Iceland Seas Experiment; Nilsen et al., 2008). The NISE dataset consists of both CTD data decimated up to 5 m, and bottle data. Winter mixed layer depth (MLD) climatology of the Norwegian Sea is calculated following Nilsen and Falck (2006). Climatology of meridional velocities along 70ºN is calculated using the thermal wind equation, and depth-average velocities are removed from it in order to eliminate the barotropic component and estimate purely baroclinic velocities (e.g., Hirschi and Marotzke, 2007).

2.4. Other datasets

Sea surface temperature (SST) for the region is obtained from monthly 1/8º global fields of SST produced by the Modular Ocean Data Assimilation System (MODAS; Barron and Kara, 2006). MODAS SST is produced by an optimal interpolation of Advanced Very-High Resolution Radiometer (AVHRR) nonlinear SST observations. Time series of the SST for the deep Lofoten Basin are of spatial averages inside the 3000 m isobath.

3. Results

3.1. The manifestation of the Lofoten Vortex in the Nordic Seas

The hydrographic data reveals the uniqueness of the Lofoten Basin in the Nordic Seas. Fig. 2a shows that AW inside the Lofoten Basin penetrates deep down to a depth of 800 m, apparently much deeper than any other location in the Nordic Seas. The zonally averaged thermal energy of AW in the Nordic Seas (Fig. 2b) is found to be largest inside the Lofoten Basin, reaching maximum at about 70ºN and decreasing to half this value outside the latitudes of the Lofoten Basin. The winter climatology of MLD shows a

maximum larger than 500 m in the deep Lofoten Basin (Fig. 2c). The Lofoten Basin thus manifests itself as a major winter convection site in the Nordic Seas. These results show the uniqueness of the deep Lofoten Basin in the Nordic Seas and this is where a quasi-permanent anticyclonic vortex is reported to reside (Ivanov and Korablev, 1995a, b; Köhl, 2007; Koszalka et al., 2011). A vortex is characterized by negative values of the Okubo-Weiss parameter (Eq. (7)). This parameter's spatial distribution in the Nordic Seas (Fig. 3a) shows that the largest negative values are found in the deep Lofoten Basin, indicating the position of the Lofoten Vortex. Analysis of surface *EKE* (Fig. 3b) further shows the existence of the Lofoten Vortex as a pronounced maximum in the deep Lofoten Basin. The weaker secondary maximum, in the eastern Lofoten Basin, is related to other eddies in the basin (Andersson et al., 2011), and will be discussed below. Fig. 2a and 3b reveal the colocation of deepest AW penetration and maximum *EKE* in the Nordic Seas.

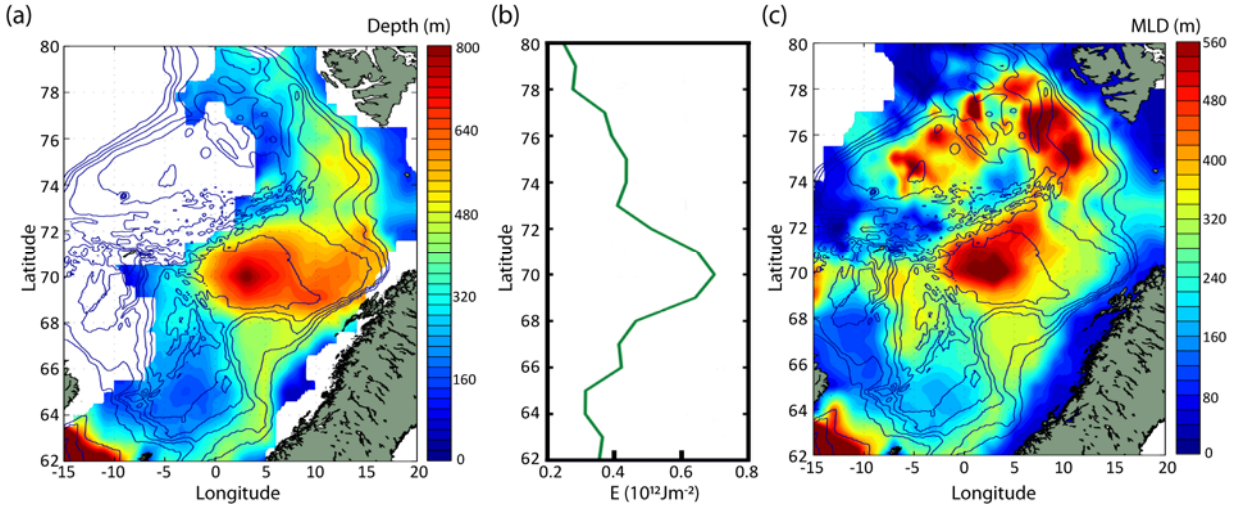

Fig. 2. (a) Maximum depth of Atlantic Water (b) zonal average thermal energy of Atlantic Water, and (c) winter mixed layer depth climatology of the Nordic Seas from NISE hydrography (1949-2008). Blue lines in panels a and c are isobaths drawn for every 600 m.

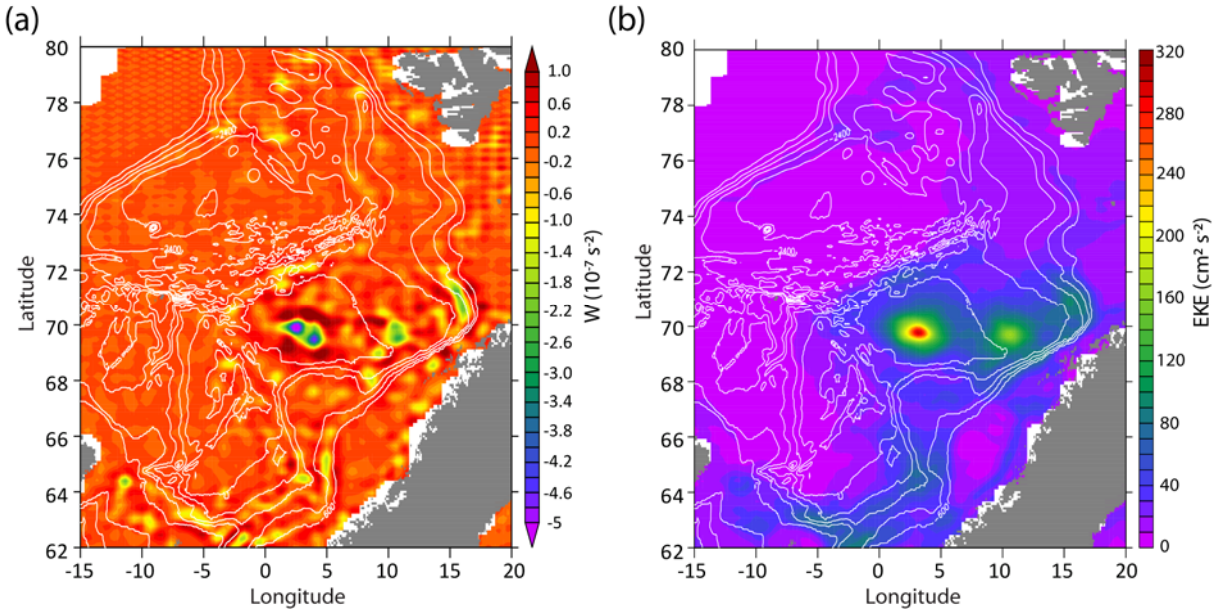

Fig. 3. Climatology (1993-2010) of (a) Okubo-Weiss parameter, *W,* and (b) *EKE* from satellite altimeter data. White lines in panel a and b are isobaths drawn for every 600 m.

3.2. The surface signature of the Lofoten Vortex

Fig. 4 shows a monthly mean example of the Lofoten Vortex situated in the deep Lofoten Basin. The spatial distribution of geostrophic velocities and *EKE* in the Lofoten Basin shows a circular maximum at the Lofoten Vortex, of approximately 30 cm s^{-1} and greater than 400 cm^2 s^{-2} respectively (Fig. 4a). The geostrophic velocities and *EKE* decrease towards the center of the vortex. This feature of the Lofoten Vortex is similar to the characteristics of eddies reported in other ocean basins (e.g., Chaigneau and Pizarro, 2005). The vortex signature is also pronounced in the simultaneous SST map, where SST at the vortex center is lower than the ambient waters (Fig. 4b).

A persistent existence of the vortex in the deep Lofoten Basin is found in approximately 80% of the dataset analyzed (754 out of 942 weeks of SLA). The persistence of the Lofoten Vortex ranges from months to years while other anticyclonic and cyclonic eddies in the Lofoten Basin rarely attains a life span of more than three months. The tracking shows that the vortex resides in a limited part of the deep Lofoten basin (Fig. 5a).

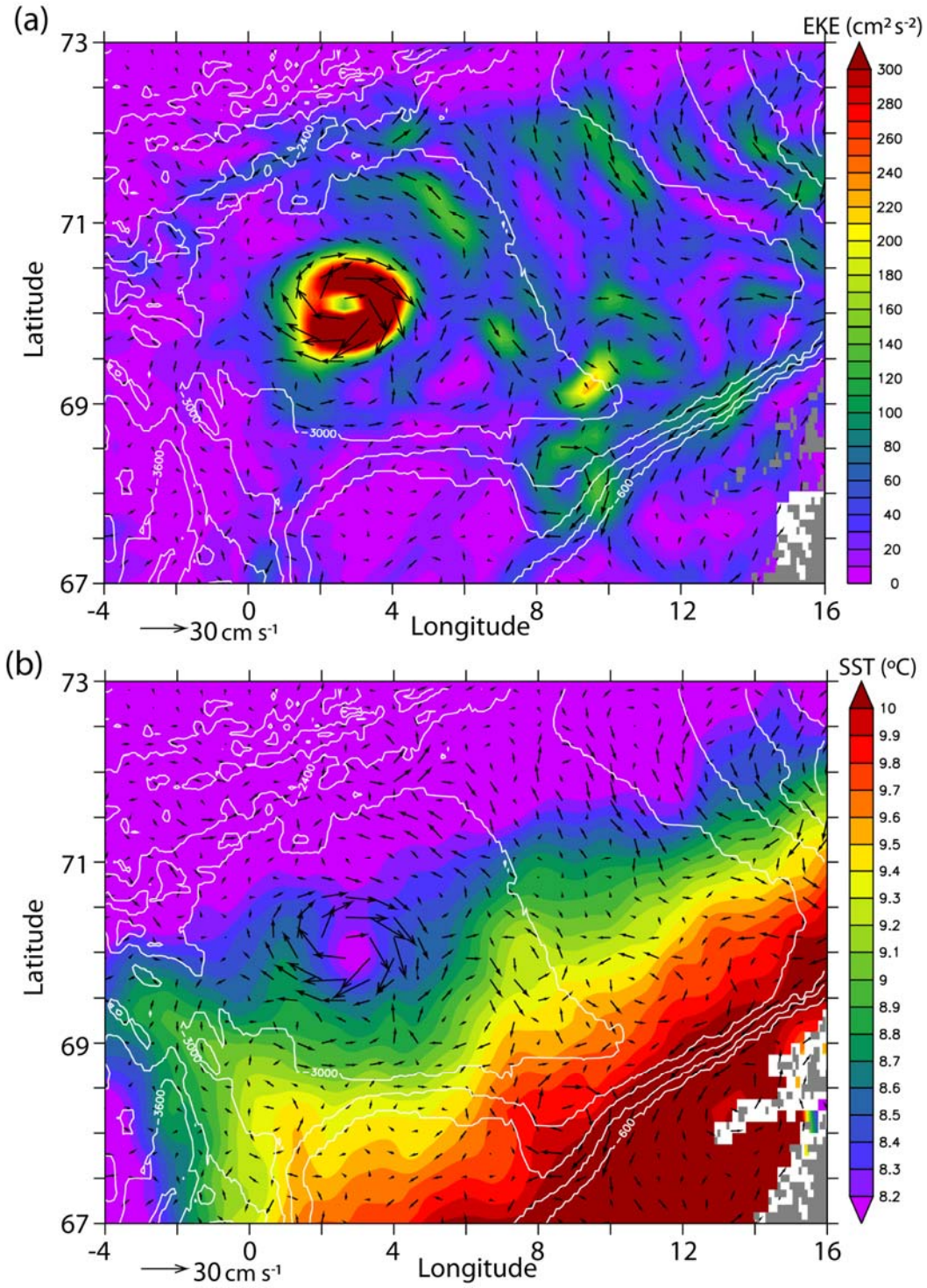

Fig. 4. Monthly (July 2000) mean satellite altimeter derived surface geostrophic velocity anomalies superimposed on (a) eddy kinetic energy and (b) MODAS SST. White lines are isobaths drawn for every 600 m.

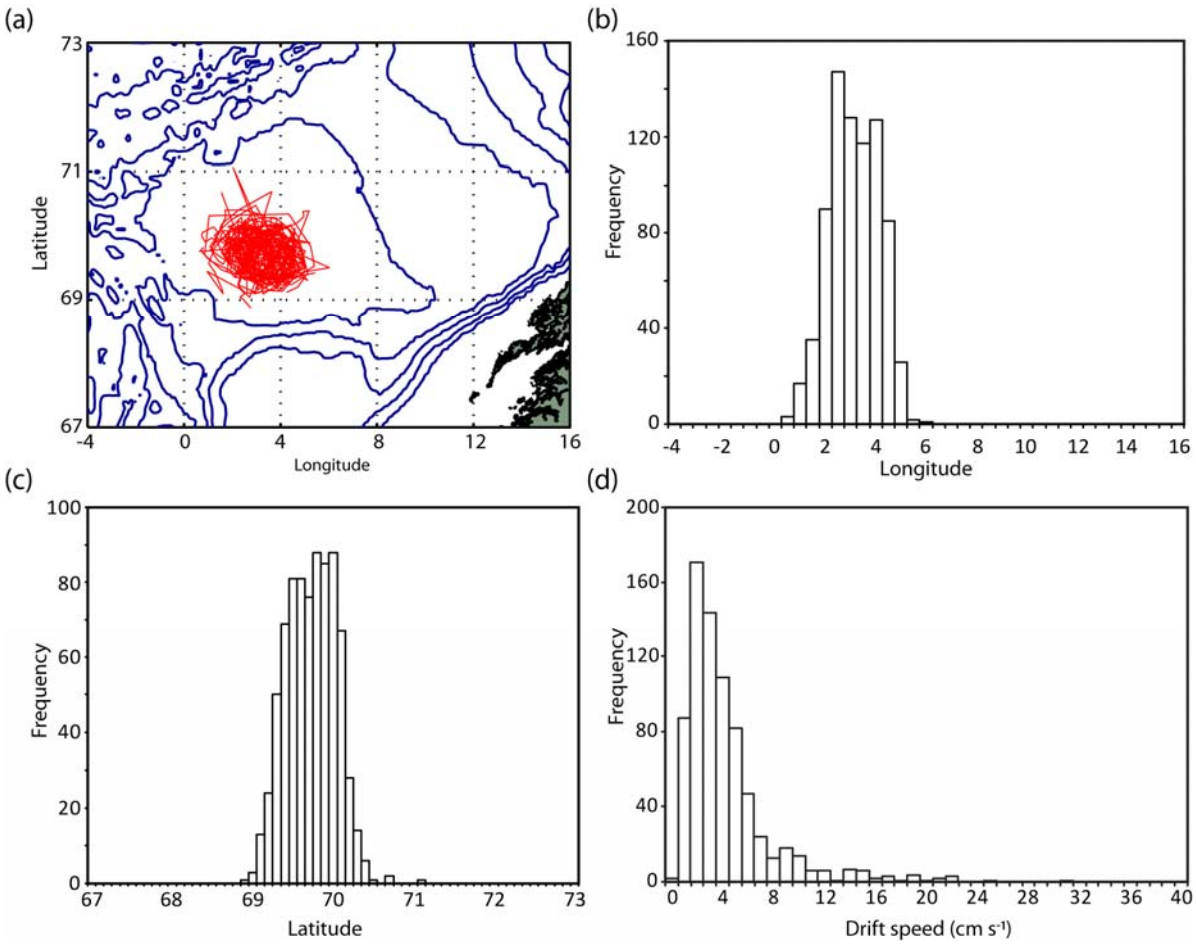

Fig. 5. (a) Track of the center of the Lofoten Vortex from weekly positions during the period 1993-2010. Frequency distribution of the (b-c) position of vortex center and (d) drift speed of the center of the vortex. Blue lines in panel a are isobaths drawn for every 600 m.

Statistically (1st and 3rd quartile), the vortex center lies within a latitude band of 69.5ºN to 70ºN and longitude band of 2.4ºE to 3.9ºE (Fig. 5b,c). The mean displacement (drift speed) of the vortex center is 3.8 cm s^{-1}. The frequency distribution of drift speed shows that typical vortex drift speed is in the range 1.6 cm s^{-1} to 4.7 cm s^{-1} (Fig. 5d). The spatial climatology of location and drift velocity of the Lofoten Vortex (Fig. 6) shows that a cyclonic drift pattern is dominating. The two-dimensional distribution of the number of occurrences of the vortex is bimodal, with distinct maxima in the proximity of two comparatively wide depressions in the sea floor of the deep Lofoten Basin.

The radius and eddy intensity of the Lofoten Vortex are determined using Eq. (10) and Eq. (11), respectively. The mean radius and EI of the vortex are found to be 46 km and 185 cm^2 s^{-2} respectively. The frequency distribution of the radius of the Lofoten Vortex shows the typical vortex radius to be in the range (1^{st} and 3^{rd} quartile) of 37 to 51 km (Fig. 7a). The frequency distribution of EI of the Lofoten Vortex shows it to be in the range of 111 cm^2 s^{-2} to 235 cm^2 s^{-2} (Fig. 7b). The radius of the Lofoten Vortex (Fig. 7c) shows distinct seasonality with maximum in summer and minimum during winter, consistent with Ivanov and Korablev (1995a). The mean radius of the vortex is less than 40 km during winter, and it increases to 50 km during spring and summer. The annual climatology of EI of the vortex also shows seasonality and has maximum during spring and minimum during late autumn and early winter (Fig. 7d).

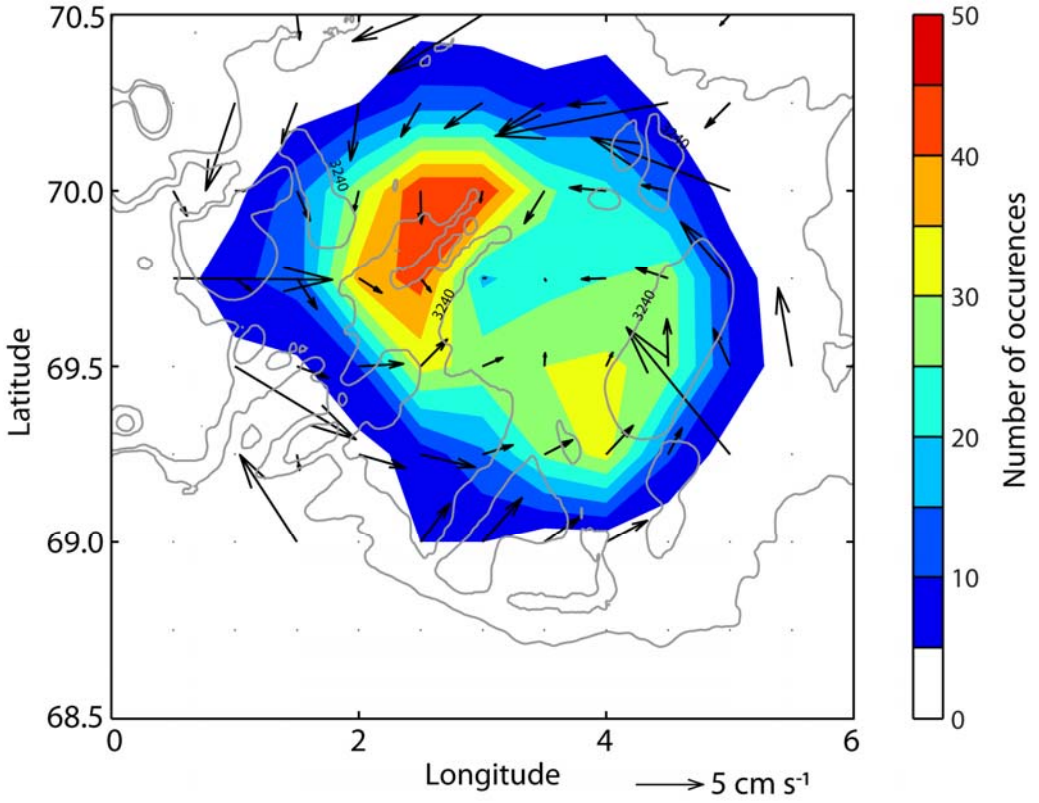

Fig. 6. Mean (bin average) of the movement of the center of the Lofoten Vortex (velocity; arrows) superimposed on its number of occurrences (color) in every 0.5° longitude and 0.25° latitude bins in the deep Lofoten Basin during 18 years time period (1993-2010). Grey lines are isobaths drawn for 3200 m and 3240 m.

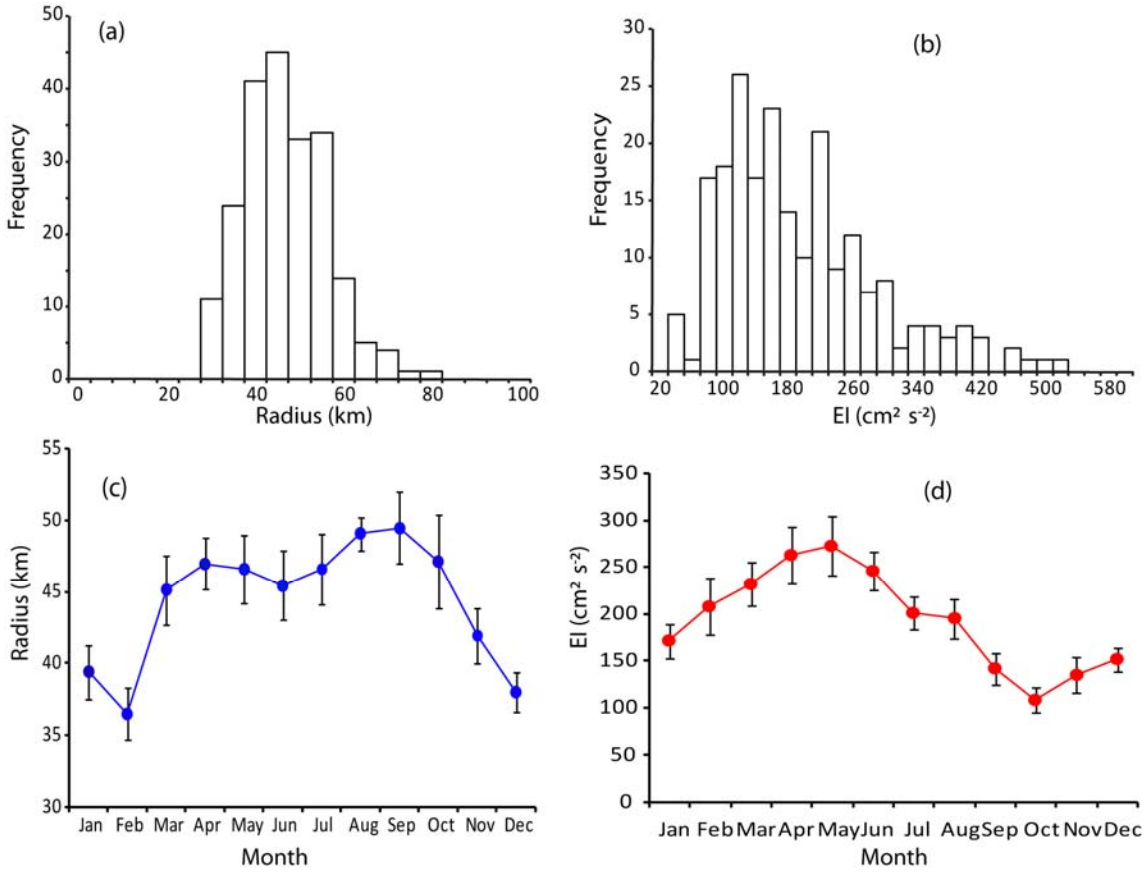

Fig. 7. (a) Frequency distribution of the (a) radius and (b) eddy intensity of the Lofoten Vortex. Annual climatology of (c) radius and (d) eddy intensity of the Lofoten Vortex together with error estimates.

3.3. The vertical structure of the vortex

Earlier studies reported the vertical structure of the Lofoten Vortex to be a doubly convex lens from a few individual hydrographic sections (Ivanov and Korablev, 1995a, b) and numerical modelling (Köhl, 2007). Our study shows a doubly convex lens structure of the Lofoten Vortex manifested in the long term hydrography (Fig. 8). The signature of the doubly convex lens is more distinct in temperature than in salinity. The figures display deep mixing and penetration of AW inside the vortex down to 800 m. The anticyclonic Lofoten Vortex is clearly manifested in the baroclinic velocity field (Fig. 8c), including a distinct maximum (5 cm s^{-1}) at mid-depth (around 400 m). The figure also shows a

maximum in surface *EKE* (200 cm^2 s^{-2}) over the Lofoten Vortex at 3°E, and the concurrence in the location of the Lofoten Vortex from satellite and hydrography derived velocities.

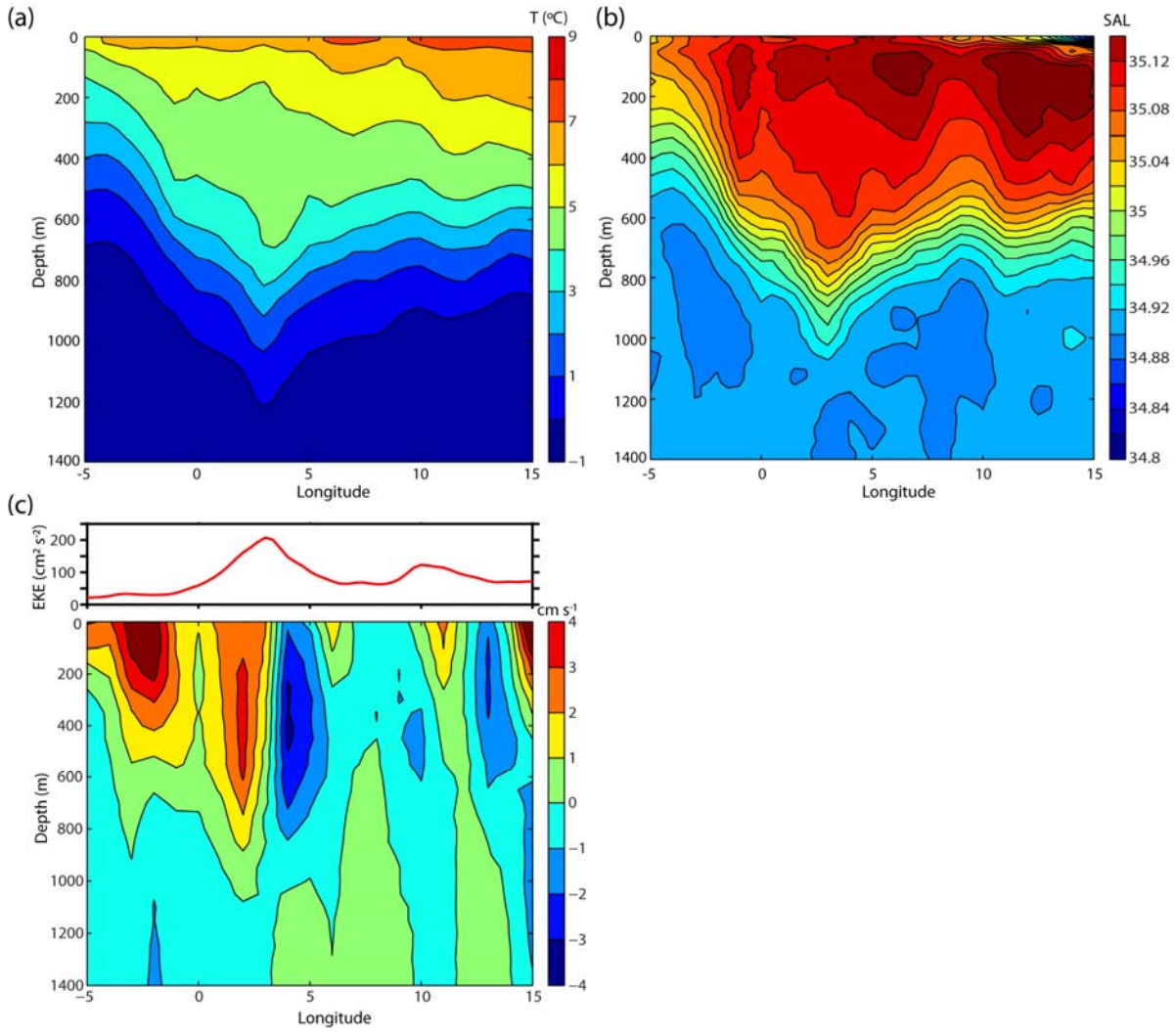

Fig. 8. Vertical structure of the Lofoten Vortex along 70°N through the Lofoten Basin (see Fig. 1). Climatology of (a) temperature, (b) salinity and (c) baroclinic northward velocity (lower panel), based on NISE hydrography (1949-2008) between 69.5ºN to 70.5ºN. (c, upper panel) Climatology of zonal average EKE across 69.9ºN from satellite altimeter data (1995-2010).

In order to assess the seasonality of the Lofoten Vortex, seasonal climatologies of temperature along 70ºN were estimated (Fig. 9). The surface temperature of the Lofoten Vortex is maximum (8ºC) during late summer, and minimum during winter and spring (6ºC). The doubly convex lens structure of the vortex is seen to develop during spring

and is most clearly defined during autumn, but less distinct during winter. Note that even though there is seasonality in the development of the doubly convex lens structure, there is no clear seasonal variability either in the penetration depth of AW within the vortex or in the location of the Lofoten Vortex.

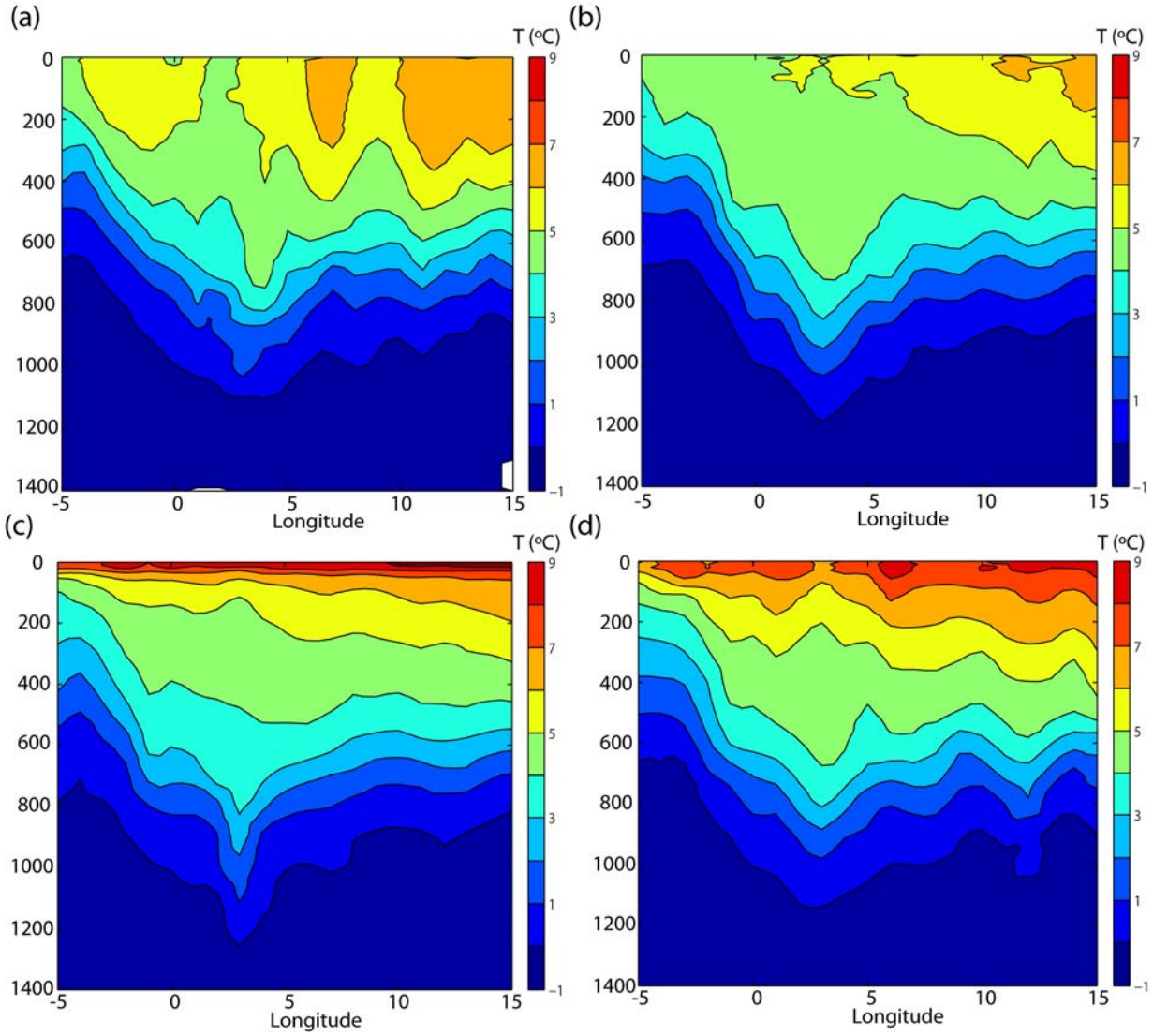

Fig. 9. Seasonal climatologies of temperature along 70°N (69.5ºN to 70.5ºN) from NISE hydrography (1949-2008) during (a) DJF, (b) MAM, (c) JJA, (d) SON.

3.4. Forcing mechanisms

Two forcing mechanisms influencing the Lofoten Vortex are examined in this section: buoyancy forcing and vortex merger. The influence of buoyancy forcing on the Lofoten

Vortex can be studied considering SST anomalies as a proxy for heat loss (e.g., Furevik, 2000). Our analysis shows that the inter-annual variability in the regional SST is similar to that of the vortex' eddy intensity (Fig. 10). Note that a one-year running mean is applied to the monthly time series of EI of the Lofoten Vortex and SST of the deep Lofoten Basin, in order to remove seasonal fluctuations and study the inter-annual variability. The correlation is estimated to r=0.62 at a lag of 11 months, where SST leads EI of the Lofoten Vortex. This indicates a possible link between buoyancy forcing and the strength of the vortex.

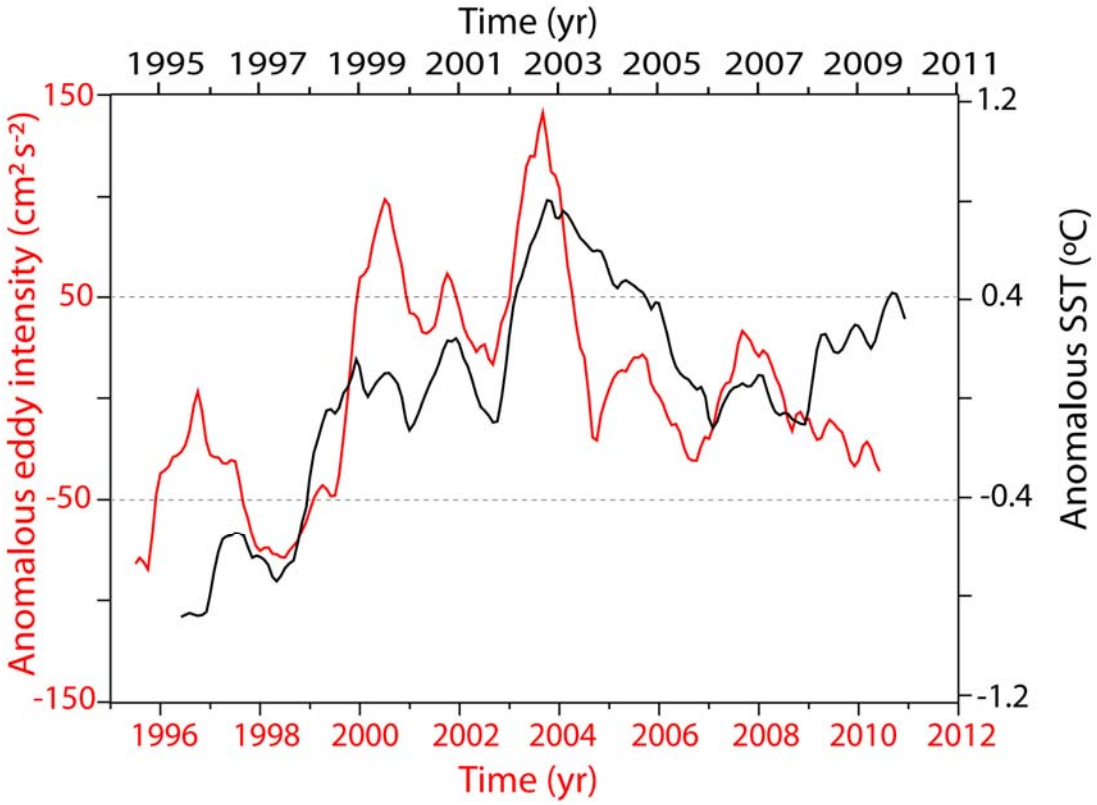

Fig. 10. Monthly time series (12 month running mean) of anomalous eddy intensity of the Lofoten Vortex (red) and SST of the deep part of the Lofoten Basin (black). Time series are de-seasoned and the vertical axes are scaled to plus/minus three standard deviations of the respective time series. The dashed grid lines represent plus/minus one standard deviation. SST has been shifted 11 months forward in time according to the lead time for maximum correlation (r = 0.62). Top and bottom X-axis represents the SST time axis (black) and eddy intensity time axis (red), respectively.

Another possible forcing mechanism influencing the Lofoten Vortex is the merger of anticyclonic eddies with the Lofoten Vortex (Fig. 11). Earlier studies argued that

mesoscale anticyclonic eddies spun from the slope current, propagate southwestward (Andersson et al., 2011; Koszalka et al., 2011), and merge with the Lofoten Vortex (Köhl, 2007).

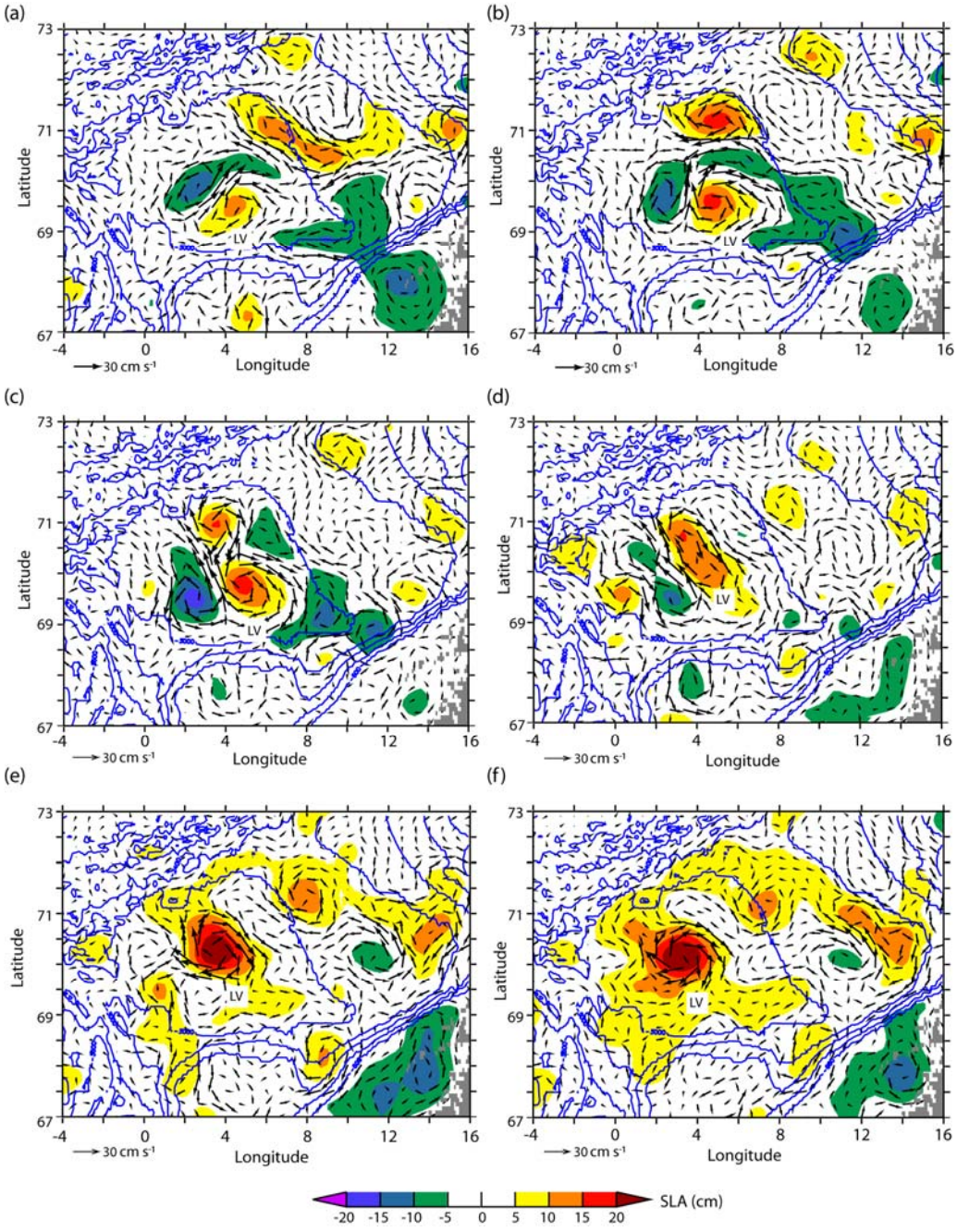

Fig. 11. Example of Lofoten Vortex-vortex mergers. Weekly absolute geostrophic velocity anomalies superimposed on SLA during the weeks of (a) 12-May-1999, (b) 19-May-1999, (c) 26-May-1999, (d) 02-June-1999, (e) 09-June-1999, (f) 16-June-1999. Blue lines are isobaths drawn for every 600 m and the Lofoten Vortex is the peak SLA marked with the symbol 'LV'.

In order to assess this vortex merger process from observations, all weekly velocity anomaly maps were superimposed on SLA maps and visually inspected. The inspection showed evidence of mergers of anticyclonic eddies with the Lofoten Vortex. Fig. 11 shows such a merger during June 1999. The drifting of anticyclonic eddies from the northeast Lofoten Basin towards the Lofoten Vortex and its merger can be seen in Fig. 11a-d. After the merging process, the rotational speed of the Lofoten Vortex increases (Fig. 11d-f). Not all anticyclonic eddies present in the Lofoten Basin were seen to merge with the Lofoten Vortex. The number of mergers identified from visual inspection of the weekly data, is in the range of 4 to 6 mergers/year. The limited and discrete range prohibits further analysis of inter-annual variability.

A distinct seasonality in the number of mergers is nevertheless evident in the annual climatology of the total number of mergers, which has maximum during winter and minimum during late autumn/early winter (Fig. 12). Out of the 72 mergers detected during the past 16 years, 48 occurred during the months February through July, while only 24 mergers were found during August through January. Note that the seasonality of mergers is not affected by any bias in the number of occurrences of the vortex (not shown), i.e. the seasonality in the mergers differs from the seasonality in the number of occurrences of the vortex.

In order to quantify the relation between the seasonality of the slope current, spinning of eddies, and the vortex mergers identified, along-slope volume transports according to Eq. (9) are estimated (Fig. 13). The general picture emerging from the representation of the along-slope transport in Fig. 13b is large variance south of 69°N, as compared to the small variability seen north of this latitude. In the time-mean sense, a distinct maximum of the transport (roughly 2.5 Sv) is found near 69.2°N, whereas the transports on each side of this peak are almost comparable. From a climatological perspective, the monthly-averaged transports (superimposed lines in Fig. 13b) confirm the general behaviour of the slope current along the continental slope of the Lofoten basin, and reveal that the

strongest/weakest transport are found during January/July, hence a winter maximum and a summer minimum dominates the seasonal pattern.

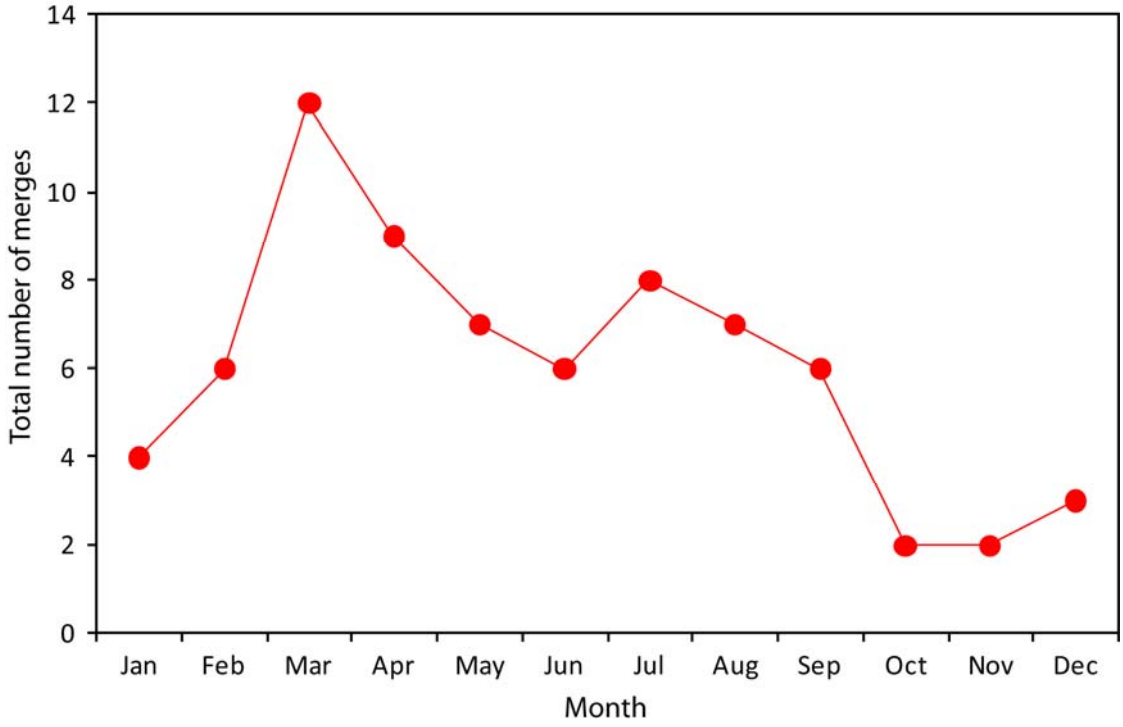

Fig. 12. Annual climatology of the number of Lofoten Vortex-vortex mergers determined from weekly SLA data during 1995-2010.

But, does this seasonal variability characterize the entire slope current? This is investigated (Fig. 13c) by analyzing the detailed seasonality of the transport peak along three locations (L1, L2 and L3) in the slope current (the exact locations are visible in Fig. 13a). In terms of seasonality, all three locations show signs of a maximum during autumn and winter, and a minimum during spring and summer. However, the seasonal amplitude is stronger and more prominent at the southern location (L1) compared to the northern (L3), and less pronounced at the location of the maximum transport (L2). A noteworthy feature is that the spread (indicated by the bars), generally tends to be larger during the cold months. Furthermore, in order to gain a statistical view of the spread we conducted an investigation of the normal probability density function for the three regions (Fig. 13d). The transports in the northern locations (L2 and L3) are characterized by narrow

widths, signifying a small variability in it as indicated by the values of the standard deviation, while the southern location (L1) transport shows a wider distribution and hence a larger variability.

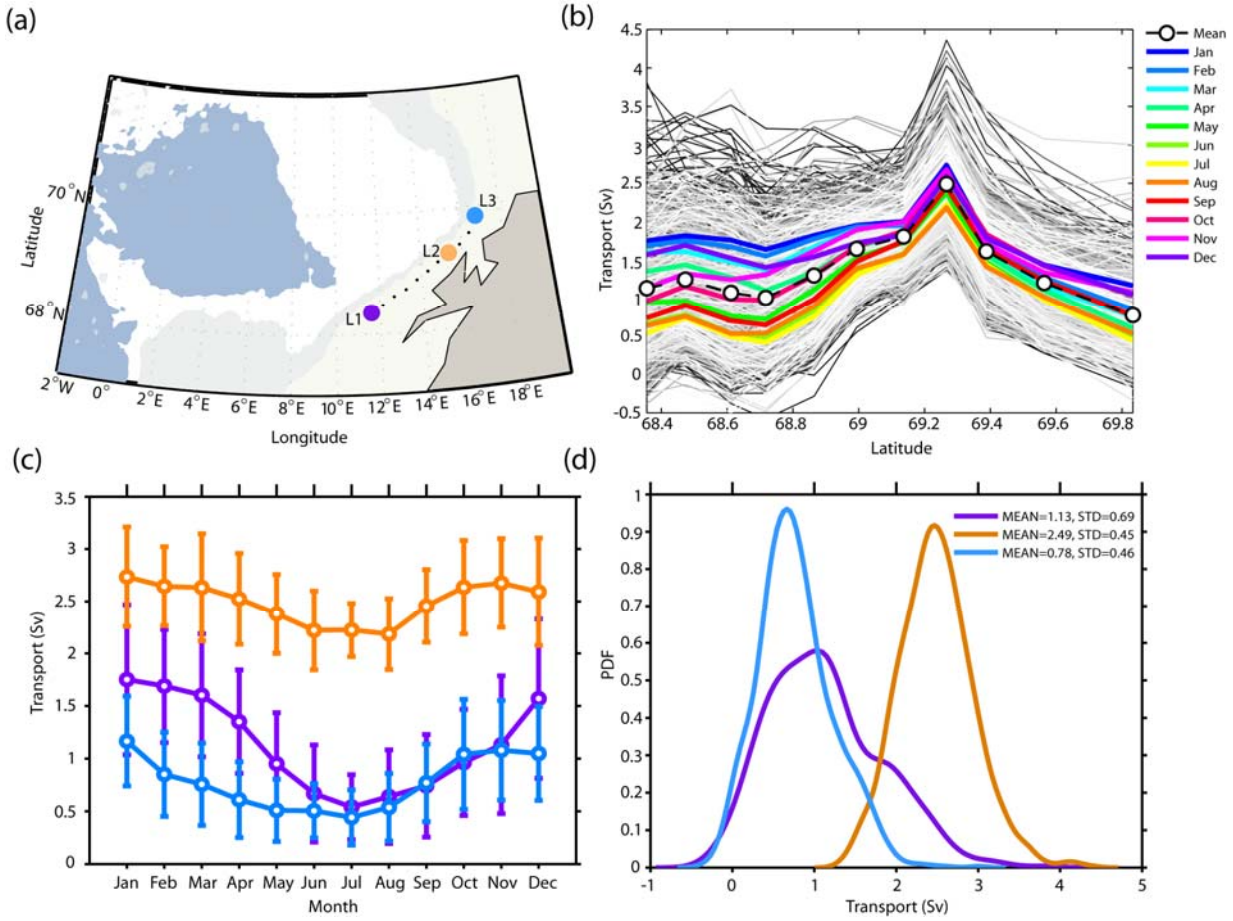

Fig. 13. (a) Map showing the location of the along-slope section used for analysing the variability of the slope current. Observations from the coloured points are used for detailed analysis in panels c and d. (b) The weekly along slope transports (grey) as a function of latitude for the entire altimetric period together with the time-mean transport (dashed and circled black line) and the monthly climatology (colors). (c) The monthly climatology of the transport for the different points seen in the map. (d) Normal probability density function of the same points as in panel c.

4. Discussion

A quasi-permanent anticyclone has been associated with the central Lofoten Basin in several studies (Ivanov and Korablev, 1995a, b; Köhl, 2007, Voet et al., 2010; Andersson et al., 2011; Koszalka et al., 2011). Our observation based study provides a comprehensive quantification of the Lofoten Vortex and highlights its importance in the

Nordic Seas. The persistence of the Lofoten Vortex and its position in the deepest part of the Lofoten Basin is here documented using satellite and hydrographic observations. Our long-term data (Fig. 8) confirms the Lofoten Vortex as a double convex structure with elevated sea surface height, and as a cold surface anomaly (Ivanov and Korablev, 1995a, b). Anticyclonic vortices in the northern hemisphere normally have warmer surface waters (McGillicuddy et al., 1999). The Lofoten Vortex on the other hand is more similar to the cold mode water eddies of the Sargasso Sea (McGillicuddy et al., 1999, 2007), suggesting an active role in ventilating the Atlantic Water in the Nordic Seas. This is further supported by the deep mixed layer inside the Lofoten Vortex indicating deep convection (Fig. 2c).

The tracking of the Lofoten Vortex from satellite observations during 754 weeks, confirms it to reside in the deepest part of the Lofoten Basin (Fig. 6) as reported earlier (Köhl, 2007; Koszalka et al., 2011). Within the deep Lofoten Basin, the Lofoten Vortex resides mainly in two regions which are in the proximity of two depressions (Fig. 6). It can be argued that the Lofoten Vortex is comparatively more stable in the deepest part of the basin. This result is consistent with observations of earlier studies which showed that bottom depressions stabilize anticyclones while bottom elevations stabilize cyclones (Benilov, 2005; Köhl, 2007). From stability analysis, Köhl, (2007) showed that a larger value of topographical parameter will extend the range of stability and argued that the large-scale topographic depression in the Lofoten Basin should stabilize most anticyclones in this region. The positioning of the Lofoten Vortex in the deepest part of the basin is argued to be also associated with topographic β effect (Köhl, 2007). Due to the topographic equivalent of the β-effect which accounts for the northwest propagation of cyclones on a β-plane, cyclones will climb up the slope in an anticyclonic spiral relative to the center of a seamount and anticylones will descent toward the center of a bottom depression in a cyclonic spiral (Carnevale et al., 1991), which explains the presence of the Lofoten Vortex in the deepest part of the basin. The tracking showed that the Lofoten Vortex generally follows a cyclonic path (Fig. 6) with a mean drift speed of

3.8 cm s^{-1} (Fig. 5d). Ivanov and Korablev (1995b) have previously suggested that the Lofoten Vortex drift is guided by the mean cyclonic circulation that largely follows f/H contours (Nøst and Isachsen, 2003). This was later contradicted by Köhl (2007), who modelled the drift of the Lofoten Vortex to be anticyclonic due to the circulation created by cyclones surrounding the vortex. Hence, it appears that the presence of cyclonic eddies in the deep Lofoten Basin is more dominant in the numerical simulation of Köhl (2007) than in the observational record.

Two potential forcing mechanisms influencing both the persistence and variability of the anticyclonic Lofoten Vortex discussed here are buoyancy forcing and vortex merger. The buoyancy forcing, from air-sea heat exchange, can be assessed using SST as a proxy as presented in Section 3.4. The Lofoten Vortex is a cold surface anomaly (Fig. 4b), but a warm anomaly at depth (Fig. 8a). Colder surface water is thus consistent with a less stratified vortex towards the surface relative to climatology (Fig. 8a), and vice versa for warmer surface water. In other words, decreasing SST (e.g., from surface cooling) of the deep Lofoten Basin contributes to a relative stretching of the vortex, and increasing SST (heat gain) to compression. This converts to anomalous cyclonic and anti-cyclonic circulation, respectively, from the conservation of potential vorticity (e.g., Gill, 1982). More quantitatively, the observed 50.1 cm^2 s^{-2} standard deviation (std) of eddy intensity (Fig. 10) corresponds to a vortex center SLA of 4.4 cm for a vortex with a radius of 44 km (cf. Fig. 7a). To explain this SLA by thermal expansion alone would require the 0.4 K std of SST (Fig. 10) to be representative of the upper 200 m of the water column (assuming a thermal expansion coefficient $\alpha = 1.5*10^{-4}$ K^{-1}). We further note that the difference between SST and interior vortex temperature in the climatology (cf. Fig. 8a) is comparable to two std of the filtered SST time series (Fig. 10). This suggests that the observed SST variance is sufficient to ventilate and "recharge" the core vortex water mass.

The above is reflected in the observed inter-annual variability to the extent that change in low-pass filtered SST leads change in EI. The maximum correlation is $r = 0.62$ with a time lag of 11 months (cf. Fig. 10). We thus argue that the variable vortex strength as quantified by EI, and also possibly the intermittent convective mixing that maintains the core vortex water mass, can partly be explained by air-sea heat exchange via variable SST. The fact that the possible cause-and-effect predominantly relates to inter-annual change (for comparison, $r = 0.33$ for the monthly de-seasoned time series), would imply that the described mechanism is not dominant for individual events, but rather manifests itself as an integrated effect. I.e. an inter-annual bias to anomalously warm SST preconditions an anomalously strong anticyclonic Lofoten Vortex. Periods of anomalous cold SST would have the opposite effect, but also make the vortex more biased to convective overturning and thus also add to the persistence of the vortex.

The other forcing mechanism suggested to influence the Lofoten Vortex, is the vortex merger process (Fig. 11). Vortex merger is the interaction of two co-rotating vortices close enough to each other to mix a significant proportion of their vorticity core, and form a single bigger vortex (Rodriguez-Marroyo and Viudez, 2011). In the Lofoten Basin, it has been argued earlier that mesoscale eddies spun from the slope current (Andersson et al., 2011; Koszalka et al., 2011; Skagseth and Mork, 2012) propagate southwestward, and maintain the Lofoten Vortex (Köhl, 2007). Here, we provide observational evidence for the merger process and in particular supporting the hypothesis that mergers contribute to EI of the Lofoten Vortex. The observed increase in vortex intensity after a merger (Fig. 11d-f) indicates such transfer of energy. A seasonal signal with maximum in March is present in the number of mergers. We herein argue that the observed peak in barotropic transport during January along the slope current is a highly plausible mechanism for the eddy shedding. This along-slope transport maximum in January is consistent with the findings of the vortex merging maximum in March, if the south-westward propagating eddies have a travel time of two months from the slope to the western Lofoten Basin as inferred by Poulain et al. (1996). The observed quasi-stable

nature (weak seasonality) of the slope current transport near the eastern rim of the Lofoten Basin (L2 in Fig. 13a) could be one of the potential reasons for the quasi-continuous eddy shedding toward the deep Lofoten basin. This feature is most probably tied to the steep bottom topography, which has a strong capacity to suppress baroclinic eddies (Isachsen et al., 2012) that tend to drift westward targeting the Lofoten Basin, as exemplified in Fig. 11. Furthermore, as the isobaths diverge (area north of L3 in Fig. 13a) there is a tendency of the flow to become turbulent, reinforcing growth of baroclinic eddies. Thus the above discussion ties the maxima in the slope current transport during January to the vortex merging maxima during March.

However, it is observed that there are more anticyclonic eddies present in the Lofoten Basin than those that merge with the Lofoten Vortex. Mesoscale eddies spun into the Lofoten Basin flux heat into the basin, which may balance the large winter heat loss there (Spall, 2010). Rossby et al. (2009) argued that roughly 20 mesoscale eddies per year is needed for this balance. The relatively low number of mergers inferred from the altimeter data indicates that a large number of eddies do not merge with the Lofoten Vortex. We hypothesize that the presence of *cyclonic* vortices in the deep Lofoten Basin (Fig. 11; Köhl, 2007) can partly explain the low number of mergers. When a cyclonic vortex is present near two anticyclonic vortices, the torque exerted by the one counter-rotating vortex on the two co-rotating vortices hinders the merger (Rodriguez-Marroyo and Viudez, 2011). The timing of EI maximum of the Lofoten Vortex (April-May) is slightly later than the maximum in the mergers, even though the input of energy is local. This may be related to the other forcing mechanism proposed, air-sea heat exchange. As discussed, cooling has an opposite effect on EI, thus contributing oppositely to the input of EI by mergers during winter.

It is known that the AW entering the Lofoten Basin has potential importance for the dense water formation of the Atlantic Meridional Overturning Circulation (Mauritzen, 1996; Eldevik et al., 2009). Hydrographic observations show that the penetration of AW

in the Lofoten Vortex is the deepest in the entire Nordic Seas (Fig. 2), suggesting that the Lofoten Basin is a major winter convection site. The concurrence in the location of the Lofoten Vortex and the deep convective site suggest that the vortex is related to this deep convection. The persistence of the Lofoten Vortex ranges from months to years, which means increased residence time of AW and storage of large quantity of AW within it. Preservation of convectively mixed waters within the Lofoten Vortex acts as a precondition for subsequent winter convection. The large heat loss associated with the Lofoten Vortex, as indicated by colder surface waters, further supports strong convection there suggesting that the vortex in particular contributes to the dense water formation of the region.

5. Summary

The Lofoten Vortex is established as an anomalous feature in the Nordic Seas. Two main characteristics of the Lofoten Vortex which distinguishes it from other eddies in the Lofoten Basin are its location and its persistence. The tracking of the center of the Lofoten Vortex confirms it to be persistently residing in the deepest part of the Lofoten basin. The eddy intensity of the Lofoten Vortex shows distinct seasonality with maximum during late winter-spring, and minimum during late autumn-early winter. Observational evidence confirms transfer of energy from other anticyclones to the Lofoten Vortex via vortex merging. While the seasonality in the eddy intensity of the Lofoten Vortex can be explained by vortex merger, the long term variability in the eddy intensity of the Lofoten Vortex is significantly influenced by the buoyancy forcing. The maximum in vortex mergers during March is further linked to the maxima in the slope current transport during January. Finally, we argue that the Lofoten Vortex plays a key role in dense water formation of the region by enhancing winter convection.

Acknowledgements

This research was supported by the European Union and Norwegian Research Council through the projects MONARCH-A, and BIAC. We thank Tore Furevik for his

encouragement. The altimeter products were produced by Ssalto/Duacs and distributed by Aviso, with support from Cnes (http://www.aviso.oceanobs.com/duacs/). The hydrographic data were provided by the Marine Research Institute, Iceland; Institute of Marine Research, Norway; the Faroese Fisheries Laboratory; Geophysical Institute, and University of Bergen, Norway through the NISE project. Léon Chafik is supported by the Swedish National Space Board. This is publication no. AXXX from the Bjerknes Centre for Climate Research.

References

Andersson, M., Orvik, K. A., LaCasce, J. H., Koszalka, I., Mauritzen, C., 2011. Variability of the Norwegian Atlantic Current and associated eddy field from surface drifters. J. Geophys. Res. 116, C08032, doi:10.1029/2011JC007078.

Barron, C. N., Kara, A. B., 2006. Satellite-based daily SSTs over the global ocean. Geophys. Res. Lett. 33, L15603, doi:10.1029/2006GL026356.

Benilov, E. S., 2005. Stability of a two-layer quasigeostrophic vortex over axisymmetric localized topography. J. Phys. Oceanogr. 35**,** 123–130.

Blindheim, J., Rey, F., 2004. Water-mass formation and distribution in the Nordic seas during the 1990s. ICES J. Mar.Sci. 61**,** 846–863.

Bunker, A.F., 1976. Computations of surface energy flux and annual air–sea interaction cycles of the North Atlantic Ocean. Monthly Weather Review. 104 (9), 1122–1140.

Carnevale, G. F., Kloosterziel, R. C., van Heijst, G. J. F., 1991. Propagation of barotropic vortices over topography in a rotating tank. J. Fluid Mech. 223**,** 119–139.

Chaigneau, A., Pizarro. O., 2005. Eddy characteristics in the eastern South Pacific, J. Geophys. Res. 110, C06005, doi:10.1029/2004JC002815.

Chaigneau, A., Gizolme, A., Grados, C., 2008. Mesoscale eddies off Peru in altimeter records: Identification algorithms and eddy spatiotemporal patterns. Prog. Oceanogr. 79, 106–119, doi:10.1016/j.pocean.2008.10.013.

Ducet, N., LeTraon, P. Y., Reverdin, G., 2000. Global high-resolution mapping of ocean circulation from TOPEX/Poseidon and ERS-1 and 2. J. Geophys. Res. 105, 19477–19498.

Eldevik, T., Nilsen, J. E. Ø., Iovino, D., Olsson, K. A., Sandø, A. B., Drange, H., 2009. Observed sources and variability of Nordic seas overflow**.** Nat. Geosci. 2, 406-410, doi: 10.1038/ngeo518.

Furevik, T., 2000. On anomalous sea surface temperatures in the Nordic Seas. J. Climate. 13 (5) 1044-1053.

Furevik, T., Nilsen, J. E. Ø., 2005. Large-Scale Atmospheric Circulation Variability and its Impacts on the Nordic Seas Ocean Climate - a Review. The Nordic Seas: An Integrated Perspective. AGU Geophysical Monograph Series. 158, 105-136.

Gascard, J.C., Mork, K. A., 2008. Climatic importance of large scale and mesoscale circulation in the Lofoten Basin deduced from lagrangian observations, in: Dickson. R. R., Meincke, Jens., Rhines, P. (Eds.), Arctic - Subarctic Ocean Fluxes: Defining the role of the Northern Seas in Climate. Springer., The Netherlands, pp. 131-143, doi: 10.1007/978-1-4020-6774-7_7.

Gill, A. E., 1982. Atmosphere-Ocean Dynamics, Academic Press, London.

Hirschi, J., Marotzke, J., 2007. Reconstructing the Meridional Overturning Circulation from Boundary Densities and the Zonal Wind Stress. J. Phys. Oceanogr. 37, 743-763, DOI: 10.1175/JPO3019.1.

Hwang, C., Wu, C. R., Kao, R., 2004. TOPEX/Poseidon observations of mesoscale eddies over the Subtropical Countercurrent: Kinematic characteristics of an anticyclonic eddy and a cyclonic eddy. J. Geophys. Res. 109, C08013, doi:10.1029/2003JC002026.

Isachsen, P. E., Mauritzen, C., Svendsen, H., 2007. Dense water formation in the Nordic Seas diagnosed from sea surface buoyancy fluxes. Deep Sea Res. Part 1 54, 22-41, doi:10.1016/j.dsr.2006.09.008.

Isachsen, P. E., Koszalka, I., LaCasce, J. H., 2012. Observed and modeled surface eddy heat fluxes in the eastern Nordic Seas. J. Geophys. Res. 117, c08020, doi:10.1029/2012JC007935.

Isern-Fontanet, J., García-Ladona, E., Font. J., 2003. Identification of marine eddies from altimetry. J. Atmos Ocean Tech. 20, 772–778.

Isern-Fontanet, J., García-Ladona, E., Font, J., 2006. Vortices of the Mediterranean Sea: an altimetric perspective. J. Phys. Oceanogr. 36, 87–103.

Ivanov, V., Korablev, A., 1995a. Formation and regeneration of the pycnocline lens in the Norwegian Sea. Russ. Meteor. Hydrol. 9, 62–69.

Ivanov, V., Korablev, A., 1995b, Interpycnocline lens dynamics in the Norwegian Sea. Russ. Meteor. Hydrol. 10**,** 32–37.

Köhl, A., 2007. Generation and stability of a quasi-permanent vortex in the Lofoten basin. J. Phys. Oceanog. 37, 2637-2651.

Koszalka. I., LaCasce, J. H., Andersson, M., Orvik, K. A., Mauritzen, C., 2011. Surface circulation in the Nordic Seas from clustered drifters. Deep Sea Res. Part 1 58, 468-485, doi:10.1016/j.dsr.2011.01.007.

Le Traon, P. Y., Ogor, F., 1998. ERS-1/2 orbit improvement using TOPEX/Poseidon: The 2 cm challenge. J. Geophys. Res. 103, 8045–8057.

Mauritzen, C., 1996. Production of dense overflow water feeding the North Atlantic across the Greenland-Scotland Ridge. Part 1: Evidence of revised circulation scheme. Deep Sea Res. Part 1 43, 769– 806.

McGillicuddy Jr, Johnson, D. J., R., Siegel, D. A., Michaels, A. F., Bates, N. R., Knap, A. H., 1999. Mesoscale variations of biogeochemical properties in the Sargasso Sea. J. Geophys. Res. 104,13381-13394.

McGillicuddy Jr, D. J., Anderson, L. A., Bates, N. R., Bibby, T., Buesseler, K.O., Carlson, C.A., Davis, C.S., Ewart, C, Falkowski, P.G., Goldthwait, S. A., Hansell, D. A., Jenkins, W. J., Johnson, R., Kosnyrev, V.K., Ledwell, J. R., Li, Q. P., Siegel, D. A., Steinberg, D. K., 2007. Eddy/Wind Interactions Stimulate Extraordinary Mid-Ocean Plankton Blooms. Science. 316, 1021-1026, DOI: 10.1126/science.1136256.

Mork, K. A., Skagseth, Ø., 2010. A quantitative description of the Norwegian Atlantic Current by combining altimetry and hydrography. Ocean Sci. 6, 901–911.

Morrow, R., Birol, F., Griffin, D., Sudre, J., 2004. Divergent pathways of cyclonic and anti-cyclonic ocean eddies. Geophys. Res. Lett. 31, L24311, doi:10.1029/2004GL020974.

Nilsen, J. E. Ø., Falck, E., 2006. Variation of mixed layer properties in the Norwegian Sea for the period 1948–1999. Prog. Oceanogr. 70, 58–90, doi:10.1016/j.pocean.2006.03.014.

Nilsen, J. E. Ø., H´at´un, H., Mork, K. A., Valdimarsson, H., 2008. The NISE Data Set. Technical Report 08-01, Faroese Fisheries Laboratory, Box 3051, T´orshavn, Faroe Islands.

Nøst, O. A., Isachsen, P. E., 2003. The large-scale time-mean ocean circulation in the Nordic Seas and the Arctic Ocean estimated from simplified dynamics. J. Mar. Res. 61, 175–210.

Okubo, A., 1970. Horizontal dispersion of floatable particles in the vicinity of velocity singularities such as convergences. Deep Sea Res. 17, 445–454.

Orvik, K. A., Niiler, P., 2002. Major pathways of Atlantic water in the northern North Atlantic and Nordic Seas toward Arctic. Geophys. Res. Lett. 29(19), 1896, doi:10.1029/2002GL015002.

Orvik, K. A., 2004. The deepening of the Atlantic water in the Lofoten Basin of the Norwegian Sea, demonstrated by using an active reduced gravity model. Geophys. Res. Lett. 31, L01306, doi:10.1029/2003GL018687.

Poulain, P. M., Warn-Varnas, A., Niiler, P. P., 1996. Near-surface circulation of the Nordic seas as measured by Lagrangian drifters. J. Geophys. Res. 101(C8), 237–258.

Rhines, P. B., Hakkinen, S., Josey, S., 2008. Is oceanic heat transport significant in the climate system?, in: Dickson. R. R., Meincke, Jens., Rhines, P. (Eds.), Arctic - Subarctic Ocean Fluxes: Defining the role of the Northern Seas in Climate. Springer., The Netherlands, pp. 87-109, doi: 10.1007/978-1-4020-6774-7_7.

Rio, M. H., Guinehut, S., Larnicol, G., 2011. New CNES-CLS09 global mean dynamic topography computed from the combination of GRACE data, altimetry, and in situ measurements. J. Geophys. Res. 116, C07018, doi: 10.1029/2010JC006505.

Rodriguez-Marroyo, R., Alvaro, V., 2011. Vortex mergers in oceanic tripoles. J. Phys. Oceanog. 41, 1239-1251, doi: 10.1175/2011JPO4582.1.

Rossby, T., Ozhigin, V., Ivshin, V., Bacon, S., 2009. An isopycnal view of the Nordic Seas hydrography with focus on properties of the Lofoten Basin. Deep Sea Res. Part 1 56, doi:10.1016/j.dsr.2009.07.005.

Skagseth, Ø., Mork. K. A., 2012. Heat content in the Norwegian Sea during 1995-2005. Ices J. Mar. Sci. 69 (5), 826-832, doi: 10.1093/icesjms/fss026.

Spall, M. A., 2010. Non-local topographic influences on deep convection: An idealized model for the Nordic Seas. Ocean Model. 32, 72-85, doi:10.1016/j.ocemod.2009.10.009.

Voet, G., Quadfasel, D., Mork, K. A., Søiland, H., 2010. The mid-depth circulation of the Nordic Seas derived from profiling float observations. Tellus A. 62 (4), 516–529. doi:10.1111/j.1600-0870.2010.00444.x.

Volkov, D. L., Pujol. I., 2012. Quality assessment of a satellite altimetry data product in the Nordic Seas, Barents, and Kara seas. J. Geophys. Res. 117, 1978-2012. doi: 10.1029/2011JC007557.

Weiss, J., 1991. The dynamics of enstrophy transfer in two-dimensional hydrodynamics. Physica D. 48, 273–294.

PAPER 4

Towards improved estimation of the dynamic topography and ocean circulation in the high latitude and Arctic Ocean: The importance of GOCE

J.A. Johannessen, R. P. Raj, J. E. Ø. Nilsen, T. Pripp, P. Knudsen, F. Counillon, D. Stammer, L. Bertino, O.B. Andersen, N. Serra and N. Koldunov

in The Earth's Hydrological Cycle. Edited by Bengtsson et al., *Springer*. Accepted

Towards improved estimation of the dynamic topography and ocean circulation in the high latitude and Arctic Ocean: The importance of GOCE

J.A. Johannessen[1], R. P. Raj[1], J. E. Ø. Nilsen[1], T. Pripp[1], P. Knudsen[2], F. Counillon[1], D. Stammer[3], L. Bertino[1], O.B. Andersen[2], N. Serra[3] and N. Koldunov[3]

[1] Nansen Environmental and Remote Sensing Center, Bergen, Norway.
[2] Technical University of Denmark, National Space Institute, Lyngby, Denmark.
[3]Center für Erdsystemforschung und Nachhaltigkeit (CEN), University of Hamburg, Hamburg, Germany

Abstract

The Arctic plays a fundamental role in the climate system and shows significant sensitivity to anthropogenic climate forcing and the ongoing climate change. Accelerated changes in the Arctic are already observed, including elevated air and ocean temperatures, declines of the summer sea ice extent and sea ice thickness influencing the albedo and CO_2 exchange, melting of the Greenland Ice Sheet and increased thawing of surrounding permafrost regions. In turn, the hydrological cycle in the high latitude and Arctic is expected to undergo changes although to date it is challenging to accurately quantify this. Moreover, changes in the temperature and salinity of surface waters in the Arctic Ocean and Nordic Seas may also influence the flow of dense water through the Denmark Strait, which are found to be a precursor for changes in the Atlantic Meridional Overturning Circulation (AMOC) with a lead time of around 10 years (Hawkins and Sutton, 2008). Evidently changes in the Arctic and surrounding seas have far reaching influences on regional and global environment and climate variability, thus emphasizing the need for advanced quantitative understanding of the ocean circulation and transport variability in the high latitude and Arctic Ocean. In this respect this study combines *in-situ* hydrographical data, surface drifter data and direct current meter measurements, with coupled sea ice - ocean models, radar altimeter data and the latest GOCE-based geoid in order to estimate and assess the quality, usefulness and validity of the new GOCE derived mean dynamic topography for studies of the ocean circulation and transport estimates in the Nordic Seas and Arctic Ocean.

1. Introduction

Changes in the dynamic topography and ocean circulation between the northern Atlantic Ocean and the Arctic Ocean result from variations in the atmospheric forcing field and convective overturning combined with changes in freshwater runoff and their pathways, mean sea level, sea ice deformation and water mass transformation. The ocean circulation in this region has been subject to investigations since Helland-Hansen and Nansen (1909). In general it can be characterized by four regional circulation regimes and cross regional exchanges and volume transports, namely: the Northeast Atlantic, the Labrador Sea and Canadian archipelago, the Nordic and Barents Seas and the Arctic Ocean as illustrated in Figure 1.

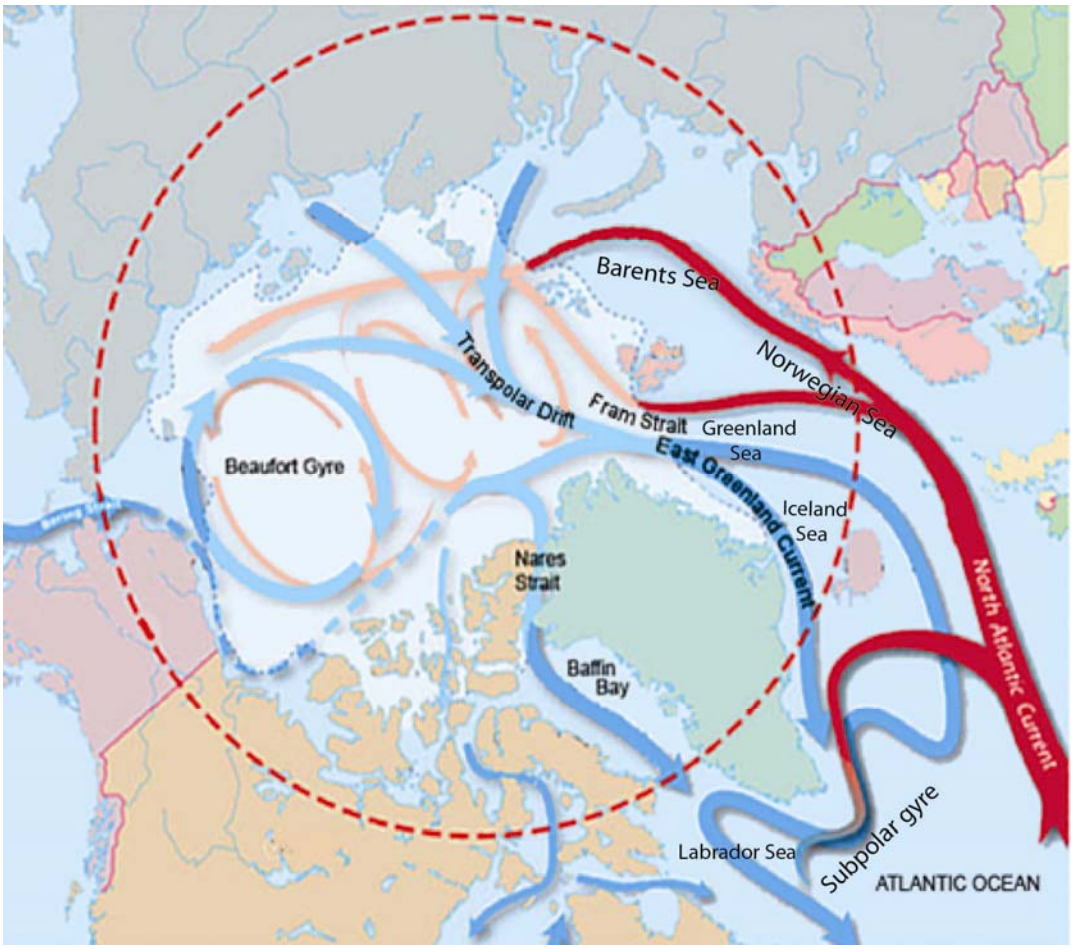

Figure 1. Large scale circulation regimes in the North Atlantic, Labrador Sea, Nordic Seas and the Arctic Ocean. Warm surface currents in red and cold surface and deep currents in blue. The study area addressed in this paper is predominantly confined to the Arctic Ocean, the Norwegian and Greenland Seas and exchanges across the Island-Shetland gap.

Accurate knowledge of the ocean transport variability together with understanding of the water mass transformations within and across these regions is highly needed to quantify changes in the overturning circulation with acceptable uncertainty. The Atlantic Meridional Overturning Circulation (AMOC) is, among other factors, influenced by: variations in the upper ocean and sea ice interaction; ice sheet mass changes and their effect on the regional sea level change; changes in freshwater fluxes and pathways; and variability in the large scale atmospheric pressure field. For instance, changes in the pathways of the freshwater from the Eurasian runoff forced by shifts in the Arctic Oscillation can lead to increased trapping of freshwater in the Arctic Ocean as presented by Morison et al. (2012) that, in turn, may alter the thermohaline circulation in the sub-Arctic Seas.

Using a new combination of the Ice Cloud and Land Elevation Satellite (ICESat) laser altimeter and the Gravity Recovery and Climate Experiment Gravity (GRACE) satellites, along with traditional hydrography, Morison et al. (2012) were able to show that the dominant freshwater changes from 2005 to 2008 were an increase of surface freshwater in the Canada basin balanced by a decrease in the Eurasian basin. These changes were due to a cyclonic (anticlockwise) shift in the ocean pathway of the Eurasian runoff forced by strengthening of the west-to-east Northern Hemisphere atmospheric circulation corresponding to a strengthening of the Arctic Oscillation index. These findings are confirmed in recent results presented by Koldunov et al. (2013). In addition the regional sea level jointly obtained from tide gauges and ERS-1, 2 and Envisat altimeter satellites together with the gravity field and ocean dynamic topography observations from GRACE and GOCE have also recently allowed new innovative studies of the climate-critical mass changes and freshwater flux variations in the high latitude and Arctic Ocean (e.g. Cheng et al., 2012; Prandi et al., 2012; Henry et al., 2012; Knudsen et al., 2011).

In this paper a new GOCE-based geoid and mean dynamic topography (MDT) for the high latitude and Arctic Ocean is obtained, assessed and compared to independent steric height observations and state-of-the-art MDTs. Furthermore, comparisons of surface velocity and transport in the Nordic Seas, based on combination of GOCE gradiometer

gravity estimates and in-situ hydrographic data, is done with estimates from several forced coupled sea ice-ocean models, ocean surface drifter data and direct measurements. The new findings and results are presented according to the ocean dynamic topography in Section 2, ocean surface circulation in Section 3 and volume transport in Section 4. A summary follows in Section 5.

2. Ocean Dynamic Topography

Measurements of the sea surface height have been routinely obtained from satellite altimeter missions, such as the TOPEX/POSEIDON (Fu et al, 2001; Shum et al., 2010) in the last 20 years. Today the annual mean sea surface (MSS) height derived from altimetry is known with millimeter accuracy (e.g. Cazenave et al., 2009) in the open ocean. In addition, knowledge of the marine geoid has drastically improved thanks to satellite gravity measurements from the NASA GRACE (Maximenko et al., 2009; Rio et al., 2011) and ESA GOCE (Johannessen et al., 2003; Bingham et al., 2011; Knudsen et al., 2011) missions in the last decade. In turn, the MDT which is simply the difference between the mean sea surface height (MSS) and the geoid (G) (both referenced to the same ellipsoid as illustrated in Figure 2), can now be determined with new and unprecedented accuracy better than ≈ 3 cm at 100 km spatial resolution (Bruinsma et al., 2013). In comparison to the use of the reference geoid obtained from the Earth Gravitational Model 2008 (EGM2008) this yields a factor 2 improvement in the MDT at this spatial resolution. However, this accuracy is not necessarily applicable to the Arctic Ocean and the neighboring sub-Arctic seas due to presence of sea ice, lack of Jason altimeter coverage and shorter dominant spatial scales.

The GOCE High level Processing Facility (HPF) delivers the Level-2 global gravity model from which geoid heights can be determined (Johannessen et al., 2003; Koop et al., 2007; Bingham et al., 2011). Based on 12 months of GOCE data acquired in the time interval 1 November 2009 to 14 April 2011 three versions of GOCE gravity model are made available: the direct (DIR) approach; the space-wise (SPW) approach; and the time-wise (TW) approach. More details of these gravity field models can be obtained from Bruinsma et al. (2010) and Pail et al. (2011). In addition, so-called combination

models such as the EIGEN-6C (Förste et al., 2011) that combines the GOCE data with terrestrial data have been developed. In this paper we apply the EIGEN-6C gravity model for the computation of the MDT. The corresponding geoid is determined in the mean-tide system and relative to a Topex-ellipsoid. This ensures consistency with the DTU MSS data set referenced to the time period 1993-2009 (Andersen and Knudsen, 2009). Subsequent to subtracting the geoid from the MSS, filtering was carried out eliminating the short wavelength geoid signals, in order to obtain a useful estimate of the MDT. This filtering was carried out using a 80 km Gaussian filter to preserve the upper bound of the mesoscale features in the study area. (Note that Knudsen et al., 2011 applied a 140 km Gaussian filter to determine the global ocean MDT.) In the forthcoming we refer to this as the GOCE-based geoid and MDT.

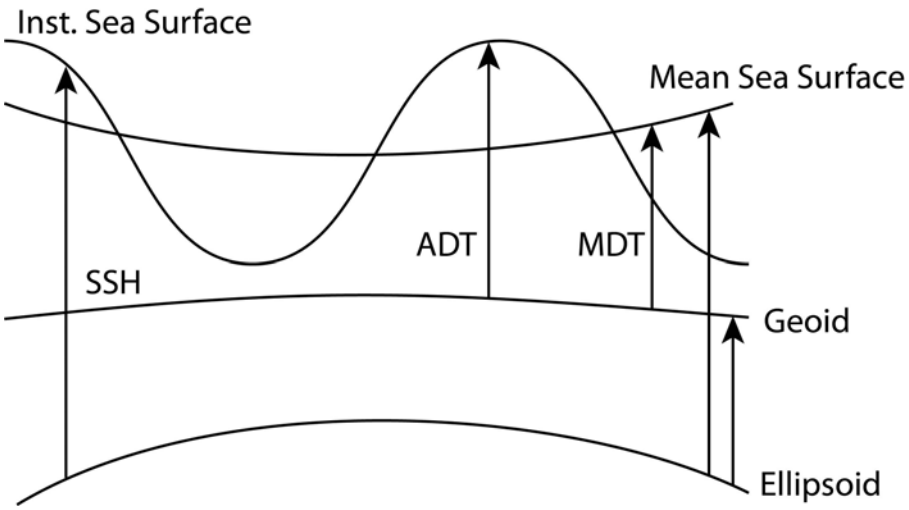

Figure 2. Schematic illustration of the relationship between the absolute and mean dynamic topography (ADT and MDT), the mean sea surface and the geoid referenced to the same ellipsoid. Note the difference between the instantaneous sea surface and the MDT.

Isolines of constant MDT (MSS – G) are usually considered as a streamfunction for the large-scale ocean surface circulation, which the surface geostrophic currents are directed along. In the northern hemisphere (southern hemisphere) the flow is clockwise (anticlockwise) around the topographic high. The magnitude of the global spatial MDT variations is around 2-3 meters, which is about two orders of magnitude smaller than the global spatial changes in the marine geoid and the MSS. This makes the computation of

the MDT and the handling of errors challenging as it is easy to fail to exploit all of the details in the geoid and the MSS when calculating the MDT because of the need to obtain a smooth solution. Herein, the separation of the MDT from the MSS and the geoid is carried out in the space domain, where the MSS is usually represented using processing tools that are available at the dedicated ESA GUT toolbox website http://earth.esa.int/gut/.

The GOCE based MDT shape and spatial pattern representing the mean from 1993-2009 for the North Atlantic, Nordic Seas and the Arctic Ocean is shown in Figure 3. The total MDT elevation range from the high in the Arctic Ocean to the low in the sub-polar gyre in the North Atlantic reaches about 0.9 m. The regional shape of the MDT with the orientation of the dominant slopes in the different sub-domains reveals the presence of the circulation pathways in: (i) the sub-polar gyre south of Greenland; (ii) the inflow of Atlantic Water respectively between Iceland and the Faroe Islands and between the Faroe and Shetland Islands; (iii) the continuous northward flowing Atlantic Water towards the Arctic Ocean; (iv) the southward flowing East Greenland Current; (v) the Beaufort Gyre; and (vi) the transpolar drift in the Arctic Ocean.

The MDT in the Arctic Ocean may display some characteristic features that are caused by problems in the data coverage. Both the GOCE data and the altimeter data do not cover the Arctic Ocean entirely, so within 300-400 km from the pole the data coverage is insufficient to calculate a reliable MDT. Also, the presence of sea ice may hamper the computation of the MSS and hence the MDT. Though care is taken to avoid erroneous data, some of the data that have been used to calculate the MSS may represent the top of the sea ice flow rather than the sea surface. Especially off the coasts of the Canadian Archipelago and northern Greenland the high values of the GOCE MDT may be caused by the influence of the permanent and thick sea ice cover.

The Arctic Ocean displays an elevation change reaching up to about 0.45 m associated with the high in the Beaufort Gyre, and with the corresponding dominant orientation of the slope mostly aligned from Siberia to the northern shores of Greenland. According to Steele and Ermold (2006) the dynamic height in the Arctic Ocean is predominantly

influenced by salinity. In the Nordic Seas the general shape of the MDT favors the cyclonic circulation pattern. This spatial pattern in the MDT agrees well with the spatial pattern in the mean steric height derived from hydrographic data (Nilsen et al., 2008) for the period 1950-2010, respectively referenced to 500m, 1000m and 1500m as shown in Figure 4 and Figure 5.

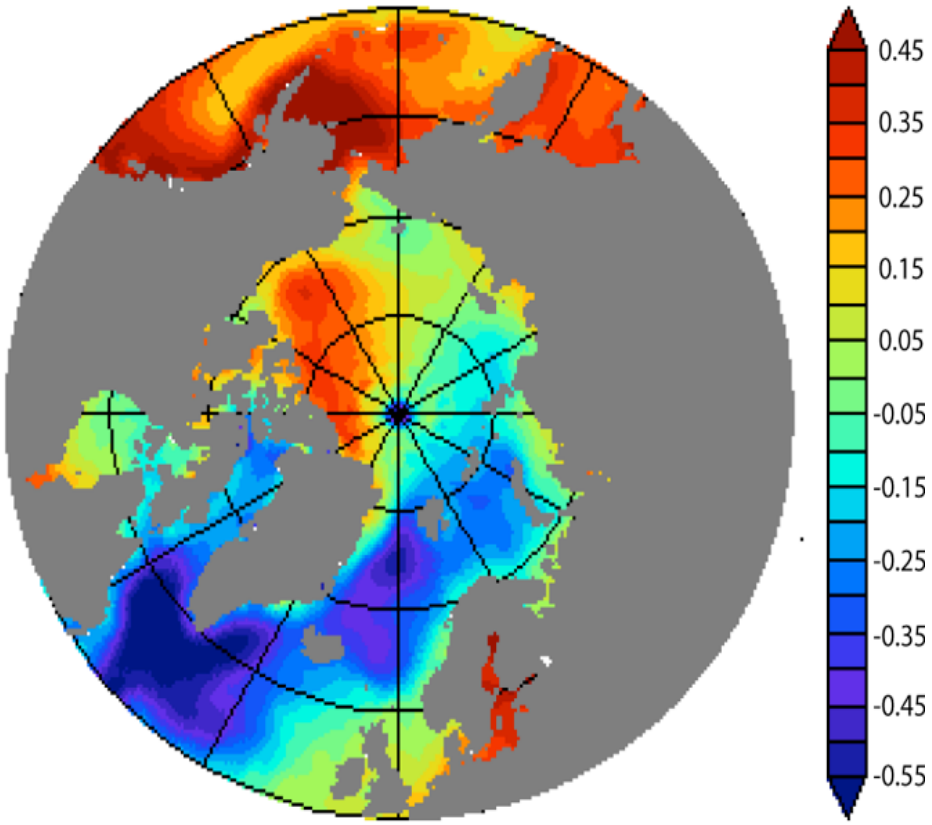

Figure 3. Mean dynamic topography (MDT) derived from the GOCE gradiometer data (release 3) and altimetry (from 1993-2009) with a spatial resolution of about 80 km. Colour bar is in units of meter. The structures in the North Pacific are not investigated further in this paper. Note that the GOCE data (release 4) available since March 2013 is more accurate due to more than a doubling in the amount of data).

The steric height calculation is done according to Siegismund et al. (2007), where the steric height is referenced to a constant density ρ_0 from salinity of 35 and temperature of 0°C. More information on the concept and application of the steric height is given by Tomczak and Godfrey (2003). The difference in these height fields primarily reveals the effect of the vertical distribution of temperature and salinity in the upper 1500 m, predominantly influenced by the advection and spreading of the Atlantic Water. Apart

from the changes occurring in the Lofoten Basin the overall structure remains largely unchanged when the density structures between 1000 and 1500 m are included. This suggests that the baroclinic circulation in the Nordic Seas is driven by the temperature and salinity structures of the Atlantic Water in the upper 1000 m.

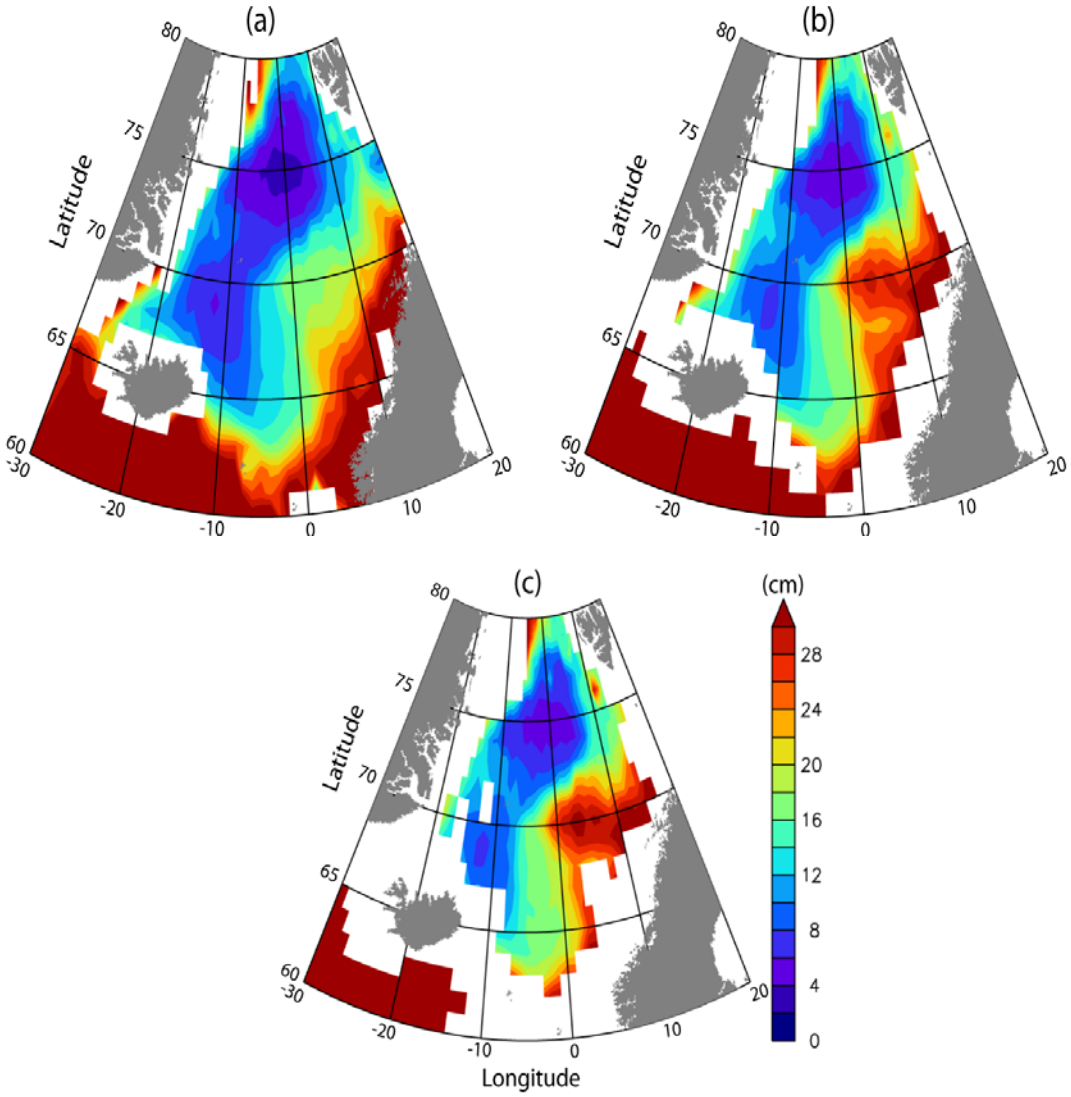

Figure 4. Observed mean steric height for the period 1950–2008 for the reference depths (a) 500 m, (b) 1000 m, and (c) 1500 m. The color-scale increment is in cm.

In the Nordic Seas the total range in the MDT derived from the combined GOCE and altimetry data is around 0.50 – 0.55 m as seen in Figure 5a. In comparison, the range of the mean steric height of 0.30 m (Figure 5b) suggests that there might be a significant contribution to the MDT pattern from the large-scale atmospheric pressure field as well

as deep barotropic currents in some of the sub-basins. Siegismund et al. (2007) moreover concluded that the seasonal cycle of the steric height (for the period 1950 to 1999) is predominantly associated with the temperature variations in agreement with previous studies on global scale (e.g., Gill and Niiler, 1973; Mork and Skagseth, 2005).

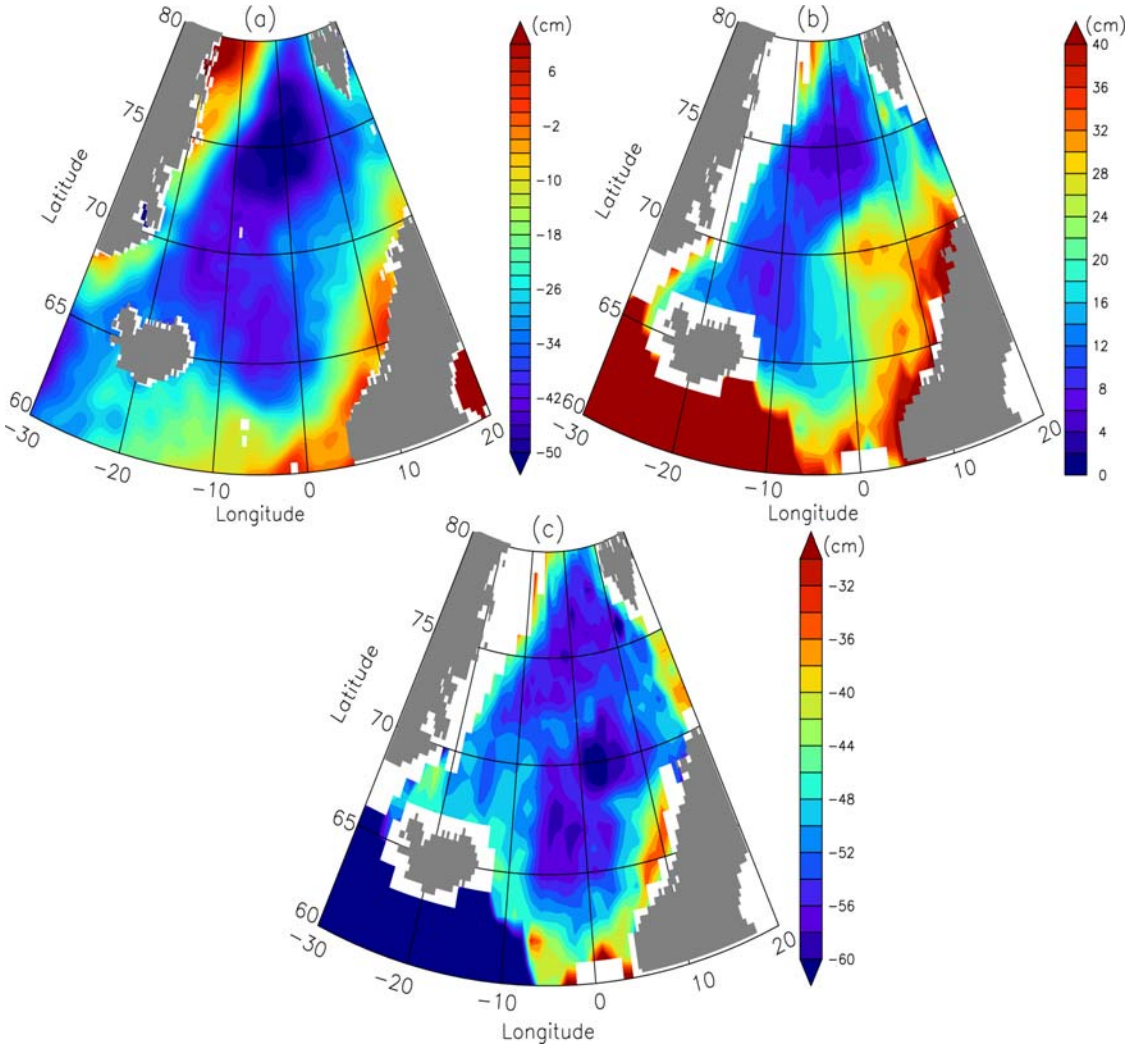

Figure 5. (a) MDT derived from combined GOCE and altimetry, (b) steric height derived from the in-situ hydrographic database where the white areas in the 1500 m reference steric height (see Figure 4) is filled with steric height values representing every 100 m from 1400 m to 500 m, and (c) difference between (a) and (b). The color bars represent the height contours in unit of cm. Note the different colour ranges.

By subtracting the GOCE based MDT from the hydrographic based steric height associated with the baroclinic structure in the water masses an estimate of the barotropic contribution to the MDT is derived as shown in Figure 5c. The barotropic contribution

contains distinct elevation changes of about 10 cm with pattern consistent with the known barotropic cyclonic circulations in the Greenland Sea, the Lofoten Basin and in the Norwegian Sea (Nøst and Isachsen, 2003). Evidence of this cyclonic barotropic circulation in the Norwegian Sea has also been observed from Argo floats in the intermediate waters below the Norwegian Atlantic Current (Søiland et al., 2008). In conclusion the assessment of the GOCE derived MDT for the Nordic Seas and the Arctic Ocean is promising.

Table 1. Characterization of the 3 coupled sea ice-ocean models used for inter-comparison to the GOCE derived MDT and mean surface geostrophic current.

Model run	Region	Spatial resolution	Period	Vertical grid of layers forcing
ATL12	Atlantic Ocean north of 33S including the Nordic Seas and the Arctic Ocean. Uses ETOPO 2min resolution bathymetry.	~8 km	1948-2009 Hindcast	z-coordinates, 50 levels NCEP-6 hourly
MICOM	North of 30 S with Nordic Seas and Arctic Ocean included. Uses ETOPO 5 min resolution bathymetry.	~15 km	1948-2007 Hindcast	Isopycnal, 35 layers NCEP-6 hourly
HYCOM	High latitude- Arctic Ocean Uses GEBCO 1 min resolution bathymetry	~12- 16 km	1993-2010 Hindcast	Hybrid coordinates 28 layers ERA Interim - 6 hourly

In view of the promising GOCE-based results presented above they are also providing a new opportunity for inter-comparison and validation of coupled ocean-ice models and re-analyses fields. As specified in Table 1, the three models used in this inter-comparison

study include the regional set-up of: the ATL (MITgcm) model (Serra et al., 2010); the MICOM model (Sandø et al., 2012); and the HYCOM model (Bleck, 2002; Sakov et al., 2012). The models are either forced by the 6 hourly NCEP reanalysis field (ATL and MICOM) or the ERA Interim field (HYCOM). Ignoring the offset in the mean MDT the three coupled sea ice – ocean models in general reproduce comparable overall spatial structure of the MDT in the Arctic Ocean, the Nordic Seas and the North Atlantic, notably the high in the Beaufort Gyre and the depressions in the Nordic Seas and the Sub-polar Gyre (Figure 6).

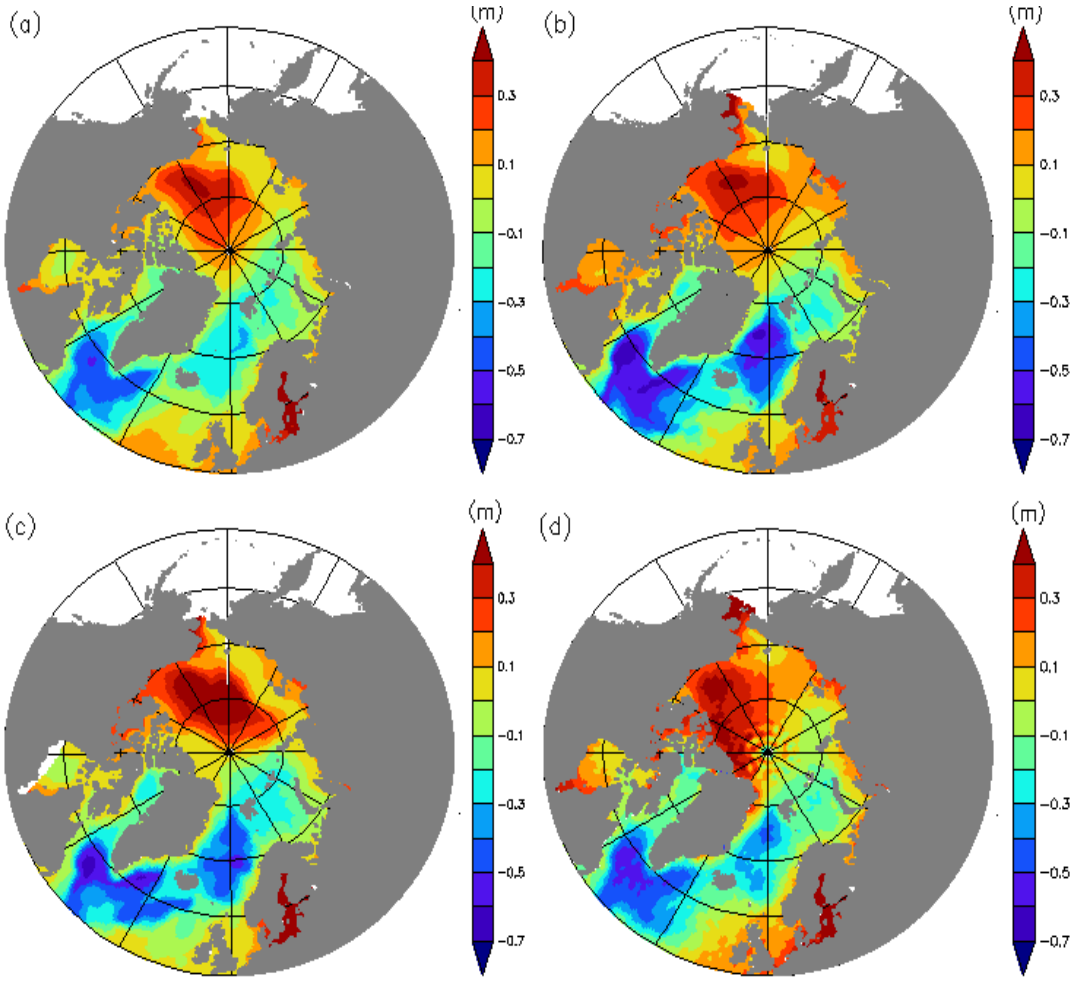

Figure 6. MDT fields referenced to the full region average: (a) the HYCOM MDT (free run) from 1993-2010; (b) the ATL from 1993-2009; (c) MICOM from 1993-2007; and (d) the GOCE-based MDT from 1993-2009. The color bars are in meters. All the fields are interpolated to a 0.25 degrees resolution grid.

The model highs in the Beaufort Gyre are circular and located towards the deep Canadian Basin with decreasing values towards the Eurasian Basin, providing an elevation difference of 0.5-0.6 m. The MICOM-field, however, has a gyre that extends into the Eurasian Basin, that, in turn, leads to incorrect transpolar drift. In comparison, the GOCE-based elevated feature in the Beaufort Sea is shifted more towards the Canadian Archipelago, while the total elevation difference remains the same. This shift in location is in agreement with the recent findings by Kwok and Morrison (2011) and Morison et al. (2012). Overall the MDT patterns in the model fields for the Arctic Ocean are in reasonably good agreement with the GOCE-based MDT map.

In the central domain of the Norwegian-Greenland Seas the suppression of the MDT in the three models corresponding to the large-scale cyclonic circulation pattern with the northward flowing Norwegian-North Atlantic Current (NwAC) and the southward flowing East Greenland Current (EGC) is consistent in location, although the magnitudes and spatial structures of the suppression differ between the models as well as in comparison to the GOCE-based MDT pattern. The largest suppression is found in the ATL model with a minimum deviation from the average of -0.6 m in the northern Greenland Sea being almost twice as large as in the GOCE-based MDT located in the same area. Similar tendencies are seen in the Sub-polar Gyre, although the difference in the minima between the ATL model and the GOCE-based MDT now is reduced by a factor of 2.

The most prominent discrepancies are the mismatch in the MDT along the Canadian Archipelago and northern Greenland coast, and the models lack of higher elevations associated with the spread of Atlantic Water in the Norwegian Sea, notably around the Vøring Plateau. The former might be related to presence of thicker multi-year sea ice that could influence the estimation of the MSS and thus the GOCE-based MDT. Kwok and Morrison (2011) did not reveal this particular high in the MDT confined to the coastal region from IceSAT data. The latter is related to the topographic steering of the baroclinic western branch of the NwAC (Nilsen and Nilsen, 2007), as well as eddy transport of buoyant waters from the slope branch of the NwAC into the Lofoten Basin

(Rossby et al., 2009), which both are challenging to model. Furthermore, although totally lacking the broadness of the NwAC, the ATL model is the only model with the doming of the densest waters of the Nordic Seas placed in the correct basin, the Greenland Basin. These differences in magnitude and spatial structure of the model and GOCE-based MDTs imply different strengths and orientations of the slopes in the MDT. In turn, the mean surface geostrophic currents are expected to have discrepancies that subsequently will lead to differences in the estimation of the associated transport of water masses. This is further assessed in the next sections.

3. Surface circulation

With access to the new GOCE-based MDT with unprecedented accuracy the uncertainties in mean ocean circulation and transport estimation are expected to improve. The mean surface geostrophic velocities are computed from the MDTs, under the assumption of the geostrophic balance, whereby:

$$u_s = \frac{-g}{f}\frac{\partial MDT}{\partial y}, \quad (1)$$

$$v_s = \frac{g}{f}\frac{\partial MDT}{\partial x}, \quad (2)$$

where u_s and v_s are components of the surface geostrophic velocity, g is the acceleration due to gravity, f is the Coriolis parameter, and x and y are the longitudinal and latitudinal directions. The corresponding surface geostrophic current derived from the GOCE MDT for the Nordic Seas over the period 1993-2009 is shown in Figure 7 and compared to the independently derived CNES-CLS09 MDT and Maximenko and Niiler MDT (which both are using a GRACE-based geoid model together with in-situ Argo floats and surface drifter data integrated over the 17 years period from 1992 to 2009), as well as the climatologic mean surface geostrophic velocities (predominantly based on drifters in the Nordic Seas from 1991-2010) from the surface drifter data (Lumpkin and Garraffo, 2005; http://www.aoml.noaa.gov/phod/dac/drifter_climatology.html).

The large-scale cyclonic surface circulation regime is well reproduced in all three fields. However, while the strongest mean surface currents of the inflowing Atlantic Water to

the Norwegian Sea reaching nearly 0.2 m/s are derived from the GOCE MDT, the inflow in the other two surface current fields is clearly weaker with maximum speed not much more than 0.10 m/s.

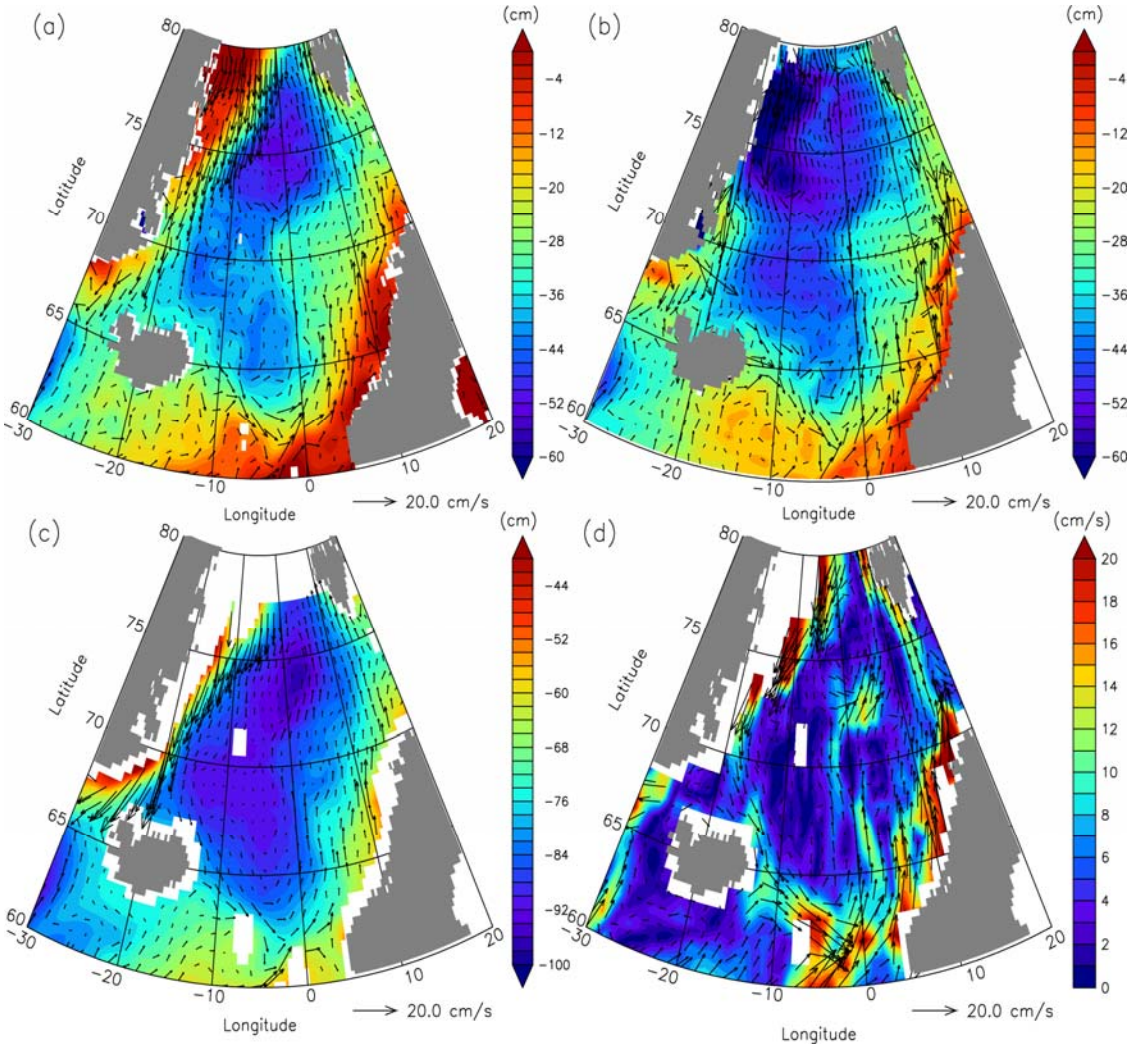

Figure 7. Mean surface geostrophic velocities shown by the vectors superimposed on mean dynamic topography (MDT) derived from (a) GOCE; (b) CNES-CLS09; (c) Maximenko et al.,2009; and (d) mean surface velocity vectors derived from the climatology of the global surface drifter data. Colour scale indicate the MDT in cm for (a) to (c) and speed in cm/s for (d). Current-vector scale shown in the lower right corner.

Moreover, it is only the GOCE-based surface geostrophic current that reveals distinct expressions of cyclonic circulation in the Greenland Basin, Norwegian Basin and Iceland Sea, as well as the broadening of the NwAC over the Vøring Plateau and in the Lofoten Basin, i.e. signs of a proper western (baroclinic) branch of the northward flowing Atlantic Water. From this intercomparison and assessment it is therefore evident that the

GOCE-based geoid provides a reliable representation of the MDT and mean ocean surface circulation in the Nordic Seas. Evidently, this is further supported by the mean surface circulation pattern derived from the climatology of the surface drifter data as shown in Figure 7 (d).

A comparison of the speed of the GOCE based mean surface geostrophic currents and corresponding model based currents for the Nordic Seas is shown in Figure 8.

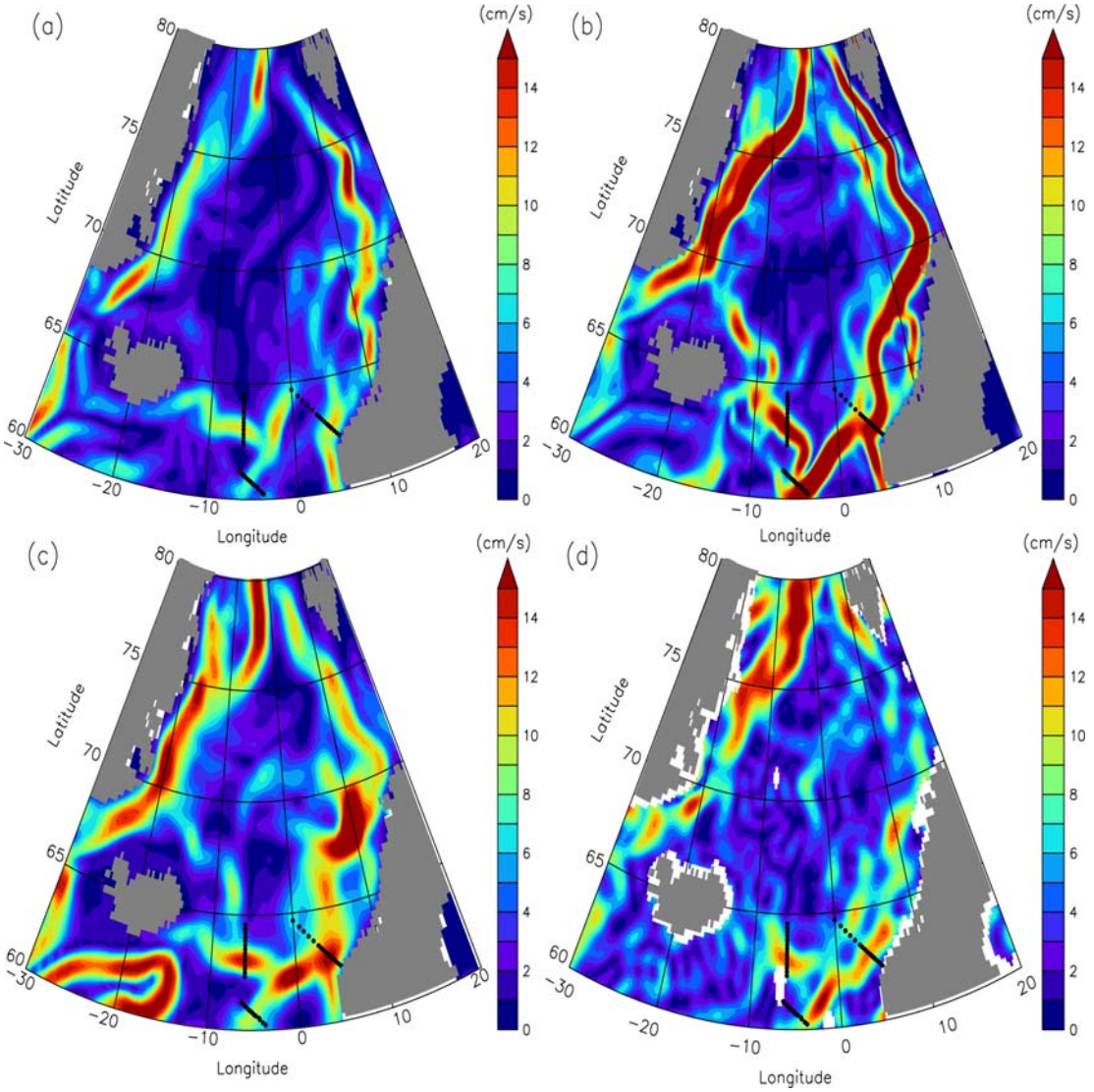

Figure 8. Inter-comparison of models and GOCE based mean absolute surface geostrophic velocity from: (a) HYCOM model from 1993-2010; (b) the ATL model from 1993- 2009; (c) MICOM model from 1993-2007; and (d) GOCE. The color bars are in cm/s. The 3 black dotted lines mark the position of the Island-Faroe Ridge section, the Faroe-Shetland Channel section and the Svinøy section.

In general it must be emphasized that the finer spatial model resolution versus GOCE may favor stronger simulated surface speeds. All models indicate intensified currents at the inflows from the northeast Atlantic Ocean, and in the boundary (slope) currents of the Nordic Seas. The ATL model shows a strengthened component of internal circulation in the Nordic Seas, by very strong currents along all the margins. Regarding the currents over the mid ocean ridges and other internal topographic features, it is only the MICOM run that shows signs of reproducing the level of intensification shown in the GOCE based speeds, however only at one location, the Mohn Ridge (as also noticed in Figure 7d).

For a more detailed study of the seasonal variability induced by the altimetric observations, the surface slopes and meridional velocities across 75°N are presented in Figure 9 together with the model derived fields. The seasonal mean velocities are estimated by replacing MDT in equation (1) and (2) with Absolute Dynamic Topography (ADT). Note that ADT is determined as the sum of MDT and monthly mean sea level anomaly (SLA) data. The new high-resolution SLA data (obtained from the CLS lead Sea Level Climate Change Initiative project funded by ESA) are referenced to the time period 1993-2009 and hence consistent with the DTU10 MSS data used in the calculation of GOCE MDT.

The main expected features of the flow towards and from the Fram Strait is revealed by the mean velocities: - The two branch northward flowing West Spitsbergen Current (WSC) around 8°E and 15°E; - the strong southbound EGC at 10°W; - and some minor, possibly cyclonic, circulation features around 0°E. Seasonal differences are most pronounced in the WSC. Both branches are strongest in wintertime, with a near doubling of the easternmost branch, which is due to the general (wind driven) intensification of the circulation in the region. This is consistent with velocity retrievals and transport estimates reported by Mork and Skagseth, (2005). The western frontal branch stays relatively strong also during the rest of the year, likely due to the summertime spread of buoyant surface water from the coast to the front (as seen further south in the NwAC; Nilsen and Falck, 2006), maintaining a steep frontal surface slope. In comparison the

model based MDT slopes along 75°N and the corresponding meridional geostrophic velocities across the same latitude consistently reveal that the ATL model has the steepest slopes and hence the strongest flow field for both the northward flowing NwAC as well as the southward flowing East Greenland Current. Moreover, it is only the ATL model that reproduces the double peak in the WSC current in agreement with the mean and seasonal observation based findings.

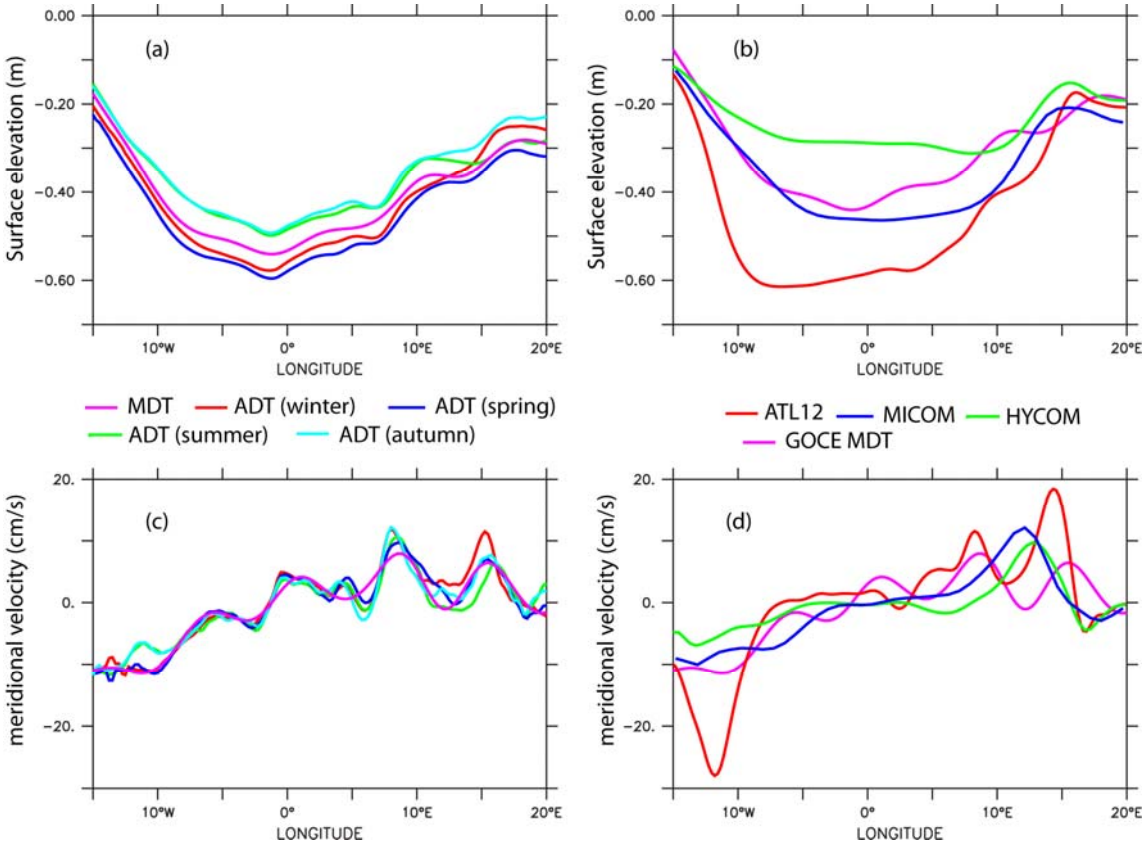

Figure 9. Climatologies of (a,b) dynamic topography across 75°N and (c,d) corresponding meridional absolute geostrophic velocities: (a,c) seasonal climatologies from combined GOCE-based MDT and altimetry and (b,d) comparison of GOCE based MDT with MDT from ATL12, MICOM, and HYCOM. Note that in (b), each MDT is referenced to its full-region average as defined in Figure 6.

4. Volume transport

By combining the GOCE derived MDT and altimetric sea level anomalies with the comprehensive hydrographic data base an estimate of the mean and variable transport of Atlantic Water entering the Nordic seas is obtained for the period 1993 – 2011. Using 44 CTD-sections for the Island-Faroe Ridge (IFR), 84 CTD-sections for the Faroe-Shetland Channel (FSC) and 76 CTD-sections taken along the Svinøy section (see Figure 8 for

locations) the baroclinic velocity structures in the Atlantic Water defined by salinity values S>35 were estimated across these sections. Combined with the barotropic velocity values the absolute velocities are then retrieved, and when these are multiplied to the area covered by the Atlantic Water we obtain estimates of the corresponding volume transports of Atlantic Water across the 3 sections (see Table 2).

Table 2. Comparison of volume transport estimates from combined GOCE, altimetry and in-situ to previous studies as well as estimates from simulation models for the Island-Faroe Ridge (IFR), Faroe-Shetland Channel (FSC), NwAFC, NwASC in the Svinøy Section and the total Svinøy Section. (* only from 1997-2007.)

Source	Data	Period	IFR [Sv]	FSC [Sv]	Svinøy [Sv]		
					NwAFC	NwASC	Total
The current study	GOCE + Altim. + hydr	1993-2011	3.5	4.1	3.0	3.9	6.9
Mork and Skagseth (2010)	Altim. + hydr.	1993-2009			1.7	3.4	5.1
Skagseth et al. (2008)	current meter	1995-2006				4.3	
Orvik and Skagseth (2003)	curr. meters	1998-2000				4.4	
Orvik et al. (2001)	curr. meters + ADCP + hydr.	1995-1999			3.4	4.2	7.6
Østerhus et al. (2005)	Bottom ADCP + hydr.	1999-2001	3.8	3.8			
Hansen et al. (2010)	Bottom ADCP + hydr.	1997-2008	3.5				
Hansen et al. (2003)	Bottom ADCP + hydr.	1997-2001	3.5				
Sandø et al. (2012)	MICOM model	1994-2007	4.7*	4.7			
The current study	HYCOM model	1993-2007	1.8	1.5	2.0	0.6	2.6
The current study	MICOM model	1993-2007	3.5	6.9	3.5	5.0	8.5
The current study	ATL model	1993-2007	3.5	4.2	3.5	4.7	8.2

From the combination of GOCE, altimetry and hydrography the mean inflows of Atlantic Water (determined by salinity >35) across the Iceland Faroe Ridge and through the

Faroe-Shetland Channel are estimated to approximately 3.5 Sv and 4.1 Sv respectively (1 Sv = 10^6 m^3s^{-1}). The former is in very good agreement with Hansen et al. (2010). The mean transport of the two branches of Atlantic Water crossing the Svinøy section, e.g. the Norwegian Atlantic Slope Current (NwASC) and the Norwegian Atlantic Front Current (NwAFC) is respectively 3.0 Sv and 3.9 Sv. The latter value is acceptable with previous transport estimates for the NwASC reported by Mork and Skagseth, (2010); Orvik and Skagseth, (2003); and Orvik et al., (2001) as documented in Table 2, taking into account the slight differences in the integration periods.

In comparison, the mean (1993-2007) transports estimated from the 3 models across these sections shows quite different values as noticed in Table 2. One explanation for this is partly related to the definition and choice of layers for the transport estimations. The best agreement between the model and the combined GOCE-based and hydrographic data is clearly obtained for the ATL simulation with transport estimates across the IFR and FSC of 3.5 Sv and 4.2 Sv respectively. For the Svinøy section the comparison is, in general, less satisfactory. The HYCOM model clearly underestimate the observed transport of 5.1 Sv reported by Mork and Skagseth (2010) as well as the GOCE-based estimate of 6.9 Sv. This is mainly due to a miss-location of the NwAFC in the HYCOM simulation as seen in Figure 8a. In contrast, the MICOM and ATL models, having comparable mean transport estimates in the range of 8.2 - 8.5 Sv overestimate both the GOCE-based estimate and the transport reported by Mork and Skagseth (2010). Overall, this large spread in mean transport estimates implies significant differences in the mean northward advection of heat and salt to the Nordic Seas and Arctic Ocean. This, in turn, affects both the evaporation-precipitation fluxes and convective overturning in the Norwegian and Greenland Seas. Further studies are needed to investigate the accuracies of these transport estimates.

Taking benefit of the temporal variability observed in the SLA and hydrographic data the mean and seasonal cycle in the transport of the inflowing Atlantic Water for the period 1993 to 2009 can also be estimated and inter-compared as shown in Figure 10. On average the NwASC contains approximately 57 % (or 3.9 Sv) of the total mean volume

transport across the Svinøy section of about 6.9 Sv. The mean seasonal variability reveals a pattern with largest transports (9.3 Sv) in winter being almost twice as large as the summer transport minimum (5.4 Sv). Moreover, the mean seasonal NwASC transport always exceeds the mean seasonal NwAFC transport, while the latter display a narrower range of seasonal variability in the volume transport. This suggests that the seasonal changes of the transport across the Svinøy section are predominantly controlled by seasonal changes in the transport of the NwASC. The partitioning of these total transport estimates (both in the mean and seasonal signals) into the respective barotropic and baroclinic components are shown in Figure 10b and Figure 10c and reveal distinct differences. While the transport in the NwASC is dominated by the barotropic flow as expected along the shelf break at the Svinøy section, the transport of the NwAFC, in contrast, is clearly larger in the baroclinic component with the exception of the autumn period.

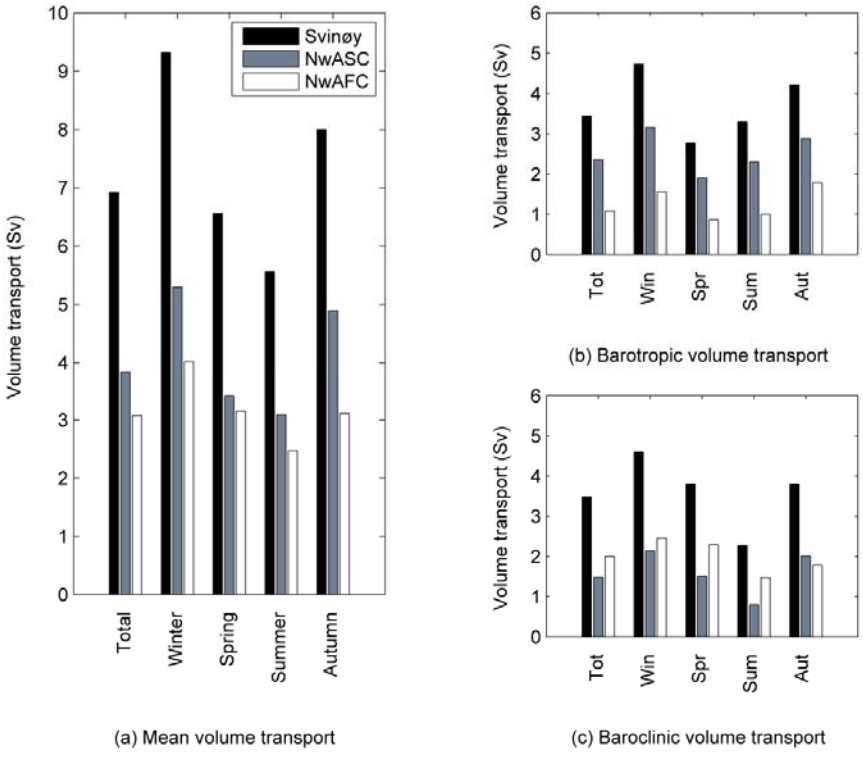

Figure 10. Mean annual and mean seasonal total volume transport estimates (a), the respective barotropic components (b) and baroclinc components (c) for the Svinøy section including the NwASC and the NwAFC for the period 1993-2010 based on combined use of GOCE, altimetry and in-situ hydrography data. The grey-scale legend is marked in (a).

These GOCE-based estimates together with high-quality in-situ hydrographic data are providing new and promising abilities to examine the seasonal transport variability (total as well as barotropic and baroclinic components) across key selected sections. As such, it is also providing an important tool for validations of model circulation and transports between the Northeast Atlantic Ocean and the Nordic Seas and Arctic Ocean.

5. Summary

In combination with *in-situ* hydrographical data, surface drifters and current meter measurements, coupled sea ice - ocean models and the latest GOCE derived geoid and MDT, the paper has investigated the quality, usefulness and validity of the new GOCE data for studies of the ocean circulation and transports in the Nordic Seas and Arctic Ocean. Using the GOCE data from release number 3 (based on 12 months of GOCE data in the time interval 1 November 2009 to 14 April 2011) the gravity model from the direct approach yield the computation of the GOCE- based geoid, and jointly with the DTU10 MSS data (based on the integration over the period 1993-2011, Knudsen et al., 2011) the MDT (MSS-G) representing the same 18-years integration period has been calculated. In summary the following key findings and results are highlighted:

(i) New knowledge of the shape and spatial pattern of the MDT is derived at a spatial resolution of around 100 km, which is superior to previous existing MDTs for this region.

(ii) Combined with the steric height estimated from hydrographic data the pure barotropic contribution to the MDT shows distinct features in consistence with known extistence of deep barotropic circulations in the central regions of the Norwegian - and Greenland Seas.

(iii) Comparison of the surface geostrophic current, inverted from the new GOCE based MDT, to existing independent surface velocity calculations derived from combined altimeter data, in-situ observations and gravity field models is in favourable support to the GOCE-derived geoid and MDT.

(iv) The transport estimates, both in the mean and seasonal signals, are also favouring the combined use of the GOCE-based surface geostrophic current and hydrographic data.

(v) New understanding of the relationship between the MDT, the mean surface geostrophic current and the magnitude of the mean ocean volume transport has been derived for the seasonal variability with regards to the inflow of Atlantic Water to the Norwegian Sea at the Svinøy section.

(vi) The NwASC contains approximately 60 % of the total volume flux across the Svinøy section with a distinct transport maximum in winter (Dec-Jan) and a minimum in summer (Jun-Aug). This transport is moreover dominated by the barotropic component.

(vii) These data and findings are also excellent for assessment and validation of model based retrieval of the MDT, the surface geostrophic current and the volume transport across selected sections and straits.

These findings add new insight on the ocean circulation and transport between the northeast Atlantic Ocean and the Arctic Ocean. They are also considered to be highly valuable for further studies of the regional sea level change in the Nordic Seas and the Arctic Ocean, notable via the contribution of the steric height and changes in the volume transport. Consistent use of the GOCE data for assimilation as suggested by Haines et al. (2011) might also become feasible in near future.

Moreover, as gravity measurements provide an integrated view of the mass variations, their interpretation in terms of mass transport is inherently multidisciplinary. Satellite gravimetry (such as combined GRACE and GOCE) is thus a vital component of a multisensor Earth observing system, which complements and relates observations of different Earth system constituents in a common and consistent global framework (Panet et al., 2012). Being closely related to changes in sea level, ocean transports, and glaciers and ice caps future mass change observations from satellites (at a 100 km scale not resolved by GRACE today) have the potential to significantly advance the ability to monitor seasonal-to annual-to decadal variability in ocean mass transport.

Acknowledgement

The work presented in this paper has partly been supported by European Union 7th framework program through the MONARCH-A Collaborative Project, FP7-Space-2009-1 contract No. 242446. In addition, it has been supported by the Norwegian Funded project SATICE, project number 200408 and the (ESA/NRS) PRODEX project IGOCE, contract number 90377. The study was also partly funded by the Centre for climate dynamics at the Bjerknes Centre.

References

Andersen, O. B and P. Knudsen (2009), The DNSC08 mean sea surface and mean dynamic topography, *J. Geophys. Res*., 114, C11, doi:10.1029/2008JC005179..

Bingham, R. J., P. Knudsen, O. Andersen and R. Pail (2011), An initial estimate of the North Atlantic steady-state geostrophic circulation from GOCE. *Geophys. Res. Lett.* 38:L01606. doi:10.1029/2010GL045633.

Bleck, R. (2002), An oceanic general circulation model framed in hybrid isopycnic-Cartesian coordinates, *Ocean model.,* 4(1), 55-88.

Bruinsma, S. L., C. Förste, O. Abrikosov, J.-C. Marty, M.-H. Rio, S. Mulet and S. Bonvalot (2013), The new ESA satellite-only gravity field model via the direct approach, *Geophy. Res. Lett.*, 40, 1–6, doi:10.1002/grl.50716.

Bruinsma, S.L., J. C. Marty, G. Balmino, R. Biancale, C. Förste, O. Abrikosov and H. Neumayer (2010), GOCE Gravity Field Recovery by Means of the Direct Numerical Method, presented at the *ESA Living Planet Symposium*, 27th June - 2nd July 2010, Bergen, Norway; See also: earth.esa.int/GOCE.

Cazenave, A. , K. Dominh , S. Guinhut, E. Berthier, W. Llovel, G. Ramillien, M. Ablain and G. Larnicol (2009), Sea level budget over 2003-2008: A re-evaluation from GRACE space gravimetry, satellite altimetry and Argo; *Global Planet. Change,* 65(1-2), 83-88.

Cheng, Y., O. Andersen and P. Knudsen (2013), Evaluation of gridded and along-track altimetric data in the Arctic Ocean for climate research, submitted to *Marine Geod*.

Fu L-L, B. Cheng, B. Qiu (2001), 25-day period large-scale oscillations in the Argentine Basin revealed by the TOPEX/POSEIDON altimeter. *J. Phys. Oceanogr, 31*,506–517.

Förste, C., S. Bruinsma, R. Shako, J-C Marty, F. Flechtner, O. Abrikosov, C. Dahle, J-M Lemoine, K. H. Neumayer, R. Biancale, F. Barthelmes, R. König, and G.

Balmino, (2011), EIGEN-6 - A new combined global gravity field model including GOCE data from the collaboration of GFZPotsdam and GRGS-Toulouse; *Geophys. Res. Abstracts, 13,* EGU2011-3242-2, EGU General Assembly.

Gill, A. E., and P. P. Niiler (1973), The theory of seasonal variability in the ocean, *Deep Sea Res.,* 20, 141–177.

Haines, K., J. A. Johannessen, P. Knudsen, D. Lea, M. H. Rio, L. Bertino, F. Davidson, F, and F. Hernandez(2011), An ocean modelling and assimilation guide to using GOCE geoid products. *Ocean Sci.,* 7.(1) , 151-164.

Hansen, B., S. Østerhus, H. Hátún, R. Kristiansen and K.M.H. Larsen (2003), The Iceland–Faroe inflow of Atlantic water to the Nordic Seas. *Prog. Oceanogr.* 59, doi: 10.1016/j.pocean.2003.10.003.

Hansen, B., H. Hatun, R. Kristiansen, S. M. Olsen, and S. Østerhus (2010), Stability and forcing of the Iceland-Faroe inflow of water, heat, and salt to the Arctic, *Ocean Sci*., 6, 1013–1026.

Hawkins, E., and R. Sutton (2008), Potential predictability of rapid changes in the Atlantic meridional overtunning circulation, *Geophys. Res. Lett.*, 35(11), L11603, doi:10.1029/2008GL034059.

Henry, O., P. Prandi, W. Llovel, A. Cazenave, S. Jevrejeva, D. Stammer, B. Meyssignac, and N. Koldunov(2012) Tide gauge-based sea level variations since 1950 along the Norwegian and russian coasts of the arctic ocean: Contribution of the steric and mass components, *J. Geophys. Res.,* 117 (C6), C06 023, doi:10.1029/2011JC007706.

Helland-Hansen, B., and F. Nansen (1909), The Norwegian Sea: its physical oceanography based upon the Norwegian Researches 1900–1904, *Report on Norwegian Fishery and Marine Investigation, vol. II*. The Royal Department of Trade, Navigation and Industries, Mallingske, Kristiania, 390 pp.

Johannessen, J.A., G. Balmino, C. Le Provost, R. Rummel, R. Sabadini,, H. Su□nkel, C.C. Tscherning, P. Visser, P. Woodworth, C. W. Hughes, P. LeGrand, N. Sneeuw, F. Perosanz, M. Aguirre-Martinez, H. Rebhan, and M. Drinkwater(2003), The European Gravity Field and Steady-State Ocean Circulation Explorer Satellite Mission: Impact in Geophysics, *Survey in Geophysics*, 24, 339-386.

Knudsen, P., R. Bingham, O. Andersen, Marie-Helene Rio (2011), A global mean dynamic topography and ocean circulation estimation using a preliminary GOCE gravity model, *J. Geod.,* doi10.1007/s00190-011-0485-8.

Koldunov, N.V., N.Serra, A. Kohl, D. Stammer, O. Henry, P. Prandi, A. Cazenave, P.

Knudsen, O.B. Andersen, Y. Gao, J. A. Johannessen, (2013), Arctic Ocean Sea Surface Height variability during the last 40 years, *to be submitted to Geophys. Res. Lett.*

Koop, R., T. Gruber, and R. Rummel (2007), The status of the GOCE high level processing facility (HPF). *Proceedings of the 3rd GOCE User Workshop*, Eur. Space Res. Inst., Eur. Space Agency, Frascati, Italy.199-204.

Kwok, R. and J. Morison (2011), Dynamic topography of the ice-covered arctic ocean from ICESat. *Geophys. Res. Lett.,* 38 (2), L02 501+, doi:10.1029/2010GL046063.

Lumpkin, R. and Z. Garraffo (2005), Evaluating the Decomposition of Tropical Atlantic Drifter Observations. *J. Atm. Oceanic Techn.* 22, 1403-1415.

Maximenko, N., P. Niiler, M-H Rio, O. Melnichenko, L. Centurioni, D. Chambers, V. Zlotnicki and B. Galperin (2009), Mean dynamic topography of the ocean derived from satellite and drifting buoy data using three different techniques. *J Atmos Ocean Tech* 26(9):1910–1919.

Mork, K. A., and Ø. Skagseth (2005), Annual sea surface height variability in the Nordic Seas, in The Nordic Seas: An Integrated Perspective, *Geophys. Monogr. Ser.,* vol. 158, edited by H. Drange et al., pp. 51– 64, AGU, Washington, D. C.

Mork, K. A., and Ø. Skagseth (2010), A quantitative description of the Norwegian Atlantic Current by combining altimetry and hydrography. *Ocean Sci.,* 6, 901–911, doi:10.5194/os-6-901-2010.

Morison, J., R. Kwok, C. Peralta-Ferriz, M. Alkire, I. Rigor, R. Andersen, and M. Steele (2012), Changing arctic ocean freshwater pathways. *Nature,* 481 (7379), 66–70, doi:10.1038/nature10705.

Nilsen, J. E. Ø., and E. Falck (2006), Variation of mixed layer properties in the Norwegian Sea for the period 1948–1999, *Prog. Oceanogr.,70*, 58–90, doi:10.1016/j.pocean.2006.03.014.

Nilsen, J. E. Ø., and F. Nilsen (2007), The Atlantic Water Flow along the Vøring Plateau: Detecting Frontal Structures in Oceanic Station Time Series, *Deep Sea Res.*, *Part 1,54(3)*, 297-319, doi:10.1016/j.dSV.2006.12.012.

Nilsen, J. E. Ø., H. Hatun, K. A. Mork, and H. Valdimarsson (2008), The NISE Data Set. *Technical Report 08-01*, Faroese Fisheries Laboratory, Box 3051, Torshavn, Faroe Islands.

Nøst, O. A., and P. E. Isachsen (2003), The large-scale time-mean ocean circulation in the Nordic Seas and Arctic Ocean estimated from simplified dynamics, *J. Mar. Res.,* 61, 175– 210.

Orvik, K.A., Ø. Skagseth, M. Mork (2001), Atlantic inflow to the Nordic Seas: current

structure and volume fluxes from moored current meters, VM-ADCP and SeaSoar-CTD observations, 1995-1999, *Deep Sea Res.,* I, 48, doi: 10.1016/S0967-0637(00)00038-8.

Orvik, K. A., and Ø. Skagseth (2003), Monitoring the Norwegian Atlantic slope current using a single moored current meter, *Cont. Shelf Res.,23*, 159–176.

Østerhus, S., W. R. Turrrell, S. Jónsson,and B. Hansen (2005), Measured volume, heat, and salt fluxes from the Atlantic to the Arctic Mediterranean, *Geophys. Res. Lett.,* 32, L07603, doi:10.1029/2004GL022188.

Pail R., S. Bruinsma, F. Migliaccio, C. Foerste, H. Goiginger, W.-D. Schuh, E. Hoeck, M. Reguzzoni, J. M. Brockmann, O. Abrikosov, M. Veicherts, T. Fecher, R. Mayrhofer, I. Krasbutter, F. Sanso, and C. C. Tscherning (2011), First GOCE gravity field models derived by three different approaches, *Journal of Geod., 85,* 11, 819-843.

Panet, I., J. Flury, R. Biancale, T. Gruber, J. A. Johannessen, M. R. van den Broeke, T. van Dam, P. Gegout, C. W. Hughes, G. Ramillien, I. Sasgen, L. Seoane, M. Thomas, (2012), Earth System Mass Transport Mission (e.motion): A Concept for Future Earth Gravity Field Measurements from Space, *Survey in Geophysics,*DOI 10.1007/s1072-012-9209-8.

Prandi, P., M. Ablain, A. Cazenave, and N. Picot (2012), Sea level variability in the Arctic Ocean observed by satellite altimetry. *Ocean Science Discussions*, 9 (4), 2375–2401, doi: 10.5194/osd-9-2375-2012.

Rio, M. H., S. Guinehut, and G. Larnicol (2011), New CNES-CLS09 global mean dynamic topography computed from the combination of GRACE data, altimetry, and in situ measurements, *J. Geophys. Res.,*116, C07018, doi: 10.1029/2010JC006505.

Rossby, T., V. Ozhigin, V. Ivshin, and S. Bacon (2009), An isopycnal view of the Nordic Seas hydrography with focus on properties of the Lofoten Basin, *Deep Sea Res.*, *Part 1, 56*, doi:10.1016/j.dsr.2009.07.005.

Sakov, P., F. Counillon, L. Bertino, K. A. Lisæter, P. R. Oke, and A. Korablev (2012), TOPAZ4: an ocean-sea ice data assimilation system for the North Atlantic and Arctic, *Ocean Sci*., 8, 633-656, doi:10.5194/os-8-633-2012.

Sandø, A. B., J. E. Ø. Nilsen, T. Eldevik, and M. Bentsen (2012), Mechanisms for variable North Atlantic–Nordic seas exchanges, J. Geophys. Res., 117, C12006, doi:10.1029/2012JC008177.

Serra, N., R.H. Käse, A. Köhl, D. Stammer, and D. Quadfasel (2010), On the low-frequency phase relation between the Denmark Strait and the Faroe-Bank Channel overflows, *Tellus*, 62, doi: 10.1111/j.1600-0870.2010.00445.x., 530—550.

Shum, C.K., H-P Plag , J. Schröter , V. Zlotnicki, P. Bender, A. Braun, A. Cazenave , D. Chamber , J. Duan, W. Emery, G. Fotopoulos, V. Gouretski, R. Gross , T. Gruber, J. Guo, G. Han, C. Hughes, M. Ishii, S. Jayne, J. A. Johannesen, P. Knudsen, C-Y Kuo, E. Leuliette, S. Levitus, N. Maximenko, L. Miller, J. Morison , H. Rashid , J. Ries , M. Rothacher , R. Rummel , K. Shibuya, M. Sideris , Y. Tony Song, D. Stammer, M. Thomas, J. Willis and P. Woodworth (2010), Geodetic observations of the ocean surface topography, geoid, currents and changes in ocean mass and volume, Plenary Session Paper, OceanObs09, Venice Italy, 21-25 Sept. 2009, *ESA Publicatiion WPP 306,* doi: 10.5270/OceanObs09, 2010.

Siegismund, F., J. A. Johannessen, H. Drange, K. A. Mork, A. Korablev (2007), Steric height variability in the Nordic Seas, *J. Geophys. Res.,.* 112, C12010, doi:10.1029/2007/JC004221.

Skagseth, Ø., T. Furevik, R. Ingvaldsen, H. Loeng, K.A. Mork, K.A. Orvik and V. Ozhigin (2008), Volume and Heat Transports to the Arctic Ocean via the Norwegian and Barents Seas. In Dickson et al. (eds.) Arctic-Subarctic Ocean Fluxes (ASOF) - Defining the Role of the Northern Seas in Climate, *Springer.* pp 45-64.

Steele M., and W. Ermold (2007), Steric Sea Level Change in the Northern Seas, *J. Climate*, 20, 403-417,doi.org/10.1175/JCLI4022.1.

Søiland, H., M. D. Prater, and T. Rossby (2008), Rigid topographic control of currents in the Nordic Seas, *Geophys. Res. Lett.,* 35, L18607, doi:10.1029/2008GL034846.

Tomczak M., and J.S. Godfrey (2003), Regional Oceanograhy: An Introduction (2nd edition), *Daya Publishing House*, New Delhi, India.